

LIBRARY COPY

## TECHNICAL NOTE

D-819

CHARTS FOR CONICAL AND TWO-DIMENSIONAL  
OBLIQUE-SHOCK FLOW PARAMETERS IN HELIUM AT  
MACH NUMBERS FROM ABOUT 1 TO 100

By Arthur Henderson, Jr., and Dorothy O. Braswell

Langley Research Center  
Langley Field, Va.

LIBRARY COPY

JUN 13 1961

SPACE FLIGHT  
LANGLEY FIELD, VIRGINIA

NATIONAL AERONAUTICS AND SPACE ADMINISTRATION  
WASHINGTON

June 1961

NATIONAL AERONAUTICS AND SPACE ADMINISTRATION

TECHNICAL NOTE D-819

CHARTS FOR CONICAL AND TWO-DIMENSIONAL  
OBLIQUE-SHOCK FLOW PARAMETERS IN HELIUM AT  
MACH NUMBERS FROM ABOUT 1 TO 100

By Arthur Henderson, Jr., and Dorothy O. Braswell

SUMMARY

Charts are presented for the determination of certain flow properties in the flow field and on the surface of cones and wedges at Mach numbers from about 1 to 100 in a perfect gas with a ratio of specific heats of 5/3. In addition, a table of the isentropic subsonic flow parameters is included.

INTRODUCTION

The present charts supplement the work of references 1 and 2. Reference 1 presents ideal-gas flow parameters for helium. It includes tables of the one-dimensional isentropic flow relations and the normal shock relations for Mach numbers from 1 to 40.

For Mach numbers of 12, 16, 20, and 24, reference 1 also presents charts of the shock angle, Mach number behind the shock, and static-pressure ratio across the shock for two dimensionally deflected flow (weak shock solution only). In addition, charts of the shock angle, surface velocity ratio, and ratio of surface static pressure to free-stream static pressure for conical flow are presented.

Reference 2 presents charts of the isentropic and normal shock relations at Mach numbers up to 20 and charts of several two-dimensional oblique-shock flow parameters at Mach numbers from about 5 to 25. Reference 2 has received only limited distribution.

The present paper presents charts of several flow parameters for both conical and two-dimensional oblique flow in helium at Mach numbers from about 1 to 100. A table of the isentropic subsonic flow parameters in helium is also given inasmuch as they are not presented elsewhere in the literature.

## SYMBOLS

A	cross-sectional area of stream tube or channel
a	speed of sound
$c_p$	specific heat at constant pressure
$c_v$	specific heat at constant volume
M	Mach number
p	pressure
q	dynamic pressure
T	absolute temperature
v	velocity of flow
$v_{\max}$	maximum velocity obtained by expanding to zero pressure
$\gamma = c_p/c_v$	
$\delta$	flow-deflection angle across oblique shock
$\epsilon$	shock wave angle
$\mu$	Mach angle
$\nu$	Prandtl-Meyer angle
$\rho$	density
$\sigma$	semivertex angle of cone

## Subscripts:

c	cone surface
n	normal shock
t	stagnation conditions

1 immediately upstream of shock

2 immediately downstream of shock

Superscript:

\* condition where local velocity equals speed of sound

## RESULTS AND DISCUSSION

The conical-flow results were computed on an IBM 704 electronic data processing machine by the procedure outlined in reference 3. A cone-surface Mach number was assumed for various values of  $\sigma$  and the flow field was iterated out toward the shock to determine the shock angle  $\epsilon$  and free-stream Mach number  $M_1$ . Figures 1 and 2 present the variations of  $\epsilon$  and  $M_c$ , respectively, with  $M_1$  for various values of  $\sigma$ . Figures 3, 4, and 5 present the variations of  $p_{t,c}/p_{t,1}$ ,  $p_c/p_1$ , and  $\rho_1/\rho_c$ , respectively, with  $M_1$ .

By using the results shown in figures 1 and 2, the results shown in figure 3 were obtained from

$$\frac{p_{t,c}}{p_{t,1}} = \left[ \frac{(\gamma + 1)M_1^2 \sin^2 \epsilon}{(\gamma - 1)M_1^2 \sin^2 \epsilon + 2} \right]^{\frac{\gamma}{\gamma-1}} \left[ \frac{\gamma + 1}{2\gamma M_1^2 \sin^2 \epsilon - (\gamma - 1)} \right]^{\frac{1}{\gamma-1}} \quad (1)$$

The curves of figure 4 were obtained from

$$\frac{p_c}{p_1} = \frac{p_c}{p_{t,c}} \left( \frac{p_1}{p_{t,1}} \right)^{-1} \frac{p_{t,c}}{p_{t,1}} \quad (2)$$

where

$$\frac{p_c}{p_{t,c}} = \left( 1 + \frac{\gamma - 1}{2} M_c^2 \right)^{-\frac{\gamma}{\gamma-1}} \quad (3)$$

$$\frac{p_1}{p_{t,1}} = \left( 1 + \frac{\gamma - 1}{2} M_1^2 \right)^{-\frac{1}{\gamma-1}} \quad (4)$$

The curves of figure 5 were obtained from

$$\frac{\rho_1}{\rho_c} = \frac{\rho_1}{\rho_{t,1}} \left( \frac{\rho_c}{\rho_{t,c}} \right)^{-\frac{1}{\gamma-1}} \frac{\rho_{t,c}}{\rho_{t,1}} \quad (5)$$

where

$$\frac{\rho_c}{\rho_{t,c}} = \left( 1 + \frac{\gamma - 1}{2} M_c^2 \right)^{-\frac{1}{\gamma-1}} \quad (6)$$

$$\frac{\rho_1}{\rho_{t,1}} = \left( 1 + \frac{\gamma - 1}{2} M_1^2 \right)^{-\frac{1}{\gamma-1}} \quad (7)$$

$$\frac{\rho_{t,c}}{\rho_{t,1}} = \frac{p_{t,c}}{p_{t,1}} \quad (8)$$

The two-dimensional results were calculated from the oblique-shock equations which may be found in reference 4, for instance. Figures 6 to 10 present charts of  $\epsilon$ ,  $M_2$ ,  $p_{t,2}/p_{t,1}$ ,  $p_2/p_1$ , and  $\rho_1/\rho_2$ , respectively, plotted against  $M_1$  for various values of flow-deflection angle  $\delta$ .

It is of interest to note that the minimum density ratio on the cone surface (fig. 5) is about 0.239 as compared with the value of 0.25 for two-dimensional flow. For comparison, it is noted that the minimum density ratio at the stagnation point behind a normal shock at  $M = \infty$  is about 0.229.

Only weak shock solutions are presented for the cones, since after the occurrence of shock detachment the mathematical solution is physically unrealistic.

Both weak and strong shock solutions are presented for the two-dimensional flow results. Although the two-dimensional results apply to conditions immediately behind the shock, when the shock is attached (weak shock solution), the results are also applicable on the surface of a wedge whose angle is identical to the flow-deflection angle across the shock, since the flow field is then uniform. Conditions immediately behind the two-dimensional shock apply to both two- and three-dimensional flow for both the weak and strong shock solutions.

Often the compression ratio  $p_2/p_c$ , the ratio of the pressure immediately behind the conical shock to the pressure on the cone surface, is desired. This ratio can be obtained from

$$\frac{p_2}{p_c} = \frac{p_2}{p_1} \left( \frac{p_c}{p_1} \right)^{-1} \quad (9)$$

The ratio  $p_c/p_1$  is given directly in figure 4, and the ratio  $p_2/p_1$  is determined from figure 9. The value of  $\delta$  to be used in figure 9 is the flow-deflection angle immediately behind the conical shock and is determined as follows: For given  $\sigma$  and  $M_1$ , the cone shock angle  $\epsilon$  is determined from figure 1. The flow-deflection angle  $\delta$  immediately behind this shock is found from figure 6 for the given value of  $M_1$  and the determined cone shock angle  $\epsilon$ .

The scales on the charts have been chosen to allow the ordinates to be read to an accuracy of at least 0.5 to 1.0 percent at Mach numbers from 1 to 40, and at least 1.0 to 2.0 percent at Mach numbers from 40 to 100.

In general, the results presented here will be used in conjunction with the isentropic and normal shock relations which may be found in references 1 or 2 for Mach numbers up to 40. At Mach numbers above 40, the hypersonic approximation applied to the isentropic and normal shock relations yields the following expressions which may be used to a high degree of accuracy. In each case, the second form of the equation applies for  $\gamma = 5/3$ .

$$\frac{p}{p_t} = \left( \frac{\gamma - 1}{2} M^2 \right)^{-\frac{\gamma}{\gamma-1}} = \frac{15.5884}{M^5} \quad (10)$$

$$\frac{\rho}{\rho_t} = \left( \frac{\gamma - 1}{2} M^2 \right)^{-\frac{1}{\gamma-1}} = \frac{5.1962}{M^3} \quad (11)$$

$$\frac{T}{T_t} = \left( \frac{\gamma - 1}{2} M^2 \right)^{-1} = \frac{3.0000}{M^2} \quad (12)$$

$$\frac{a}{a_t} = \left( \frac{\gamma - 1}{2} M^2 \right)^{-1/2} = \frac{1.7321}{M} \quad (13)$$

$$\frac{q}{p_t} = \frac{\gamma}{\gamma - 1} \left( \frac{\gamma - 1}{2} M^2 \right)^{-\frac{1}{\gamma-1}} = \frac{12.9905}{M^3} \quad (14)$$

$$\frac{A^*}{A} = \left( \frac{\gamma + 1}{2} \right)^{\frac{\gamma+1}{2(\gamma-1)}} M \left( \frac{\gamma - 1}{2} M^2 \right)^{-\frac{\gamma+1}{2(\gamma-1)}} = \frac{16.0000}{M^3} \quad (15)$$

$$\frac{V}{V_{\max}} = 1 - \frac{1}{(\gamma - 1)M^2} = 1.0000 - \frac{1.5000}{M^2} \quad (16)$$

$$\frac{V}{a^*} = \left( \frac{\gamma + 1}{\gamma - 1} \right)^{1/2} \left[ 1 - \frac{1}{(\gamma - 1)M^2} \right] = 2.0000 - \frac{3.0000}{M^2} \quad (17)$$

$$\mu = \frac{57.2958}{M} \quad (18)$$

$$v = 57.2958 \left( 1.5708 - \frac{3.0000}{M} \right) \quad (19)$$

$$M_{2,n} = \left( \frac{\gamma - 1}{2\gamma} \right)^{1/2} = 0.4472 \quad (20)$$

$$\frac{p_{2,n}}{p_1} = \left( \frac{2\gamma}{\gamma + 1} \right) M_1^2 = 1.2500 M_1^2 \quad (21)$$

$$\frac{\rho_{2,n}}{\rho_1} = \frac{\gamma + 1}{\gamma - 1} = 4.0000 \quad (22)$$

$$\frac{T_{2,n}}{T_1} = \frac{2\gamma(\gamma - 1)}{(\gamma + 1)^2} M_1^2 = 0.3125 M_1^2 \quad (23)$$

$$\frac{p_{t,2,n}}{p_{t,1}} = \frac{\gamma + 1}{\gamma - 1} \left[ \frac{(\gamma + 1)^2}{2\gamma(\gamma - 1)M_1^2} \right]^{\frac{1}{\gamma-1}} = \frac{22.8970}{M_1^3} \quad (24)$$

$$\frac{p_{t,2,n}}{p_1} = \frac{\gamma + 1}{2} \left[ \frac{(\gamma + 1)^2}{4\gamma} \right]^{\frac{1}{\gamma-1}} M_1^2 = 1.4689 M_1^2 \quad (25)$$

References 1 and 2 do not present the subsonic isentropic flow relations for helium. Inasmuch as these relations are of value in the stagnation region of blunt bodies and in the subsonic portion of boundary layers, they are given in table I.

Langley Research Center,  
 National Aeronautics and Space Administration,  
 Langley Field, Va., March 8, 1961.

## REFERENCES

1. Mueller, James N.: Equations, Tables, and Figures for Use in the Analysis of Helium Flow at Supersonic and Hypersonic Speeds. NACA TN 4063, 1957.
2. Staff of the Gas Dynamics Lab., Princeton Univ.: Charts for Flow Parameters of Helium at Hypersonic Speeds - Mach Number 10 to 20. WADC Tech. Note 57-377, ASTIA Doc. No. AD 142310, U.S. Air Force, 1957.
3. Ferri, Antonio: Elements of Aerodynamics of Supersonic Flows. The MacMillan Co., 1949.
4. Ames Research Staff: Equations, Tables, and Charts for Compressible Flow. NACA Rep. 1135, 1953. (Supersedes NACA TN 1428.)

TABLE I.- SUBSONIC ISENTROPIC FLOW RELATIONS FOR HELIUM

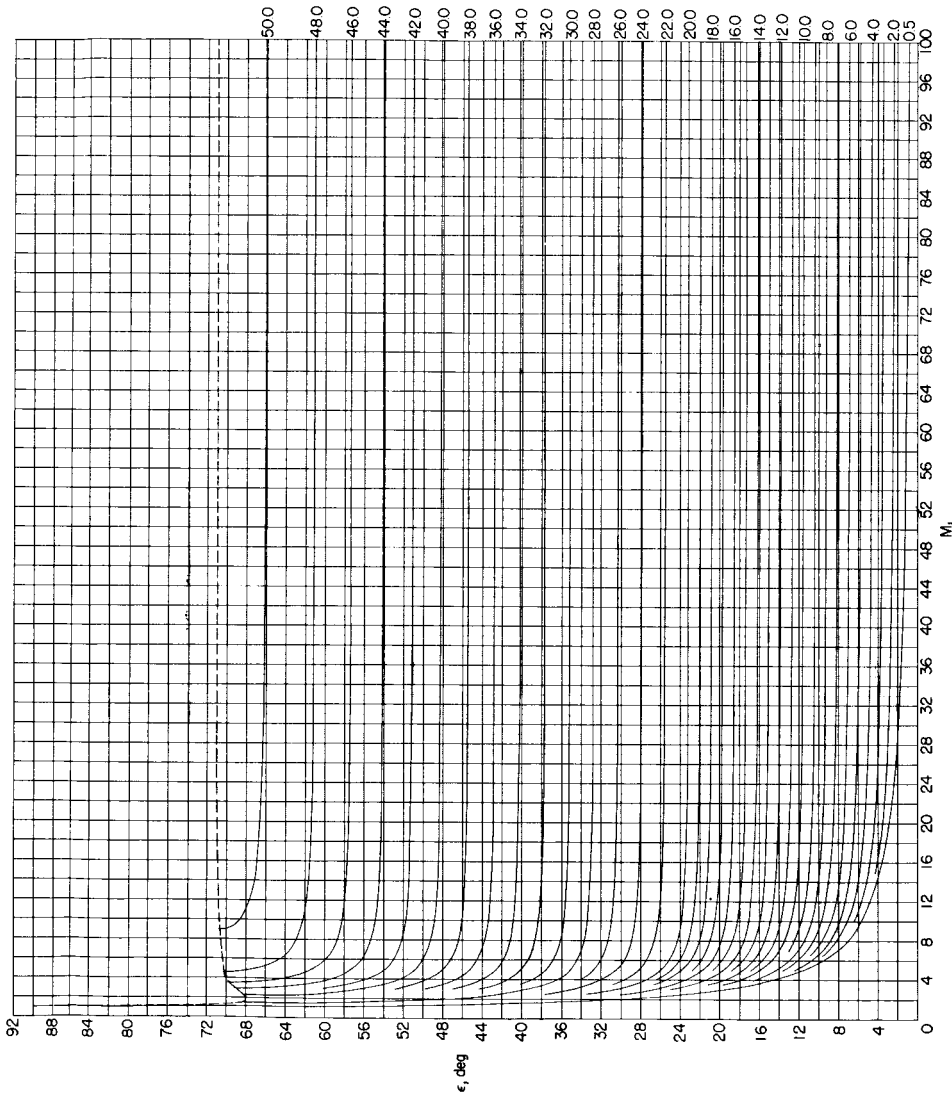
M	p/p <sub>t</sub>	$\rho/\rho_t$	T/T <sub>t</sub>	a/a <sub>t</sub>	q/p <sub>t</sub>	A/A*	v/v <sub>max</sub>	v/a
0	1.0000	1.0000	1.0000	1.0000	0	0	0	0
.01	.9999	.9999	1.0000	1.0000	.0001	.0178	.0058	.0115
.02	.9997	.9998	.9999	.9999	.0003	.0355	.0115	.0231
.03	.9993	.9996	.9997	.9999	.0007	.0533	.0173	.0346
.04	.9987	.9992	.9995	.9997	.0013	.0710	.0231	.0462
.05	.9979	.9988	.9992	.9996	.0021	.0887	.0289	.0577
.06	.9970	.9982	.9988	.9994	.0030	.1064	.0346	.0692
.07	.9959	.9976	.9984	.9992	.0041	.1240	.0404	.0808
.08	.9947	.9968	.9979	.9989	.0053	.1416	.0461	.0923
.09	.9933	.9960	.9973	.9987	.0067	.1591	.0519	.1038
.10	.9917	.9950	.9967	.9983	.0083	.1766	.0576	.1153
.11	.9900	.9940	.9960	.9980	.0100	.1940	.0634	.1268
.12	.9881	.9928	.9952	.9976	.0119	.2113	.0691	.1382
.13	.9861	.9916	.9944	.9972	.0139	.2285	.0748	.1497
.14	.9839	.9903	.9935	.9967	.0161	.2457	.0806	.1611
.15	.9815	.9889	.9926	.9963	.0184	.2627	.0863	.1726
.16	.9790	.9873	.9915	.9958	.0209	.2796	.0920	.1840
.17	.9763	.9857	.9905	.9952	.0235	.2965	.0977	.1954
.18	.9735	.9840	.9893	.9946	.0263	.3132	.1033	.2067
.19	.9705	.9822	.9881	.9940	.0292	.3298	.1090	.2181
.20	.9674	.9803	.9868	.9934	.0322	.3463	.1147	.2294
.21	.9642	.9783	.9855	.9927	.0354	.3626	.1204	.2407
.22	.9608	.9763	.9841	.9920	.0388	.3788	.1260	.2520
.23	.9572	.9741	.9827	.9913	.0422	.3948	.1316	.2633
.24	.9536	.9719	.9812	.9905	.0458	.4108	.1372	.2745
.25	.9498	.9695	.9796	.9897	.0495	.4265	.1429	.2857
.26	.9458	.9671	.9780	.9889	.0533	.4421	.1484	.2969
.27	.9417	.9646	.9763	.9881	.0572	.4575	.1540	.3081
.28	.9379	.9620	.9745	.9872	.0613	.4727	.1596	.3192
.29	.9332	.9594	.9727	.9863	.0654	.4878	.1651	.3303
.30	.9288	.9566	.9709	.9853	.0697	.5027	.1707	.3413
.31	.9242	.9538	.9690	.9844	.0740	.5174	.1762	.3524
.32	.9195	.9509	.9670	.9834	.0785	.5320	.1817	.3634
.33	.9147	.9479	.9650	.9823	.0830	.5463	.1872	.3743

TABLE I.- SUBSONIC ISENTROPIC FLOW RELATIONS FOR HELIUM - Continued

M	p/p <sub>t</sub>	$\rho/\rho_t$	T/T <sub>t</sub>	a/a <sub>t</sub>	q/p <sub>t</sub>	A/A <sup>*</sup>	V/V <sub>max</sub>	V/a
.34	0.9098	0.9449	0.9629	0.9813	0.0876	0.5604	0.1926	0.3853
.35	.9048	.9417	.9608	.9802	.0924	.5744	.1981	.3961
.36	.8997	.9385	.9586	.9791	.0972	.5881	.2035	.4070
.37	.8944	.9353	.9564	.9779	.1020	.6016	.2089	.4178
.38	.8891	.9319	.9541	.9768	.1070	.6150	.2143	.4286
.39	.8837	.9285	.9517	.9756	.1120	.6280	.2197	.4393
.40	.8782	.9250	.9494	.9744	.1171	.6409	.2250	.4501
.41	.8726	.9215	.9469	.9731	.1222	.6536	.2303	.4607
.42	.8669	.9179	.9445	.9718	.1274	.6660	.2356	.4713
.43	.8611	.9142	.9419	.9705	.1327	.6783	.2409	.4819
.44	.8553	.9105	.9394	.9692	.1380	.6902	.2462	.4924
.45	.8493	.9067	.9368	.9679	.1433	.7020	.2515	.5029
.46	.8433	.9028	.9341	.9665	.1487	.7136	.2567	.5134
.47	.8373	.8989	.9314	.9651	.1541	.7248	.2619	.5238
.48	.8311	.8949	.9287	.9637	.1596	.7359	.2671	.5341
.49	.8249	.8909	.9259	.9622	.1650	.7468	.2722	.5441
.50	.8186	.8869	.9231	.9608	.1705	.7574	.2774	.5547
.51	.8123	.8827	.9202	.9593	.1761	.7678	.2825	.5649
.52	.8059	.8786	.9173	.9578	.1816	.7779	.2876	.5751
.53	.7995	.8744	.9144	.9562	.1871	.7878	.2926	.5852
.54	.7930	.8701	.9114	.9547	.1927	.7975	.2976	.5953
.55	.7865	.8658	.9084	.9531	.1983	.8069	.3026	.6053
.56	.7799	.8615	.9054	.9515	.2038	.8161	.3076	.6153
.57	.7733	.8571	.9023	.9499	.2094	.8250	.3126	.6252
.58	.7667	.8526	.8992	.9482	.2149	.8337	.3175	.6350
.59	.7600	.8482	.8960	.9466	.2205	.8422	.3224	.6449
.60	.7533	.8437	.8929	.9449	.2260	.8503	.3273	.6546
.61	.7465	.8391	.8897	.9432	.2315	.8583	.3322	.6644
.62	.7398	.8346	.8864	.9415	.2370	.8660	.3370	.6740
.63	.7330	.8300	.8832	.9398	.2424	.8736	.3418	.6837
.64	.7262	.8253	.8799	.9380	.2479	.8809	.3466	.6932
.65	.7194	.8207	.8766	.9362	.2533	.8878	.3513	.7027
.66	.7125	.8160	.8732	.9345	.2586	.8947	.3561	.7122
.67	.7057	.8113	.8698	.9327	.2640	.9012	.3608	.7216

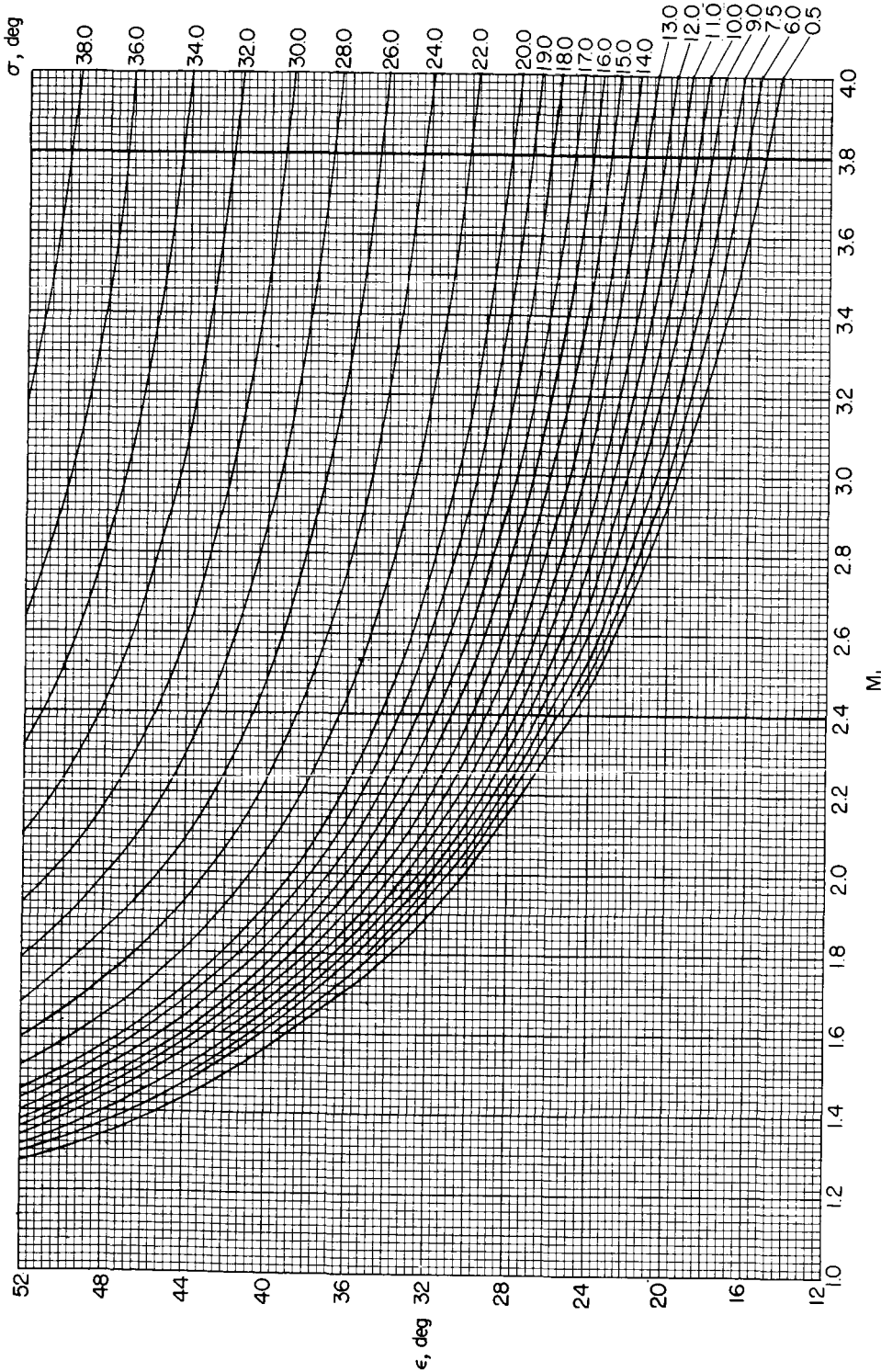
TABLE I.- SUBSONIC ISENTROPIC FLOW RELATIONS FOR HELIUM - Concluded

M	$p/p_t$	$\rho/\rho_t$	$T/T_t$	$a/a_t$	$q/p_t$	$A/A^*$	$v/v_{max}$	v/a
.68	0.6988	0.8065	0.8665	0.9308	0.2693	0.9075	0.3654	0.7309
.69	.6919	.8018	.8630	.9290	.2745	.9136	.3701	.7402
.70	.6851	.7970	.8596	.9271	.2797	.9195	.3747	.7494
.71	.6782	.7922	.8561	.9253	.2849	.9252	.3793	.7586
.72	.6713	.7873	.8527	.9234	.2900	.9306	.3839	.7677
.73	.6645	.7825	.8492	.9215	.2951	.9358	.3884	.7768
.74	.6576	.7776	.8456	.9196	.3001	.9408	.3929	.7858
.75	.6508	.7728	.8421	.9177	.3051	.9455	.3974	.7948
.76	.6439	.7679	.8386	.9157	.3099	.9501	.4018	.8036
.77	.6371	.7630	.8350	.9138	.3148	.9544	.4062	.8125
.78	.6303	.7581	.8314	.9118	.3195	.9585	.4106	.8212
.79	.6235	.7532	.8278	.9098	.3243	.9623	.4150	.8299
.80	.6167	.7482	.8242	.9078	.3289	.9661	.4193	.8386
.81	.6099	.7433	.8205	.9058	.3334	.9696	.4236	.8472
.82	.6032	.7383	.8169	.9038	.3380	.9728	.4279	.8558
.83	.5964	.7334	.8133	.9018	.3424	.9759	.4321	.8643
.84	.5897	.7284	.8096	.8998	.3467	.9787	.4364	.8728
.85	.5831	.7235	.8059	.8977	.3511	.9815	.4405	.8811
.86	.5764	.7185	.8022	.8957	.3552	.9840	.4447	.8895
.87	.5698	.7136	.7985	.8936	.3594	.9863	.4489	.8977
.88	.5632	.7086	.7948	.8915	.3634	.9884	.4529	.9059
.89	.5567	.7037	.7911	.8894	.3675	.9903	.4570	.9140
.90	.5502	.6987	.7874	.8874	.3714	.9920	.4611	.9222
.91	.5437	.6938	.7837	.8853	.3752	.9936	.4651	.9303
.92	.5372	.6888	.7800	.8831	.3789	.9949	.4691	.9381
.93	.5308	.6839	.7762	.8810	.3826	.9961	.4730	.9461
.94	.5245	.6789	.7725	.8789	.3862	.9972	.4770	.9540
.95	.5181	.6740	.7687	.8768	.3896	.9981	.4809	.9618
.96	.5119	.6691	.7650	.8746	.3931	.9987	.4848	.9695
.97	.5056	.6642	.7612	.8725	.3964	.9993	.4886	.9773
.98	.4994	.6593	.7575	.8703	.3997	.9997	.4924	.9848
.99	.4933	.6544	.7537	.8682	.4029	.9999	.4962	.9925
1.00	.4871	.6495	.7500	.8660	.4059	1.0000	.5000	1.0000



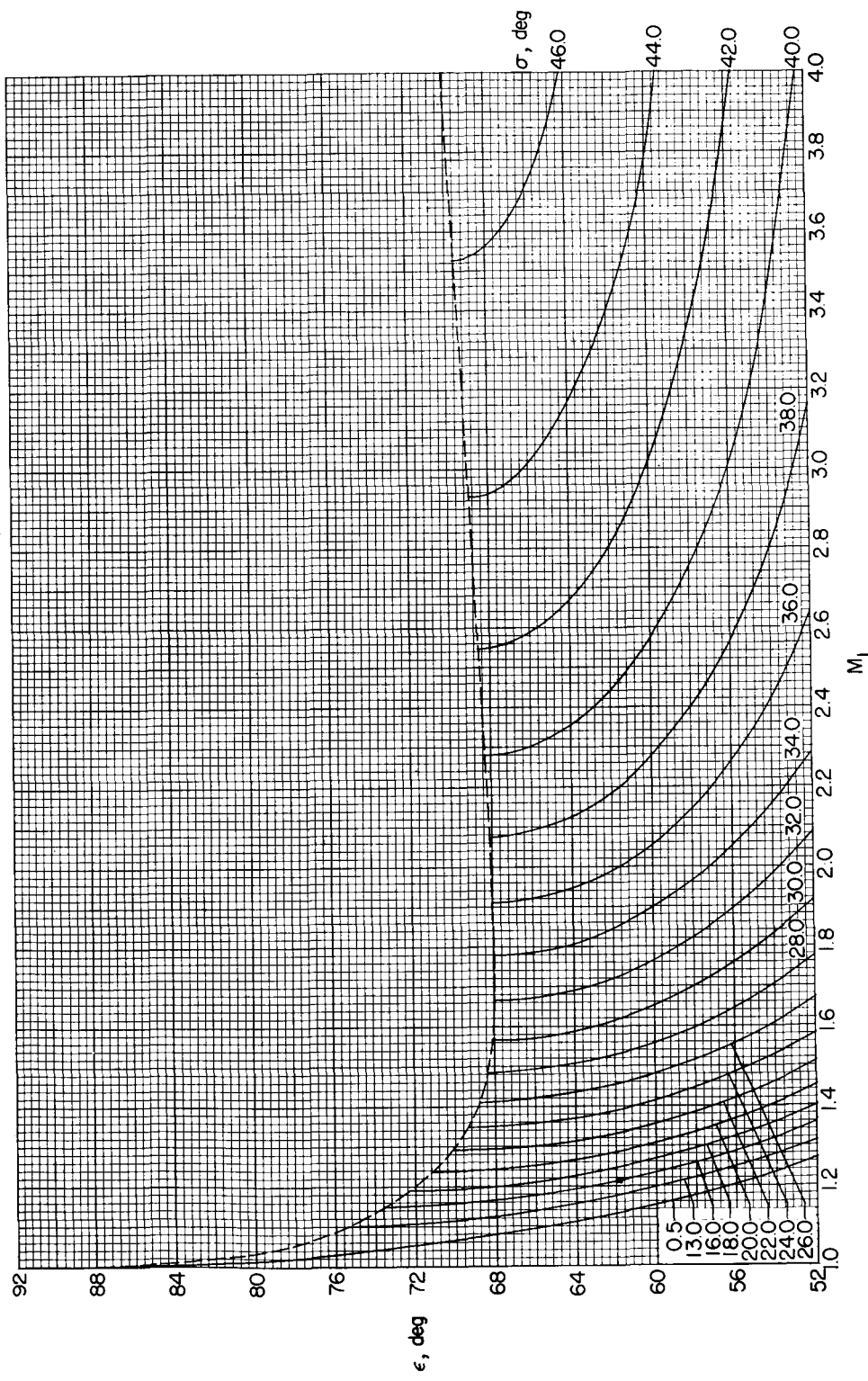
(a)  $M_1 = 1$  to 100;  $\epsilon = 0^\circ$  to  $90^\circ$ .

Figure 1.- Variation of cone shock angle with free-stream Mach number for various cone angles.  
(Dashed line denotes limit of weak shock solution.)



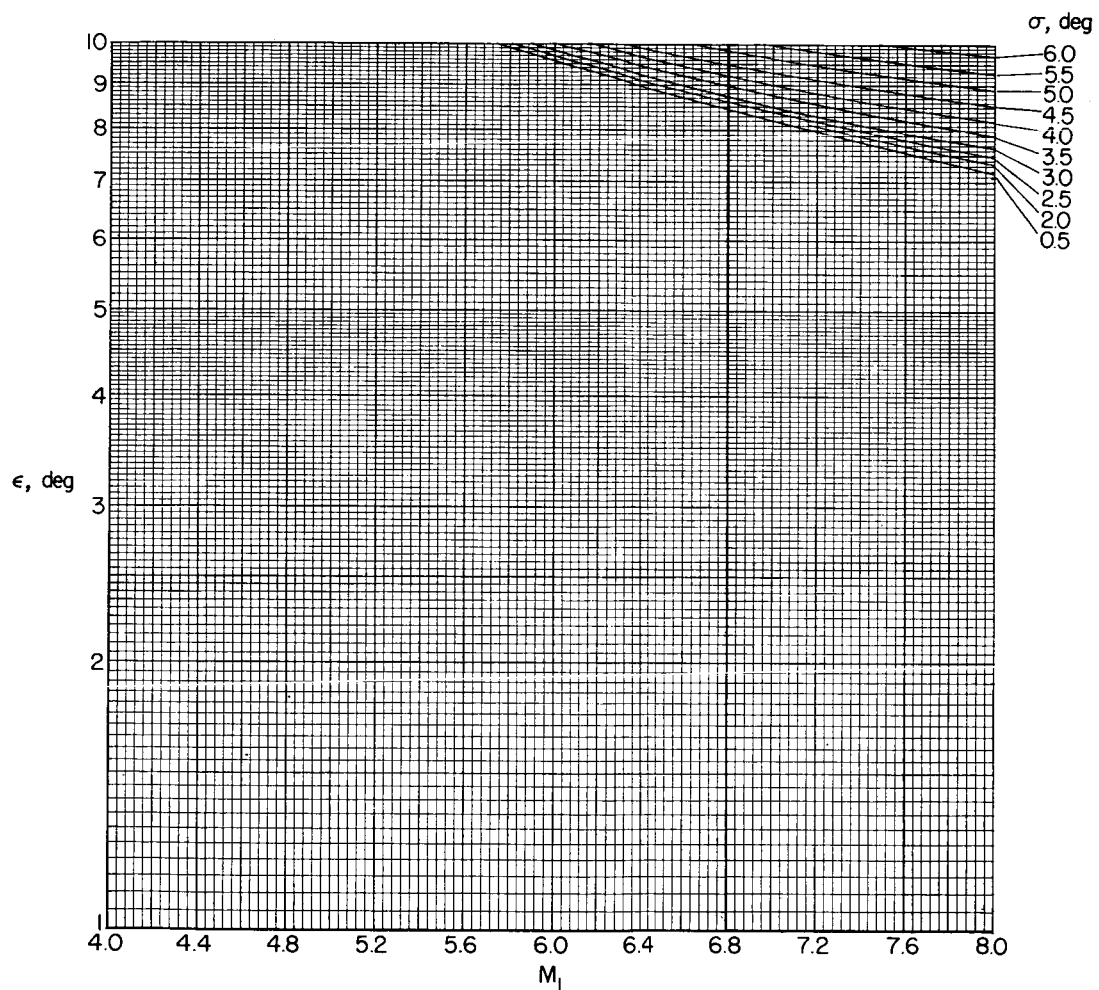
(b)  $M_L = 1$  to 4;  $\epsilon = 120^\circ$  to  $52^\circ$ .

Figure 1.- Continued.

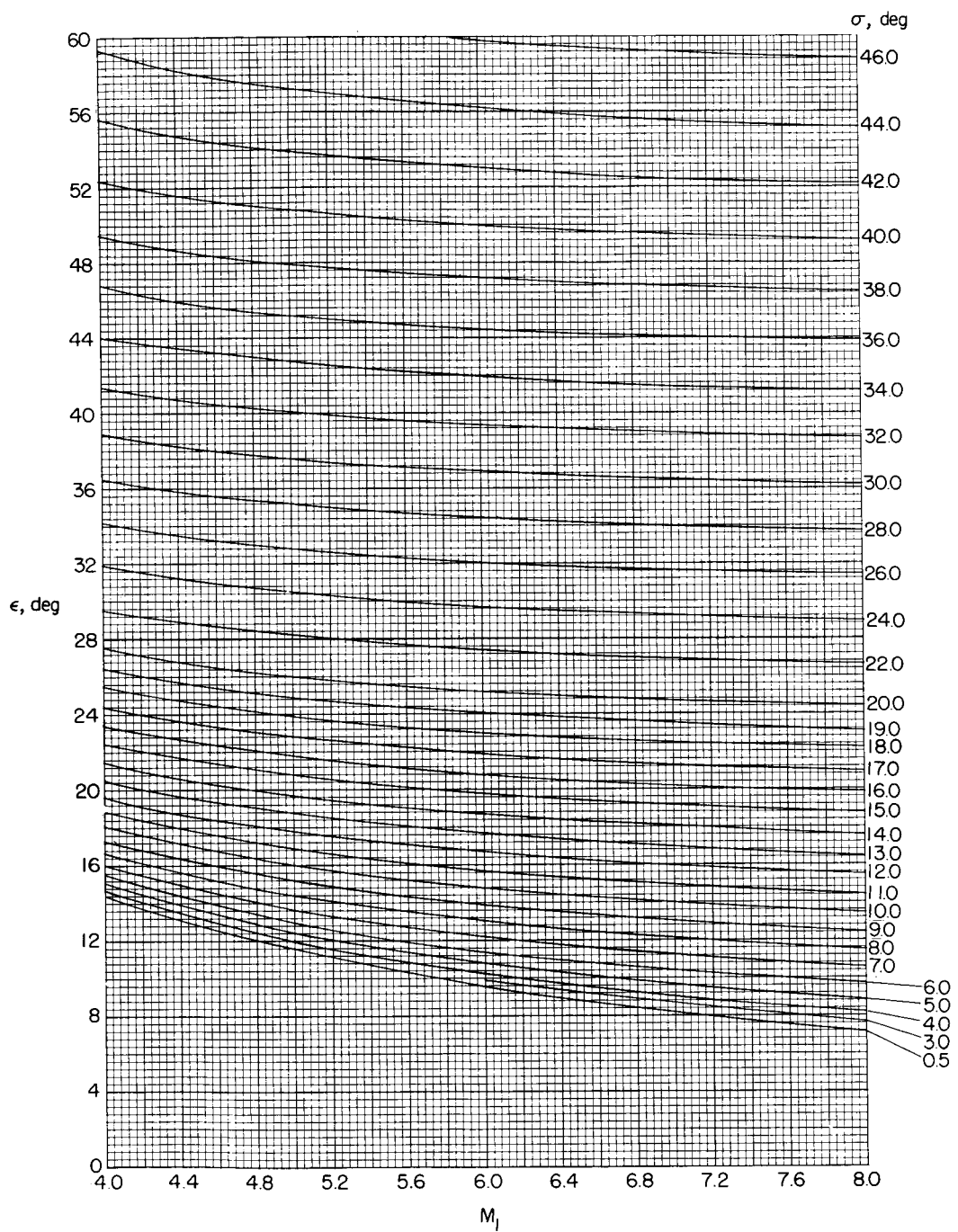


(c)  $M_1 = 1$  to 4;  $\epsilon = 52^\circ$  to  $90^\circ$ .

Figure 1.- Continued.

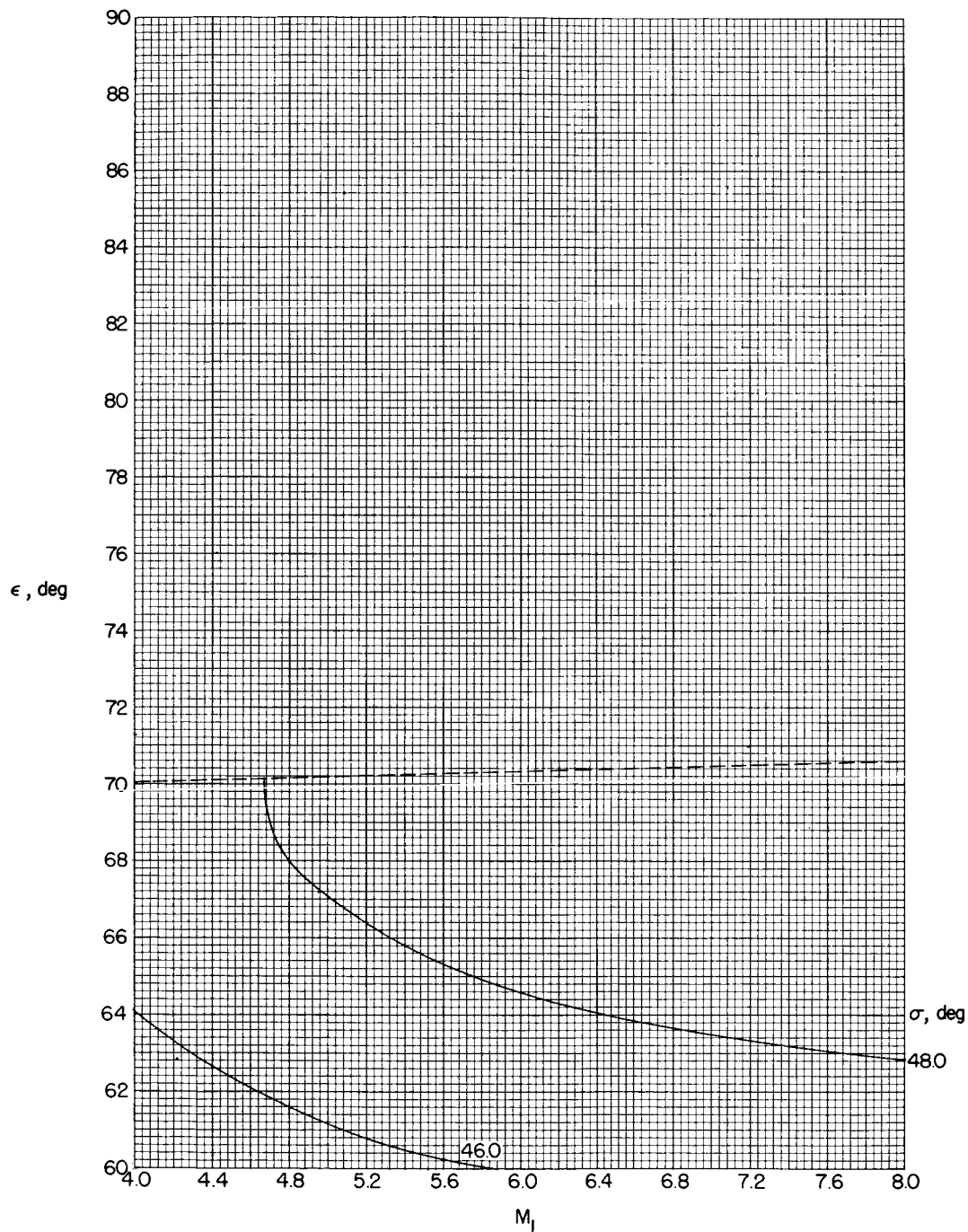


(d)  $M_1 = 4$  to 8;  $\epsilon = 1^\circ$  to  $10^\circ$ .



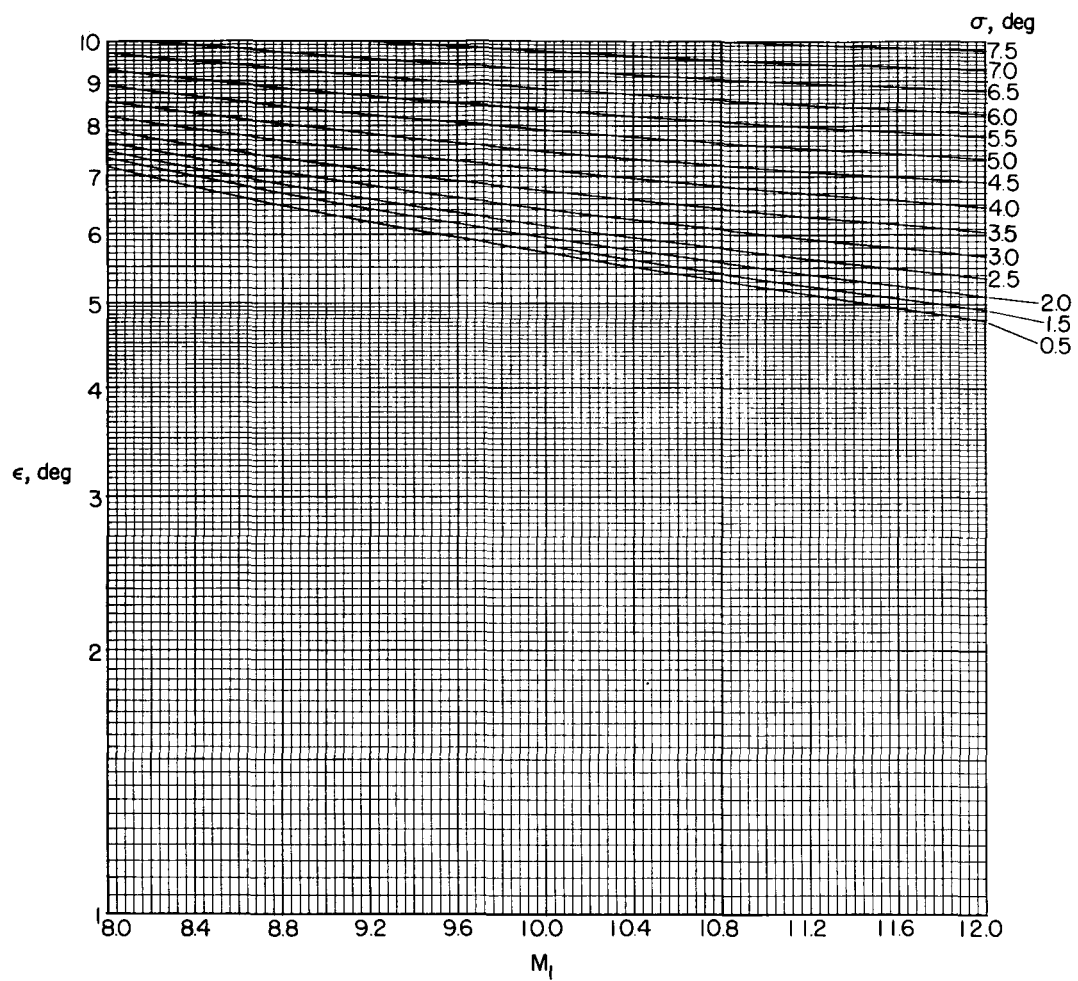
(e)  $M_1 = 4$  to 8;  $\epsilon = 0^\circ$  to  $60^\circ$ .

Figure 1.- Continued.



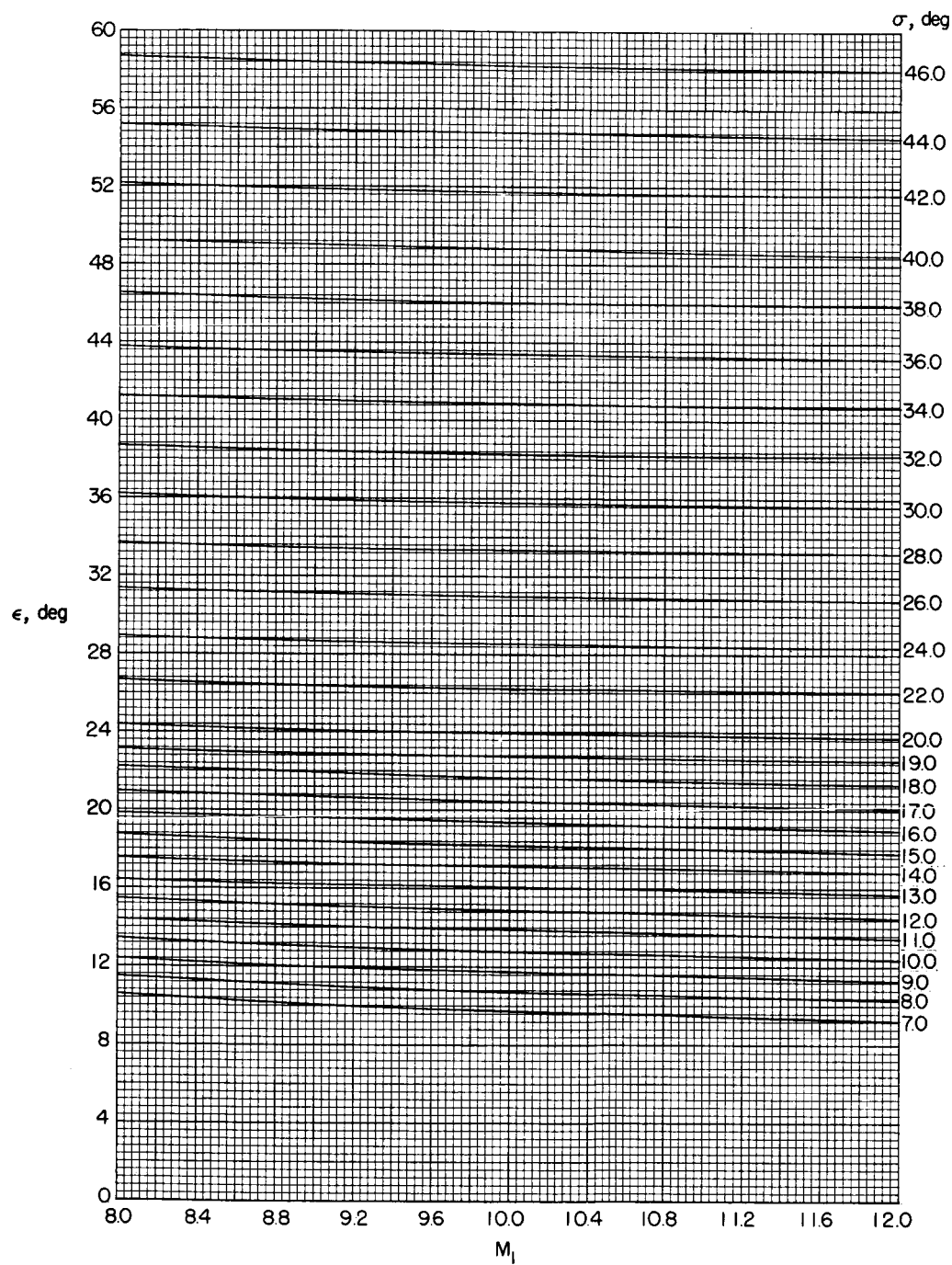
(f)  $M_l = 4$  to 8;  $\epsilon = 60^\circ$  to  $90^\circ$ .

Figure 1.- Continued.



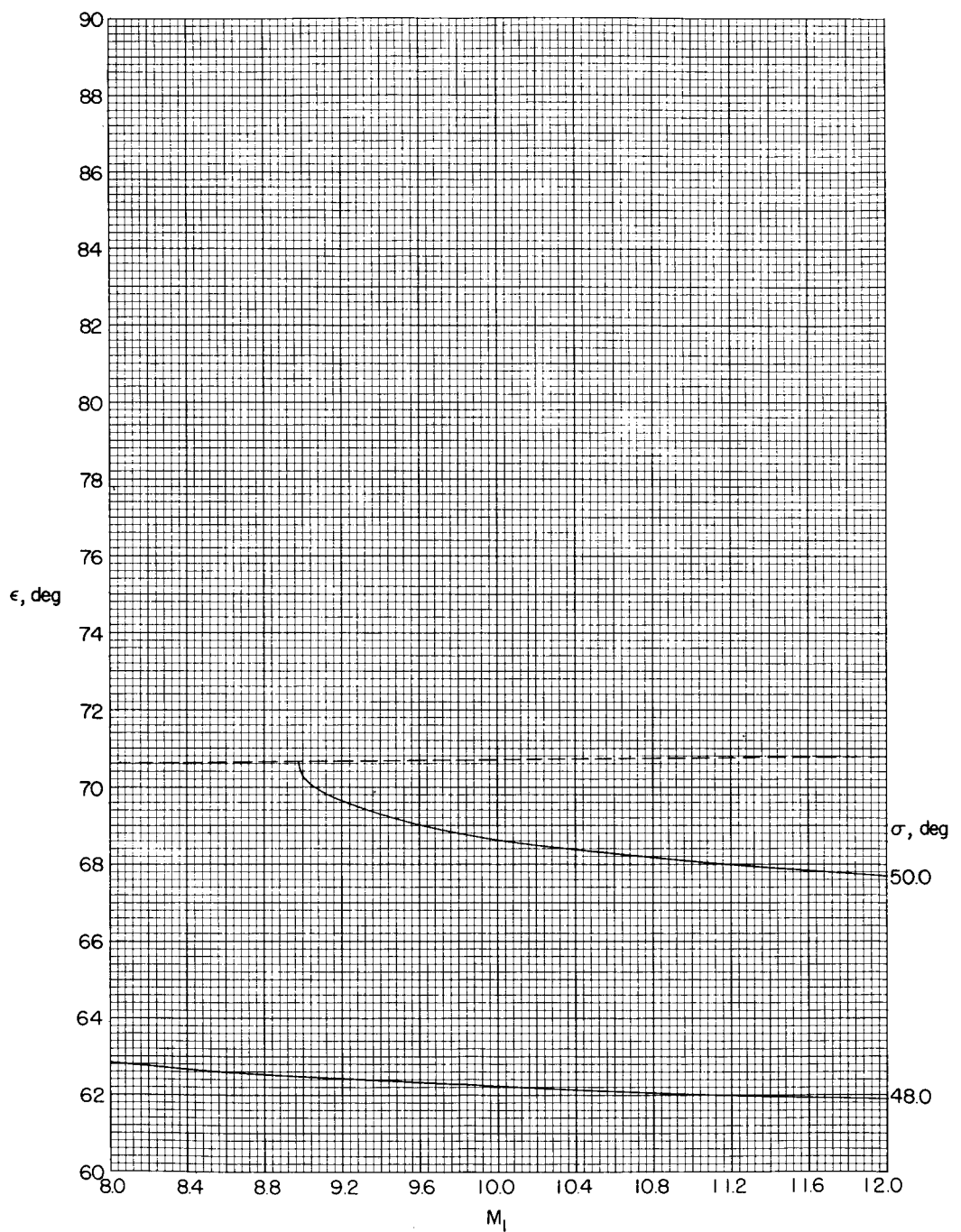
(g)  $M_l = 8$  to  $12$ ;  $\epsilon = 1^\circ$  to  $10^\circ$ .

Figure 1.- Continued.



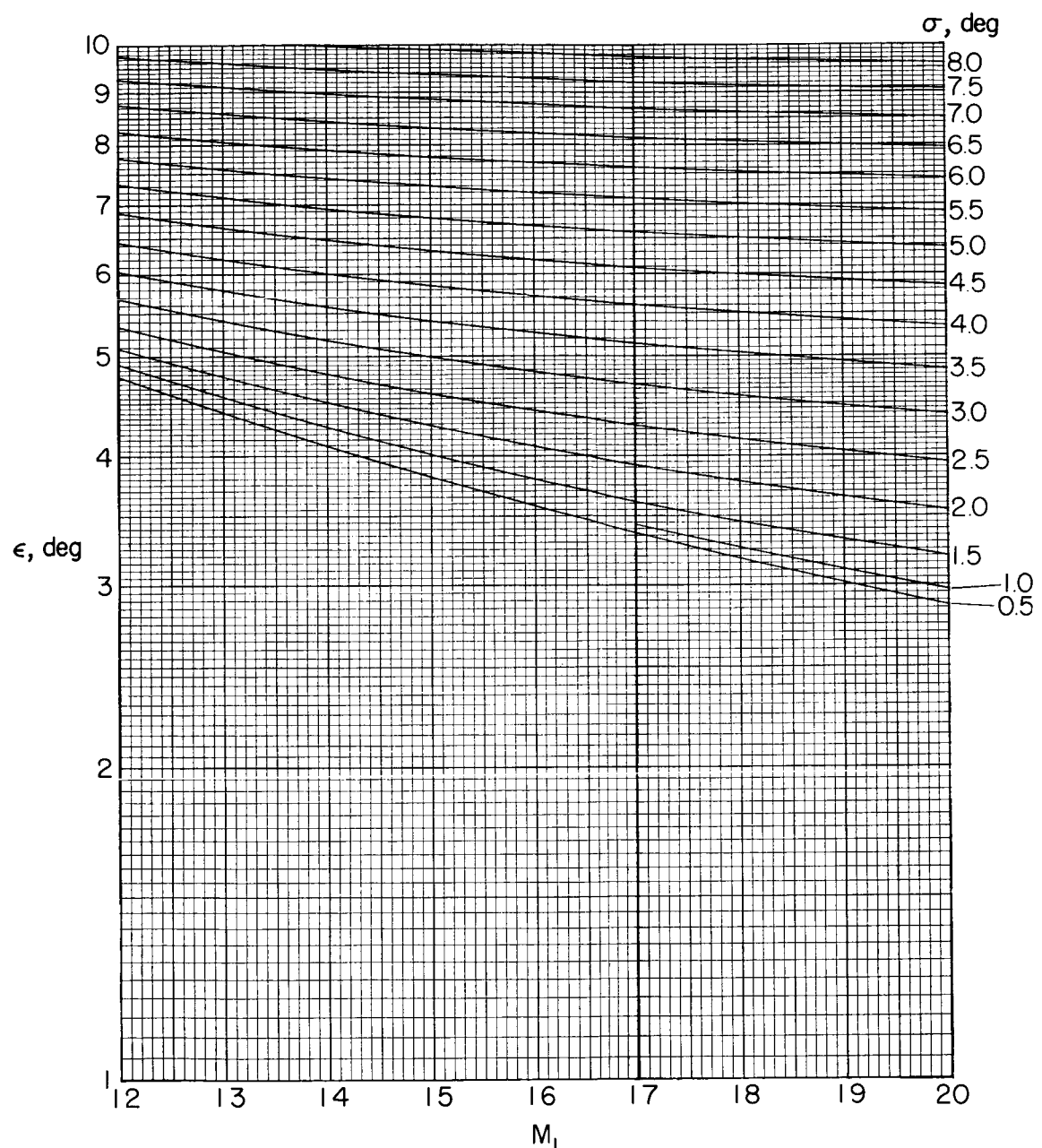
(h)  $M_1 = 8$  to  $12$ ;  $\epsilon = 0^\circ$  to  $60^\circ$ .

Figure 1.- Continued.



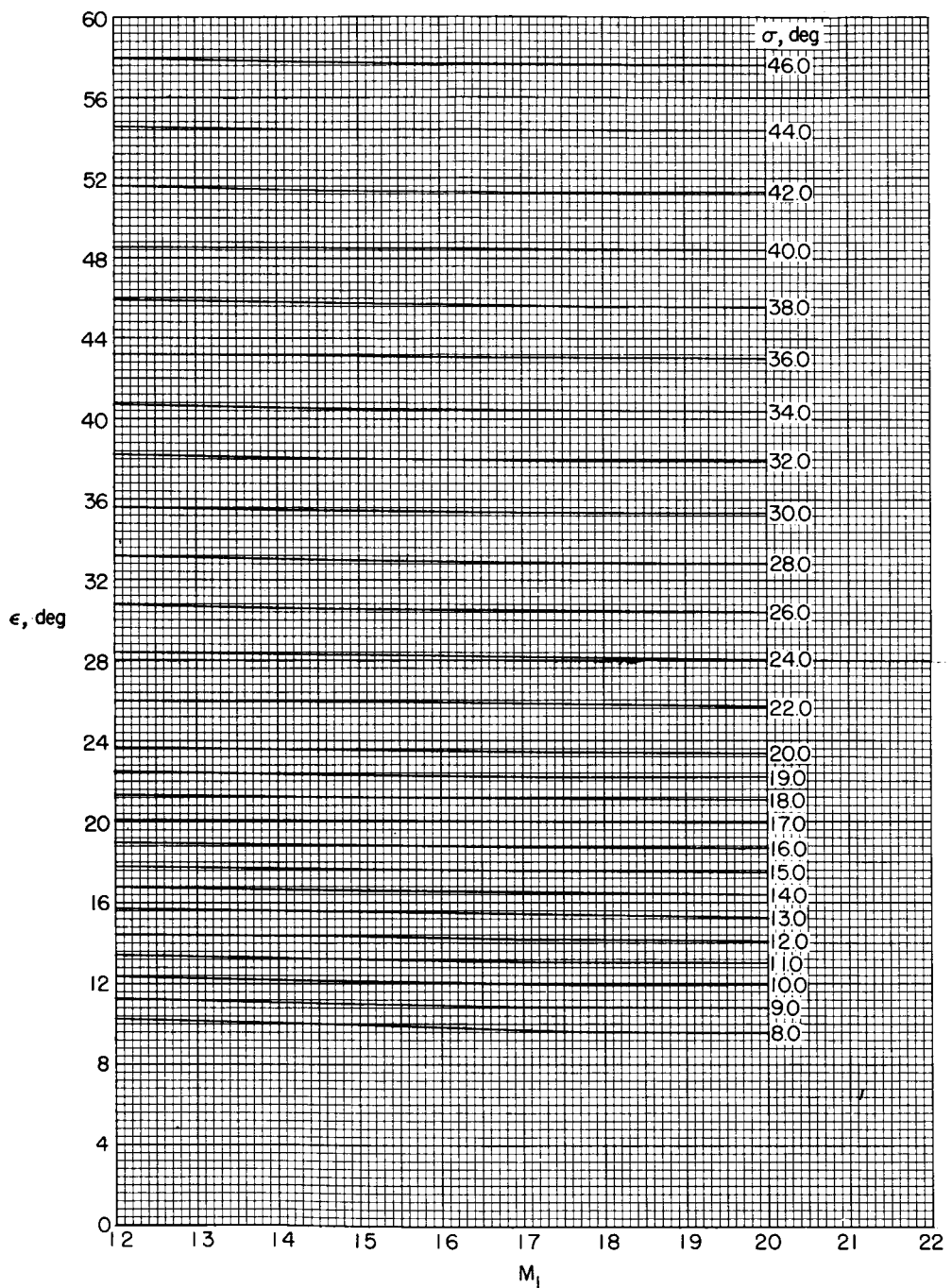
(i)  $M_1 = 8$  to  $12$ ;  $\epsilon = 60^\circ$  to  $90^\circ$ .

Figure 1.- Continued.



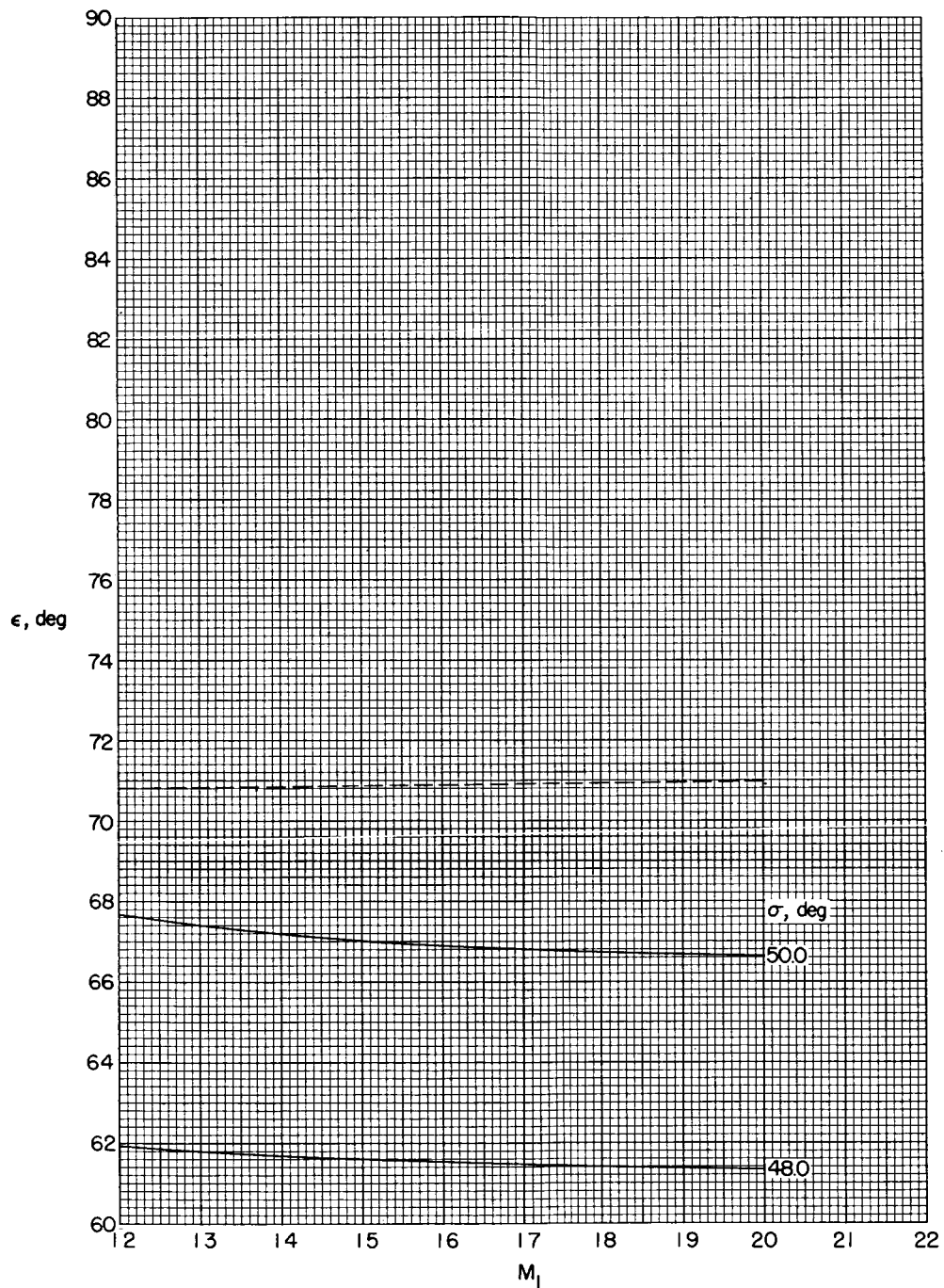
(j)  $M_I = 12$  to  $20$ ;  $\epsilon = 1^\circ$  to  $10^\circ$ .

Figure 1.- Continued.



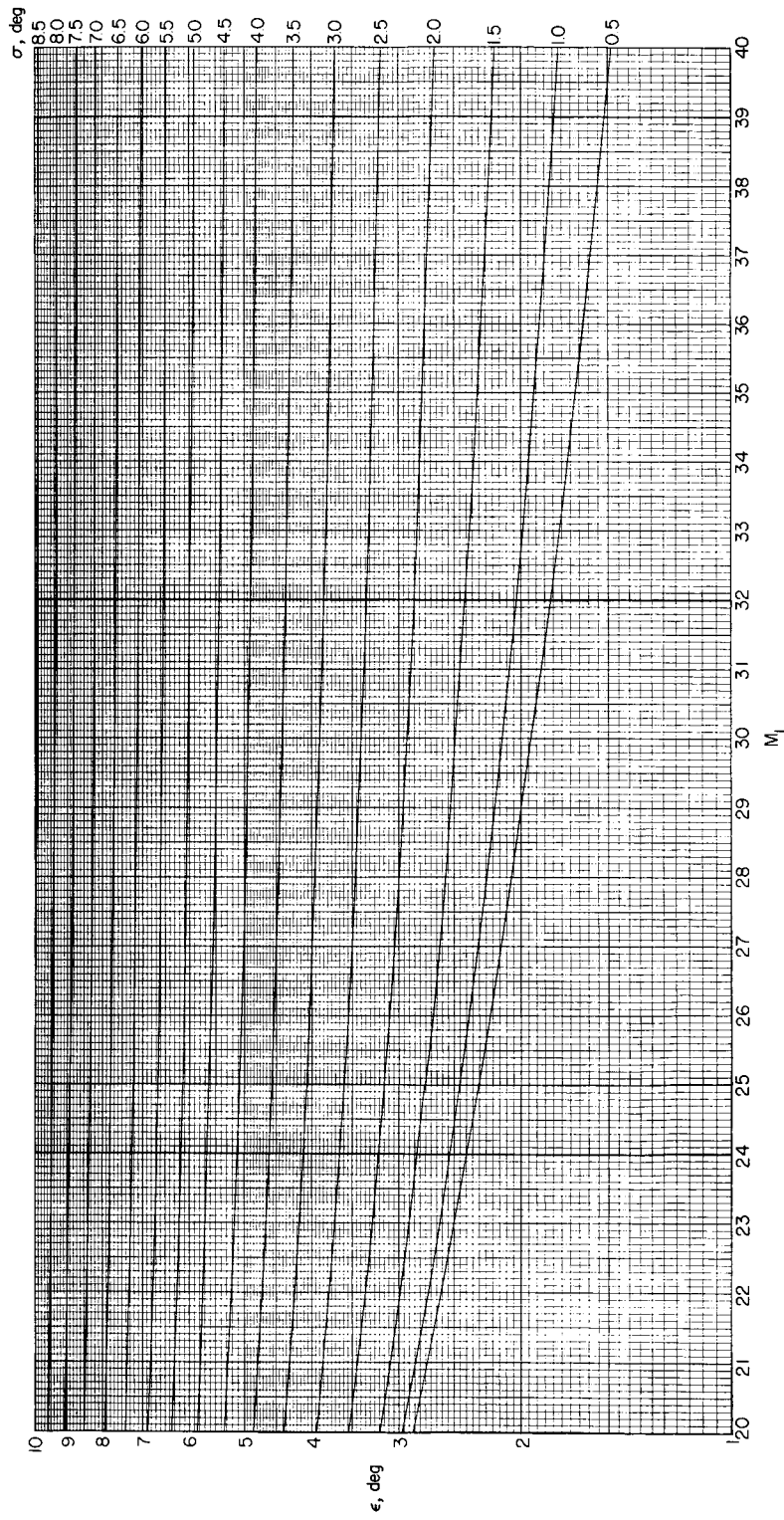
(k)  $M_1 = 12$  to  $20$ ;  $\epsilon = 0^\circ$  to  $60^\circ$ .

Figure 1.- Continued.



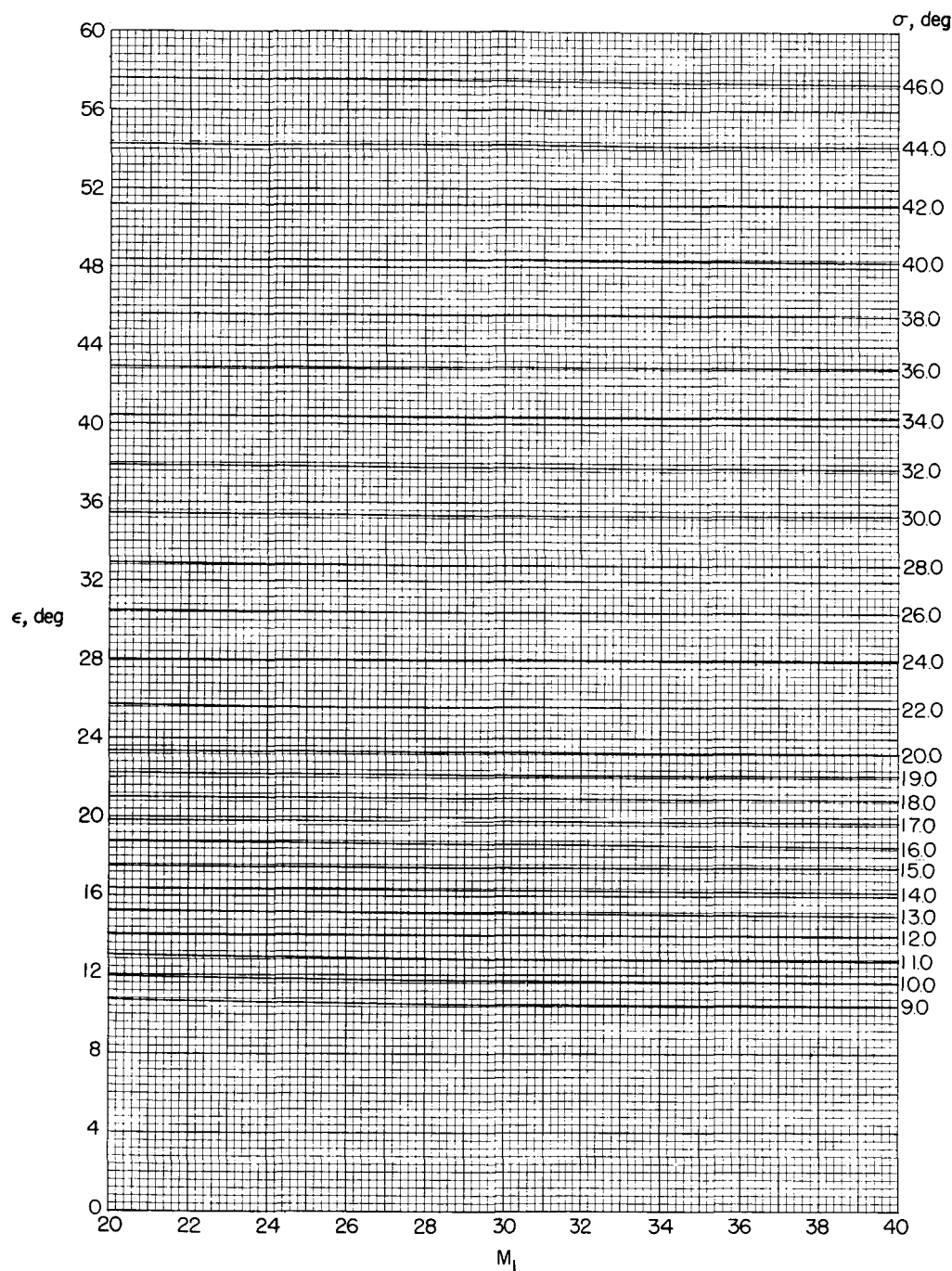
(i)  $M_1 = 12$  to  $20$ ;  $\epsilon = 60^\circ$  to  $90^\circ$ .

Figure 1.- Continued.



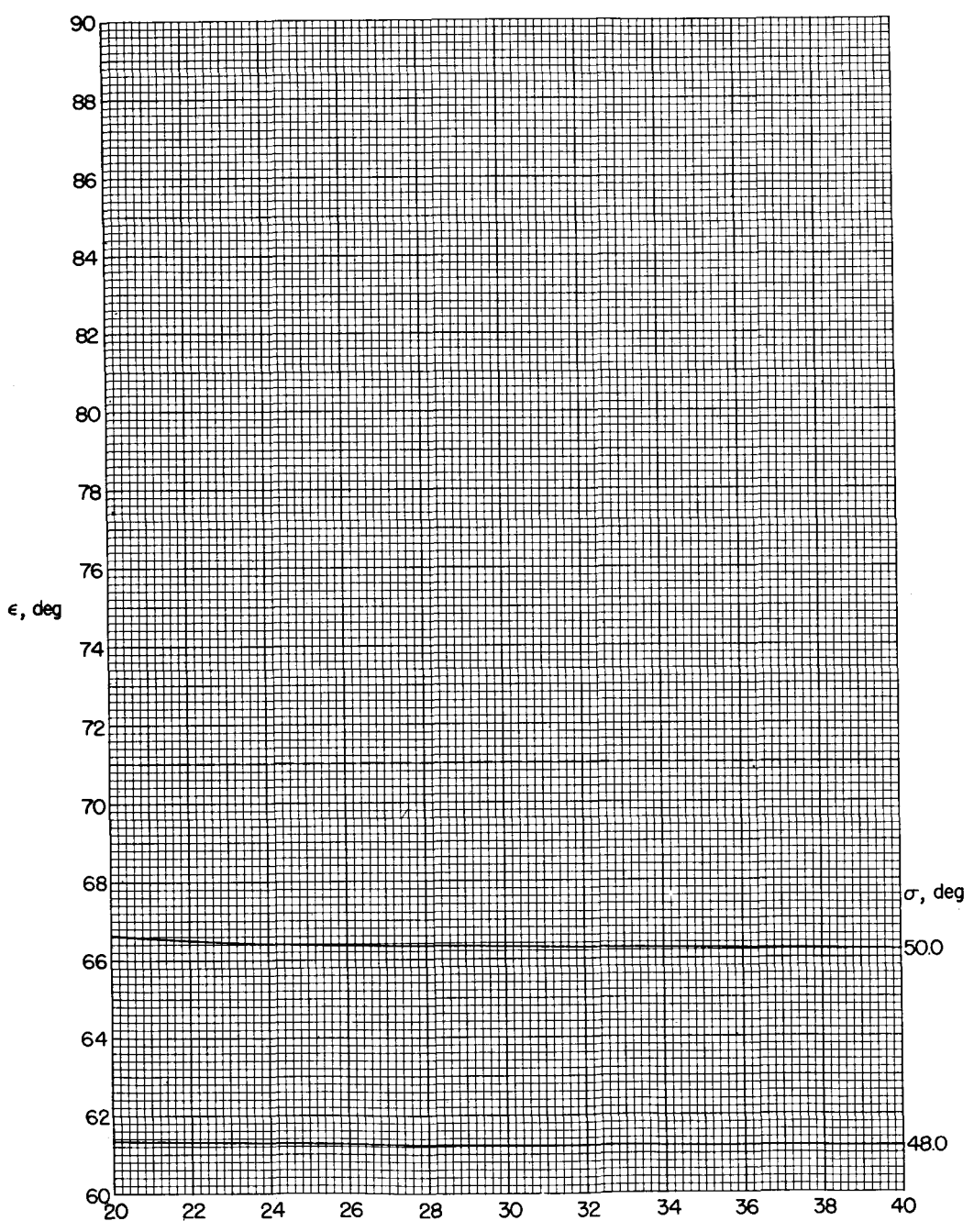
(m)  $M_1 = 20$  to  $40$ ;  $\epsilon = 1^\circ$  to  $10^\circ$ .

Figure 1.- Continued.



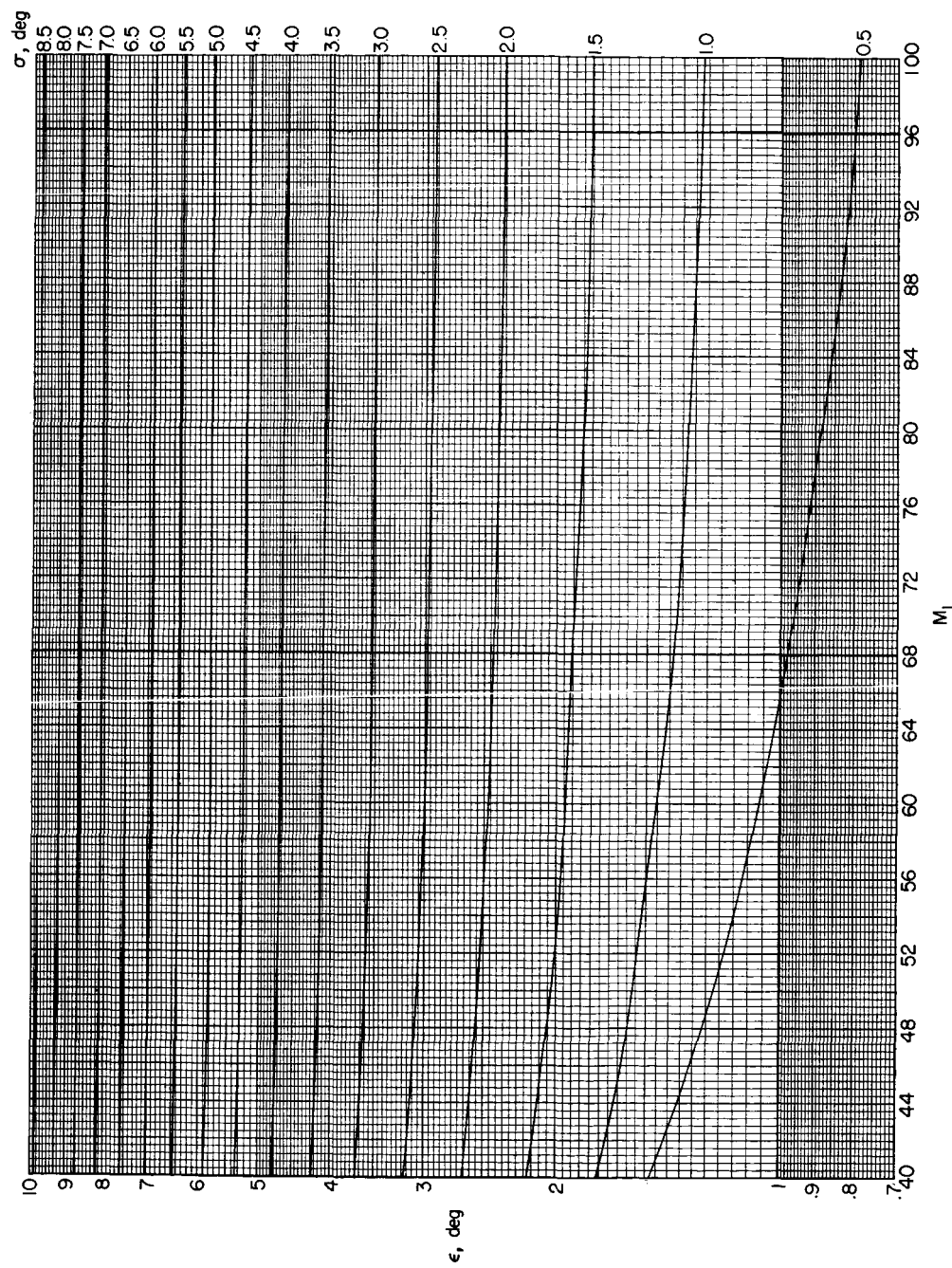
(n)  $M_1 = 20$  to  $40$ ;  $\epsilon = 0^\circ$  to  $60^\circ$ .

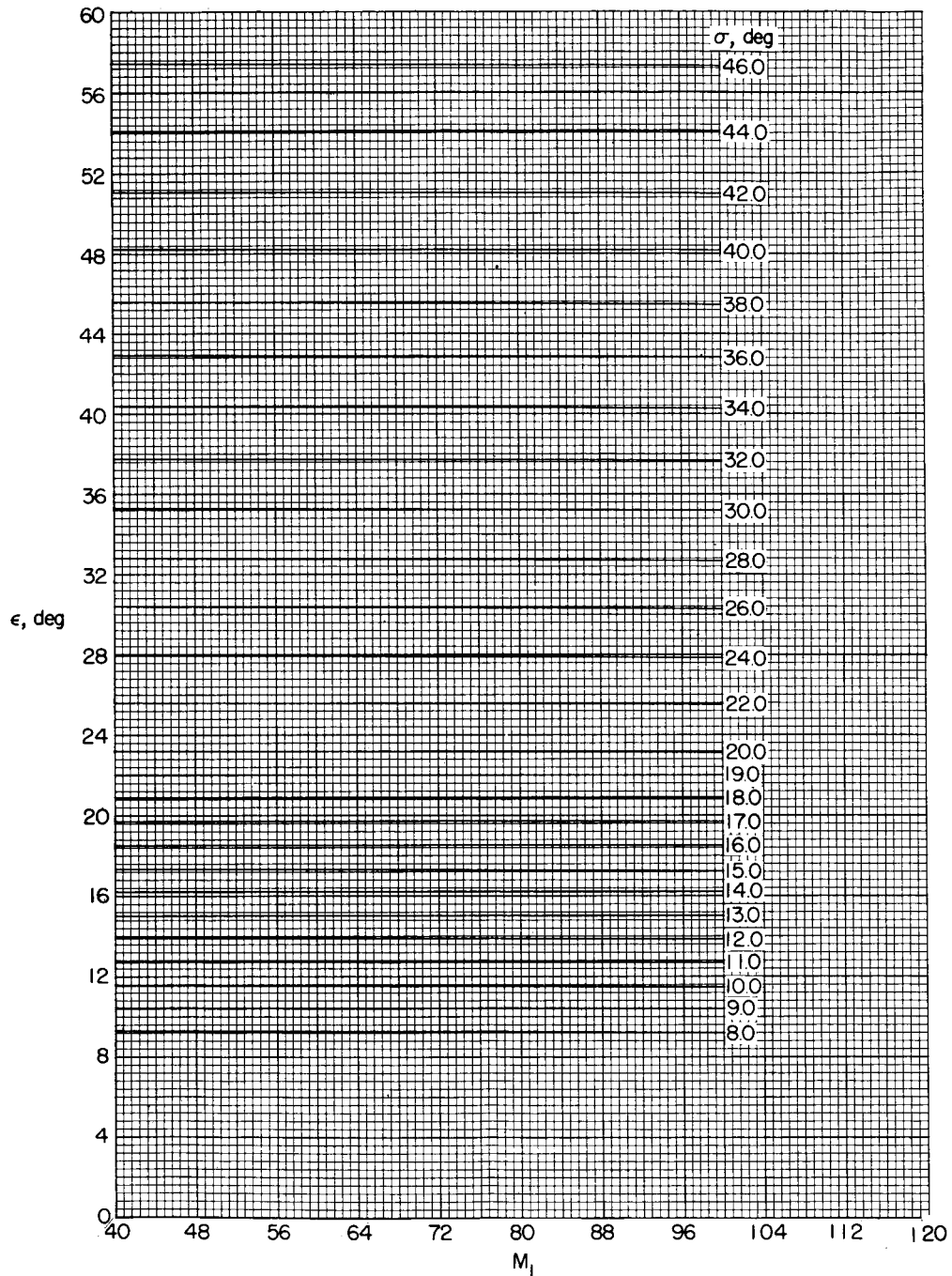
Figure 1.- Continued.



(o)  $M_1 = 20$  to  $40$ ;  $\epsilon = 60^\circ$  to  $90^\circ$ .

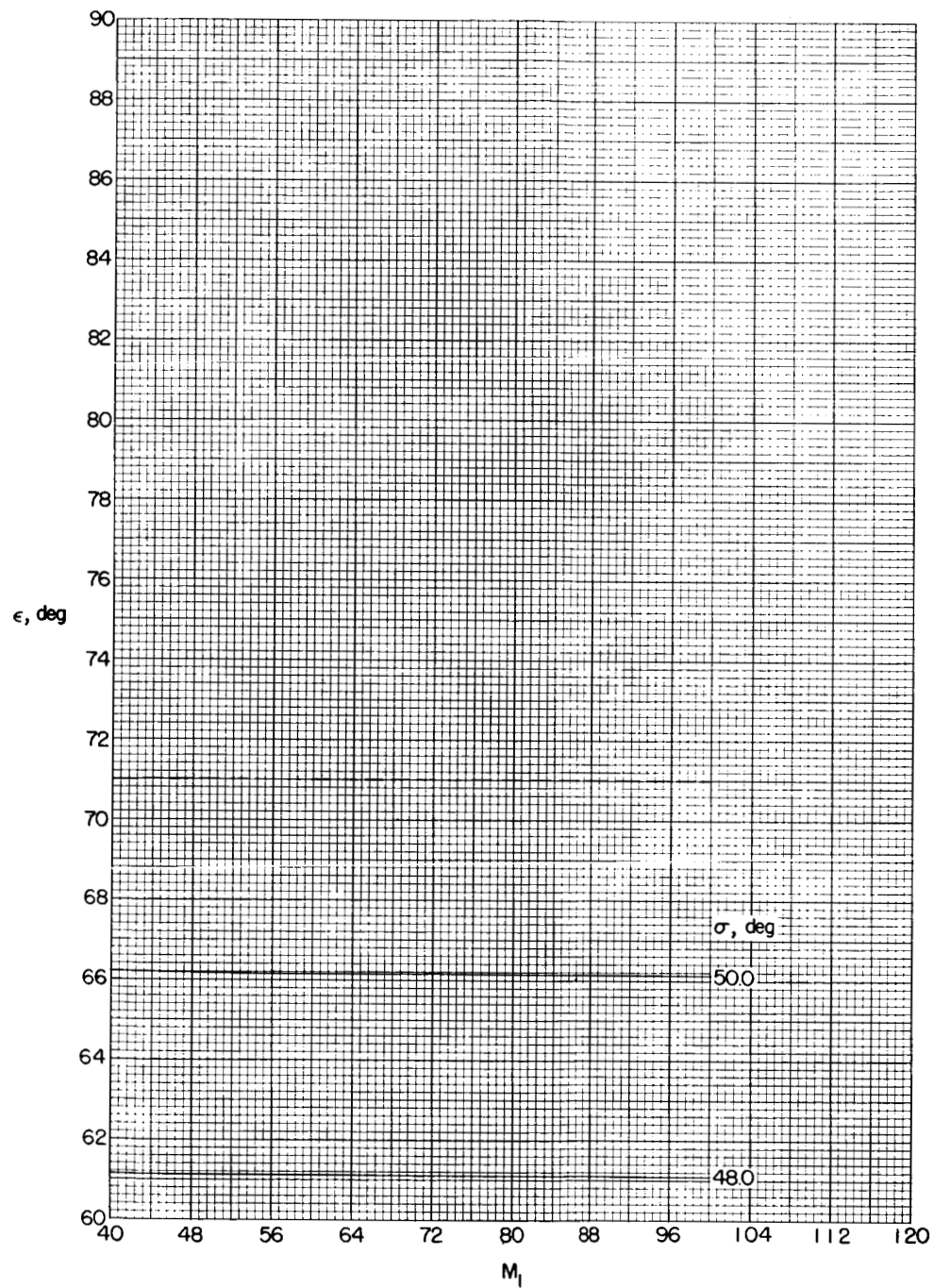
Figure 1.- Continued.





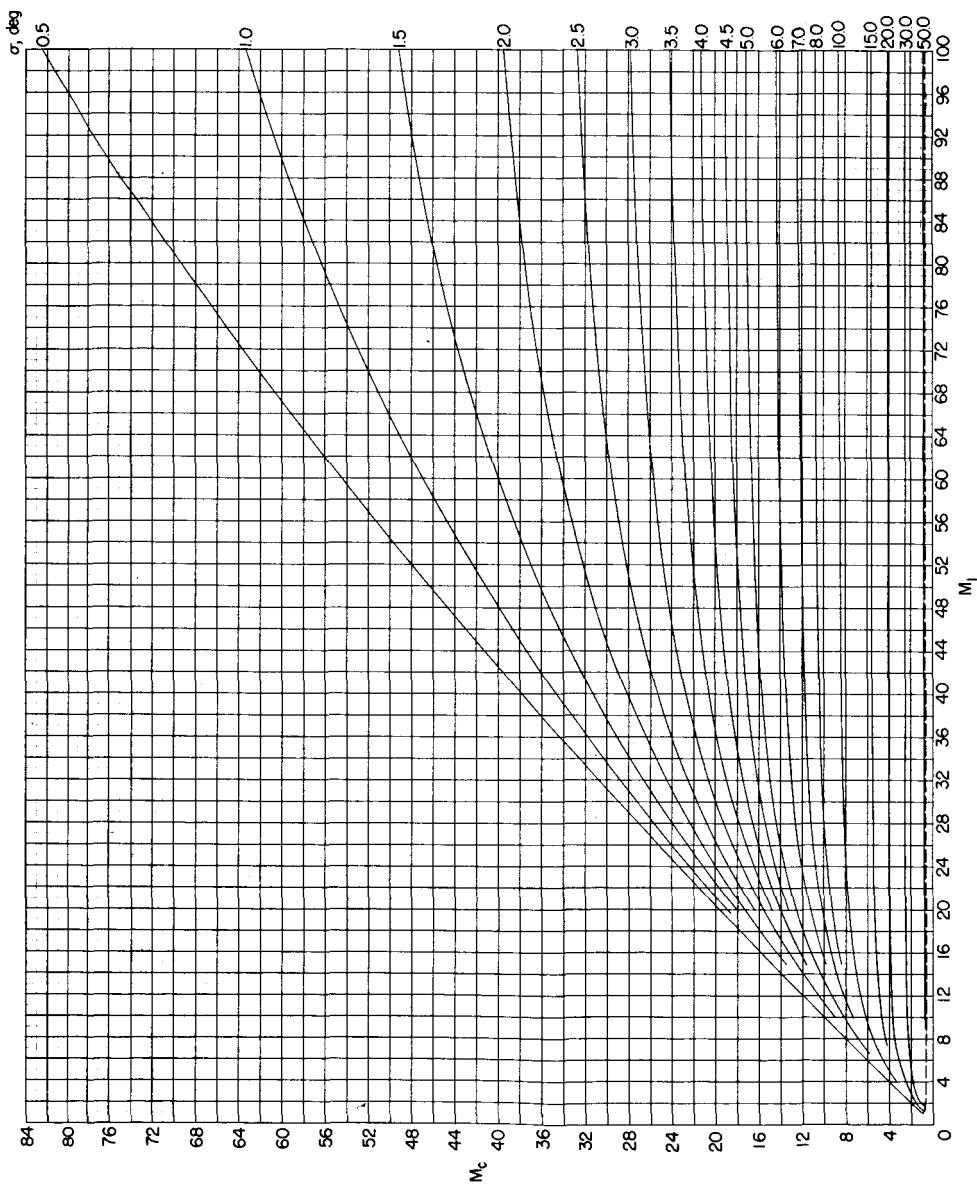
(q)  $M_{\perp} = 40$  to  $100$ ;  $\epsilon = 0^\circ$  to  $60^\circ$ .

Figure 1.- Continued.



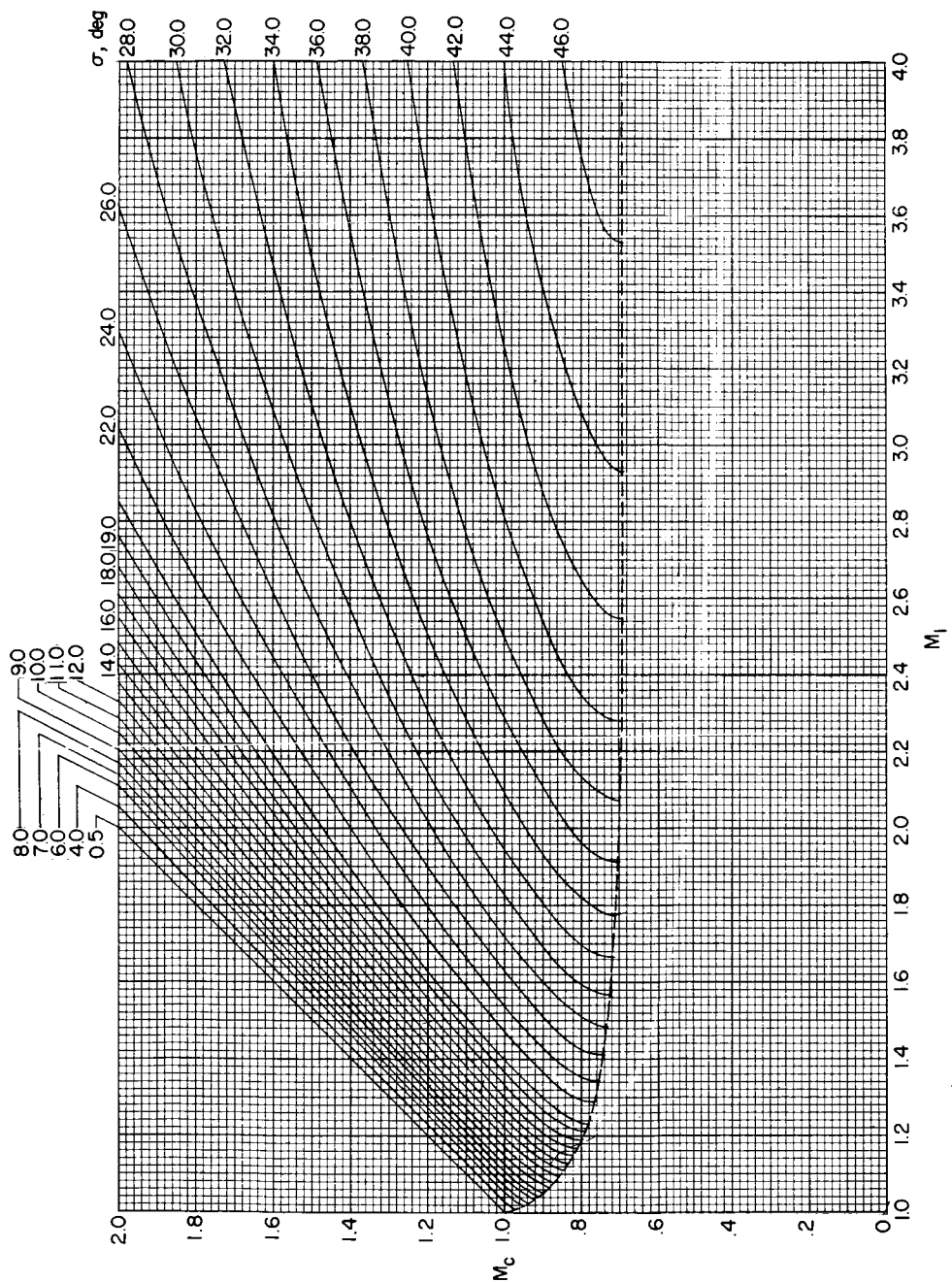
(r)  $M_1 = 40$  to  $100$ ;  $\epsilon = 60^\circ$  to  $90^\circ$ .

Figure 1.- Concluded.



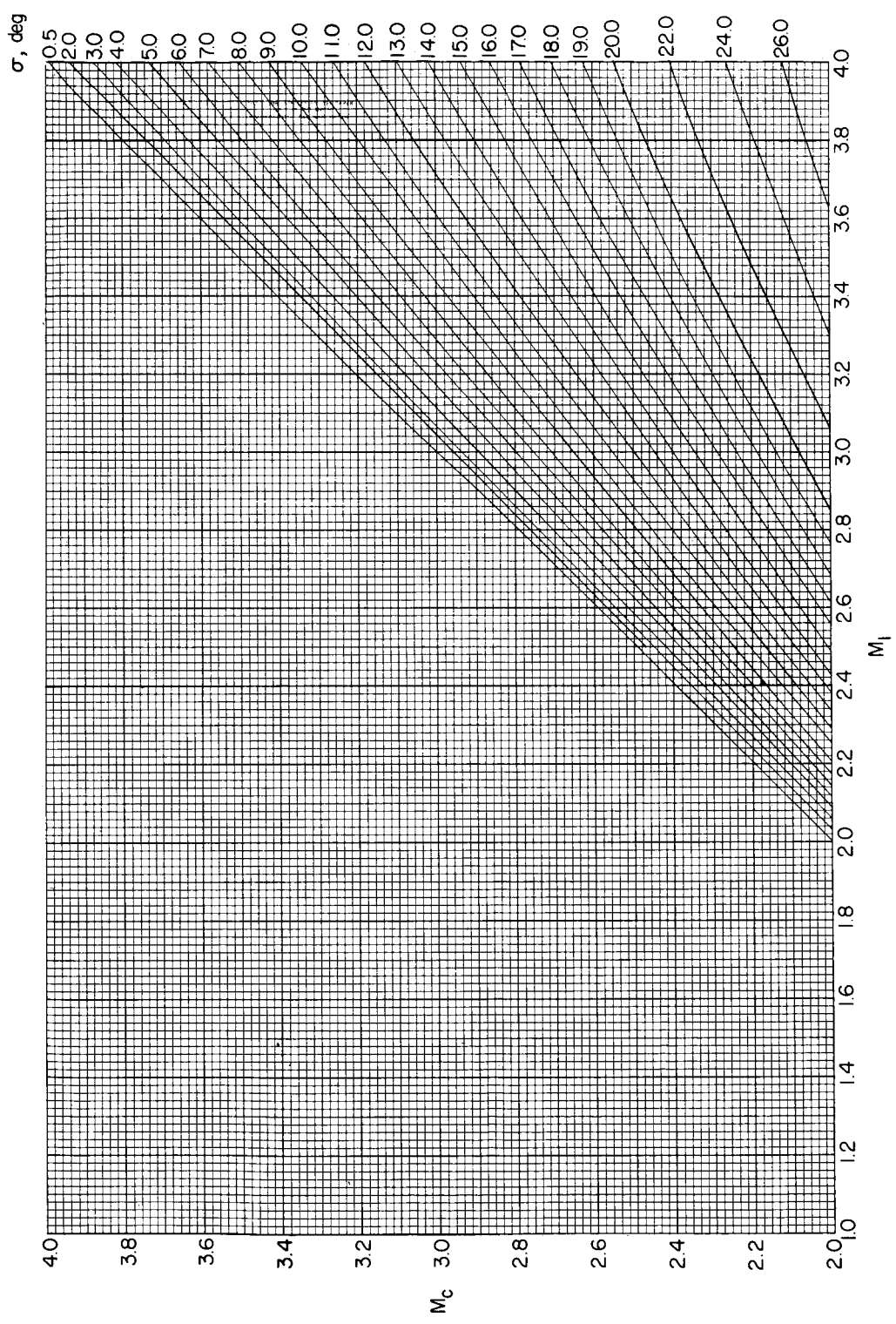
(a)  $M_1 = 1$  to 100;  $M_c = 0$  to 84.

Figure 2.- Variation of cone surface Mach number with free-stream Mach number for various cone angles. (Dashed line denotes limit of weak shock solution.)



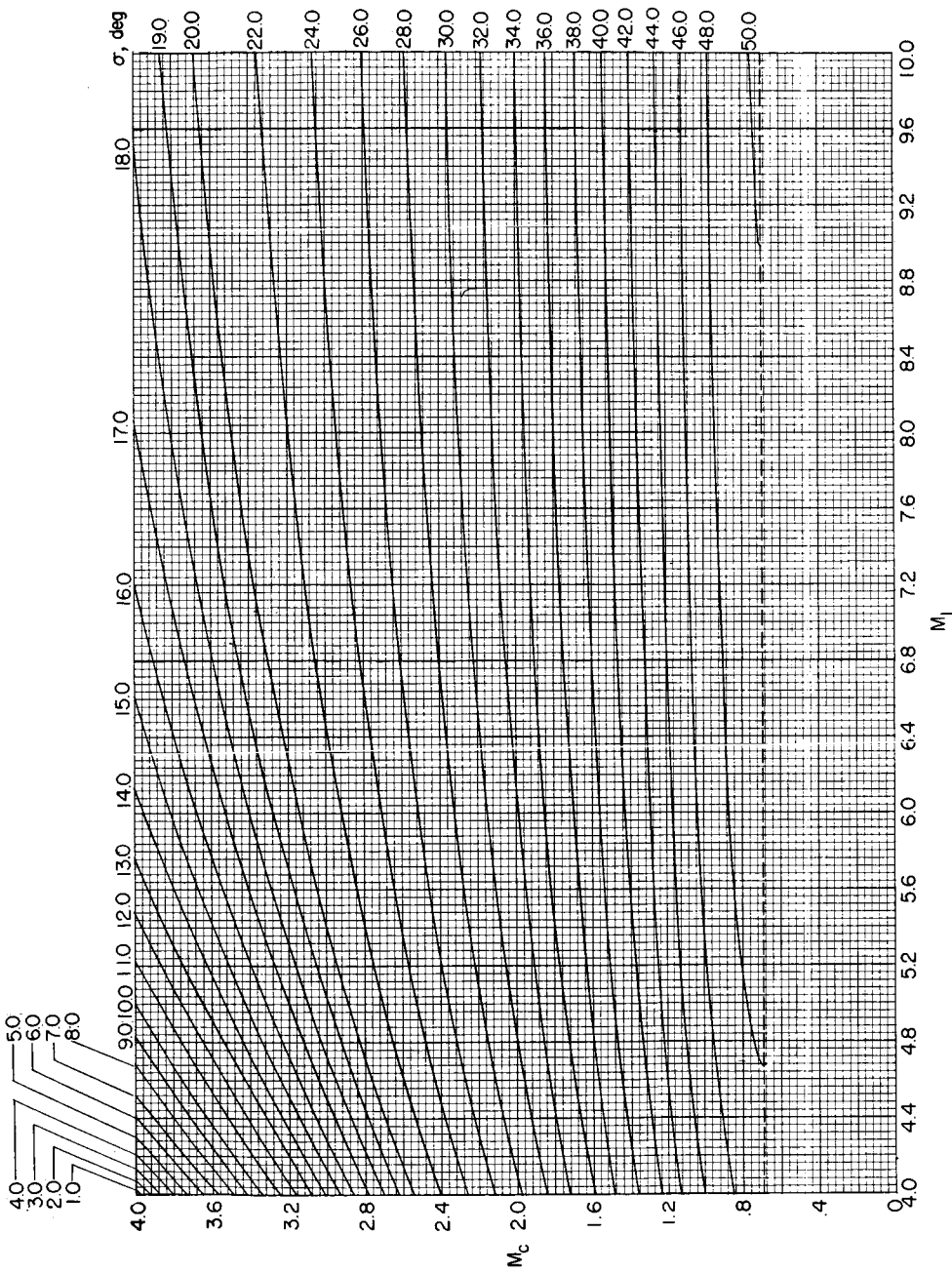
(b)  $M_1 = 1 \text{ to } 4; M_c = 0 \text{ to } 2.$

Figure 2.- Continued.



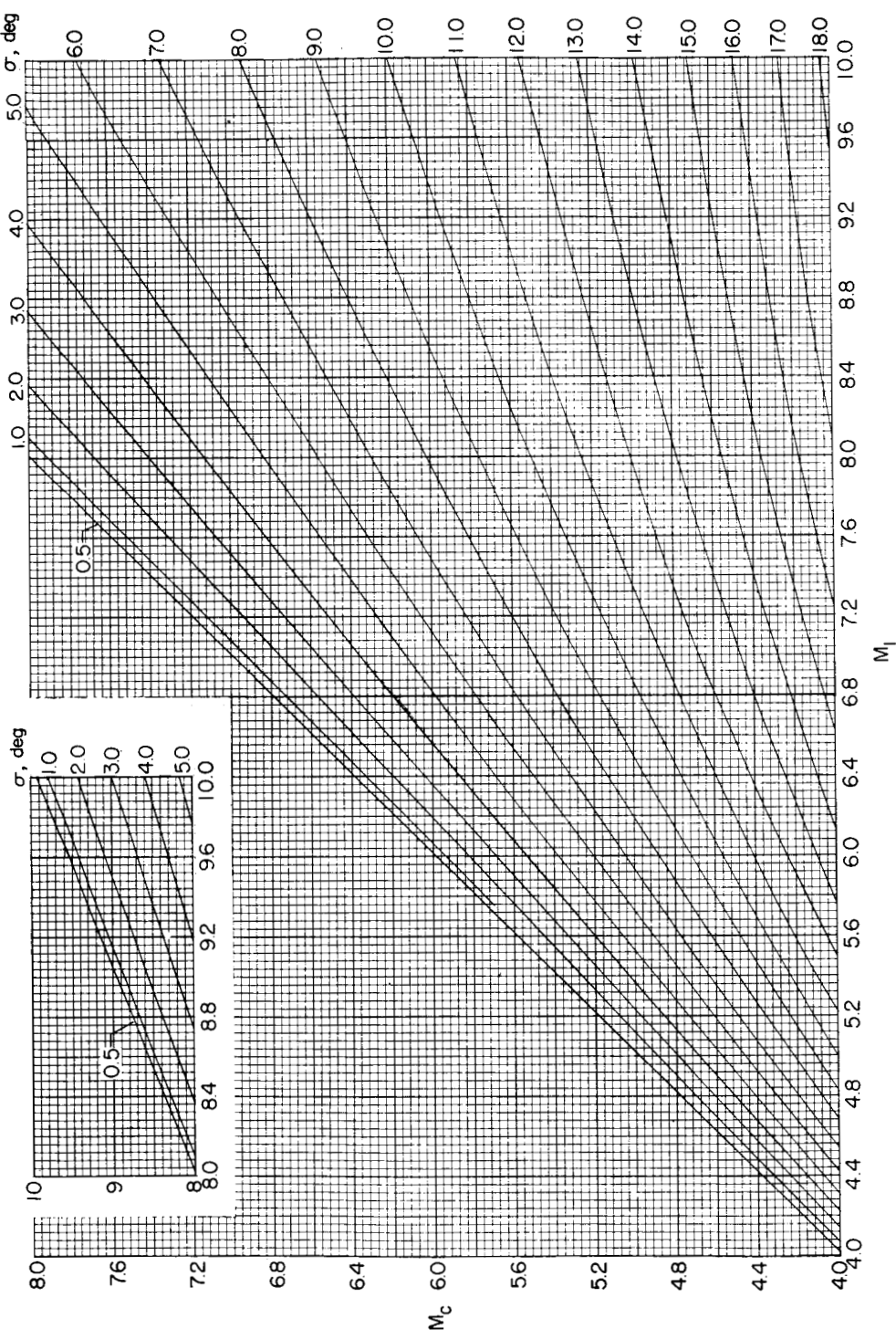
(c)  $M_L = 1$  to 4;  $M_c = 2$  to 4.

Figure 2.- Continued.



(d)  $M_{l\perp} = 4$  to 10;  $M_c = 0$  to 4.

Figure 2.- Continued.



(e)  $M_{U_1} = 4$  to 10;  $M_C = 4$  to 10.

Figure 2.- Continued.

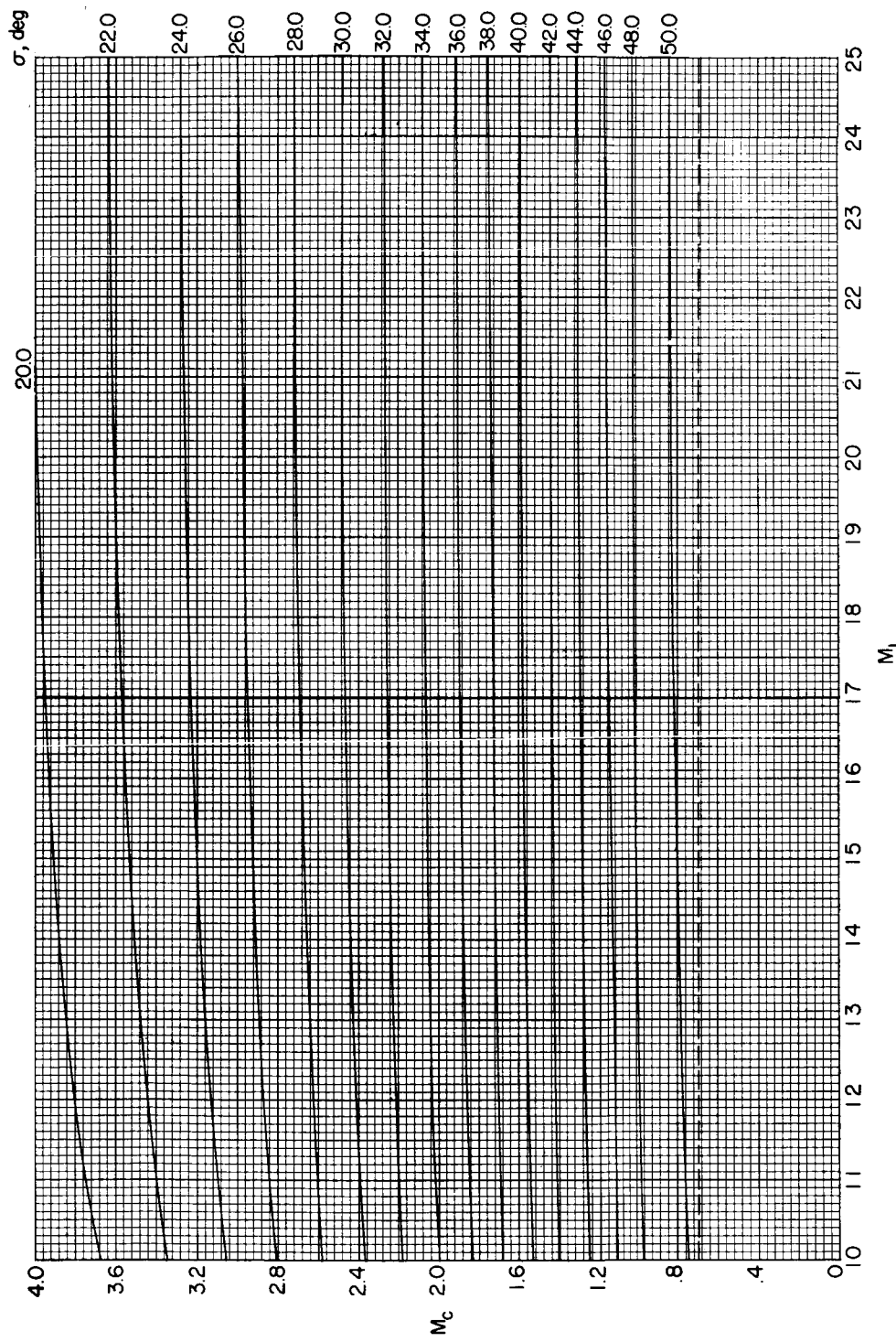
(f)  $M_1 = 10 \text{ to } 25; M_c = 0 \text{ to } 4.$ 

Figure 2.- Continued.

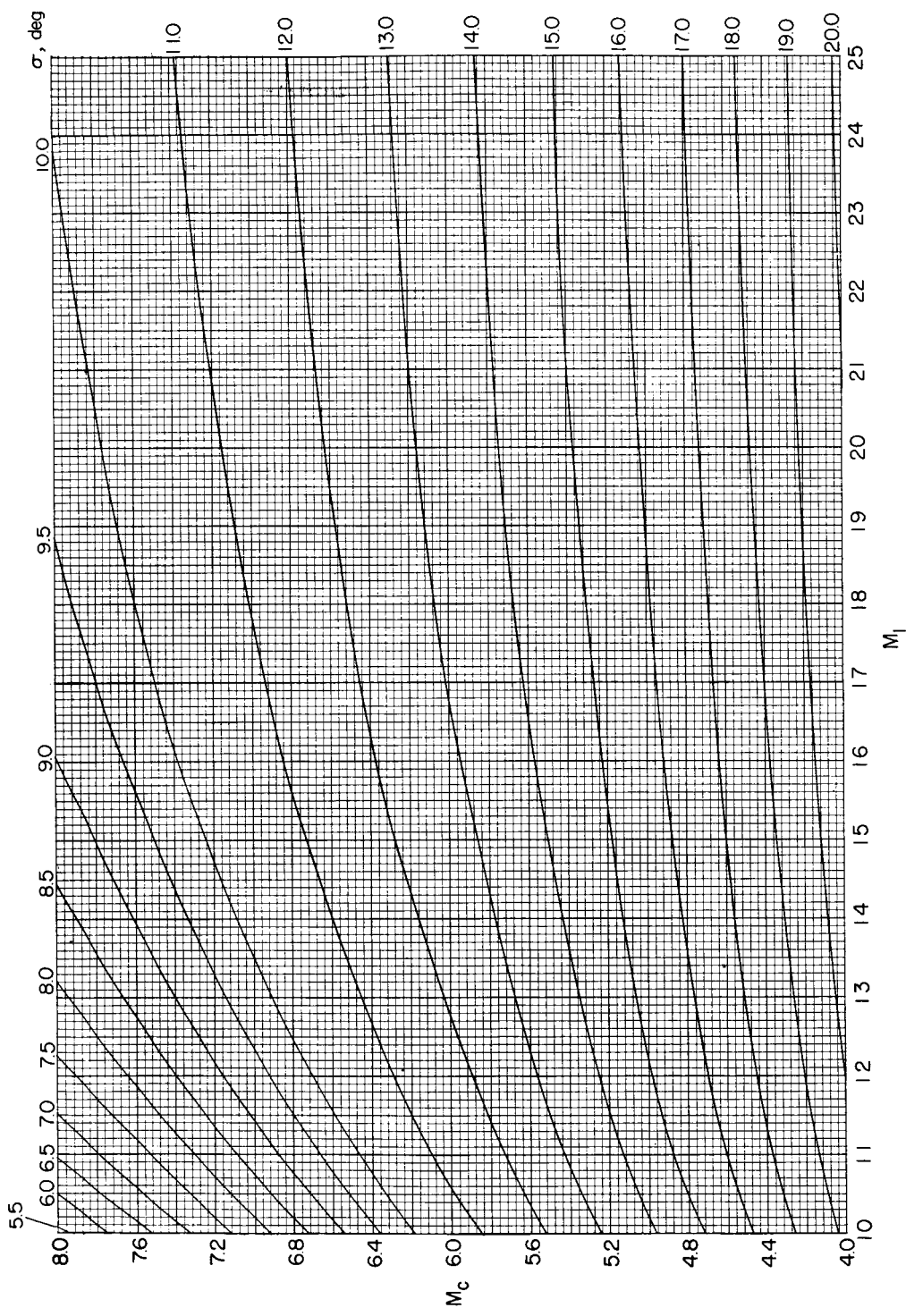
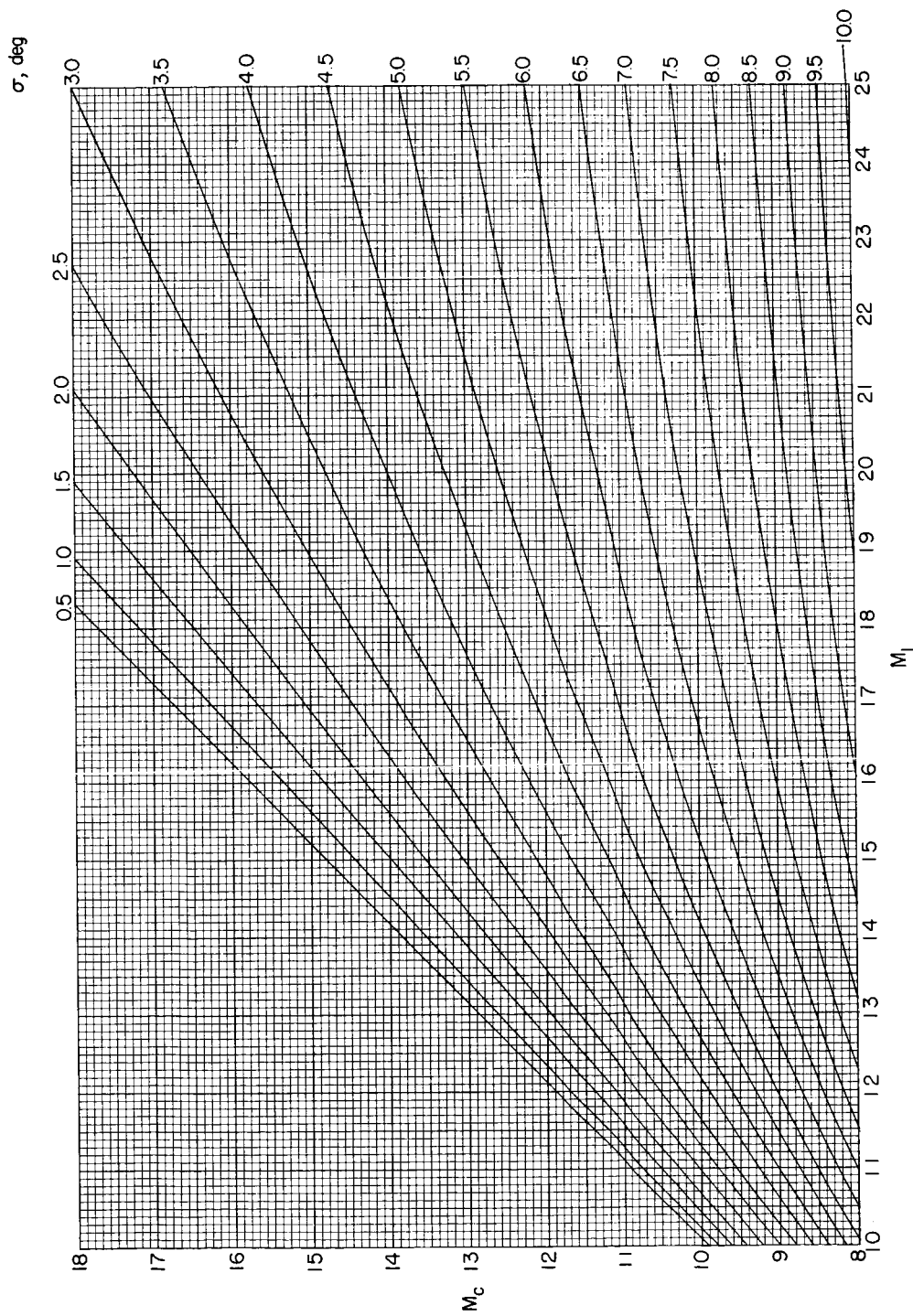
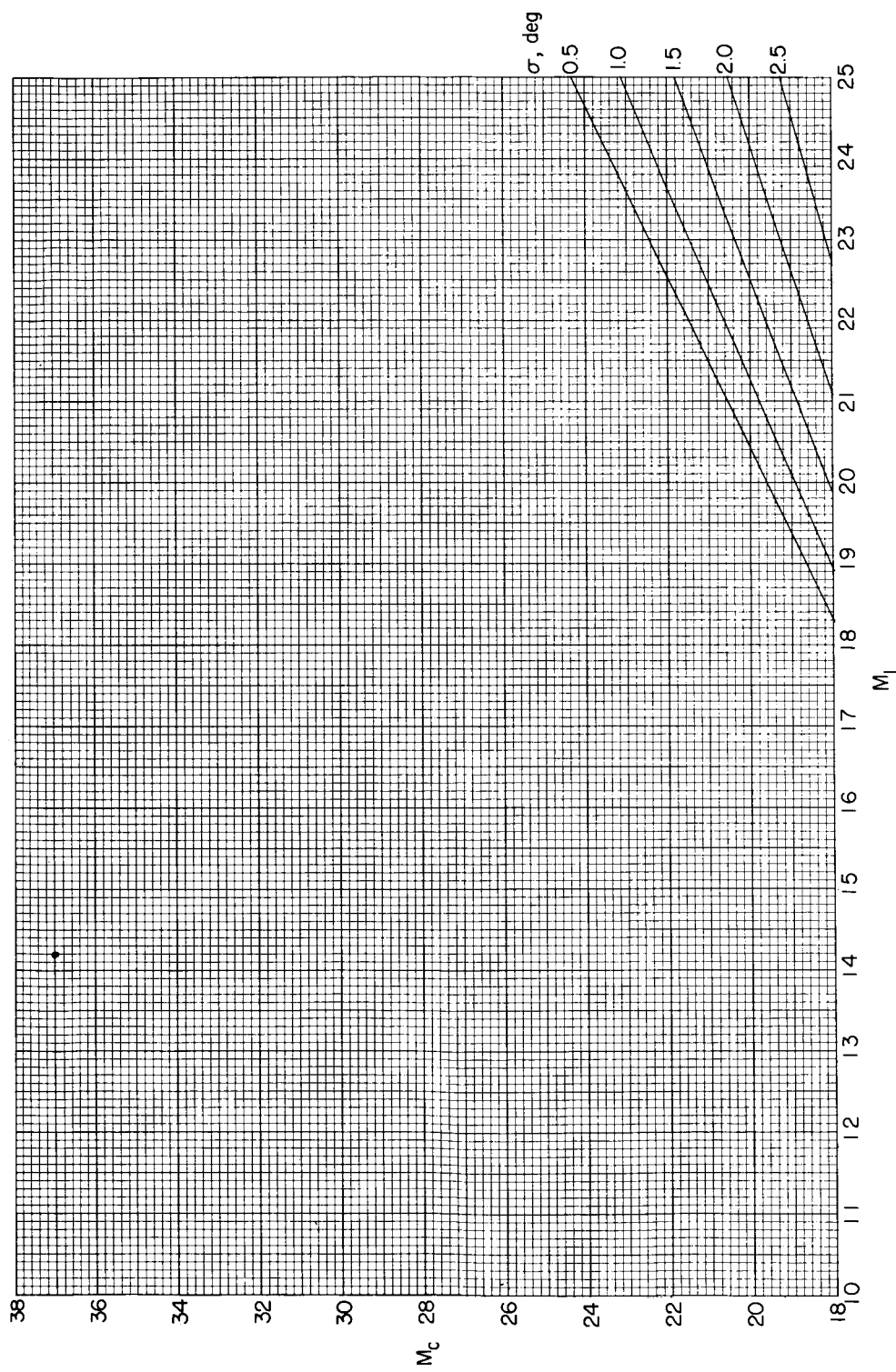
(g)  $M_L = 10$  to  $25$ ;  $M_C = 4$  to  $8$ .

Figure 2.- Continued.



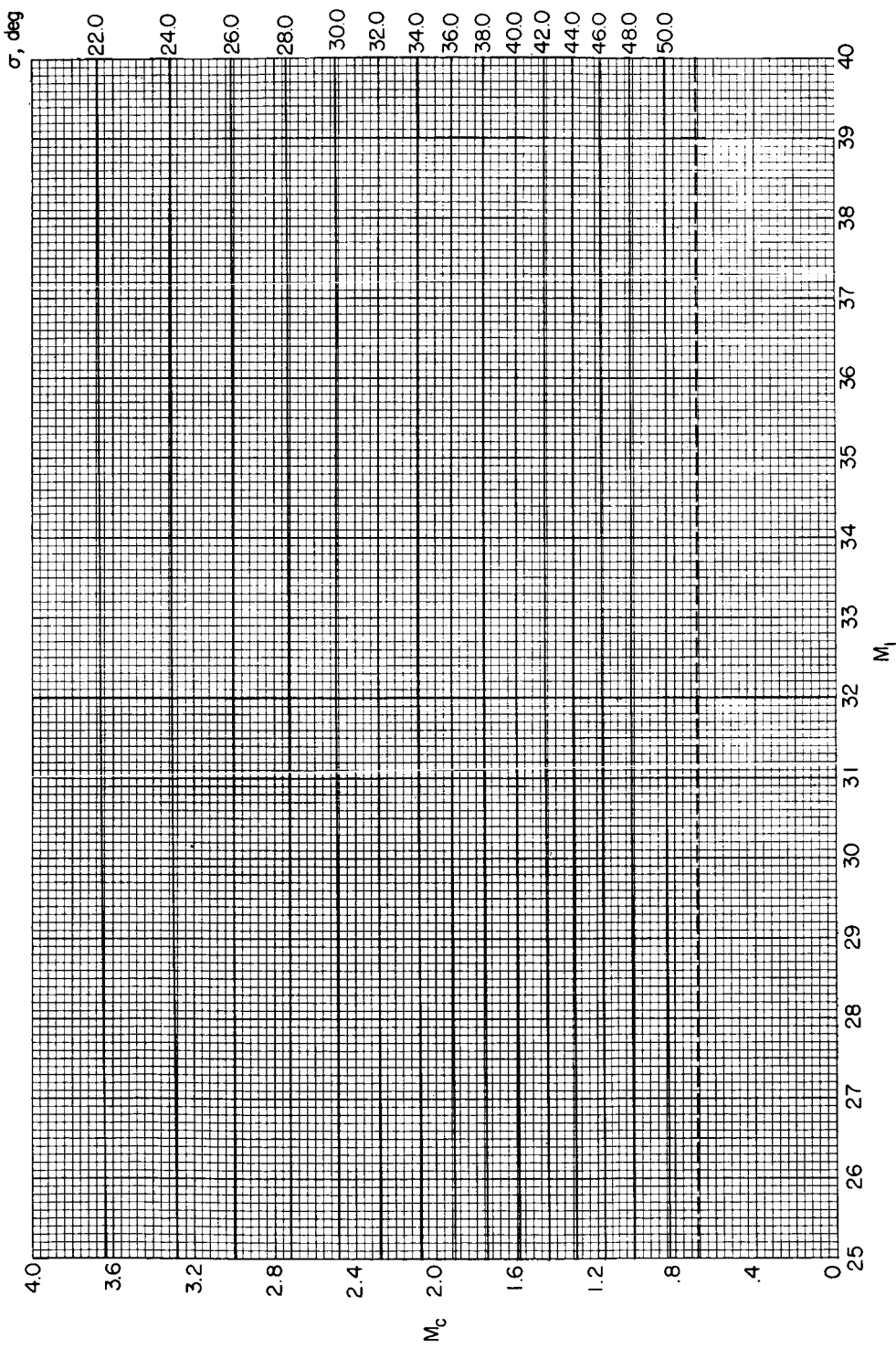
(h)  $M_{l\perp} = 10$  to 25;  $M_c = 8$  to 18.

Figure 2.- Continued.



(i)  $M_1 = 10$  to  $25$ ;  $M_c = 18$  to  $38$ .

Figure 2.- Continued.



(j)  $M_{\perp} = 25$  to 40;  $M_c = 0$  to 4.

Figure 2.- Continued.

40

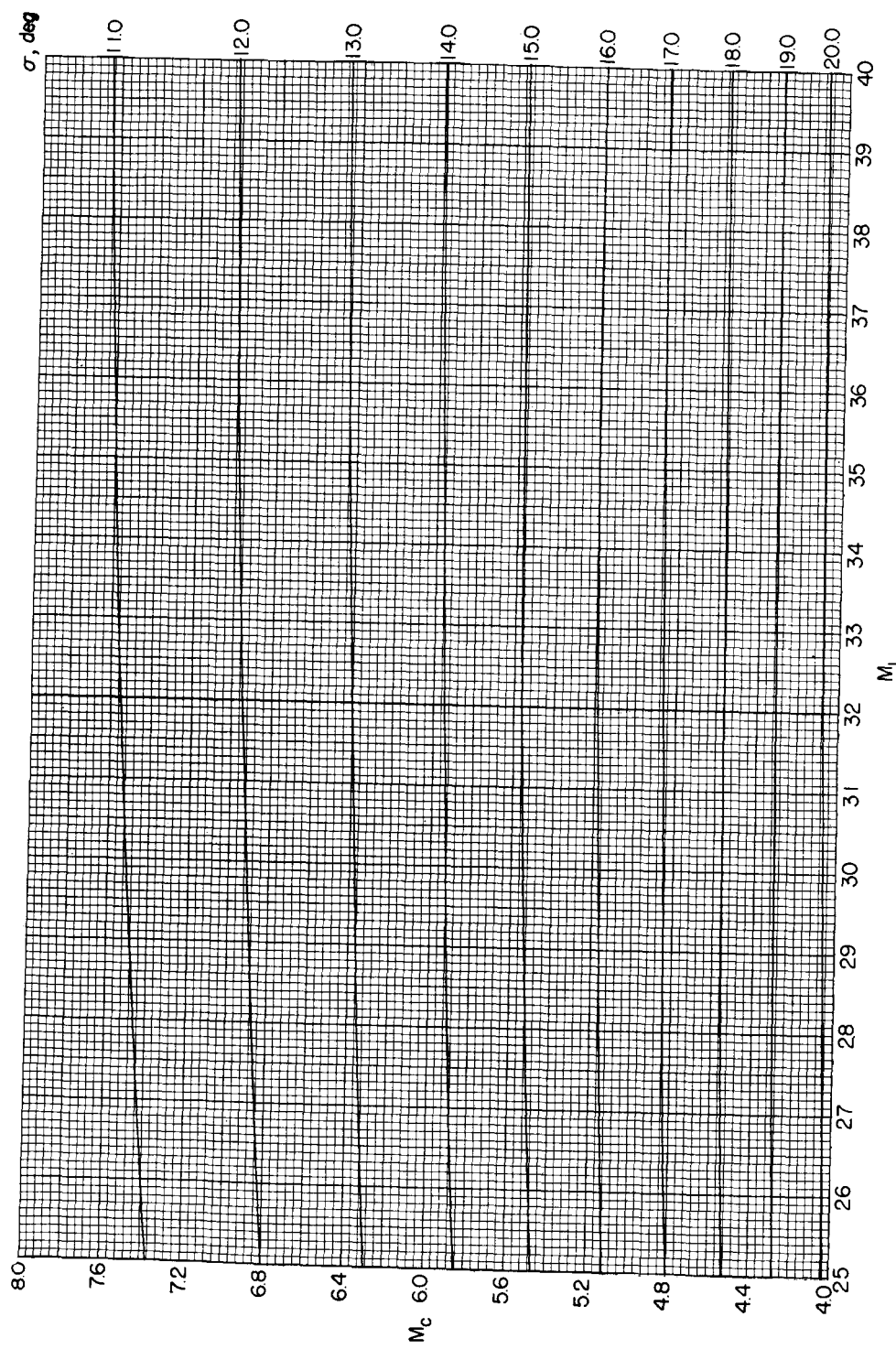
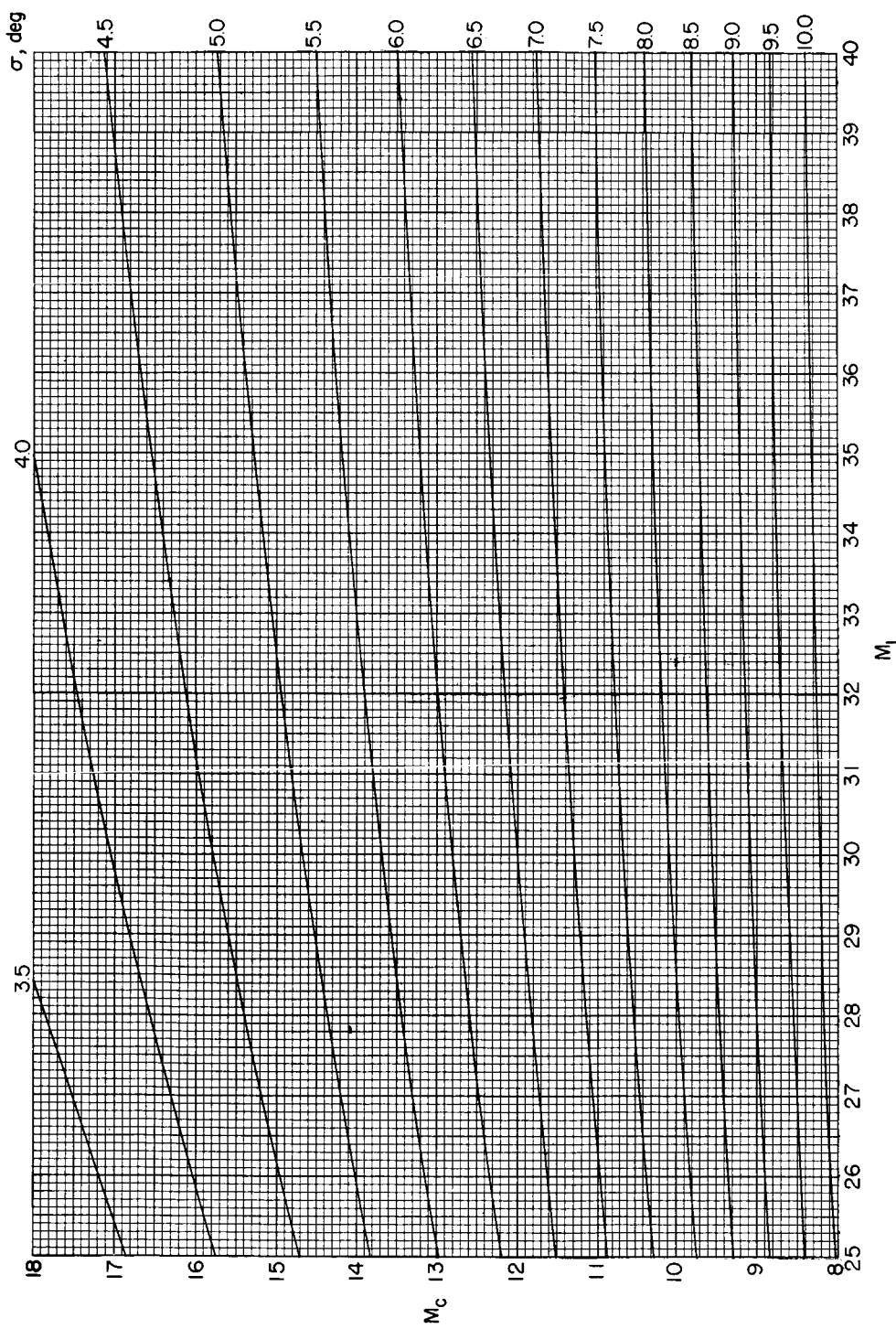
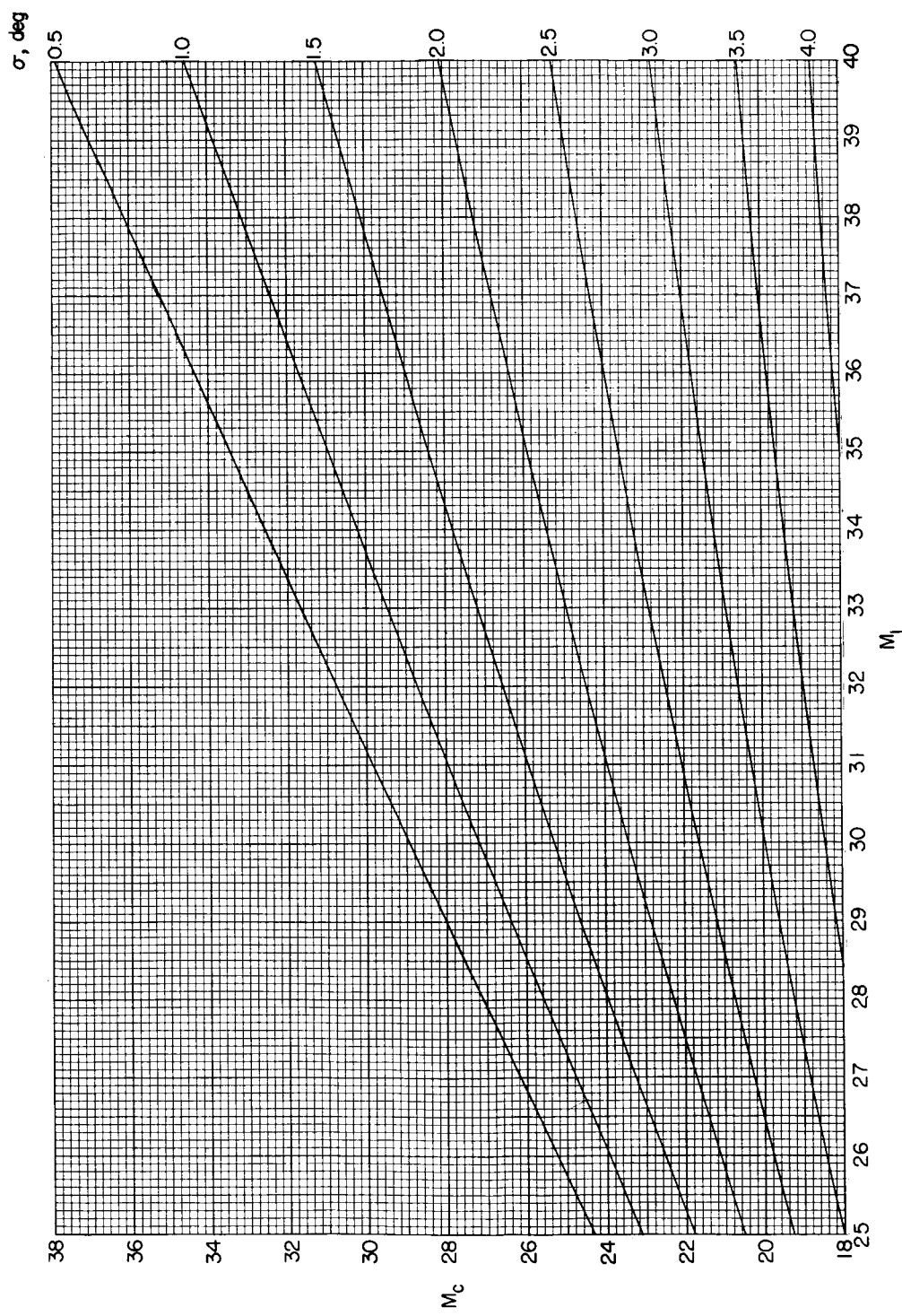
(k)  $M_l = 25$  to 40;  $M_c = 4$  to 8.

Figure 2.- Continued.



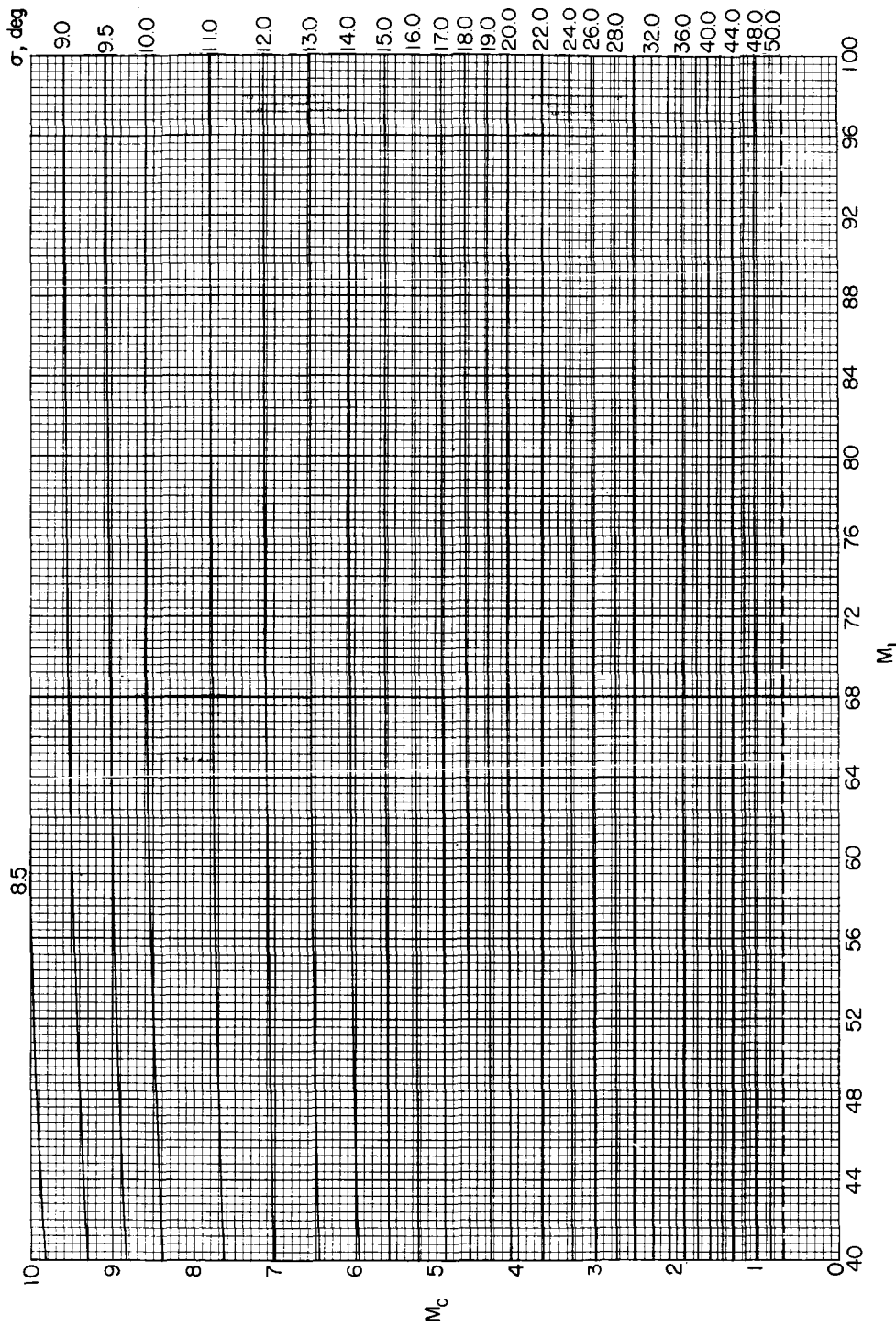
(l)  $M_1 = 25$  to 40;  $M_C = 8$  to 18.

Figure 2.- Continued.



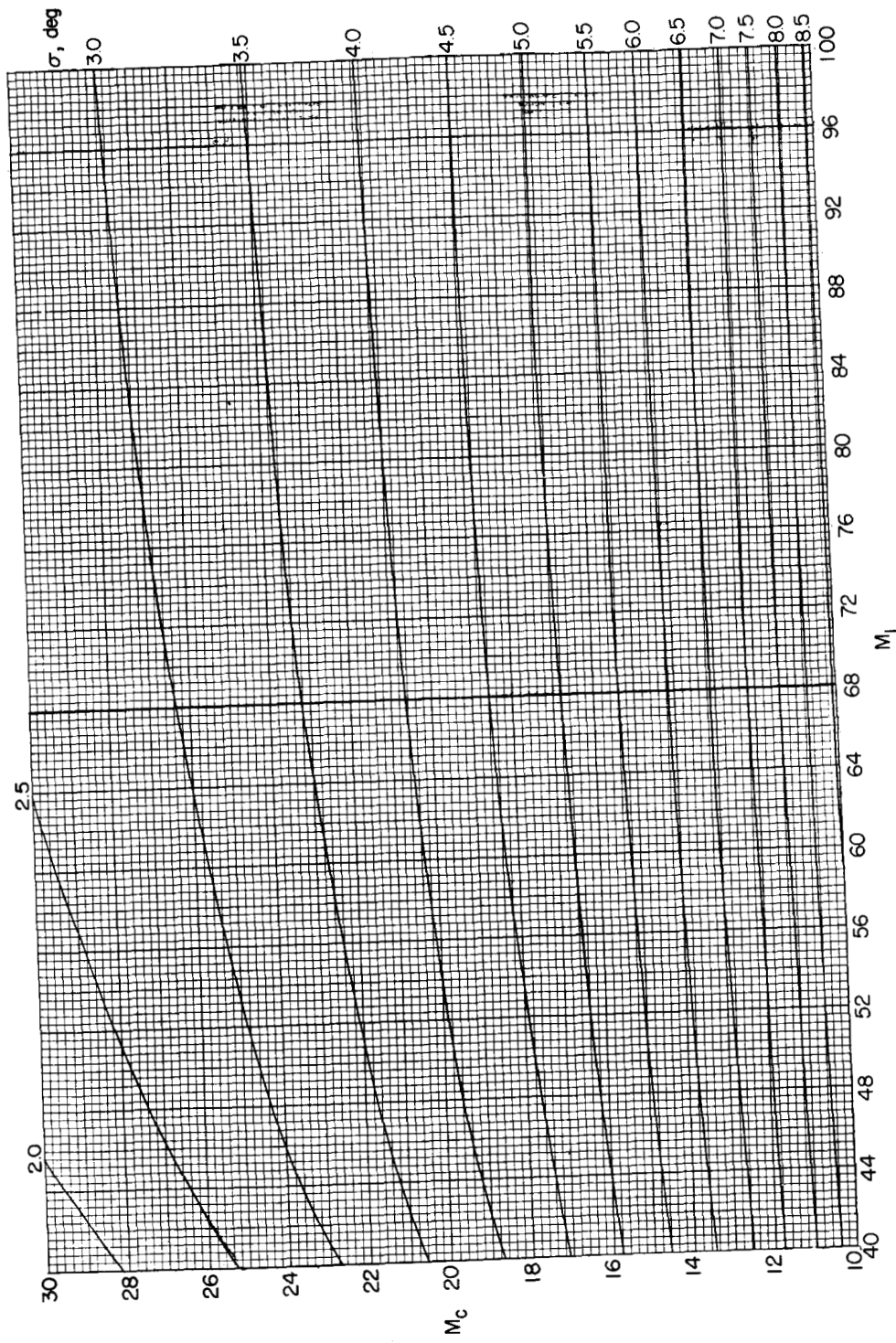
(m)  $M_l = 25$  to 40;  $M_C = 18$  to 38.

Figure 2.- Continued.



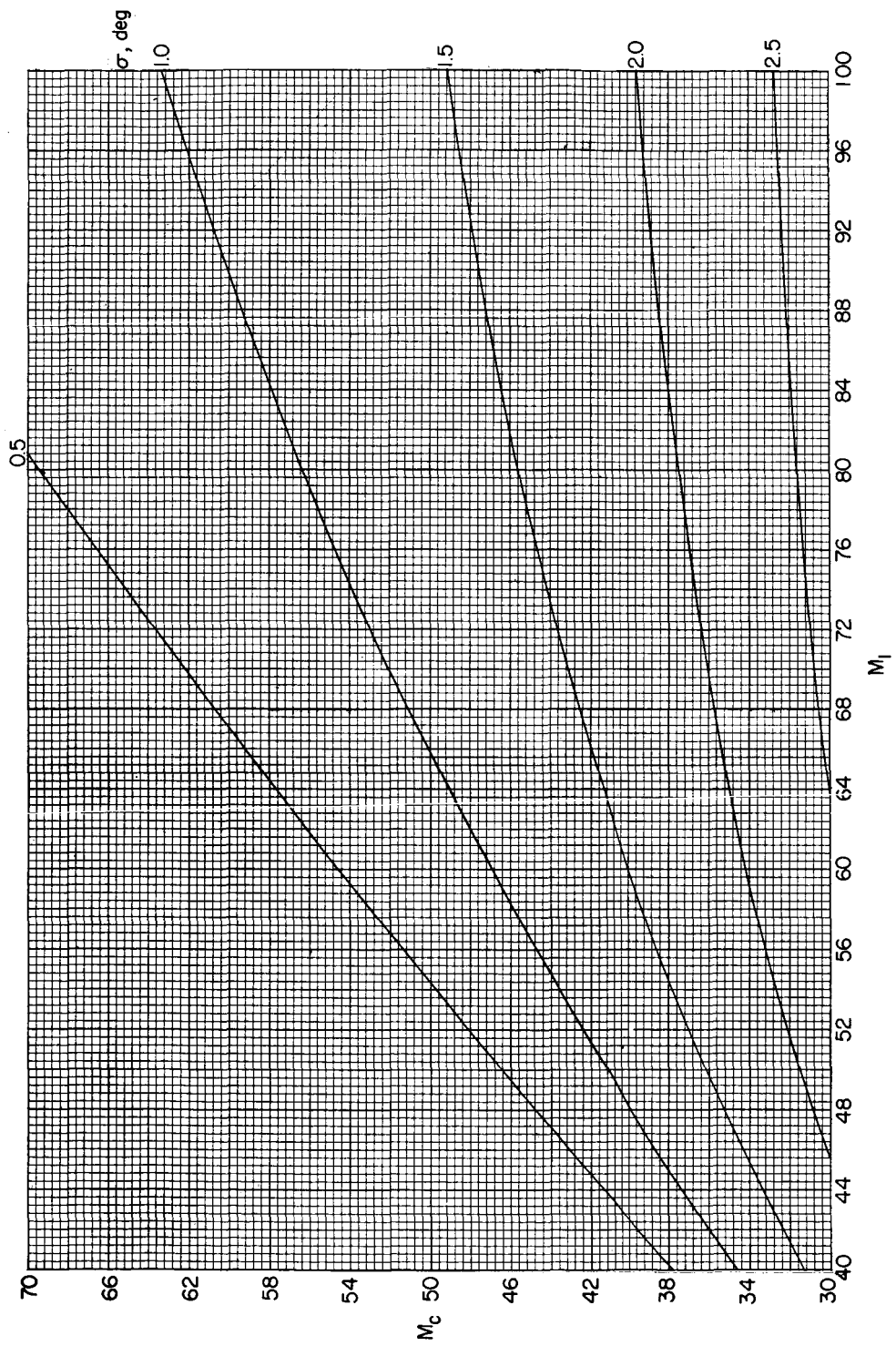
(n)  $M_l = 40$  to  $100$ ;  $M_c = 0$  to  $10$ .

Figure 2.- Continued.



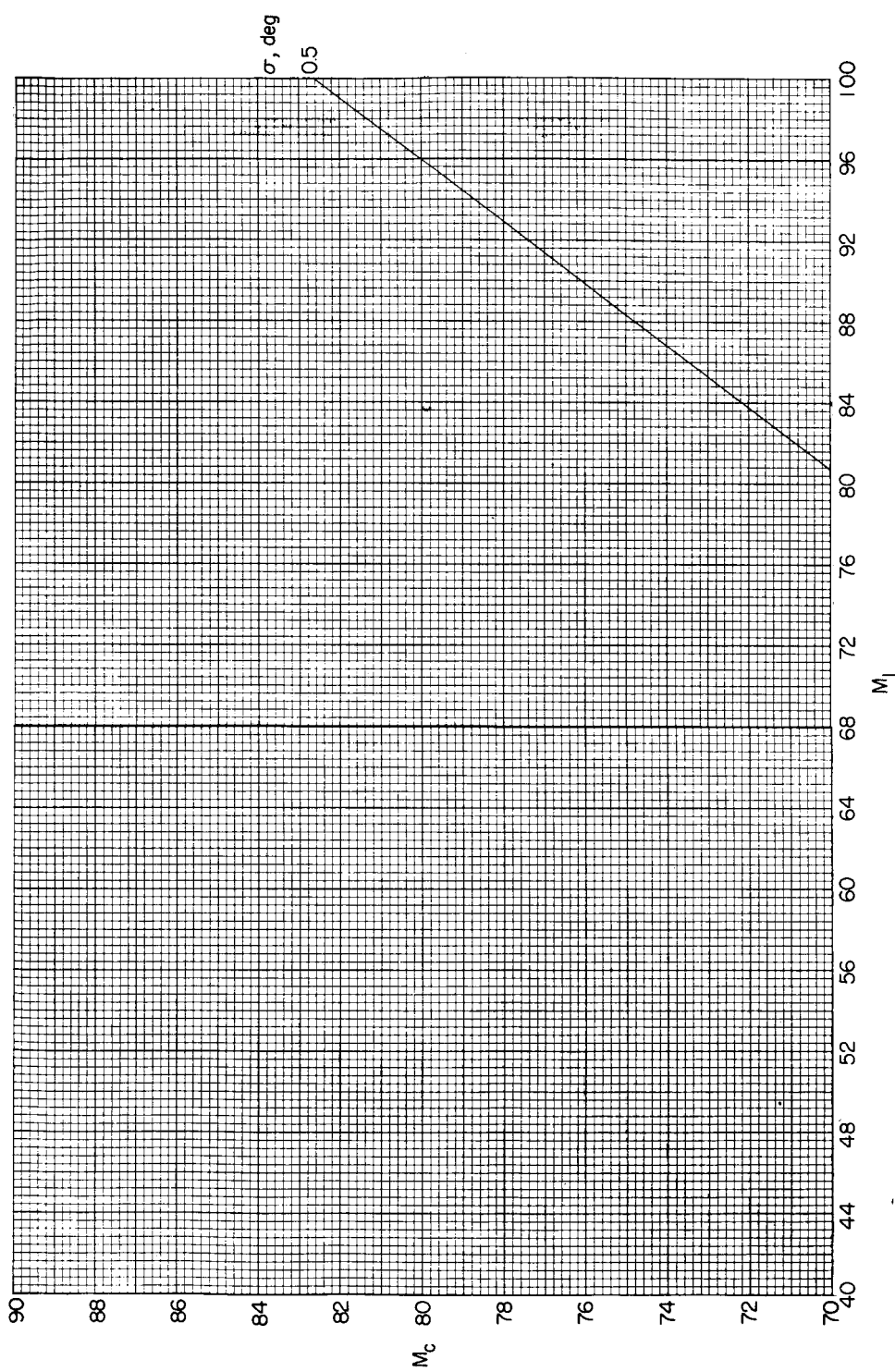
(o)  $M_1 = 40$  to  $100$ ;  $M_C = 10$  to  $30$ .

Figure 2.- Continued.



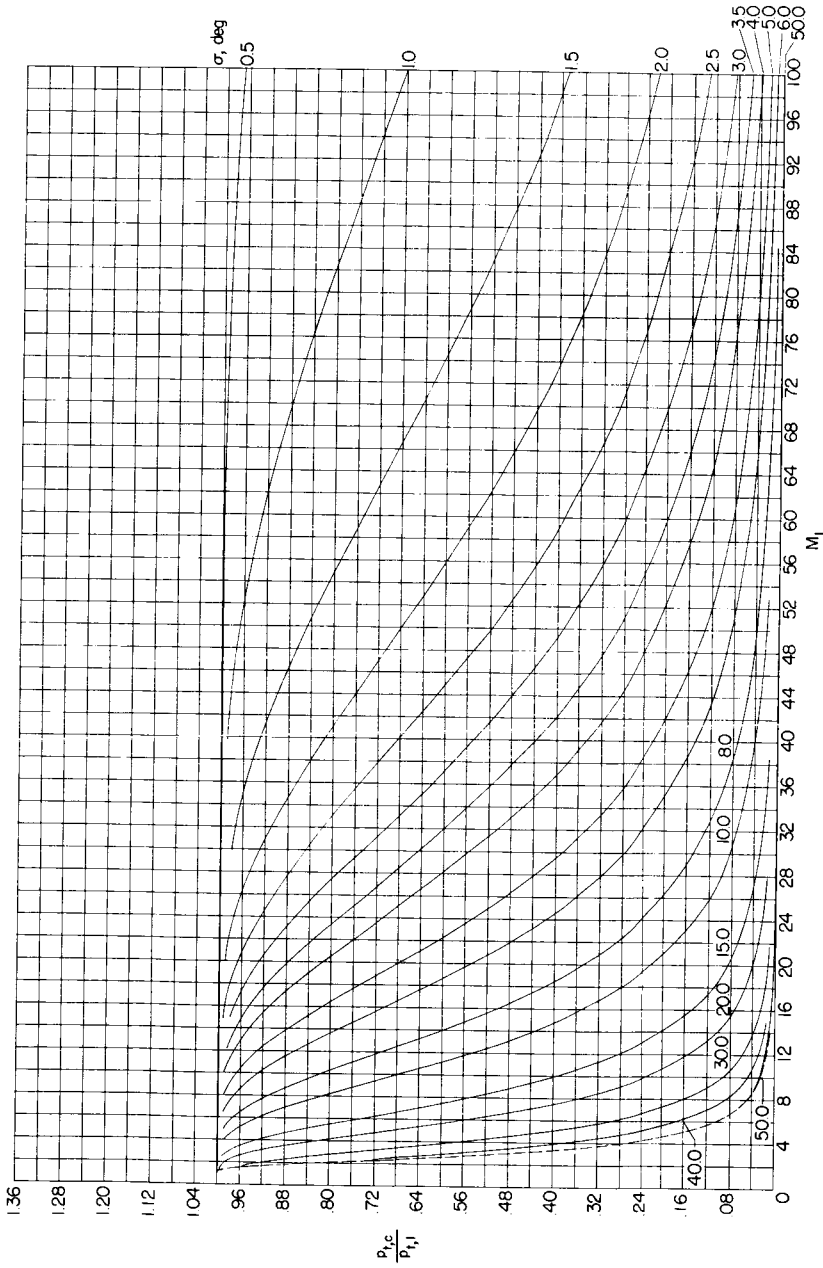
(p)  $M_l = 40$  to  $100$ ;  $M_c = 30$  to  $70$ .

Figure 2.- Continued.



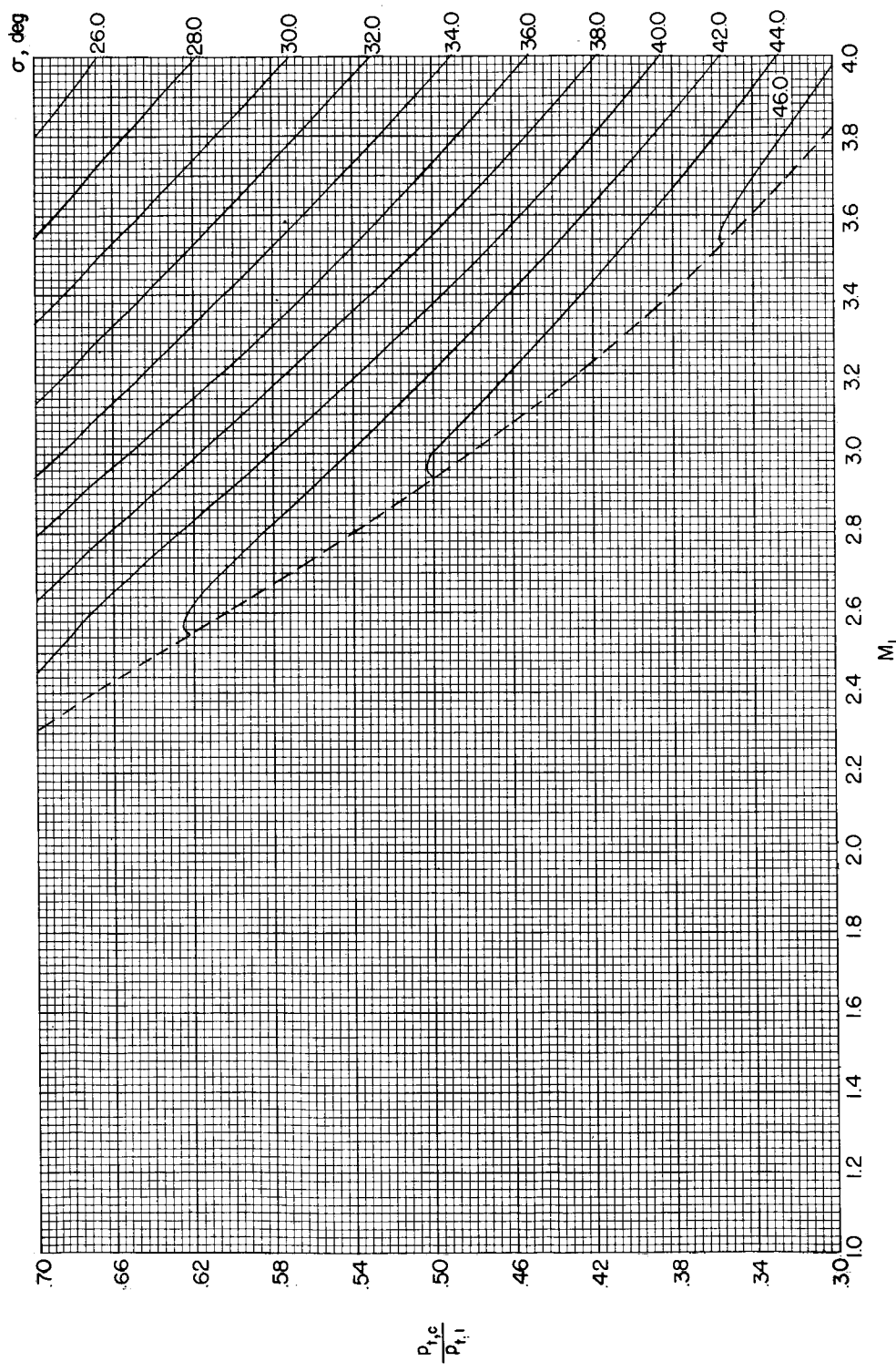
(q<sub>1</sub>)  $M_l = 40$  to  $100$ ;  $M_c = 70$  to  $90$ .

Figure 2.- Concluded.



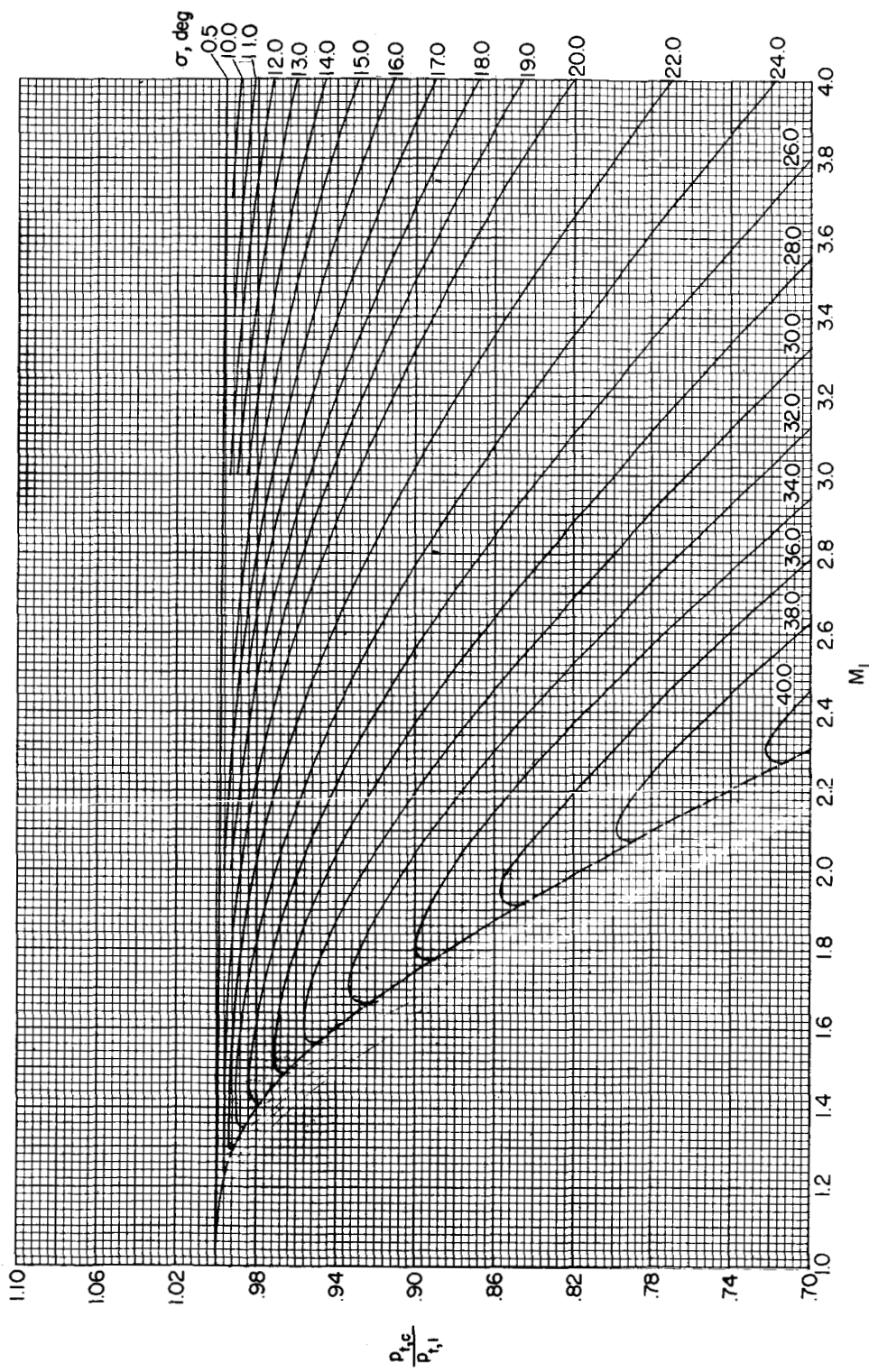
$$(a) \quad M_1 = 1 \text{ to } 100; \quad \frac{P_{t,c}}{P_{t,1}} = 0 \text{ to } 1.$$

Figure 3.- Variation of ratio of total pressure behind cone shock to free-stream total pressure with free-stream Mach number. (Dashed line denotes limit of weak shock solution.)



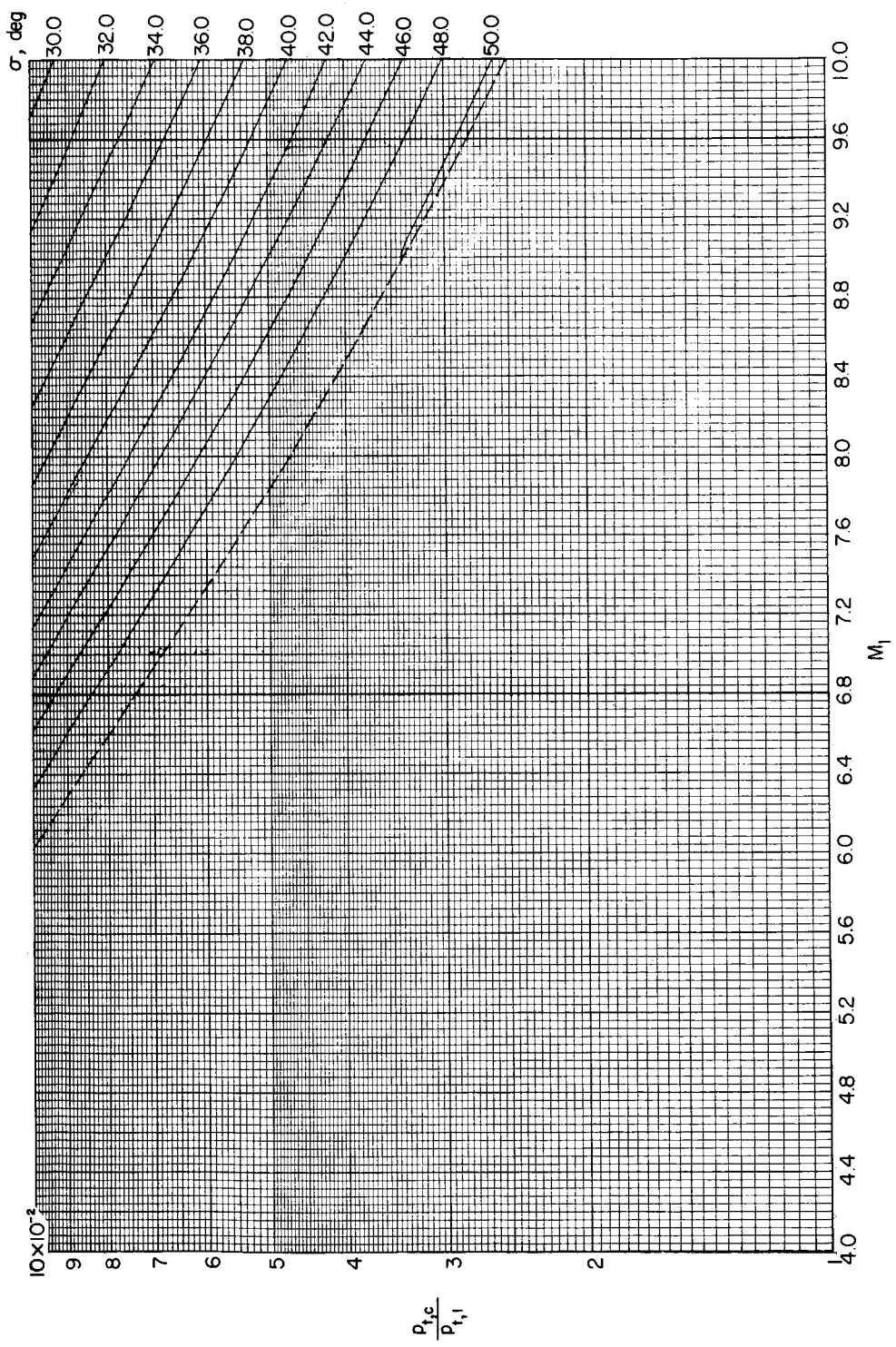
(b)  $M_1 = 1$  to 4;  $\frac{p_{t,c}}{p_{t,1}} = 0.3$  to 0.7.

Figure 3.- Continued.



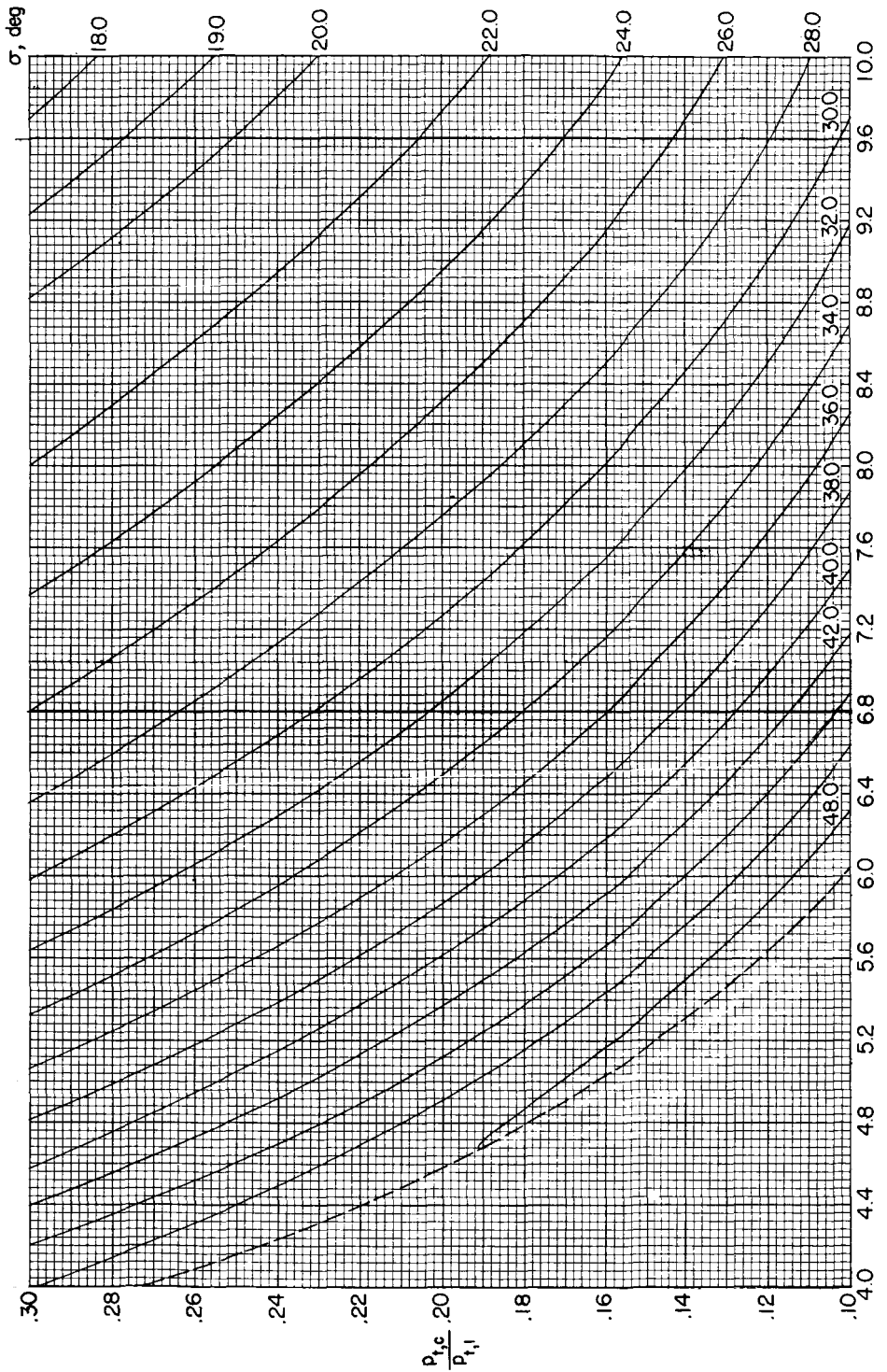
(c)  $M_1 = 1$  to 4;  $\frac{P_{t,2c}}{P_{t,1}} = 0.7$  to 1.

Figure 3.- Continued.



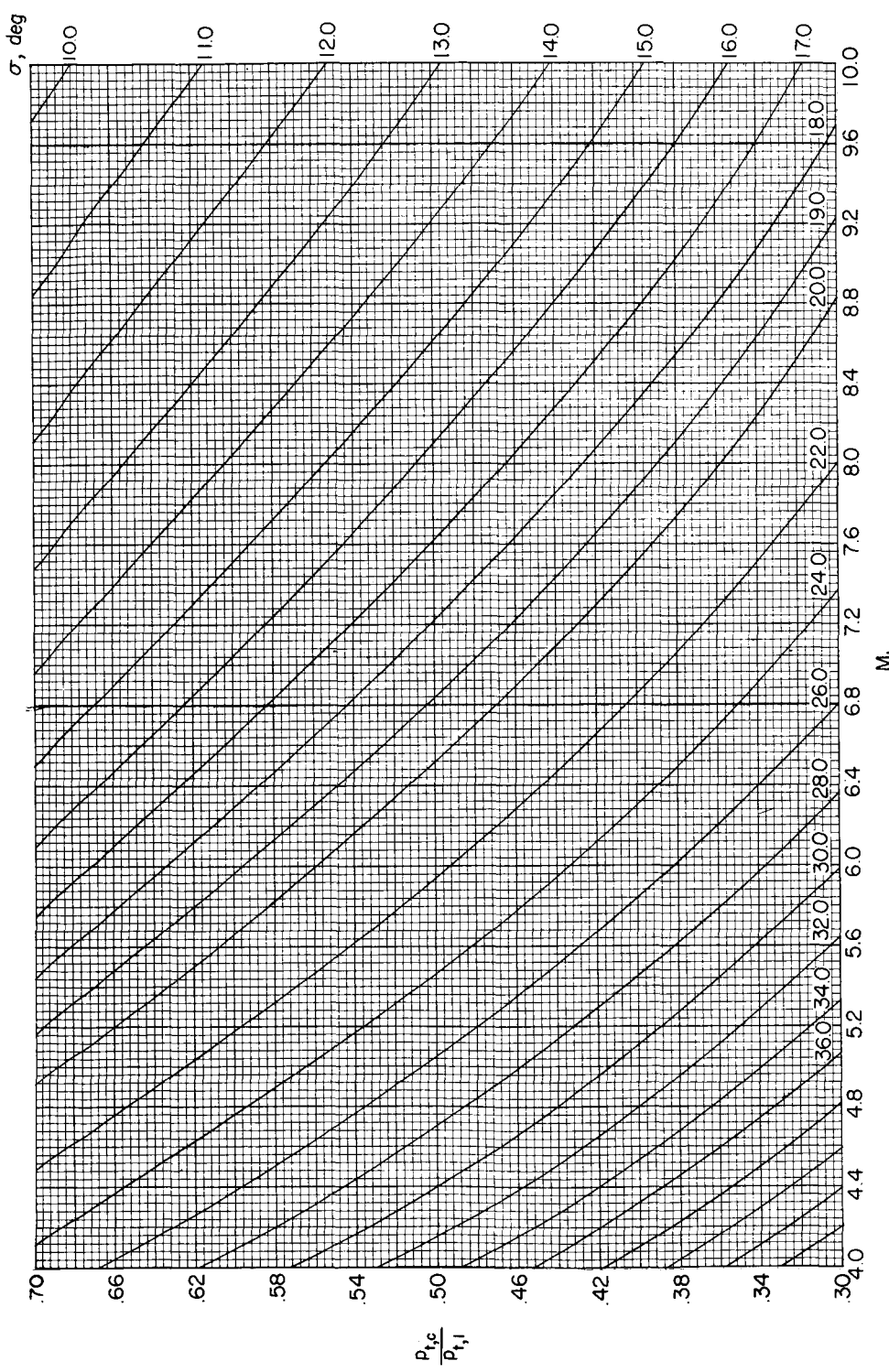
(d)  $M_1 = 4$  to 10;  $\frac{P_{t,c}}{P_{t,I}} = 1 \times 10^{-2}$  to  $10 \times 10^{-2}$ .

Figure 3.- Continued.



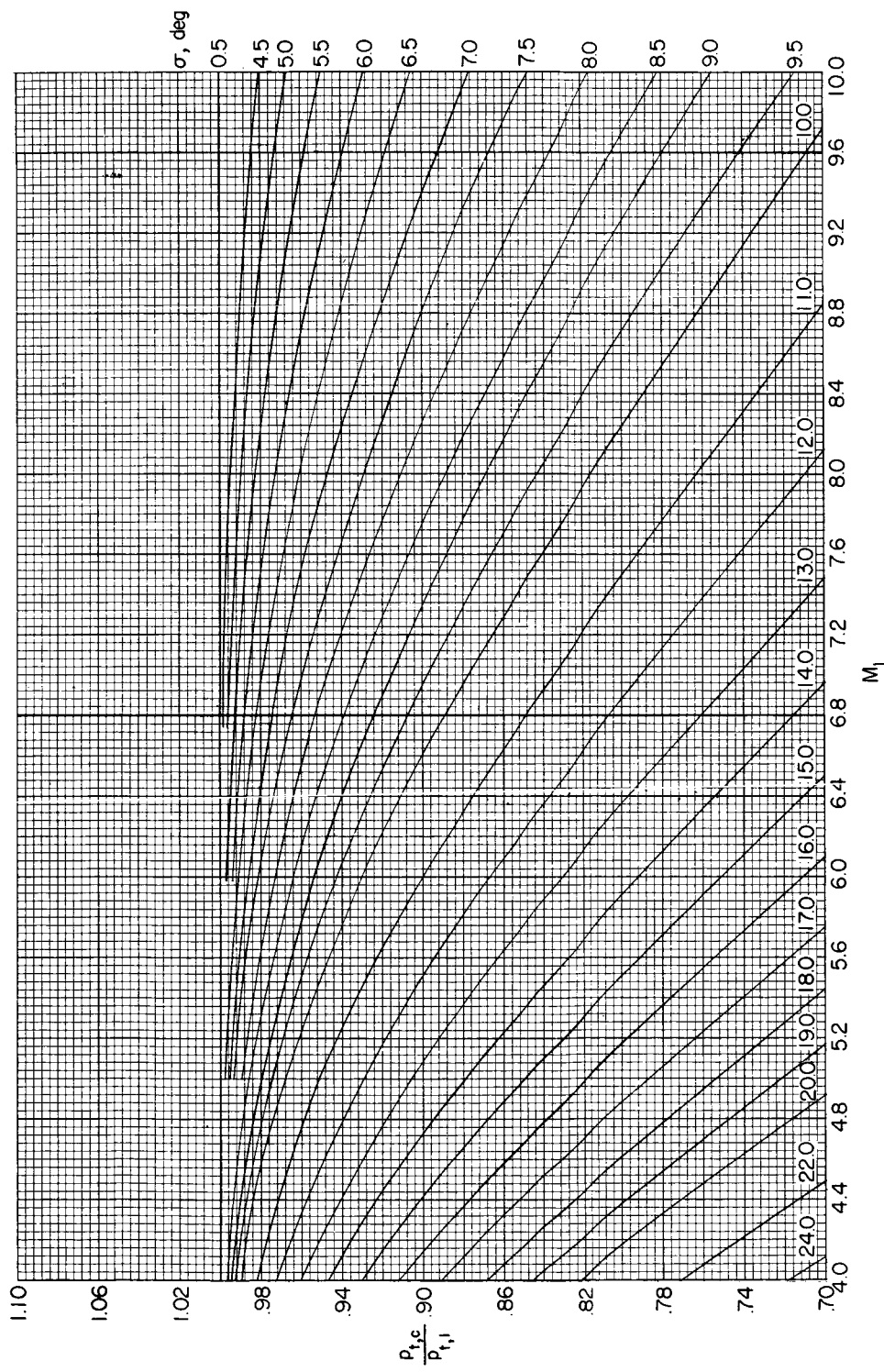
(e)  $M_1 = 4$  to 10;  $\frac{p_{t,c}}{p_{t,i}} = 0.1$  to 0.3.

Figure 3.- Continued.



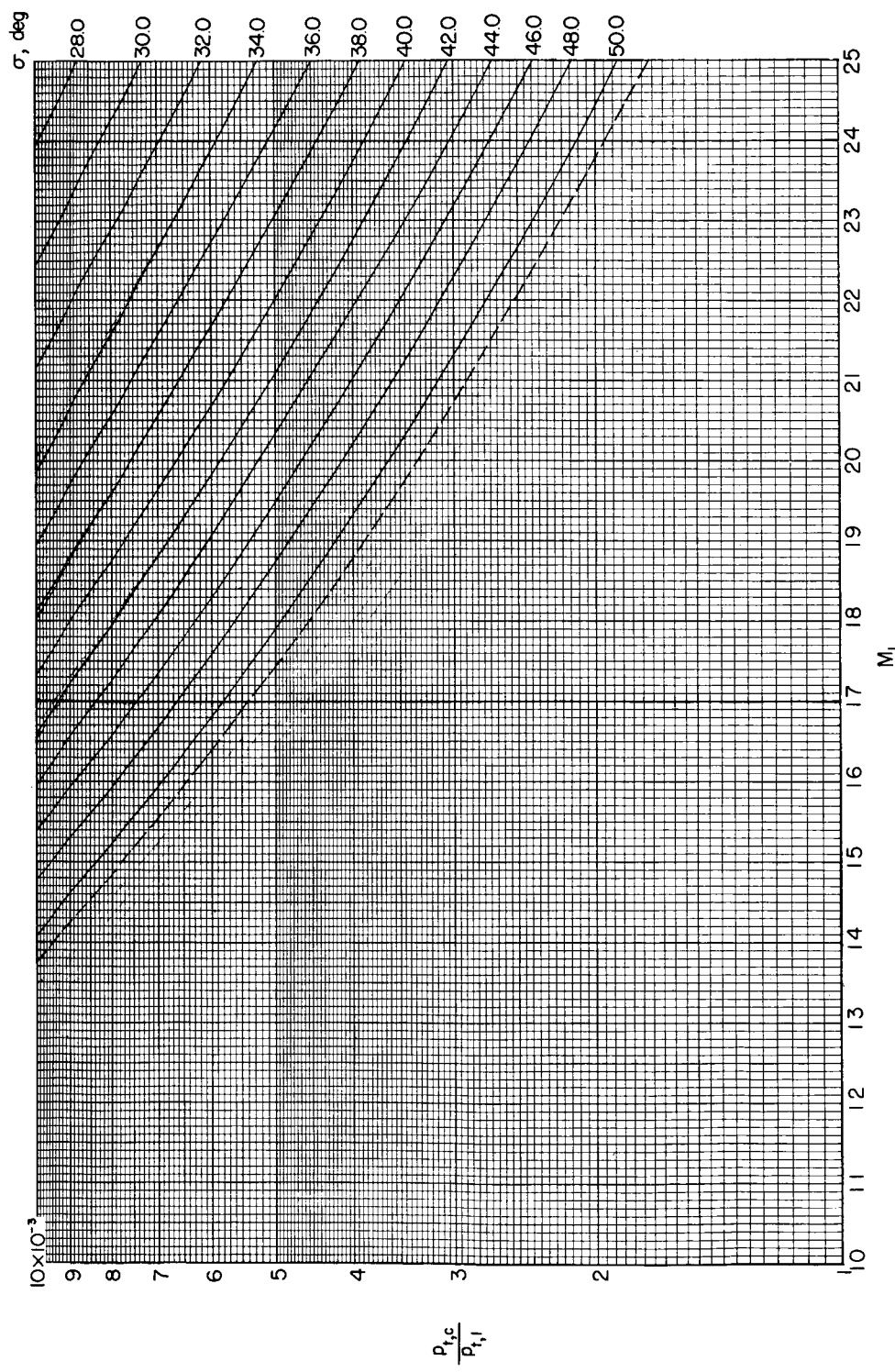
(f)  $M_1 = 4$  to 10;  $\frac{P_{t,c}}{P_{t,1}} = 0.3$  to 0.7.

Figure 3.- Continued.



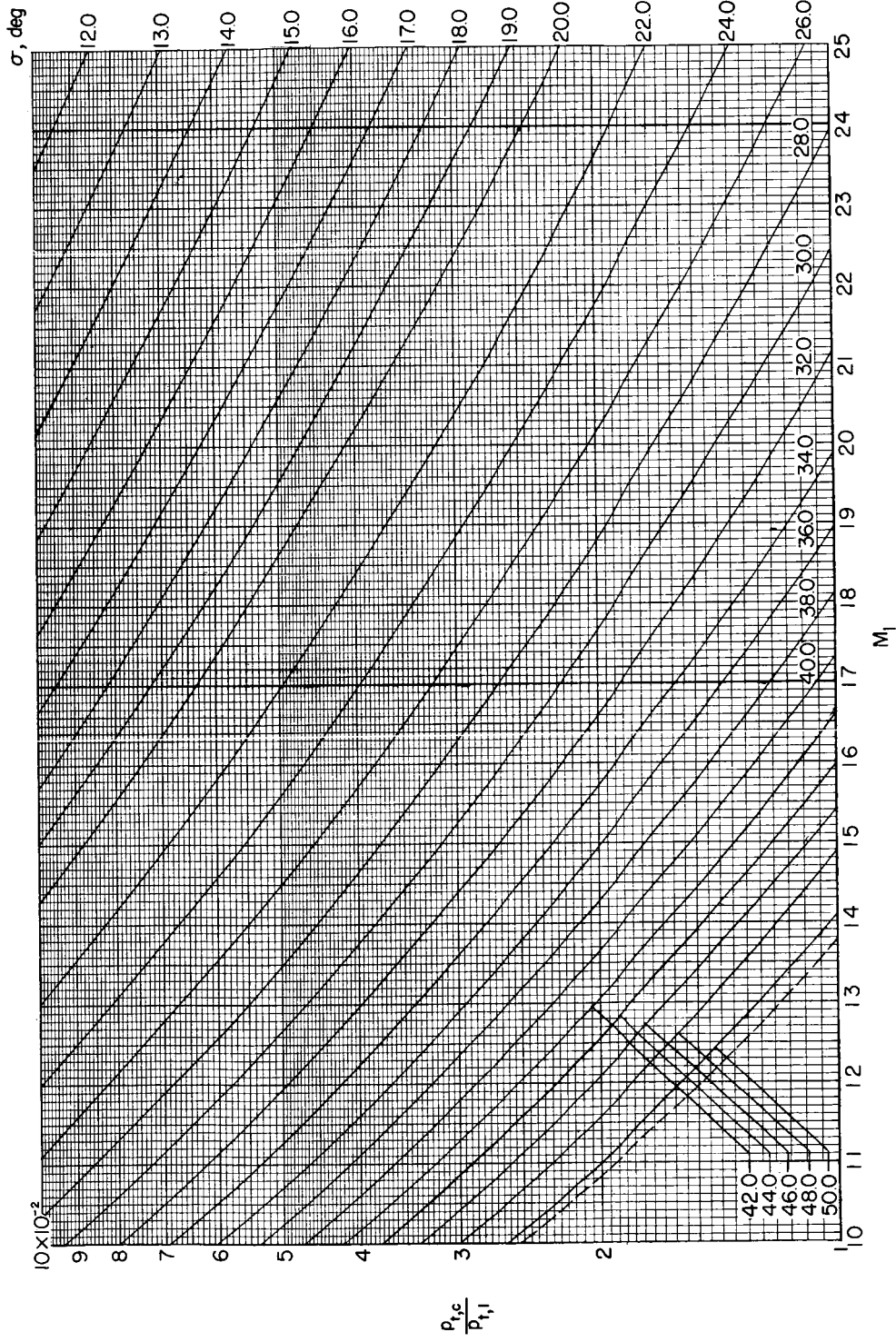
(g)  $M_I = 4$  to 10;  $\frac{p_{t,c}}{p_{t,I}} = 0.7$  to 1.

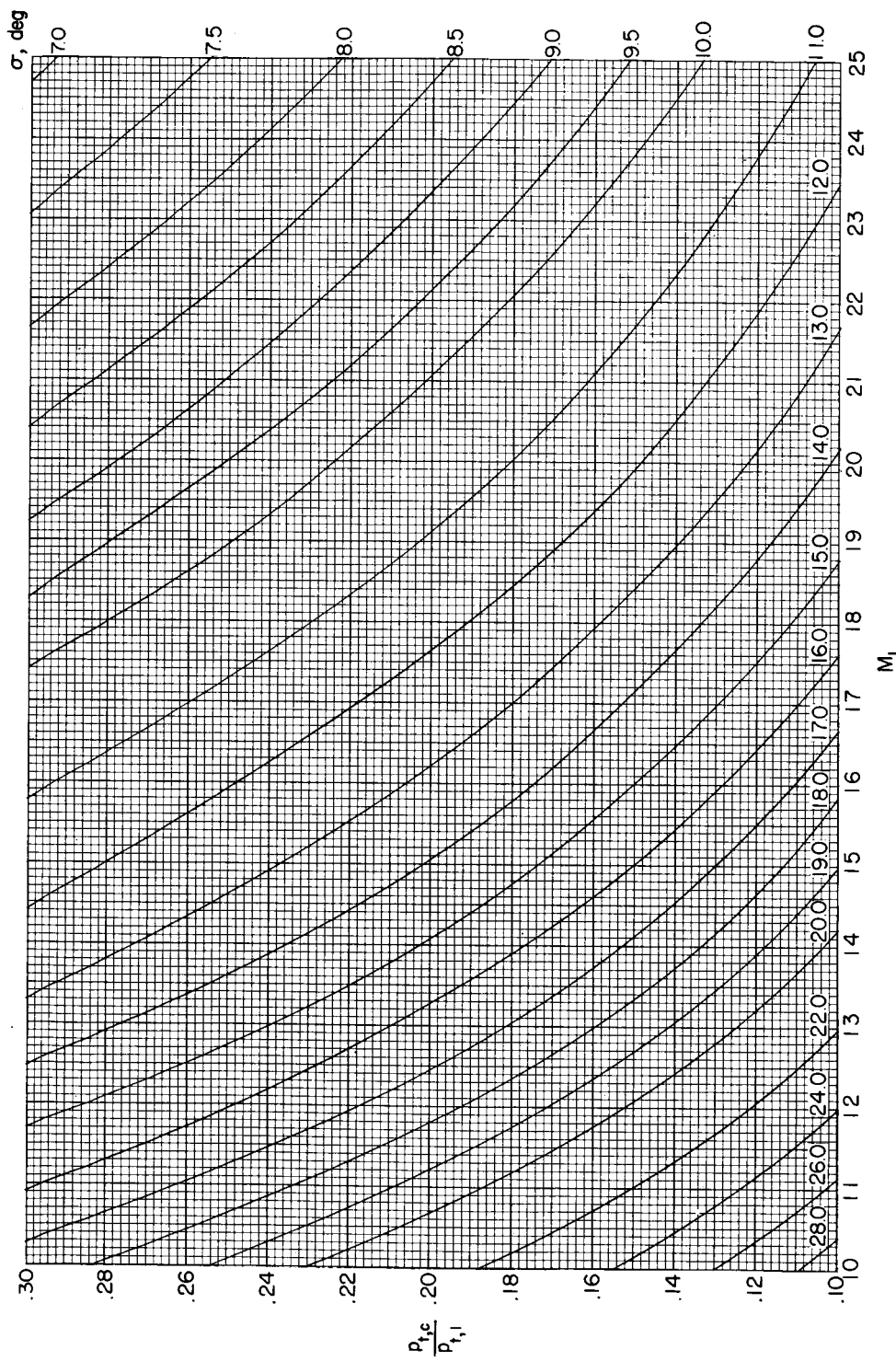
Figure 3.- Continued.



(h)  $M_1 = 10$  to  $25$ ;  $\frac{P_{t,c}}{P_{f,l}} = 1 \times 10^{-3}$  to  $10 \times 10^{-3}$ .

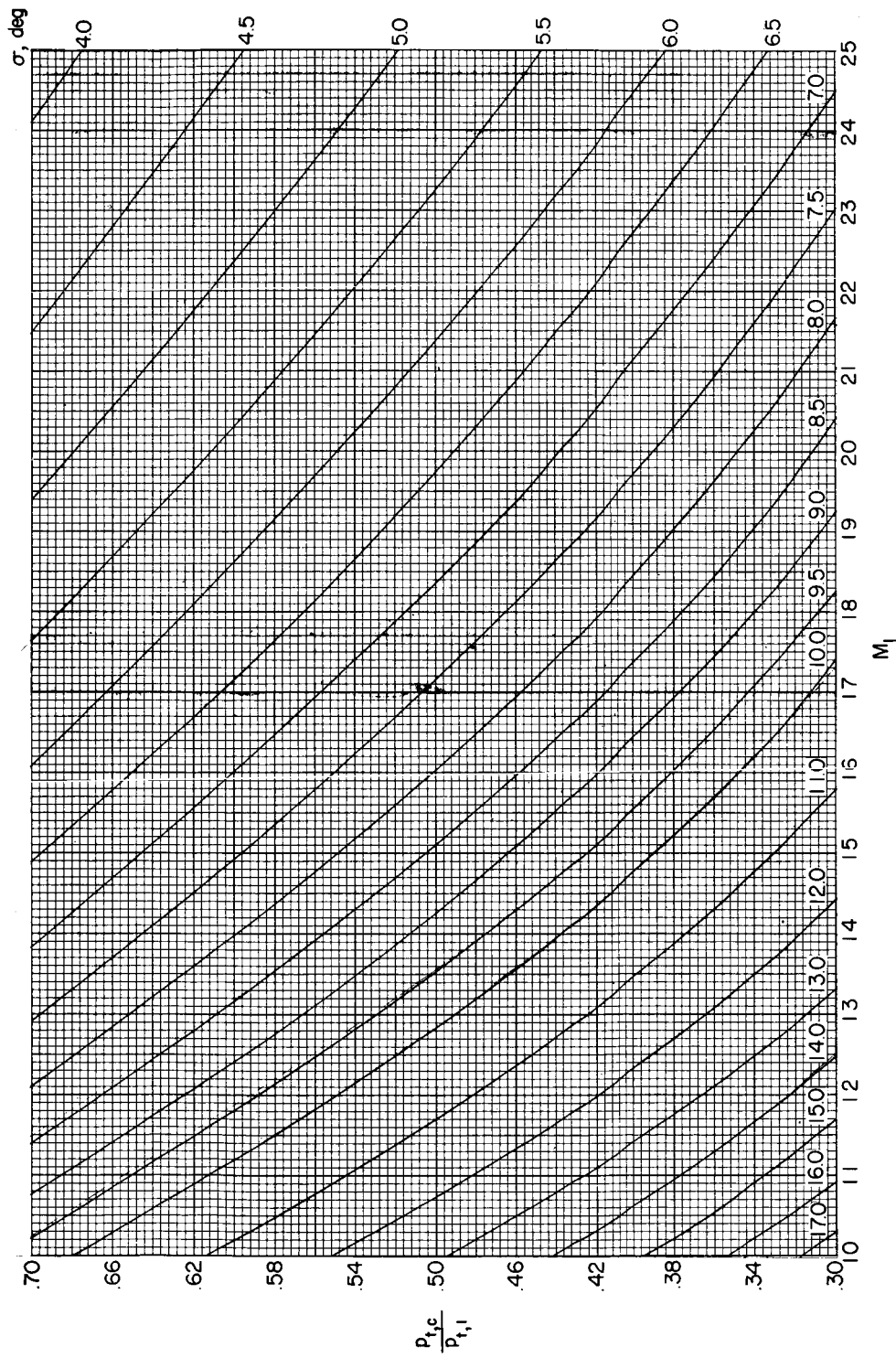
Figure 3. - Continued.





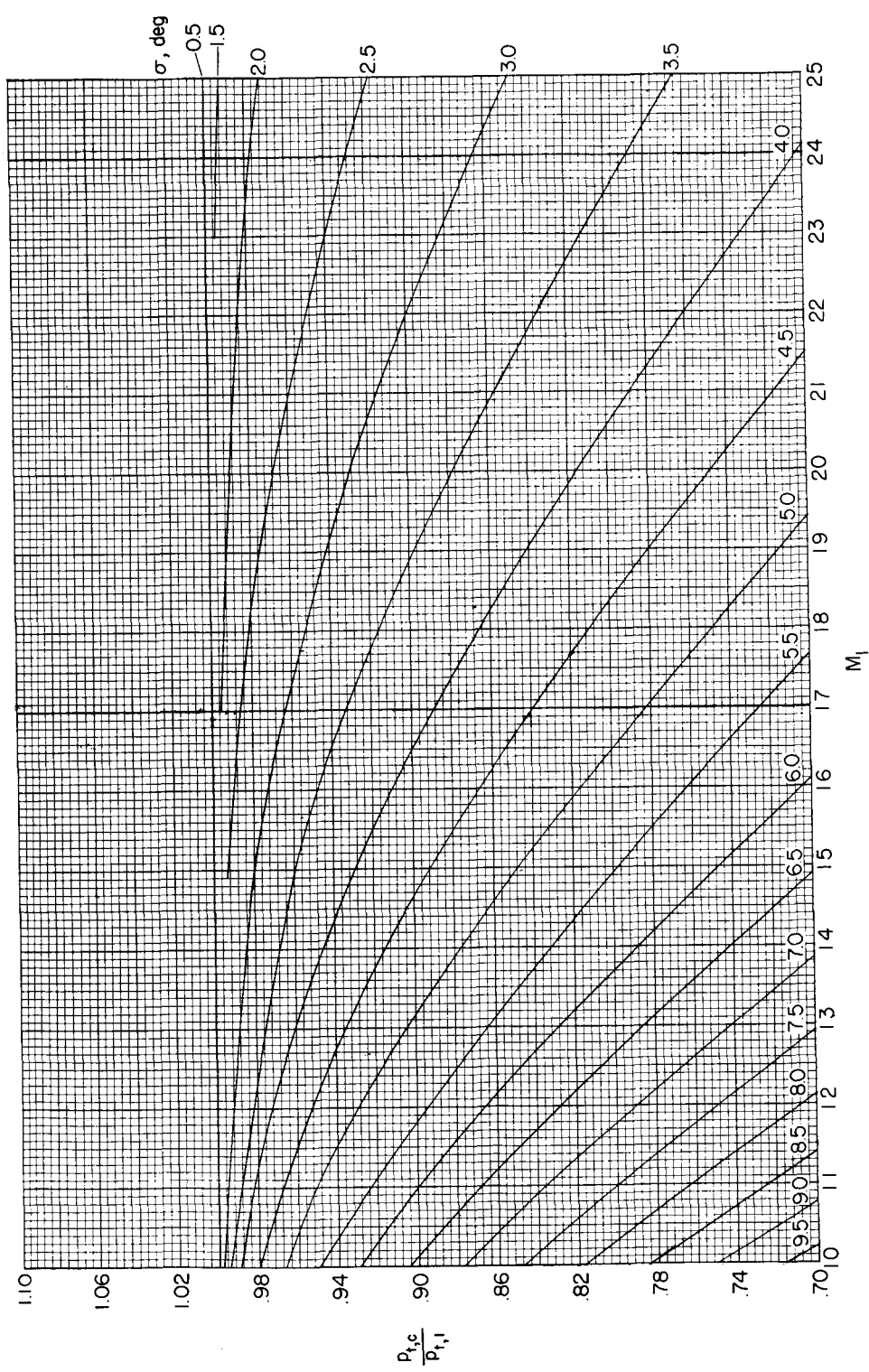
(j)  $M_1 = 10$  to  $25$ ;  $\frac{P_{t,c}}{P_{t,i}} = 0.1$  to  $0.3$ .

Figure 3.- Continued.



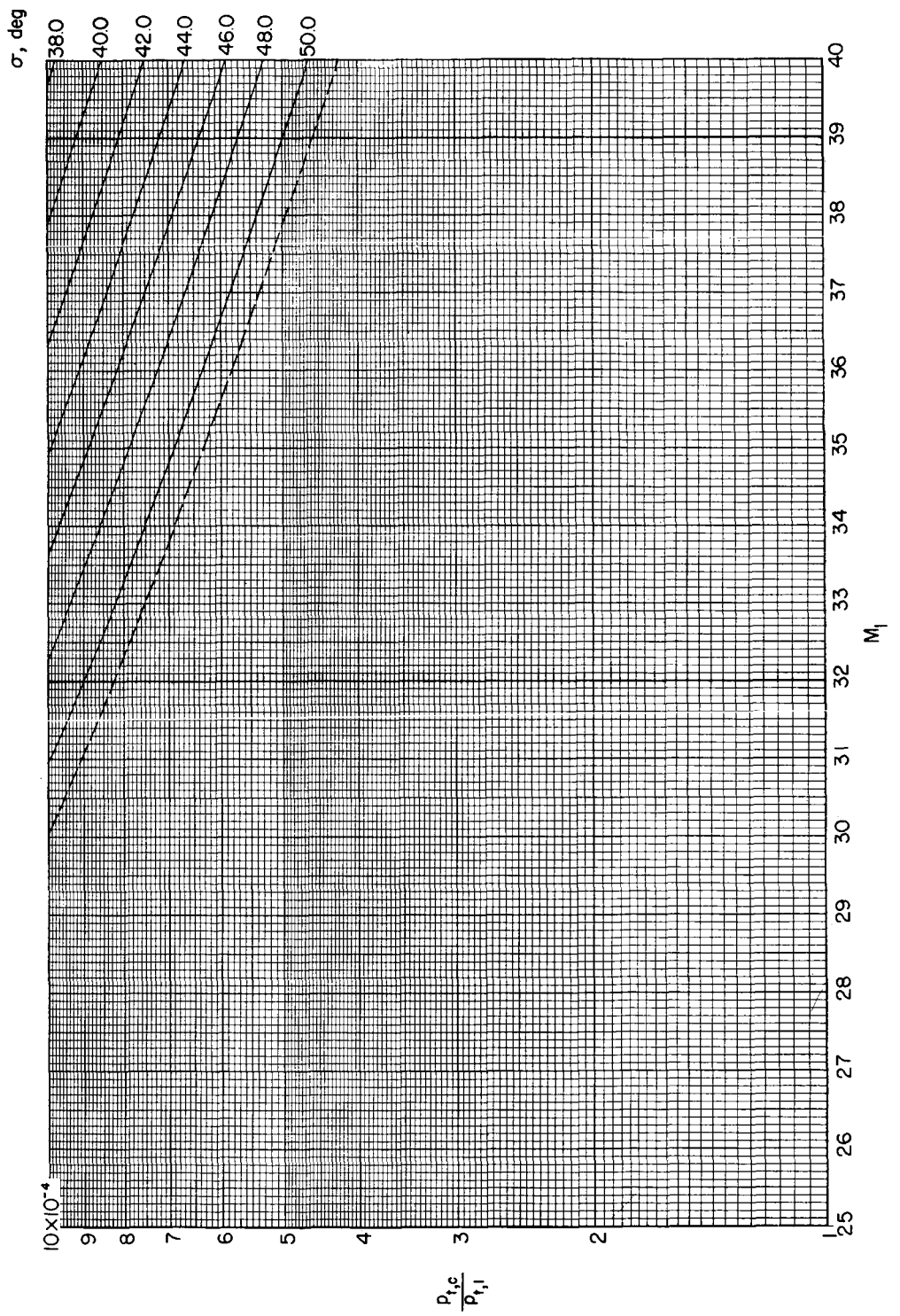
(k)  $M_1 = 10$  to  $25$ ;  $\frac{p_{t,c}}{p_{t,1}} = 0.3$  to  $0.7$ .

Figure 3.- Continued.



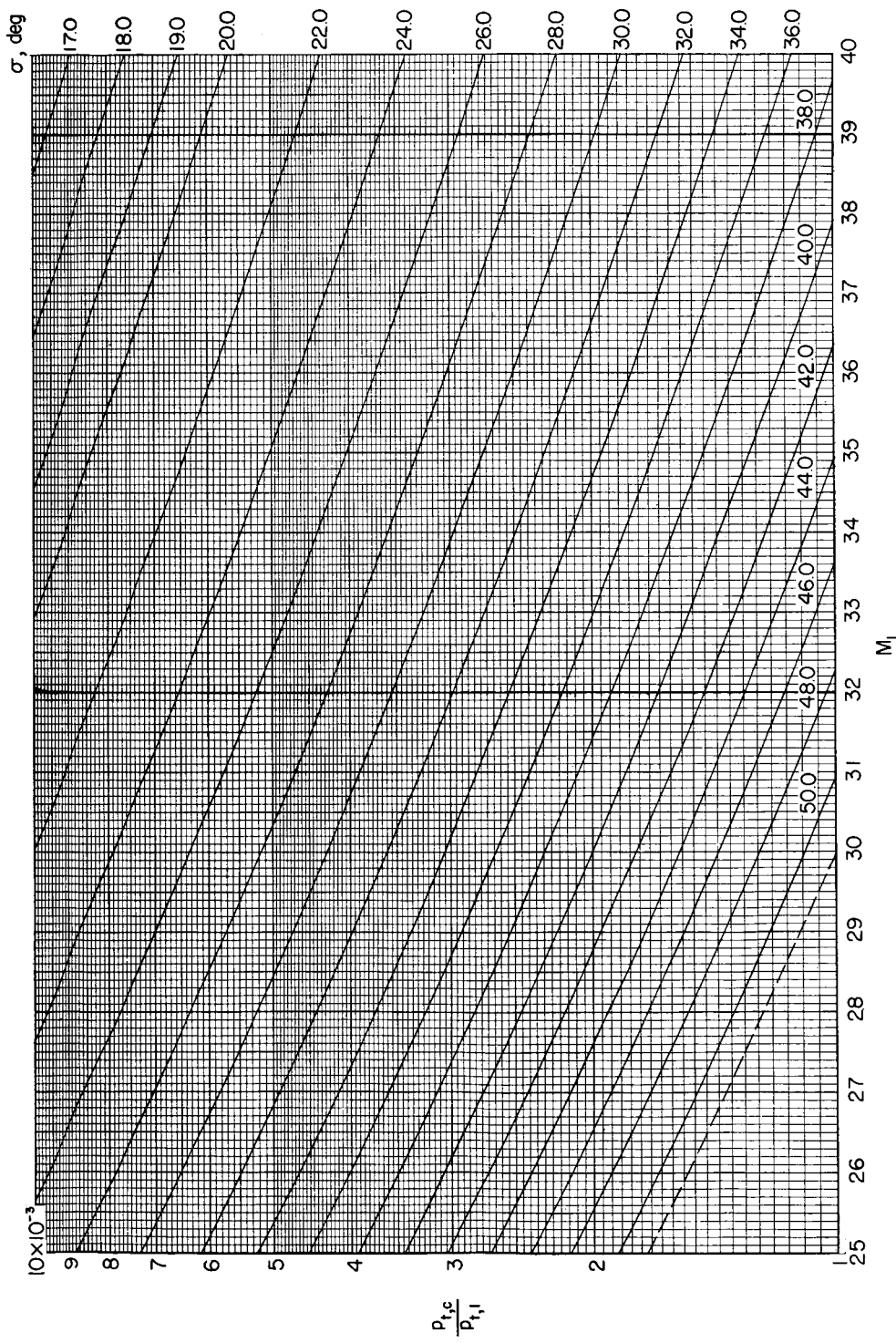
(1)  $M_1 = 10 \text{ to } 25; \frac{p_{t,c}}{p_{r,1}} = 0.7 \text{ to } 1.$

Figure 3. - Continued.



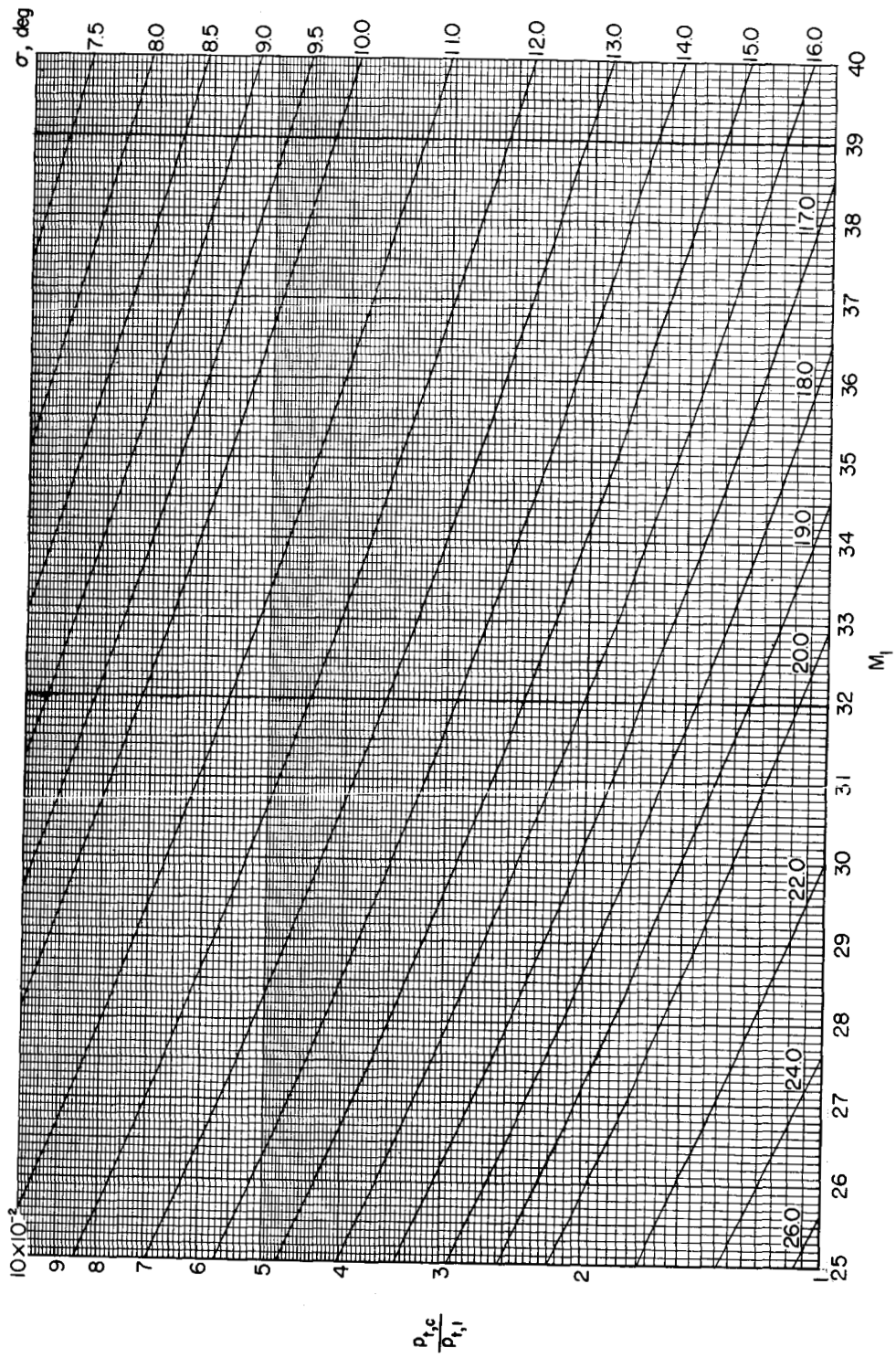
(m)  $M_1 = 25$  to 40;  $\frac{p_{t,1}}{p_{\infty,1}} = 1 \times 10^{-4}$  to  $10 \times 10^{-4}$ .

Figure 3.- Continued.



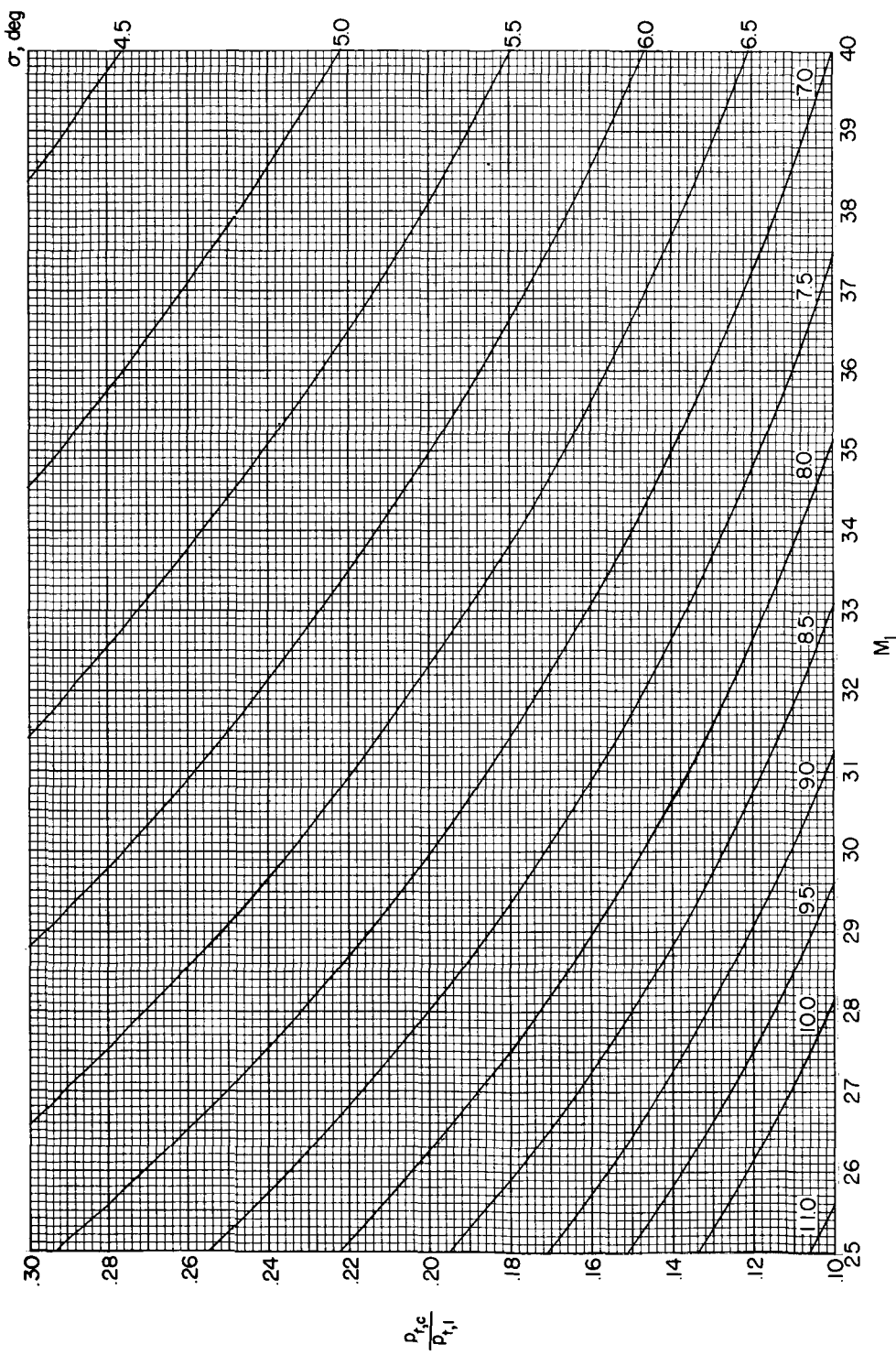
(n)  $M_1 = 25$  to 40;  $\frac{p_{t,c}}{p_{t,1}} = 1 \times 10^{-3}$  to  $10 \times 10^{-3}$ .

Figure 3.- Continued.



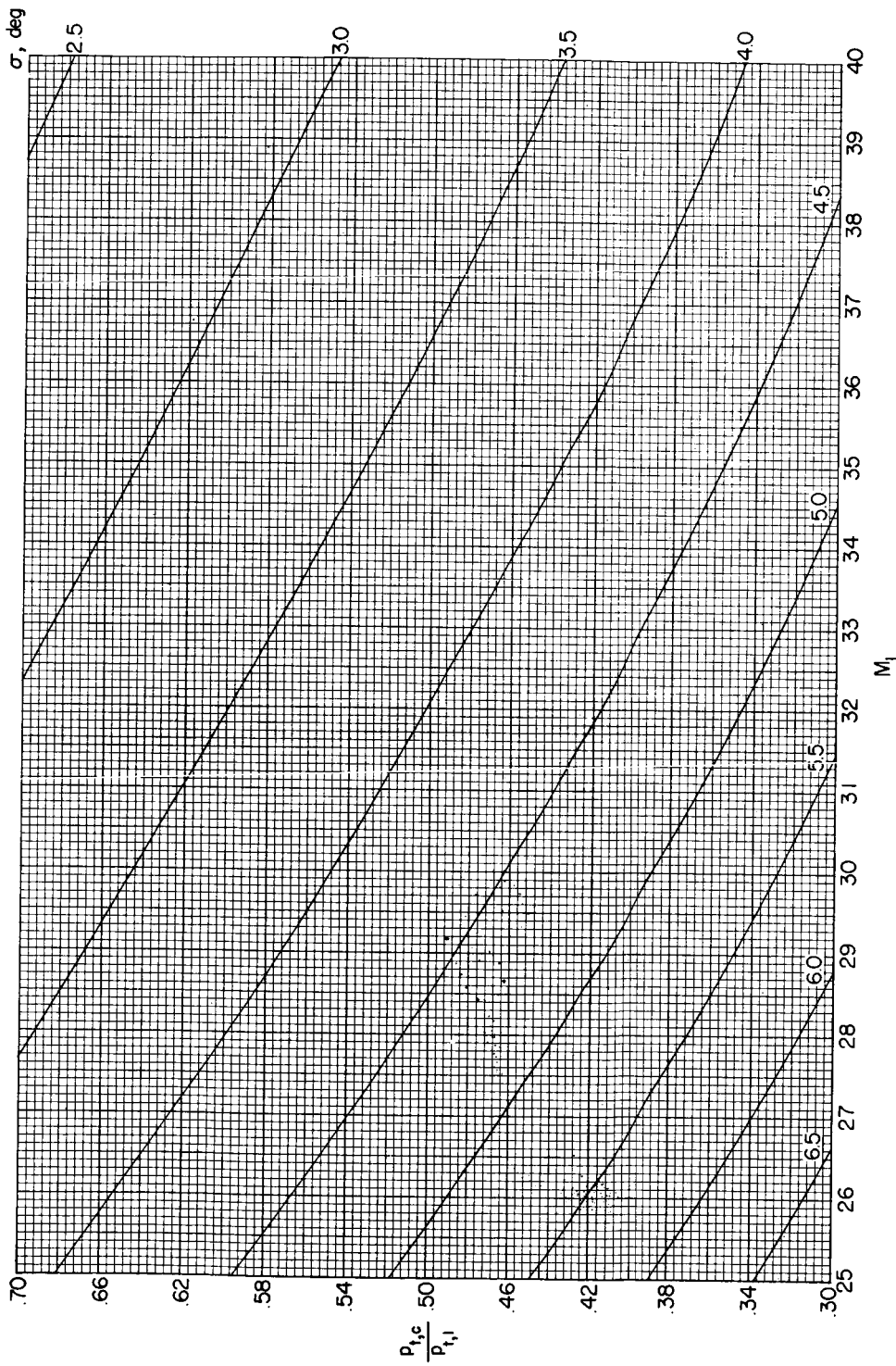
(o)  $M_1 = 25$  to 40;  $\frac{p_{t,c}}{p_{t,1}} = 1 \times 10^{-2}$  to  $10 \times 10^{-2}$ .

Figure 3.- Continued.



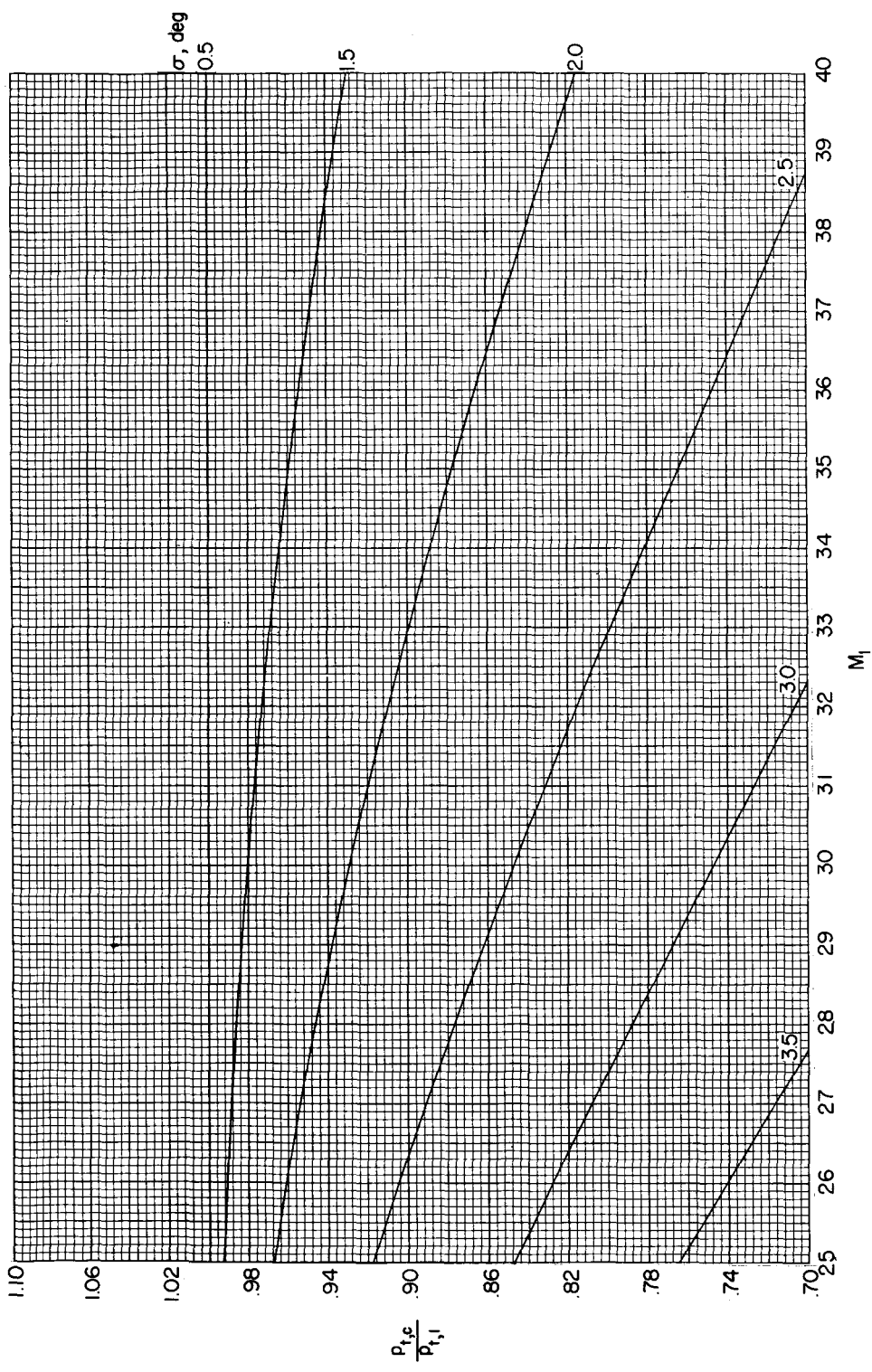
(p)  $M_1 = 25$  to 40;  $\frac{P_{t,c}}{P_{t,i}} = 0.1$  to 0.3.

Figure 3.- Continued.



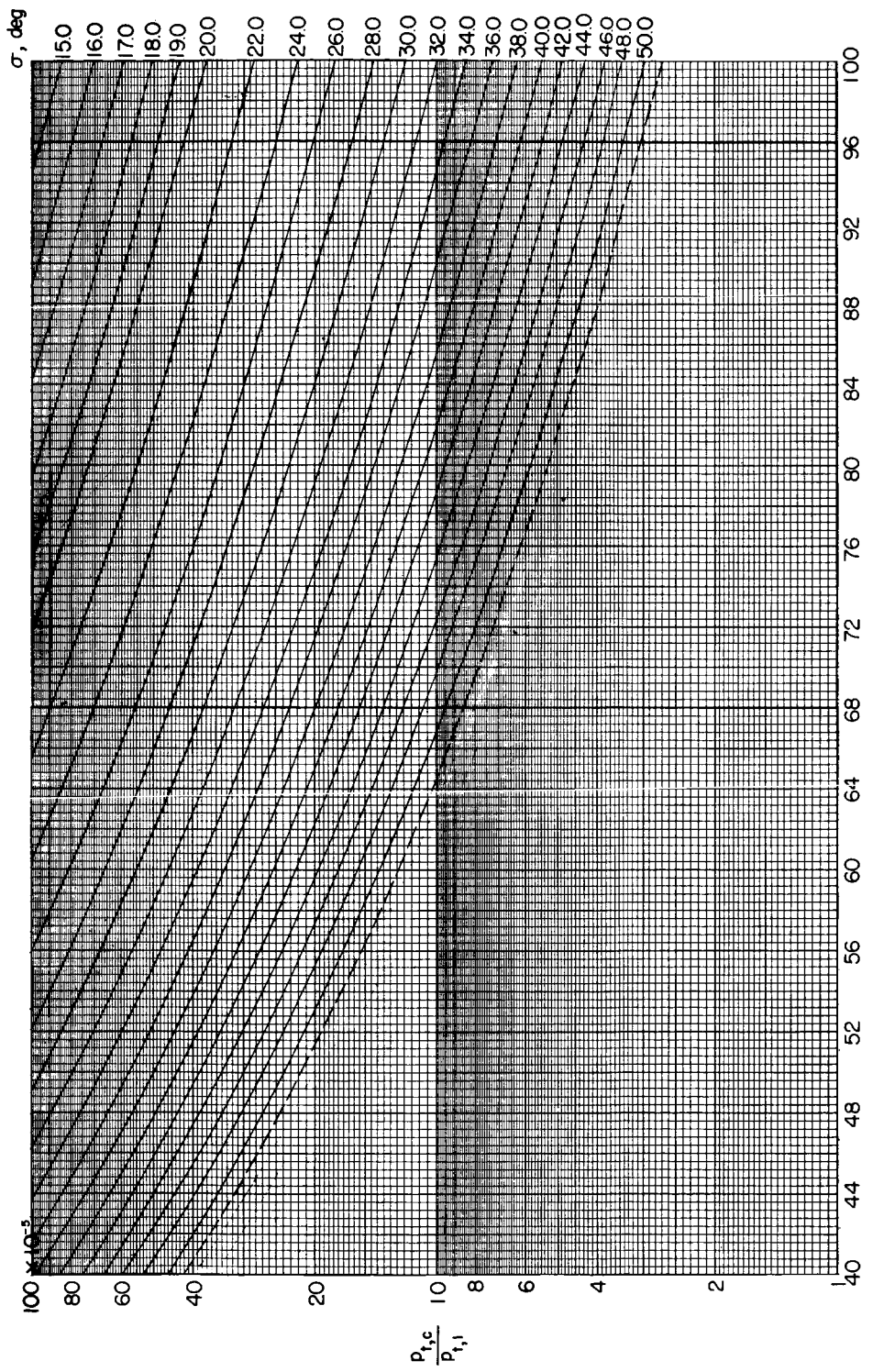
(q)  $M_{\perp} = 25$  to 40;  $\frac{P_{t,c}}{P_{t,i}} = 0.3$  to 0.7.

Figure 3.- Continued.



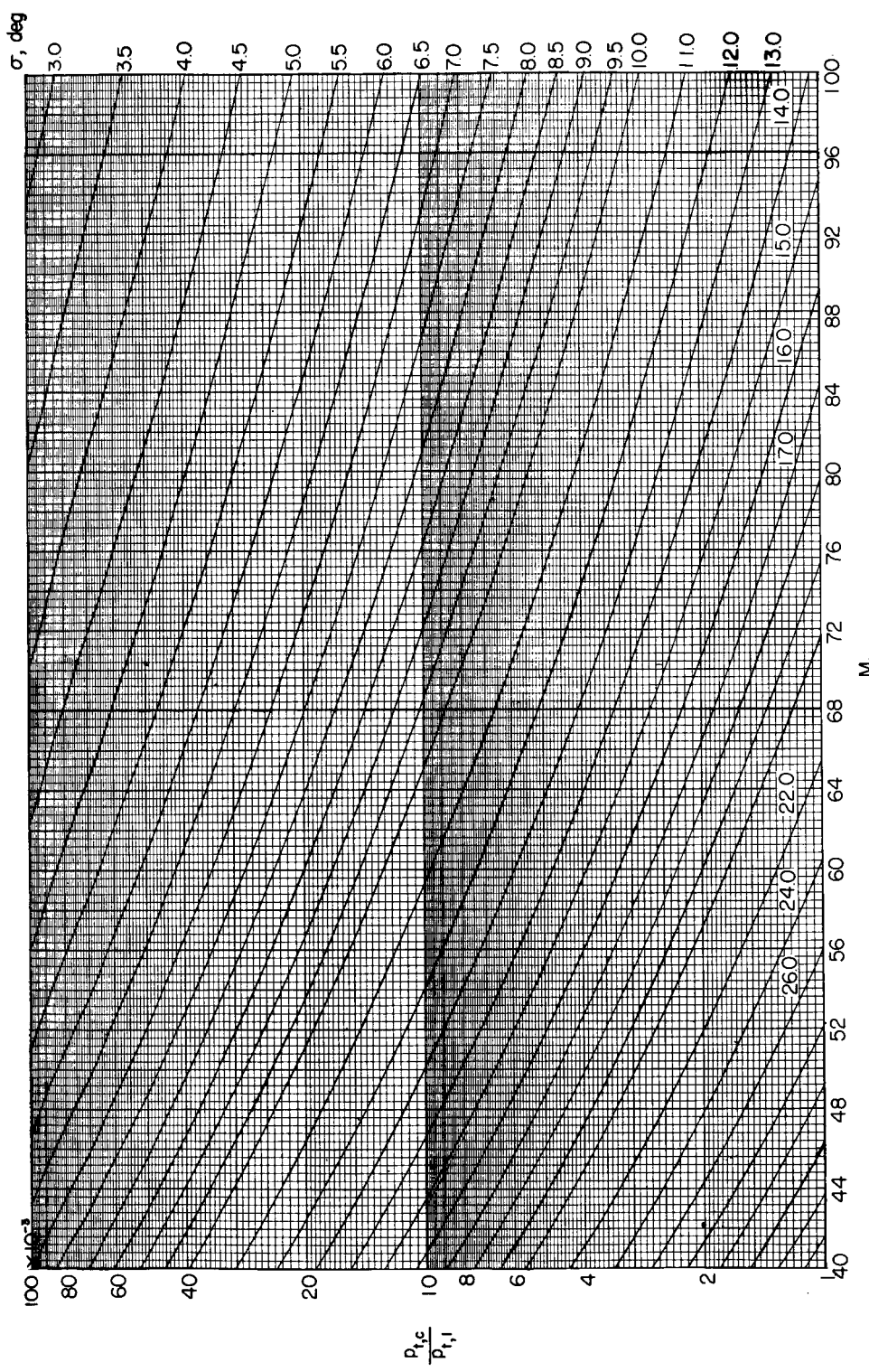
(r)  $M_1 = 25$  to 40;  $\frac{P_{t,c}}{P_{t,1}} = 0.7$  to 1.

Figure 3.- Continued.



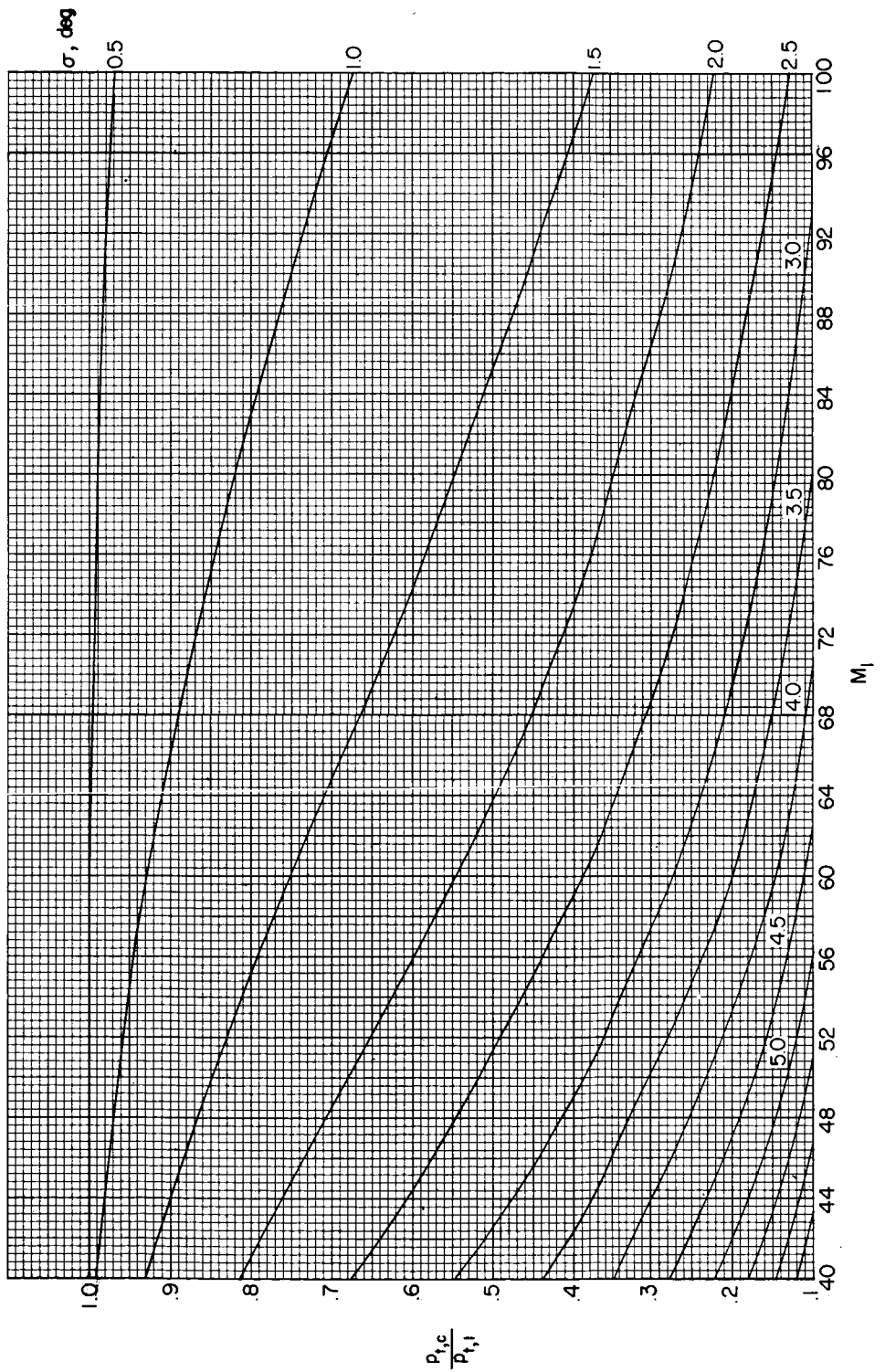
(s)  $M_1 = 40$  to  $100$ ;  $\frac{p_{t,c}}{p_{t,1}} = 1 \times 10^{-5}$  to  $100 \times 10^{-5}$ .

Figure 3.- Continued.



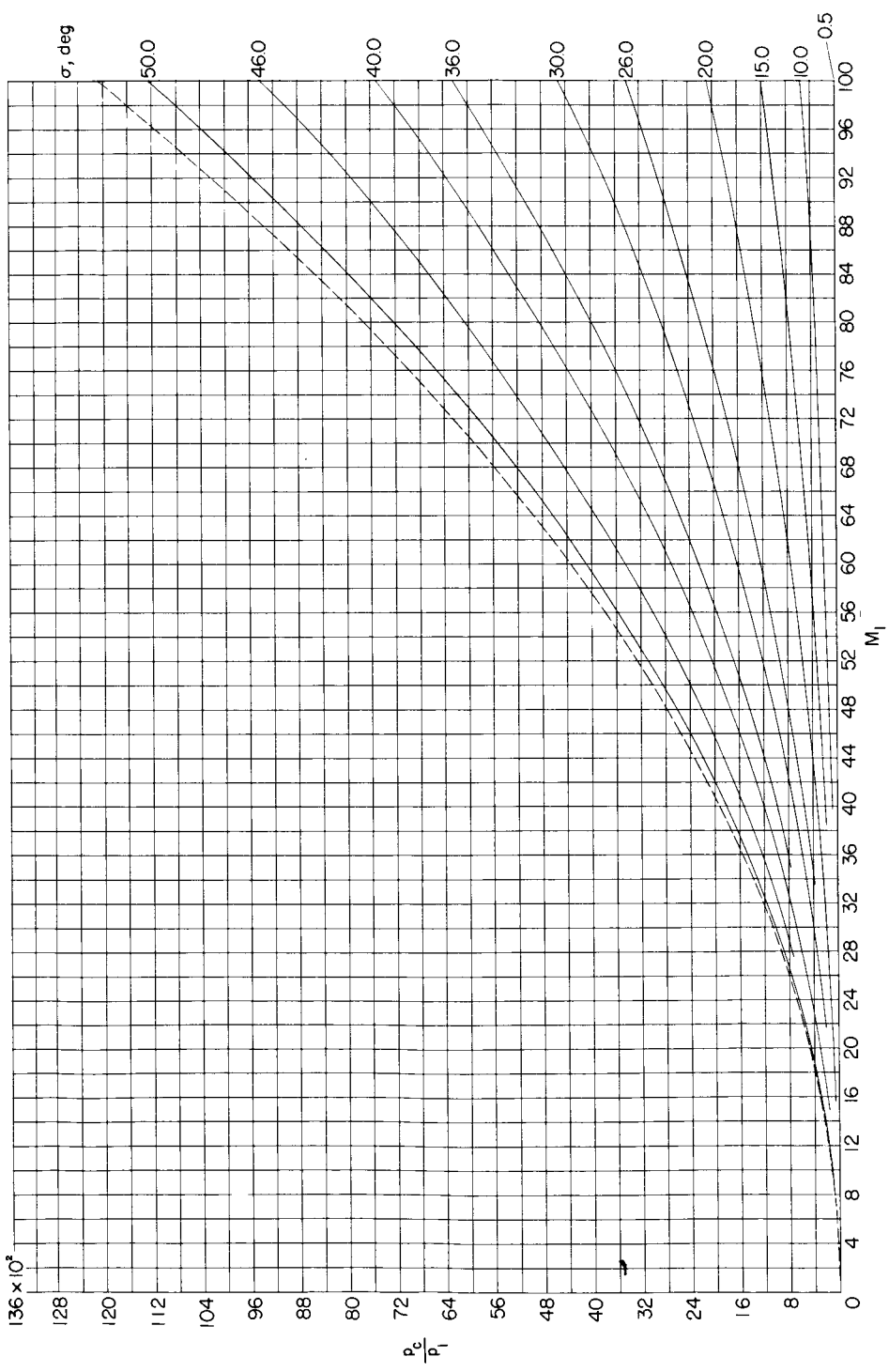
(t)  $M_1 = 40$  to  $100$ ;  $\frac{p_{t,c}}{p_{t,1}} = 1 \times 10^{-3}$  to  $100 \times 10^{-3}$ .

Figure 3.- Continued.



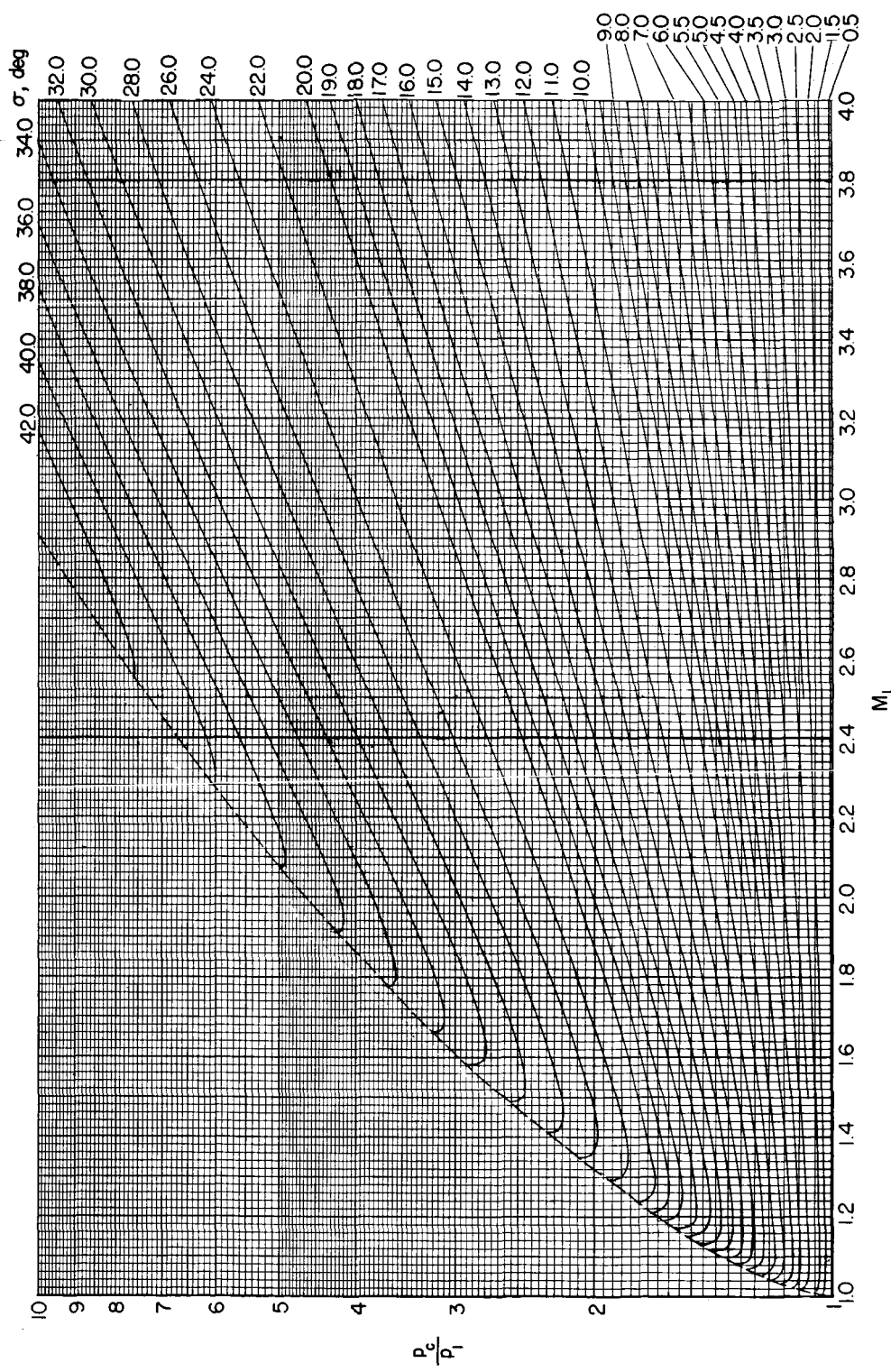
(u)  $M_{1\perp} = 40$  to 100;  $\frac{P_{t,c}}{P_{t,i}} = 0.1$  to 1.

Figure 3.- Concluded.



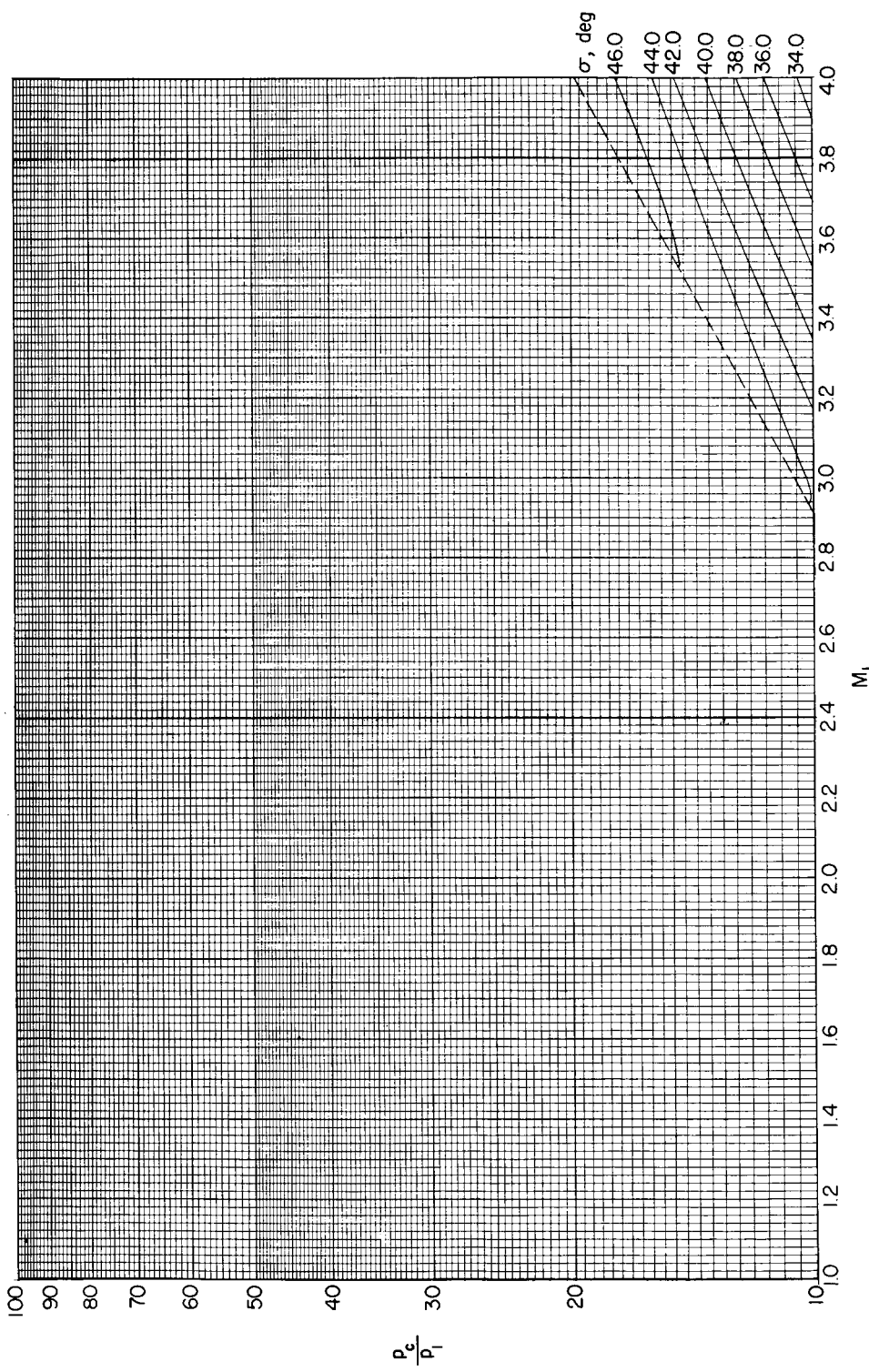
(a)  $M_1 = 1$  to 100;  $p_c/p_1 = 0$  to  $136 \times 10^2$ .

Figure 4.- Variation of ratio of cone surface static pressure to free-stream static pressure with free-stream Mach number. (Dashed line denotes limit of weak shock solution.)



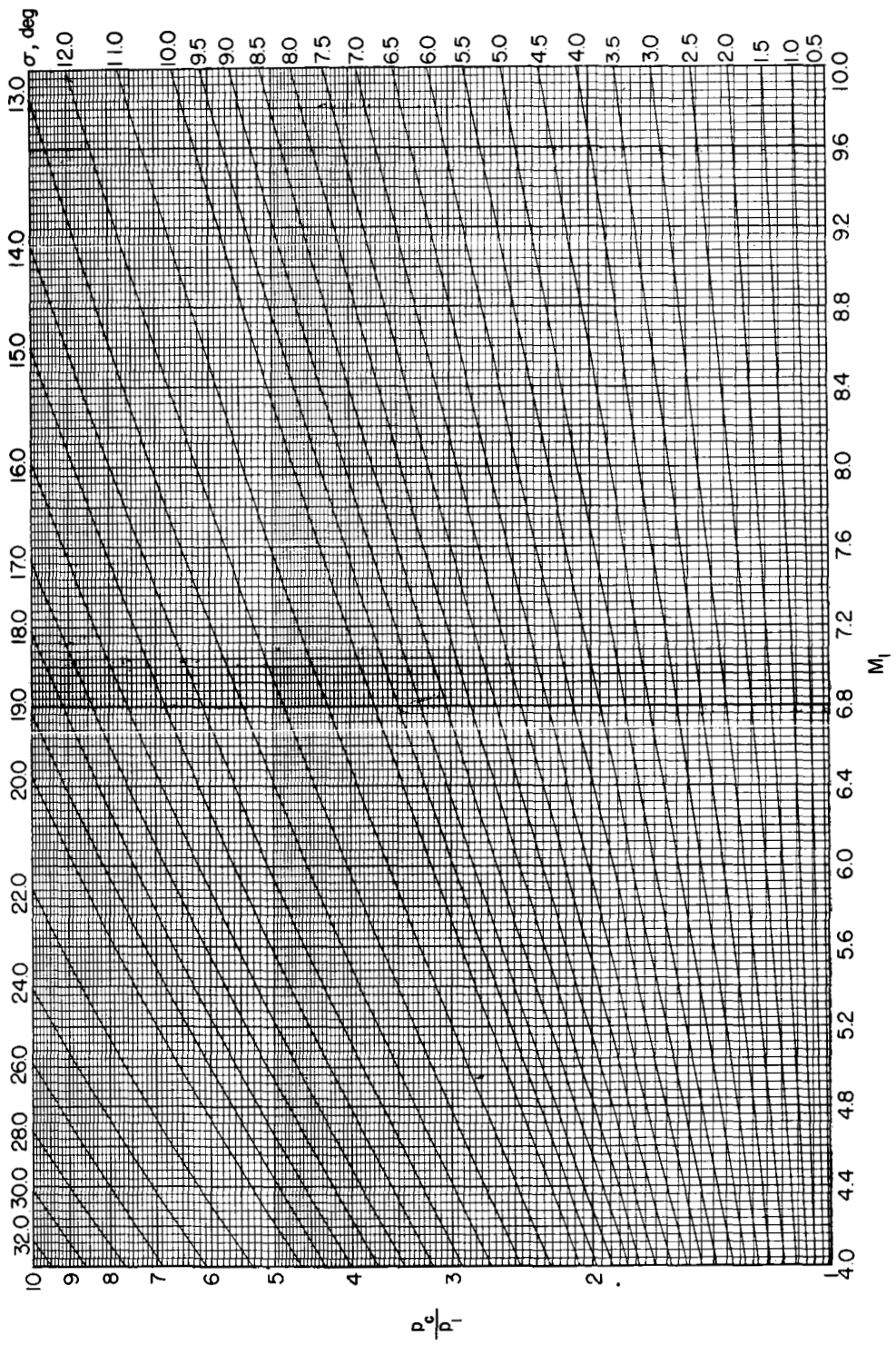
(b)  $M_1 = 1$  to 4;  $p_c/p_1 = 1$  to 10.

Figure 4. - Continued.



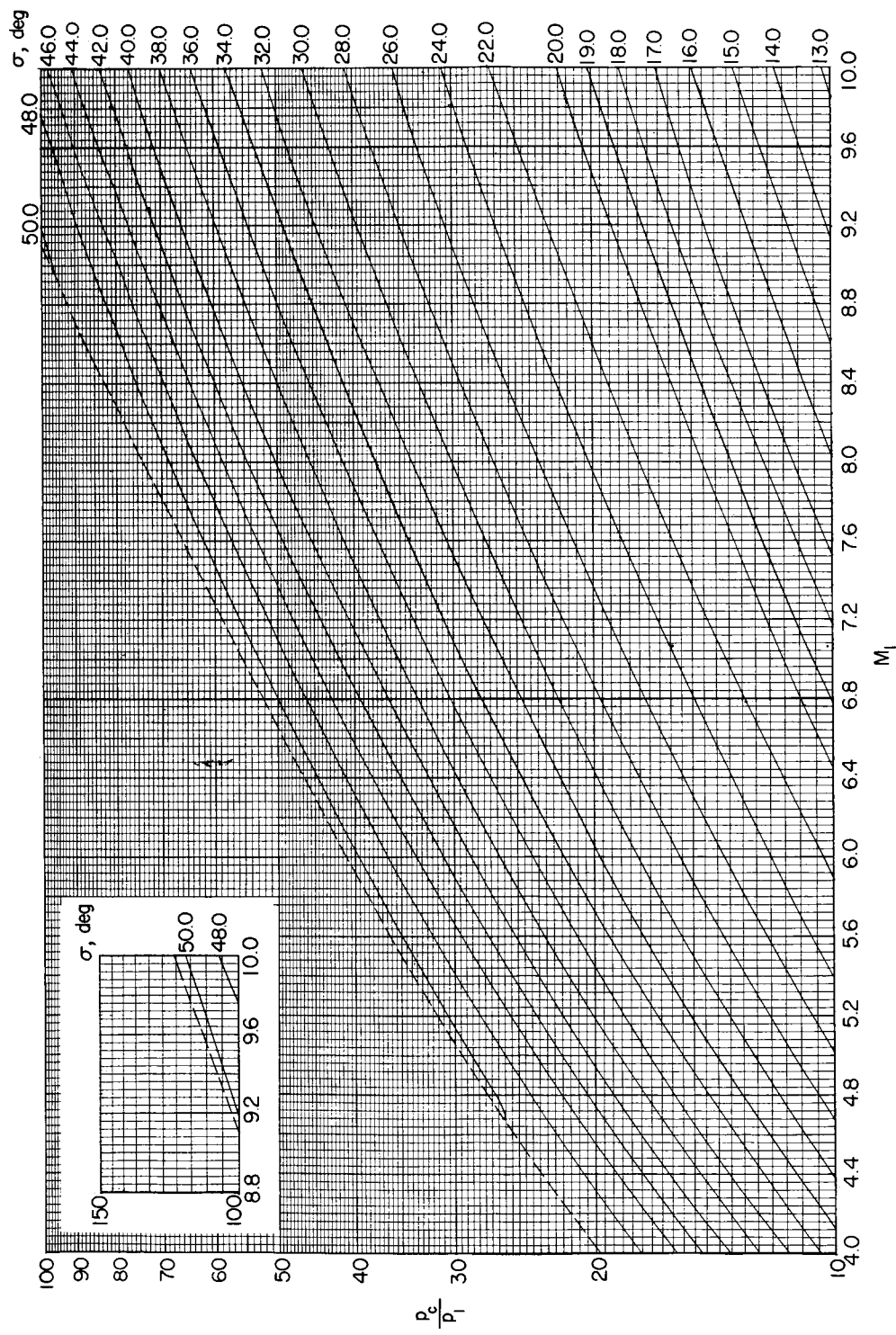
(c)  $M_1 = 1$  to 4;  $P_e/P_1 = 10$  to 100.

Figure 4.- Continued.



(d)  $M_1 = 4$  to 10;  $p_c/p_1 = 1$  to 10.

Figure 4.- Continued.



(e)  $M_1 = 4$  to 10;  $p_e/p_1 = 10$  to 100.

Figure 4.- Continued.

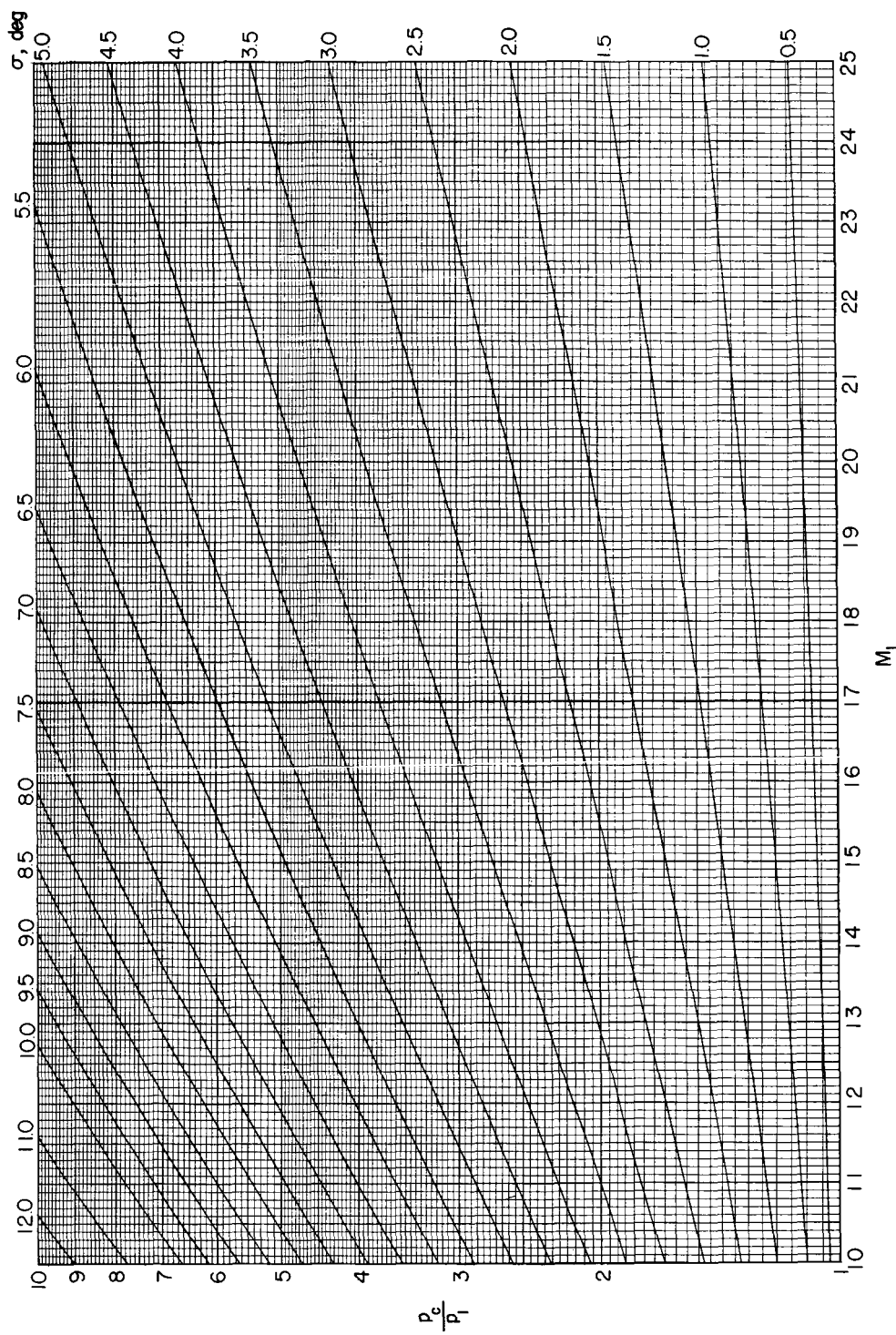
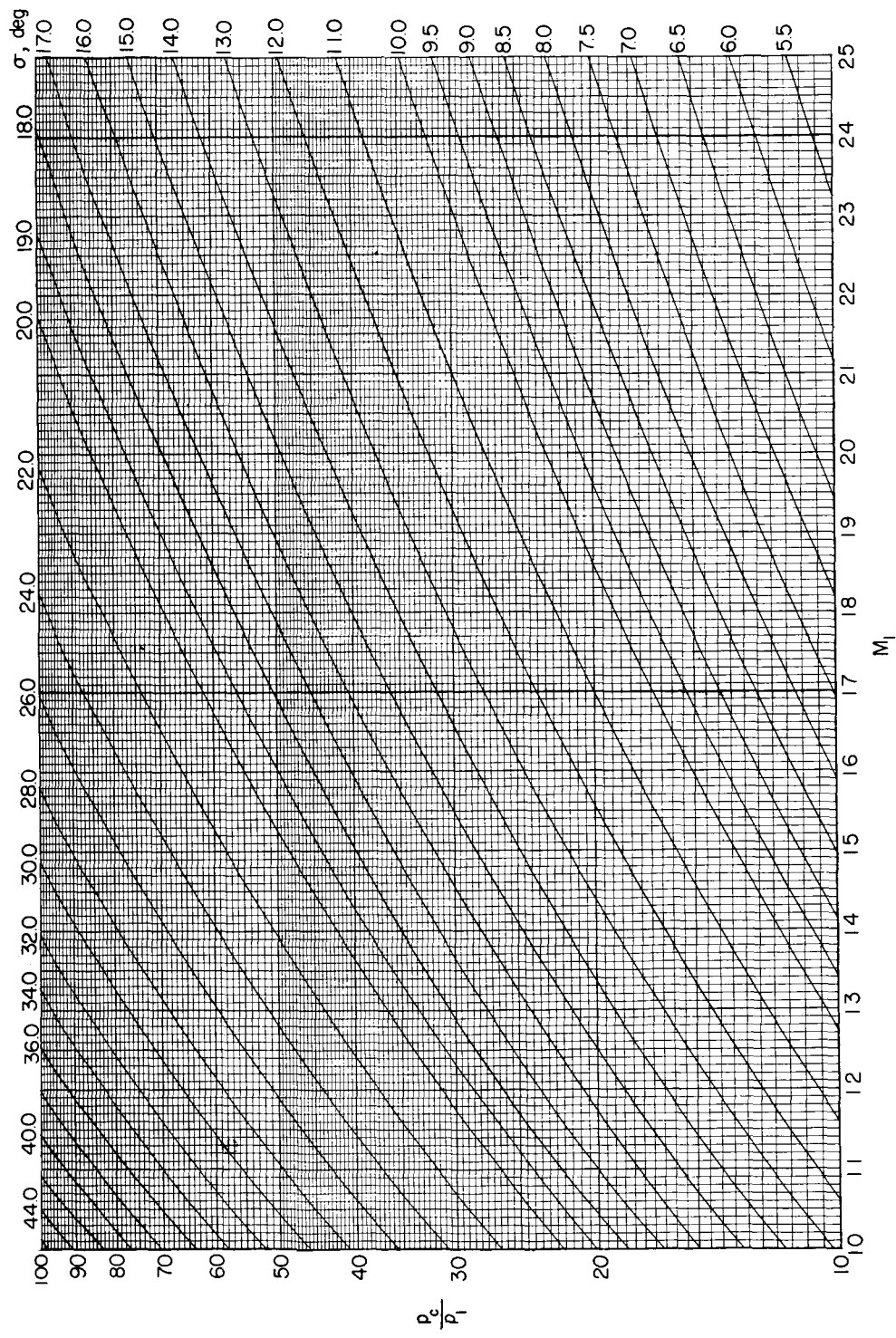
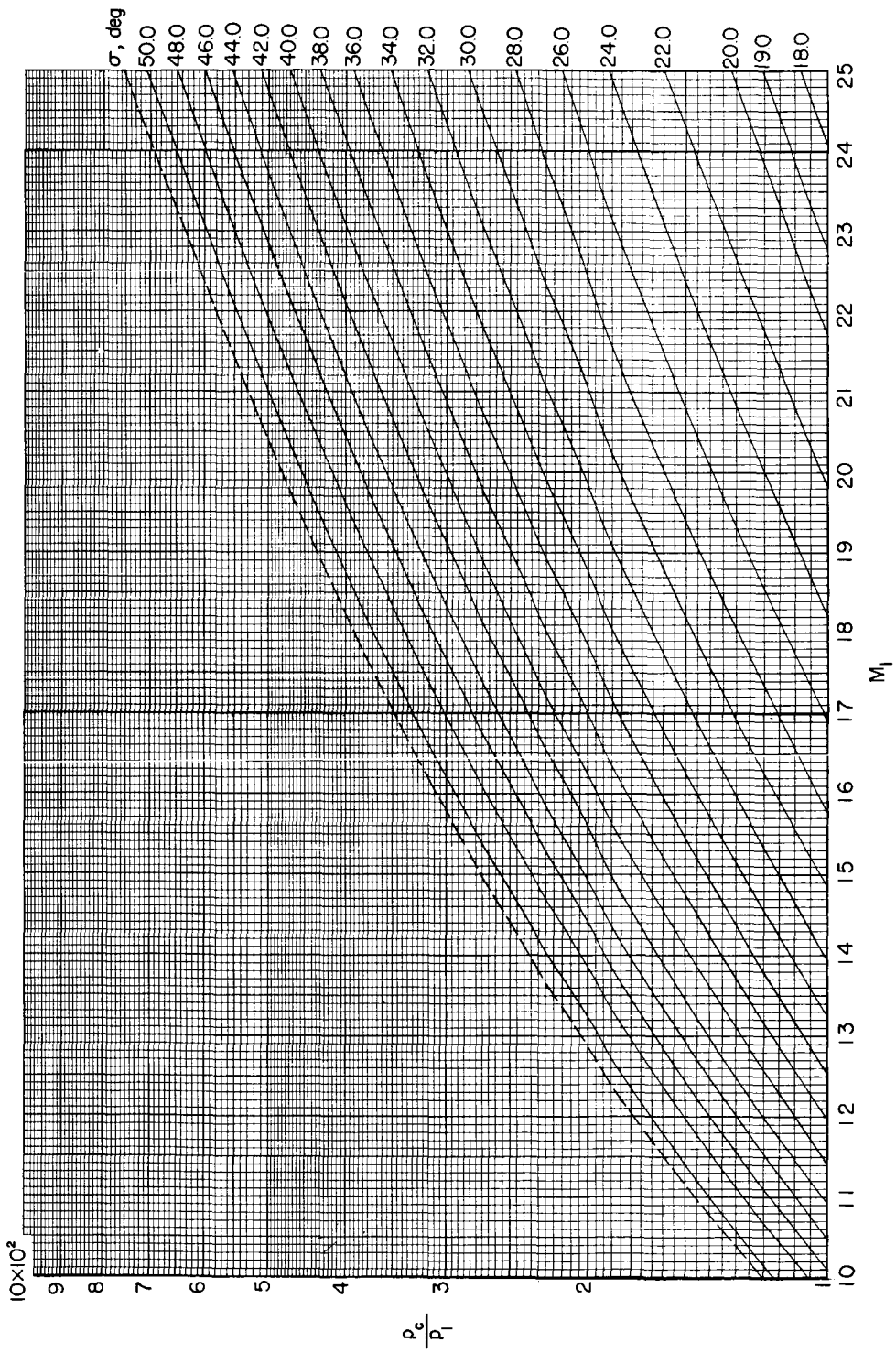
(f)  $M_1 = 10$  to  $25$ ;  $p_c/p_1 = 1$  to  $10$ .

Figure 4.- Continued.



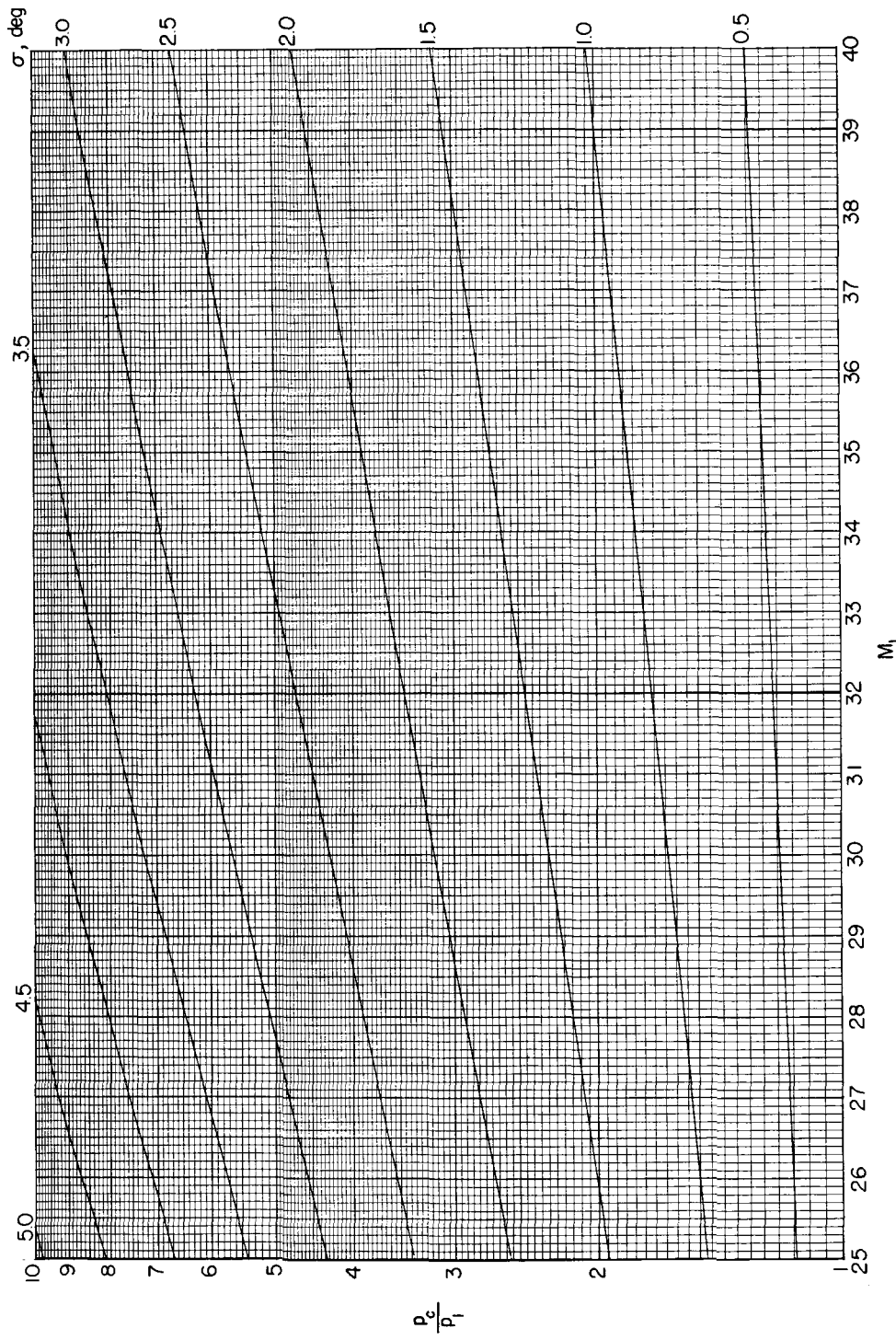
(g)  $M_1 = 10$  to  $25$ ;  $P_c/P_1 = 10$  to  $100$ .

Figure 4.- Continued.



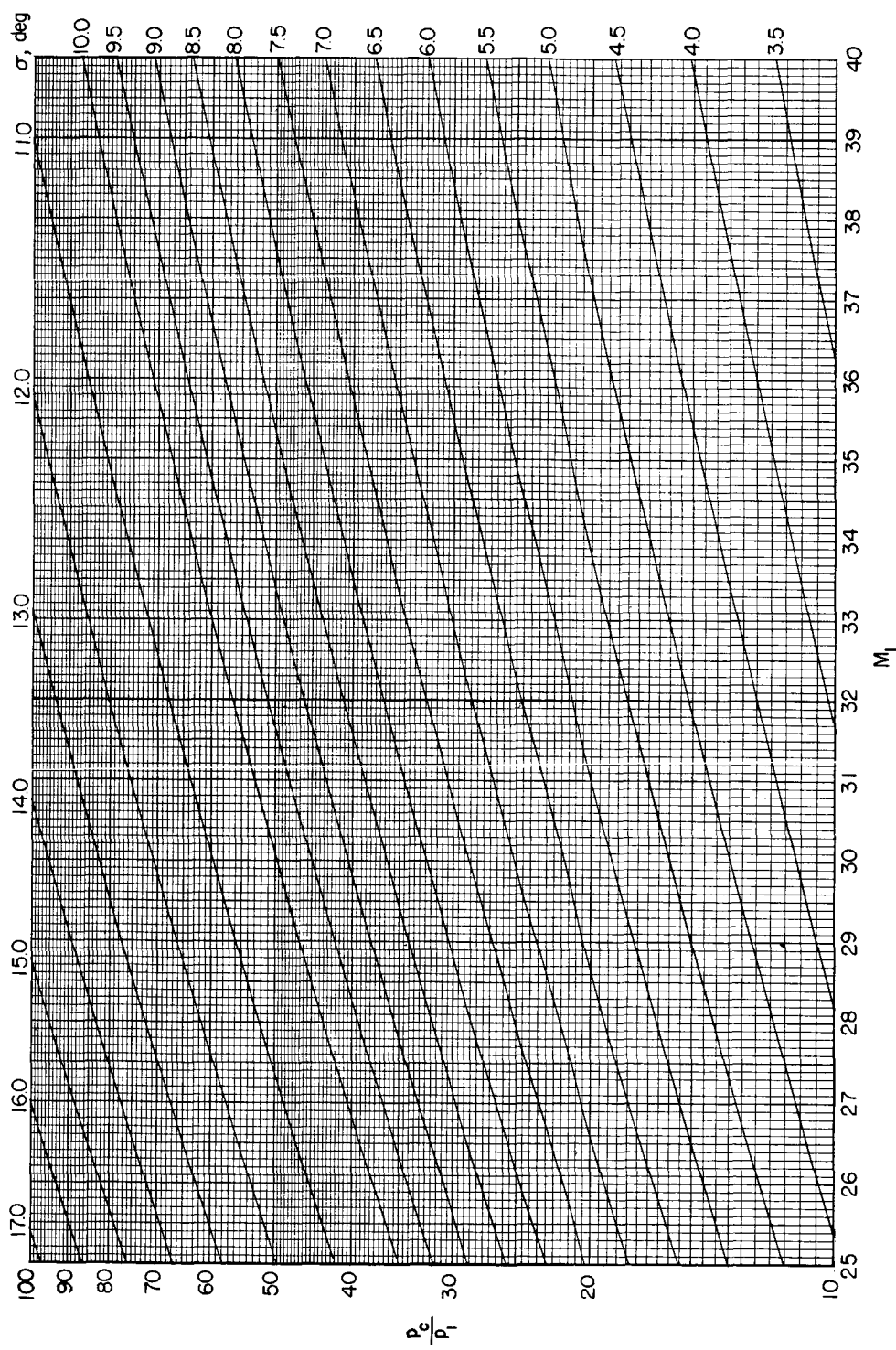
(h)  $M_1 = 10$  to 25;  $P_c/P_1 = 1 \times 10^2$  to  $10 \times 10^2$ .

Figure 4.- Continued.



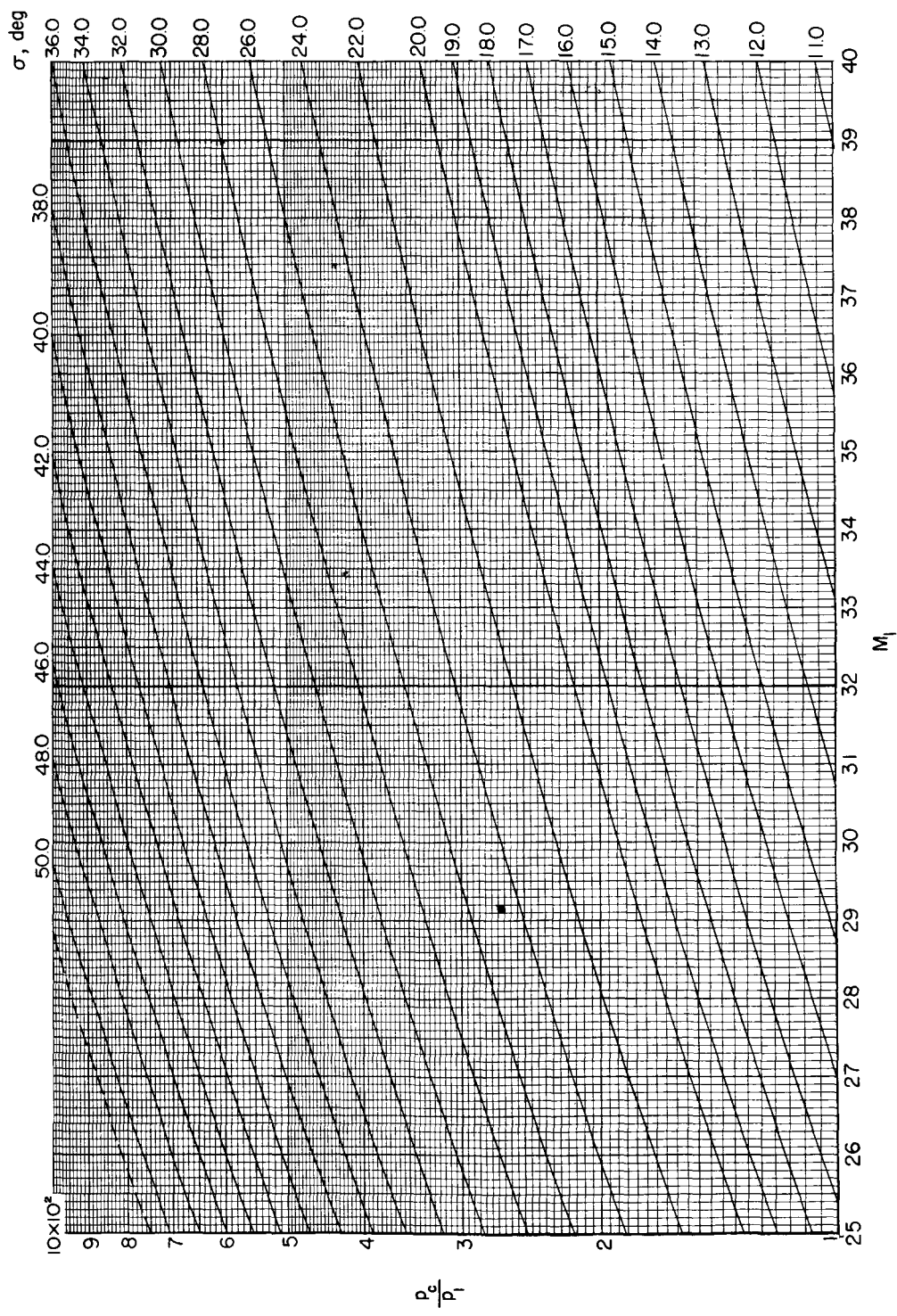
(1)  $M_1 = 25$  to 40;  $p_c/p_{\perp} = 1$  to 10.

Figure 4.- Continued.



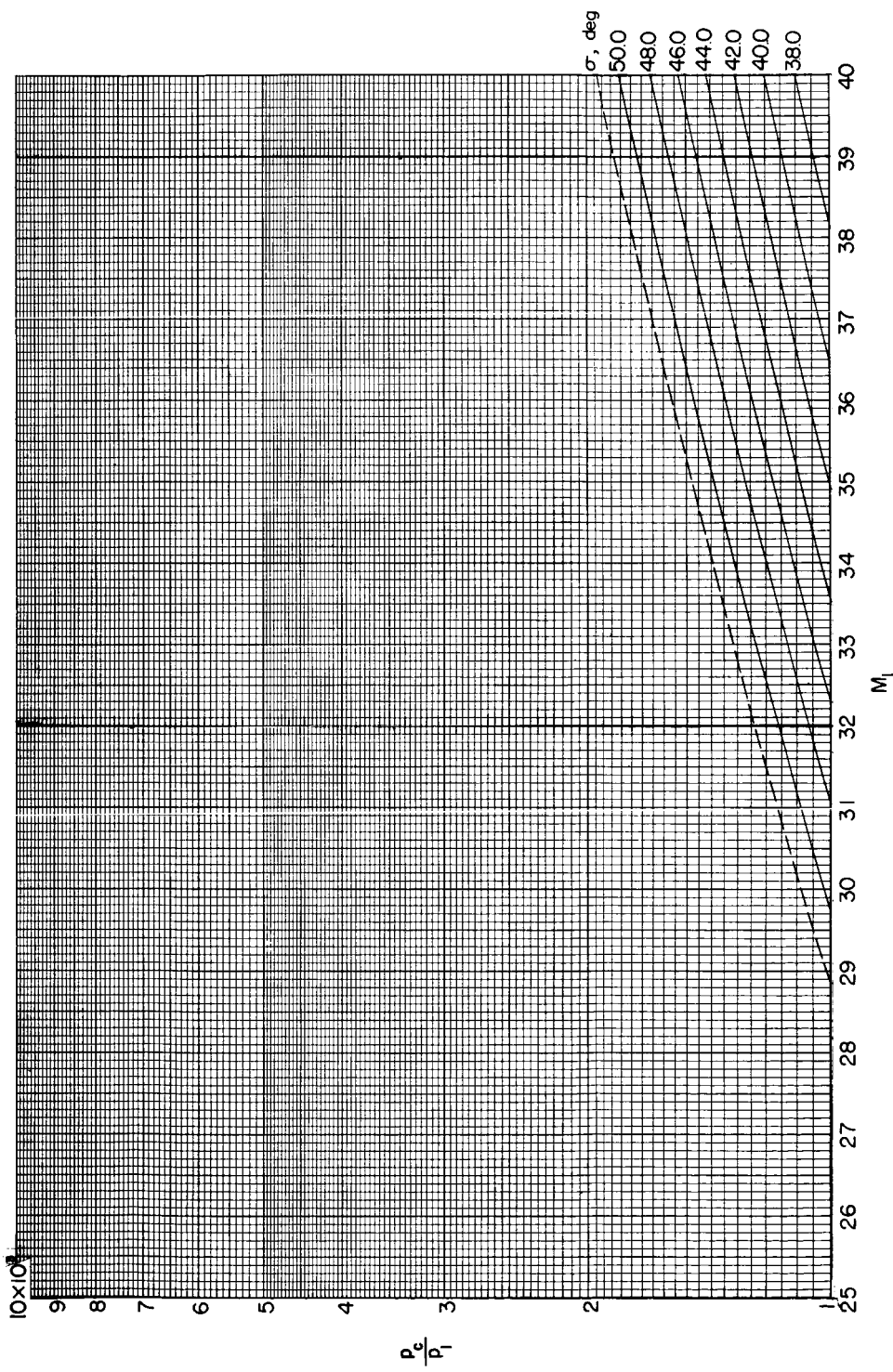
(j)  $M_1 = 25$  to 40;  $p_c/p_1 = 10$  to 100.

Figure 4.- Continued.



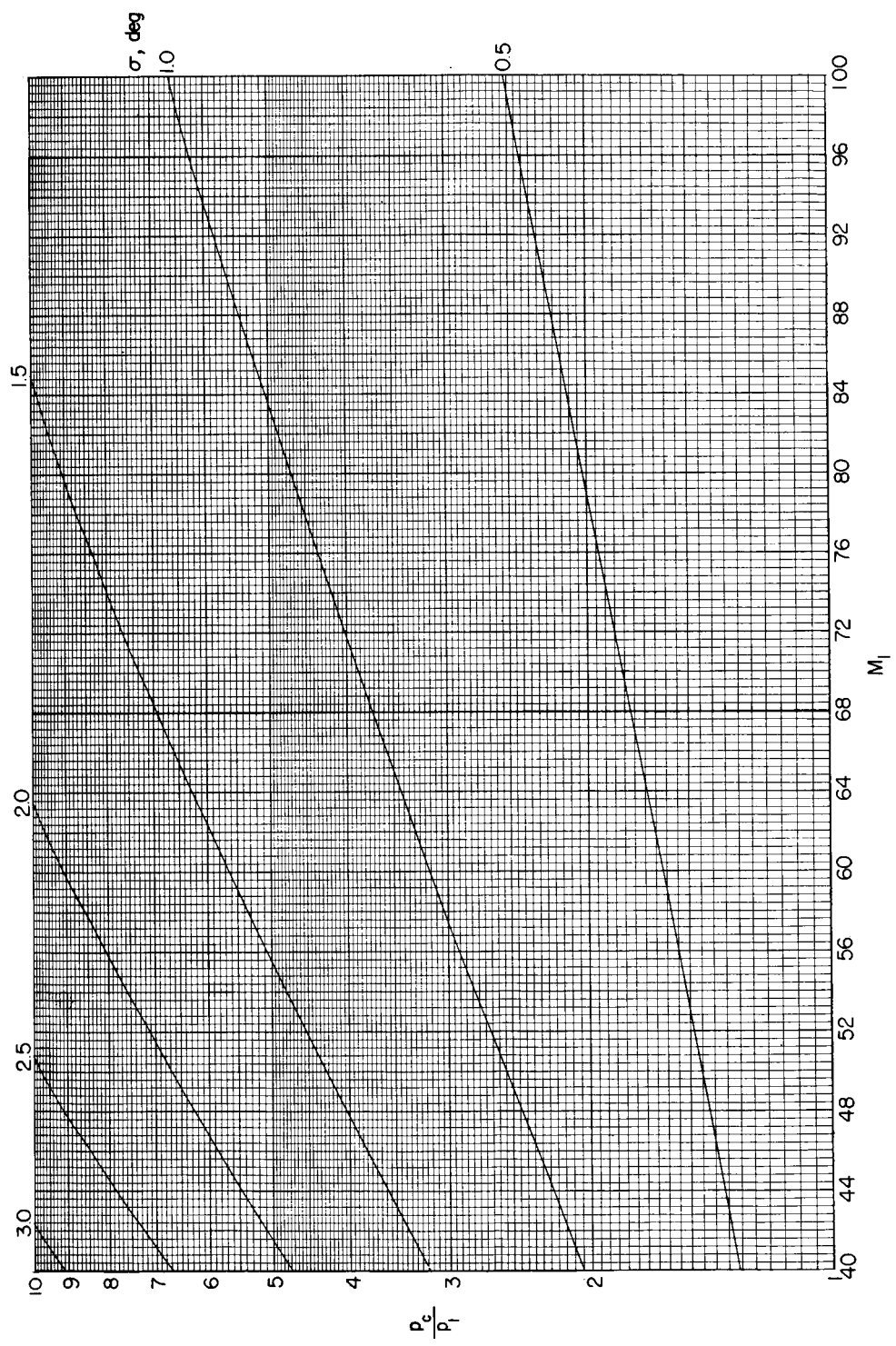
(k)  $M_1 = 25$  to 40;  $P_c/P_1 = 1 \times 10^2$  to  $10 \times 10^2$ .

Figure 4.- Continued.



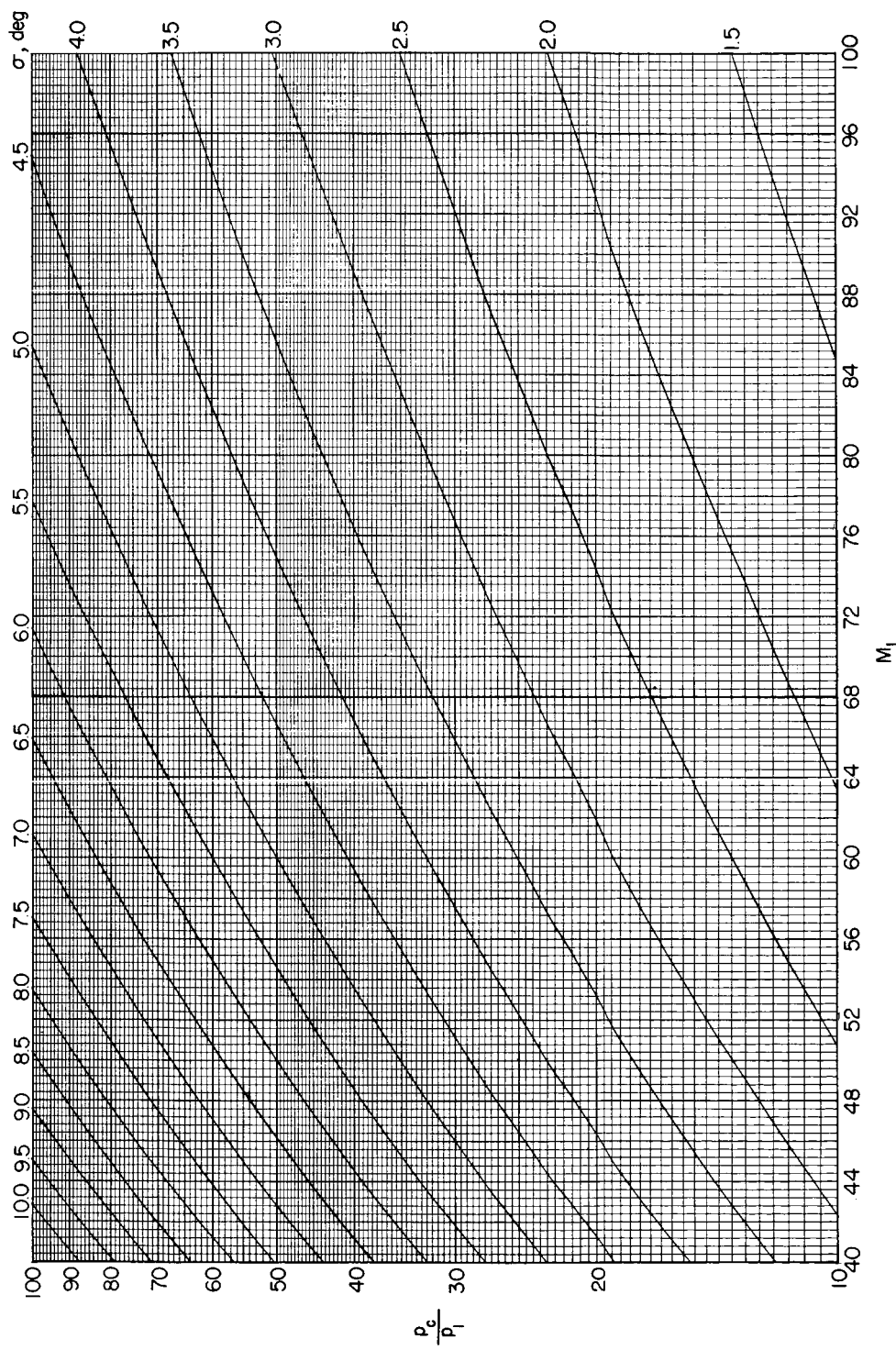
(1)  $M_{\perp} = 25$  to 40;  $p_c/p_{\perp} = 1 \times 10^3$  to  $10 \times 10^3$ .

Figure 4.- Continued.



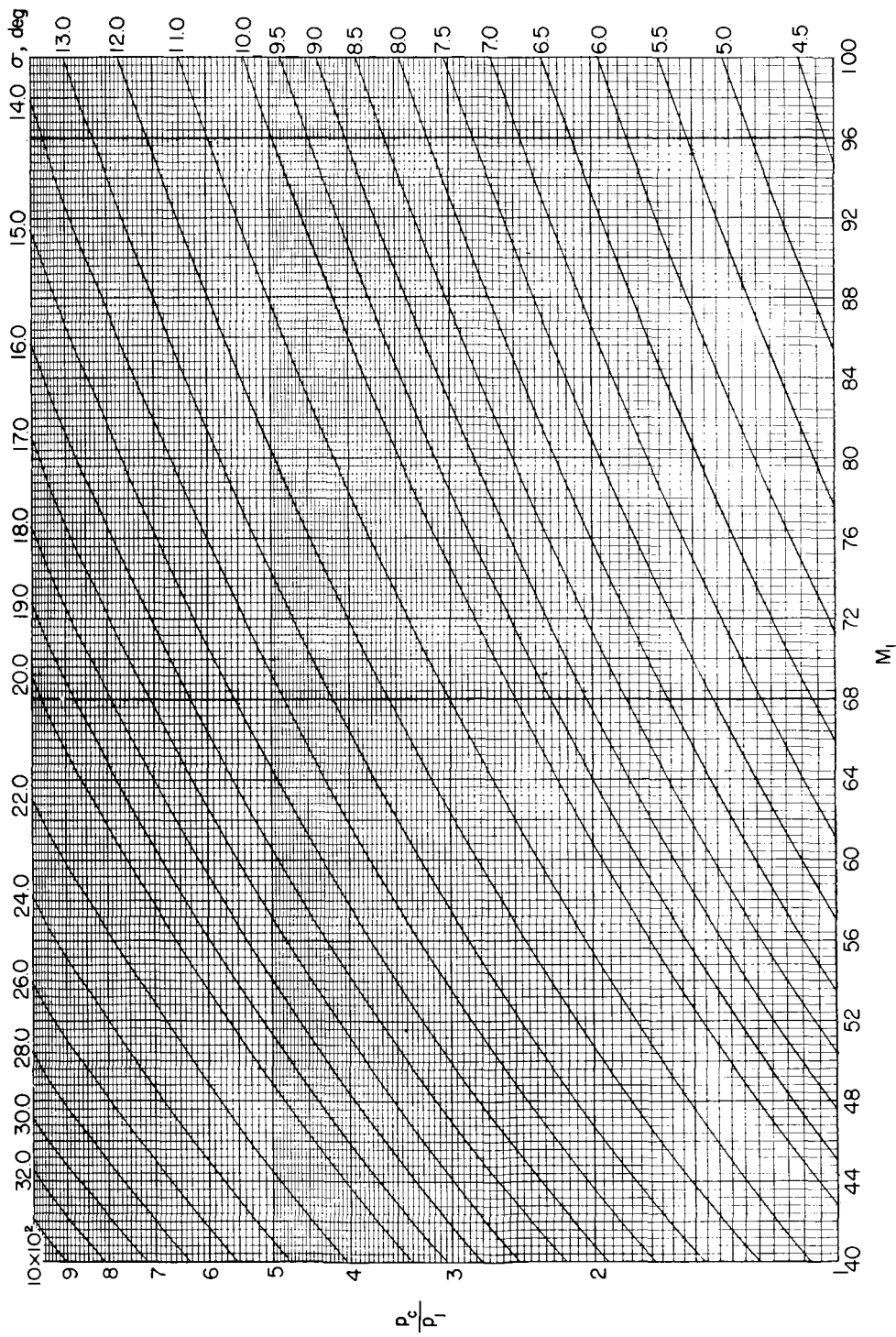
(m)  $M_1 = 40$  to 100;  $p_c/p_1 = 1$  to 10.

Figure 4.- Continued.



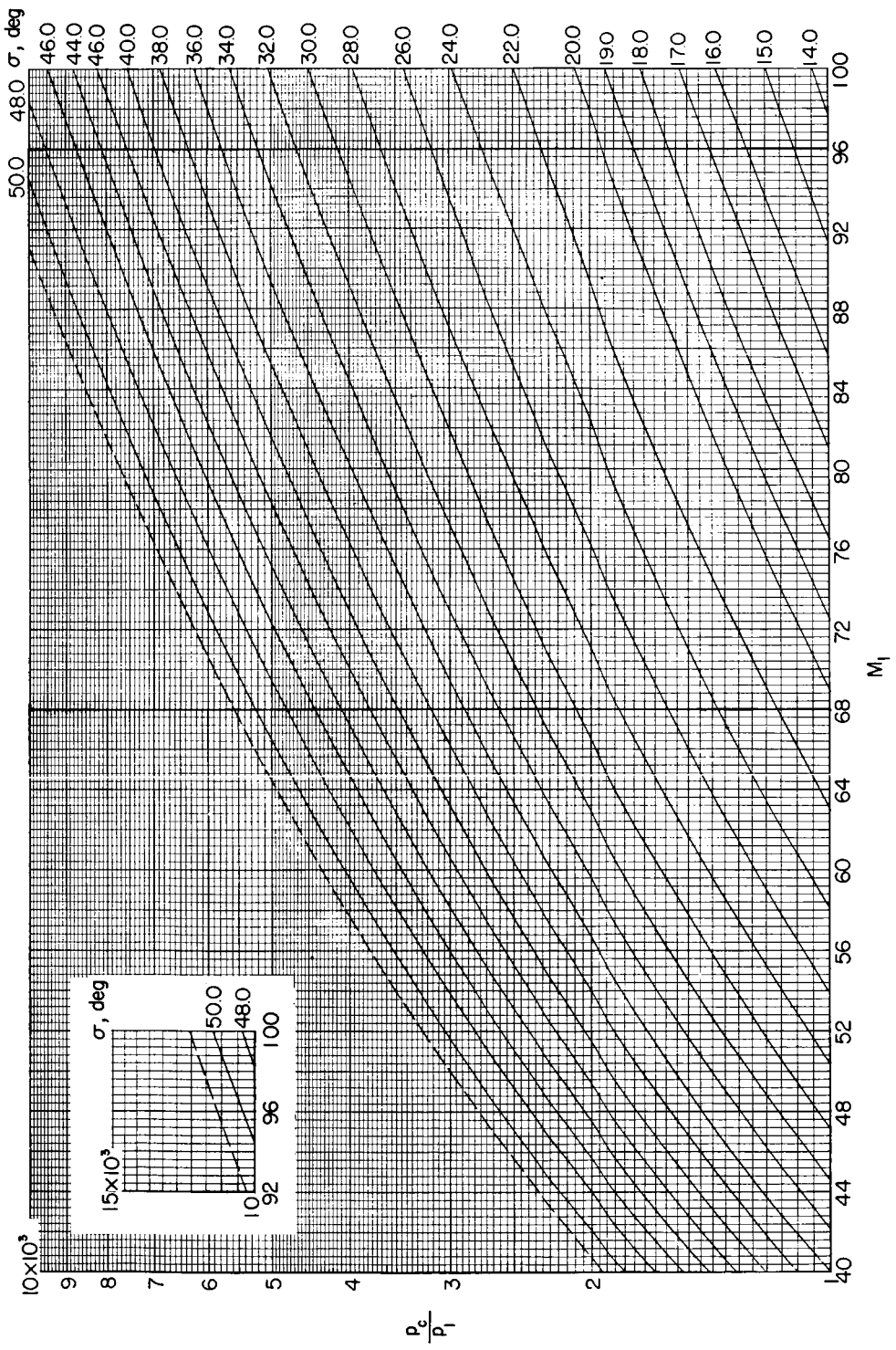
(n)  $M_1 = 40$  to 100;  $p_c/p_1 = 10$  to 100.

Figure 4.- Continued.



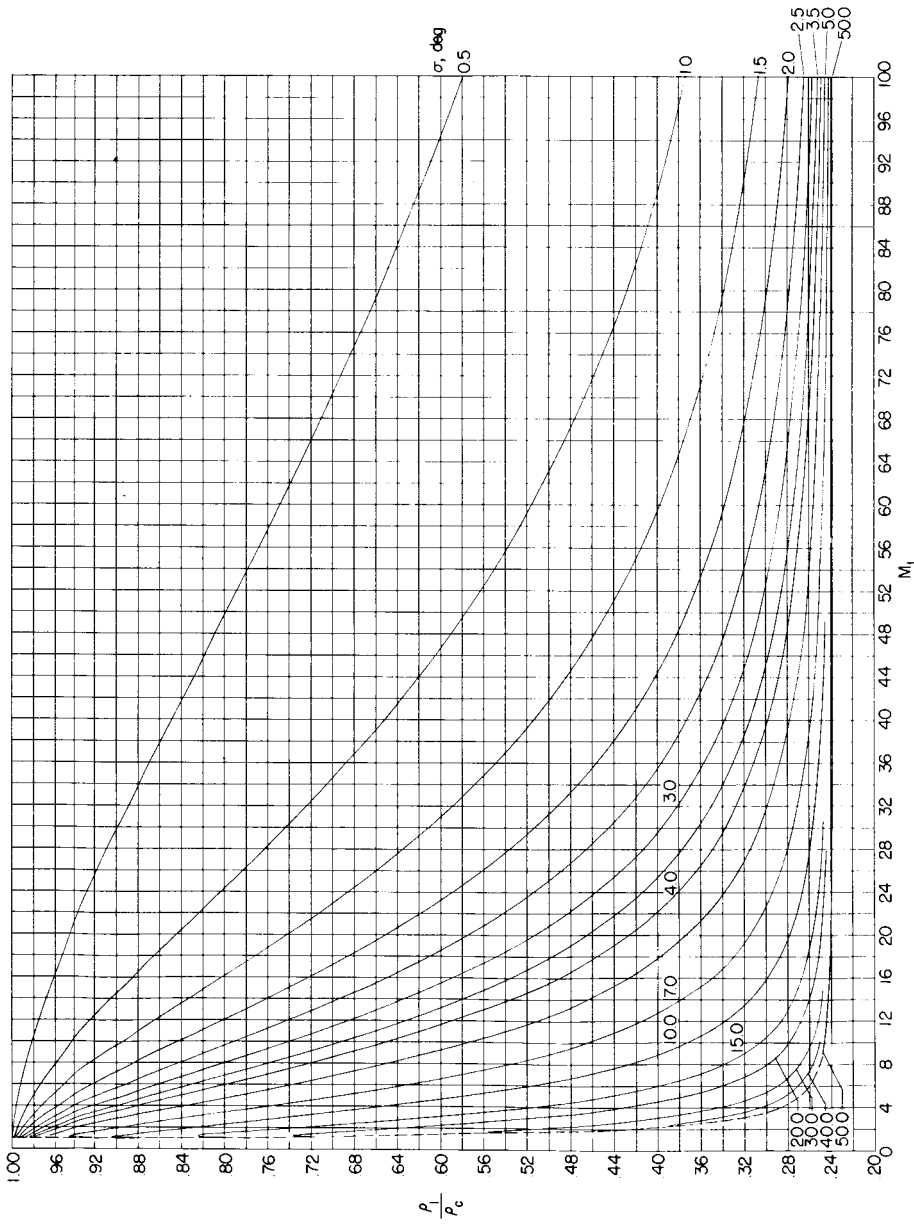
(o)  $M_1 = 40$  to  $100$ ;  $p_c/p_1 = 1 \times 10^2$  to  $10 \times 10^2$ .

Figure 4.- Continued.



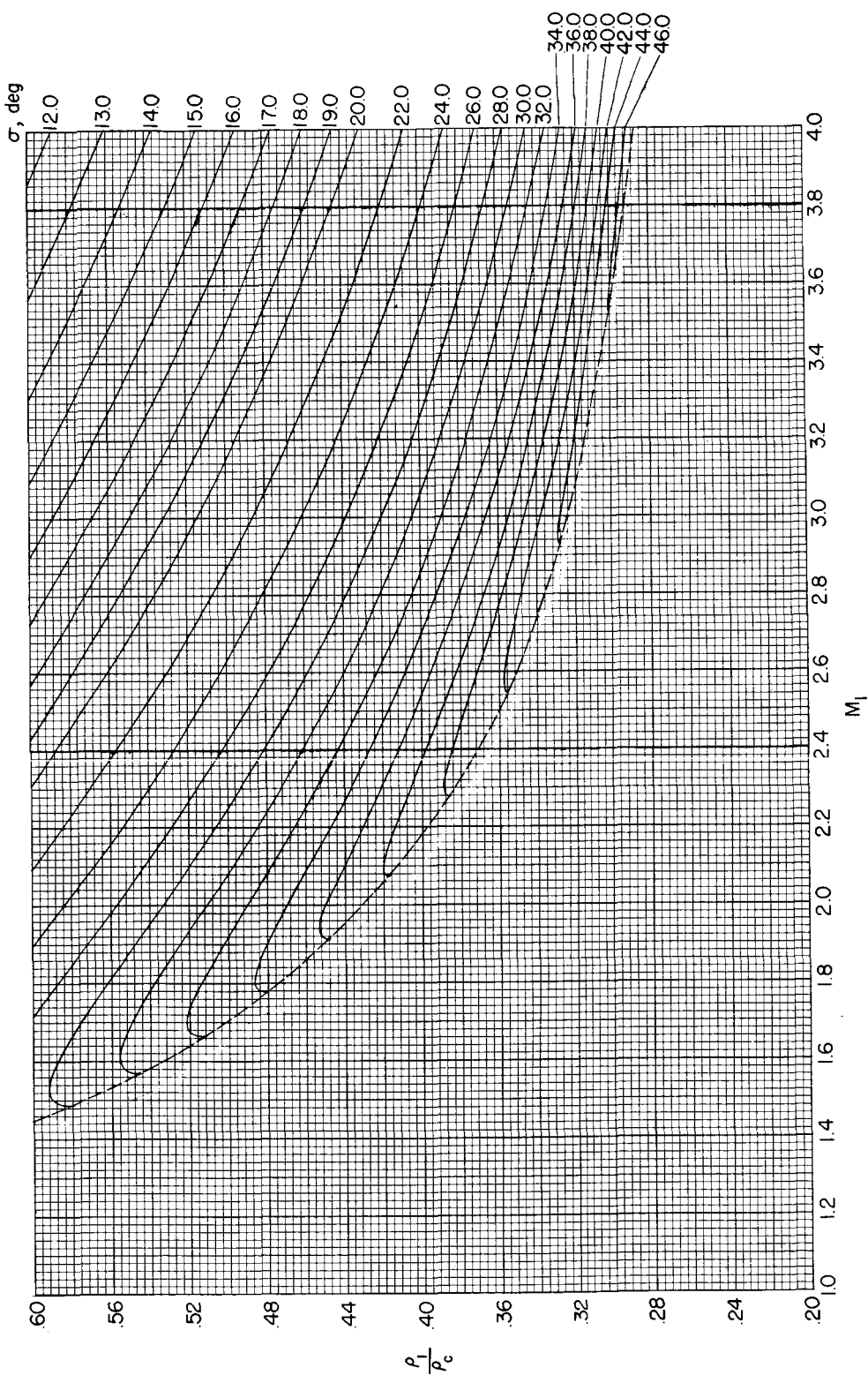
(p)  $M_1 = 40 \text{ to } 100; p_c/p_1 = 1 \times 10^3 \text{ to } 10 \times 10^3$ .

Figure 4.- Concluded.



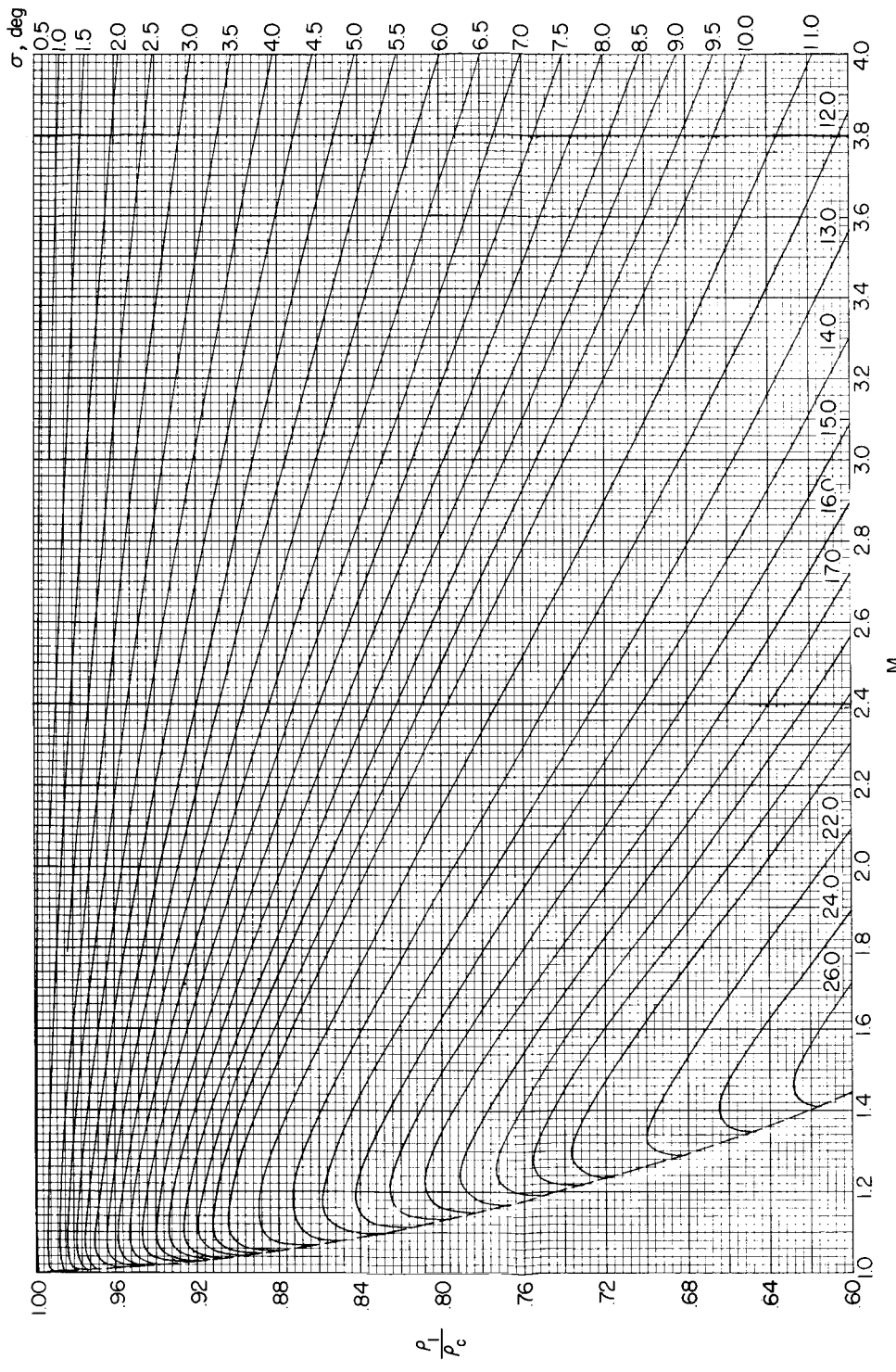
(a)  $M_1 = 1$  to 100;  $\rho_1/\rho_c = 0.2$  to 1.

Figure 5.- Variation of ratio of free-stream static density to cone surface static density with free-stream Mach number. (Dashed line denotes limit of weak shock solution.)



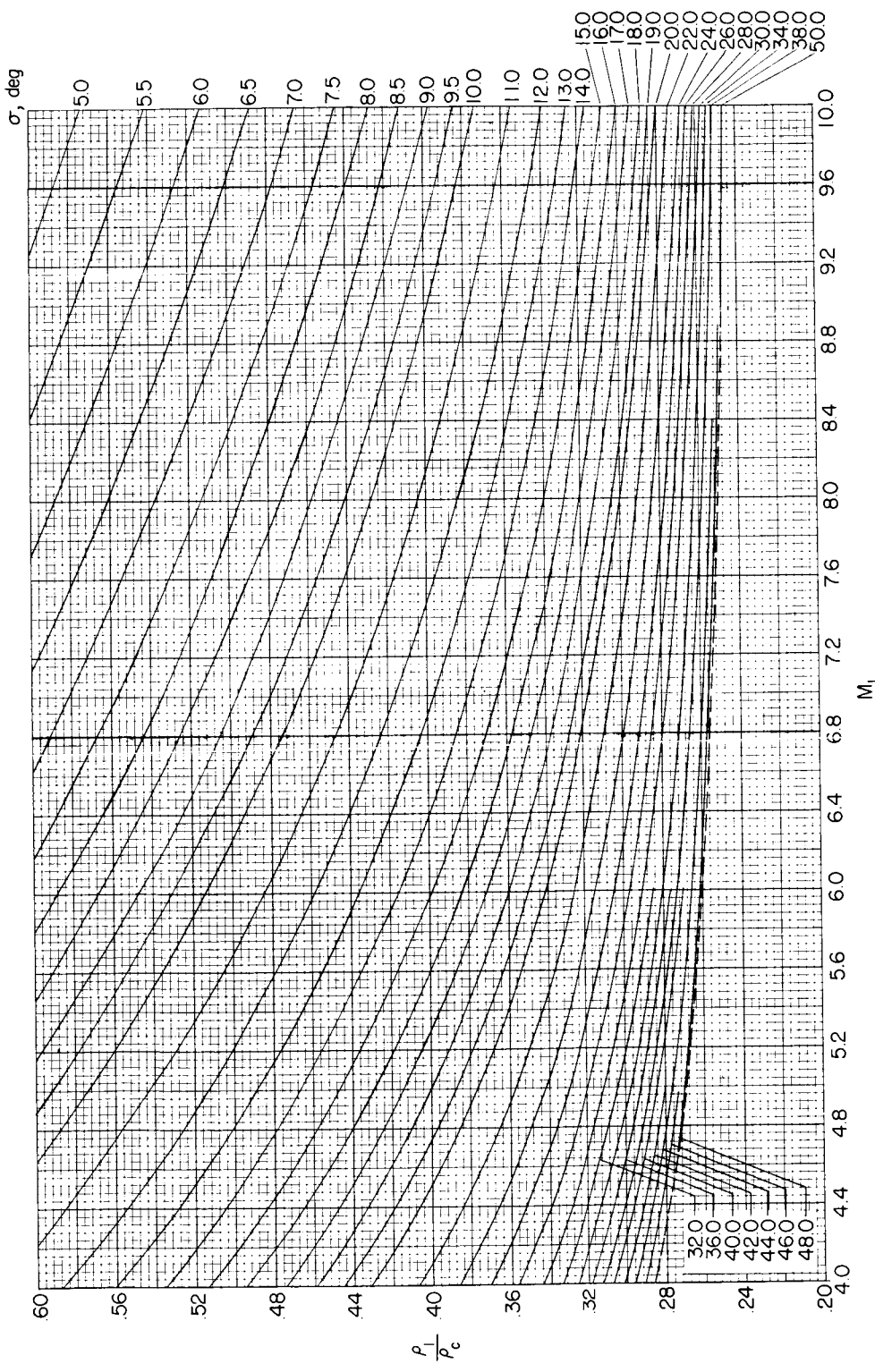
(b)  $M_1 = 1$  to 4;  $\rho_1/\rho_c = 0.2$  to 0.6.

Figure 5.- Continued.



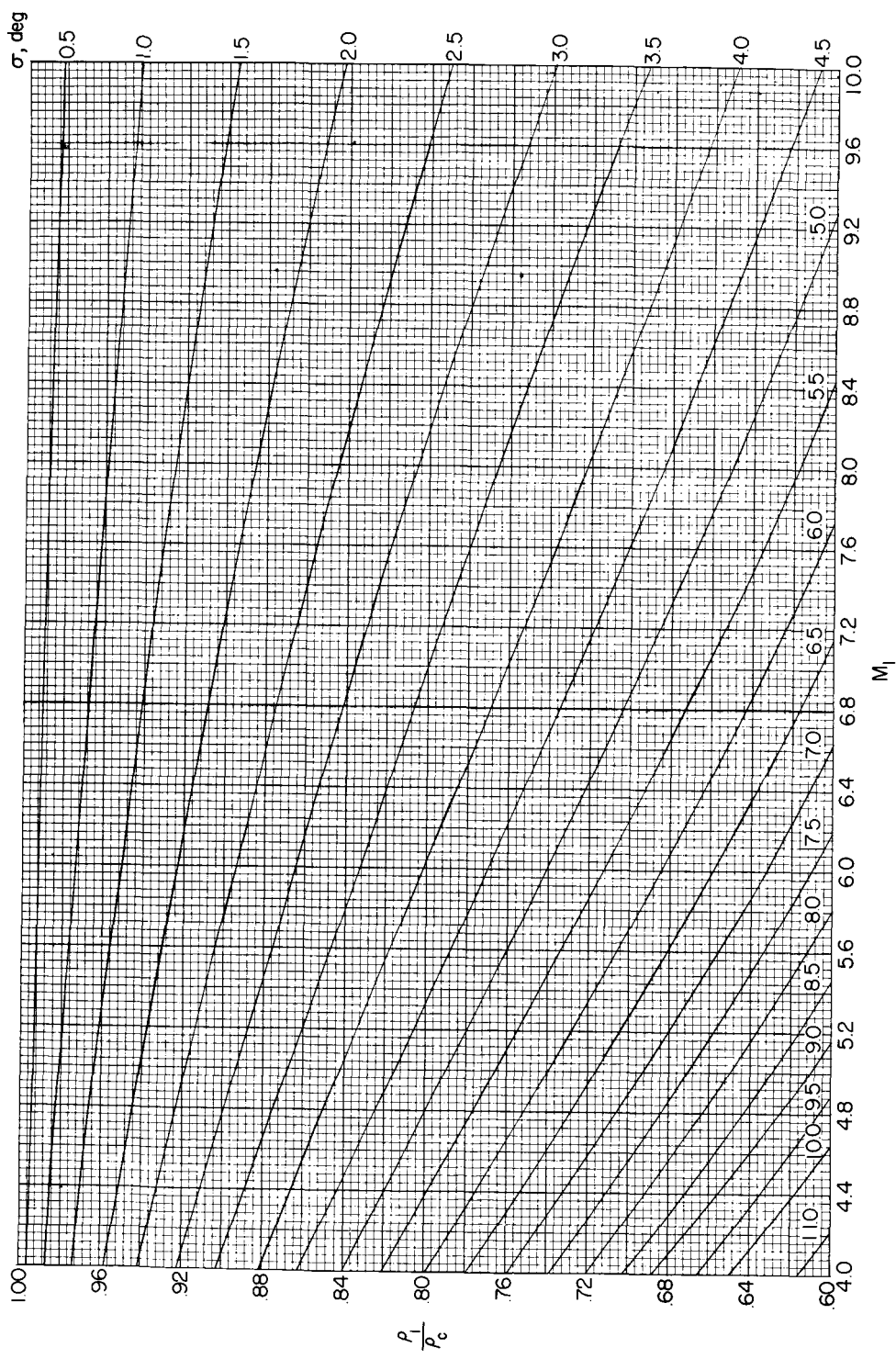
(c)  $M_1 = 1$  to 4;  $\rho_1/\rho_c = 0.6$  to 1.

Figure 5.- Continued.



(d)  $M_1 = 4$  to 10;  $\rho_1/\rho_c = 0.2$  to 0.6.

Figure 5.- Continued.



(e)  $M_1 = 4$  to 10;  $\rho_1/\rho_c = 0.6$  to 1.

Figure 5.- Continued.

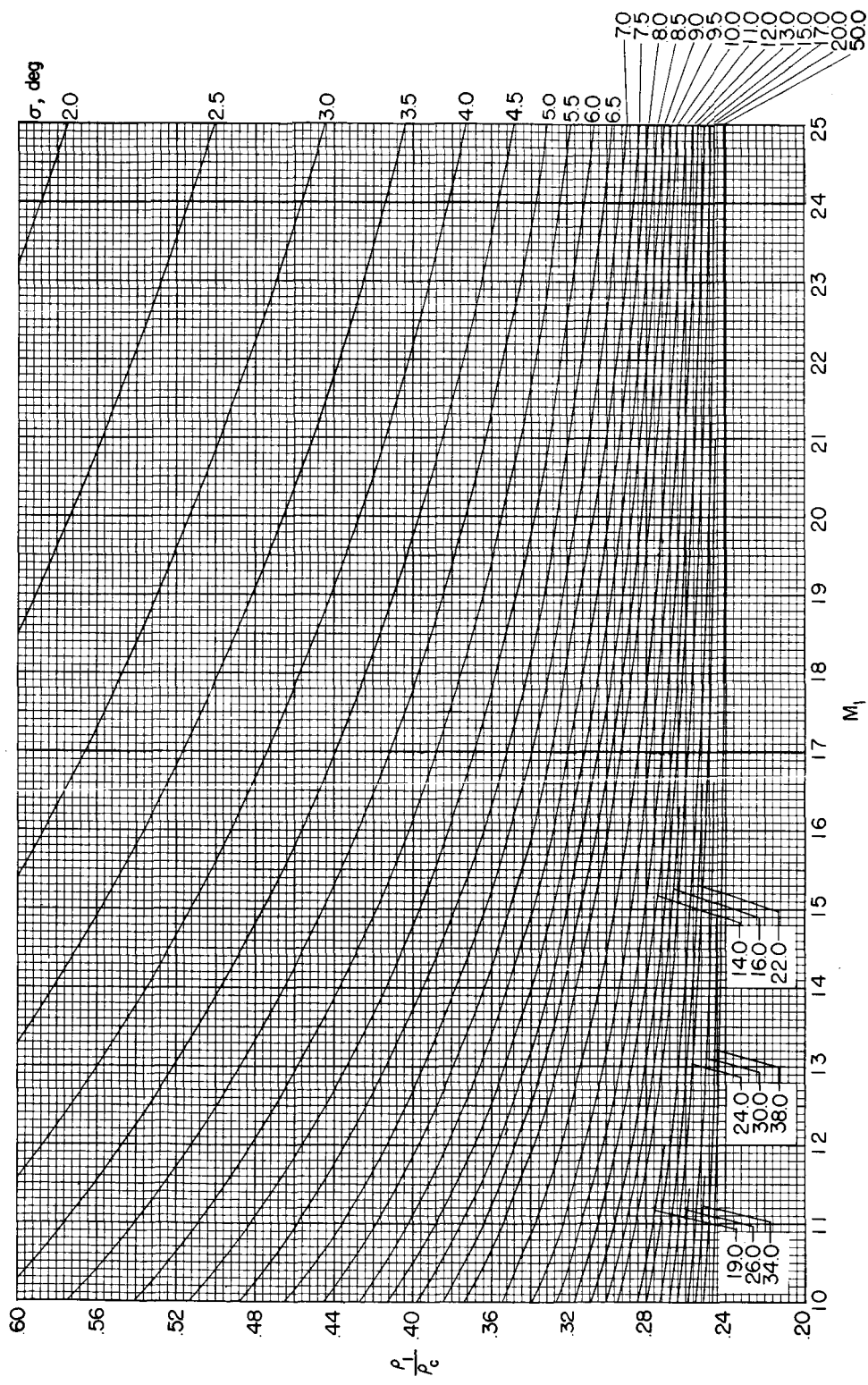
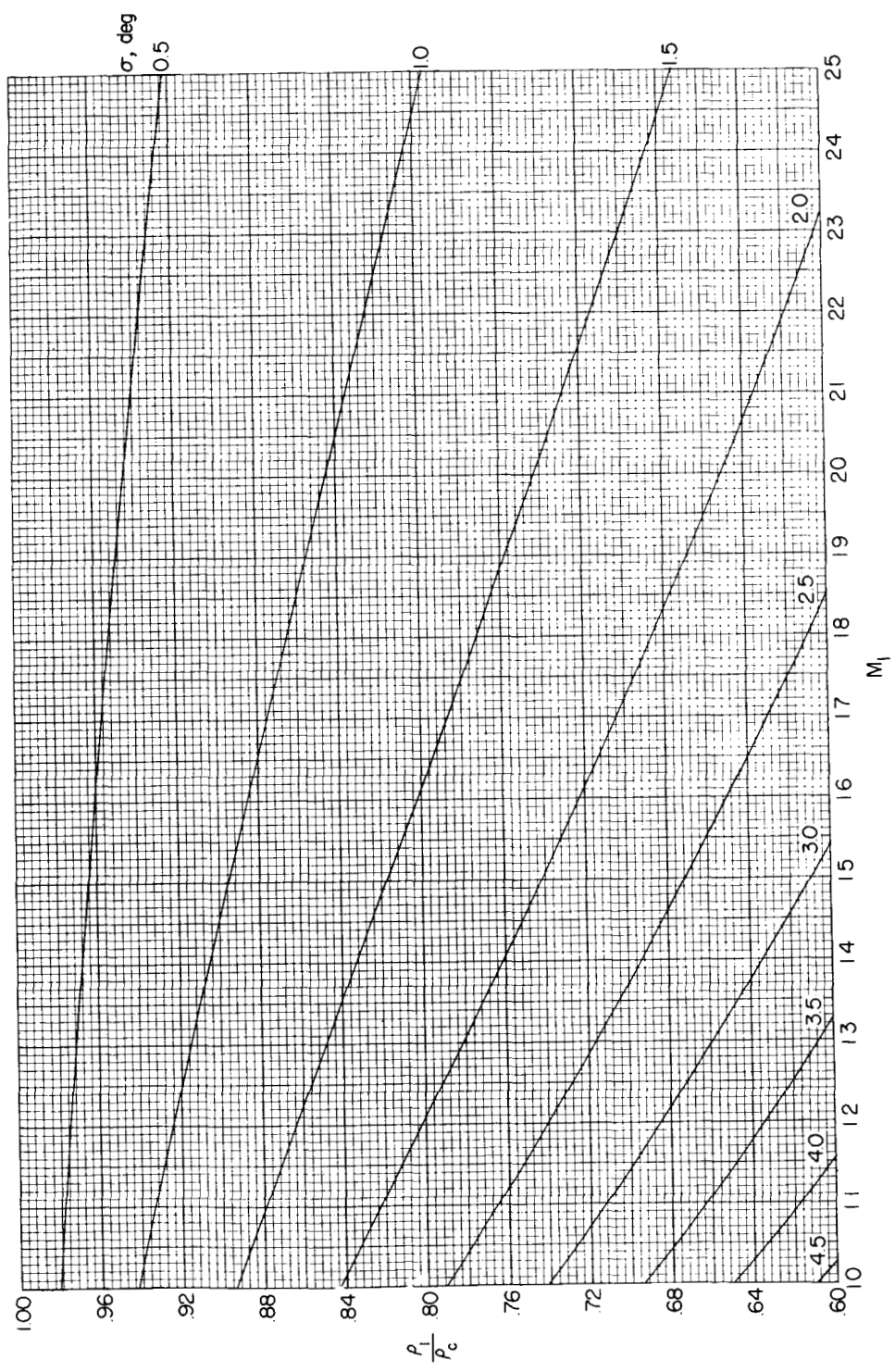
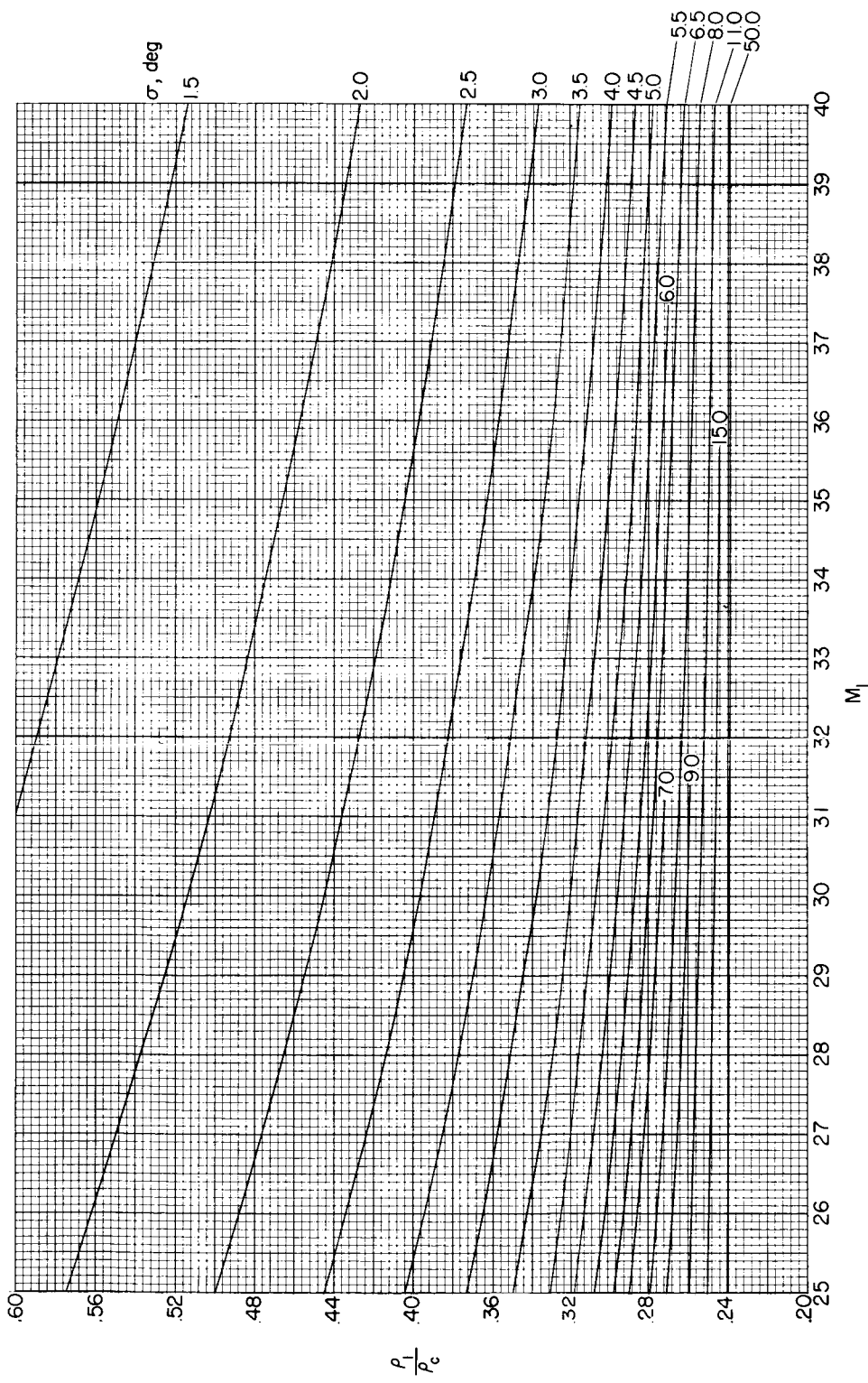
(f)  $M_1 = 10 \text{ to } 25; \rho_1/\rho_c = 0.2 \text{ to } 0.6.$ 

Figure 5.- Continued.



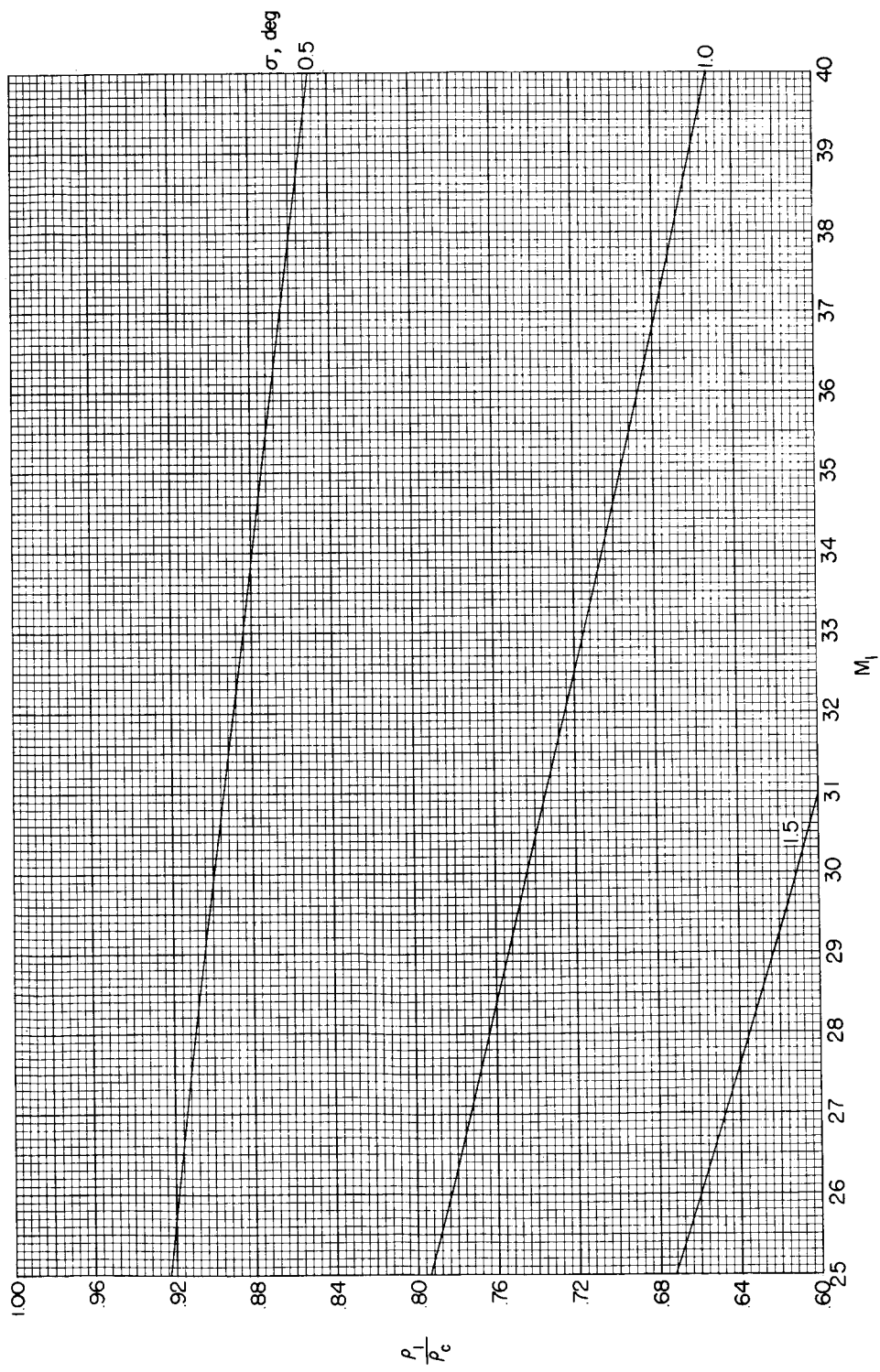
(g)  $M_1 = 10$  to  $25$ ;  $\rho_1/\rho_c = 0.6$  to  $1$ .

Figure 5.- Continued.



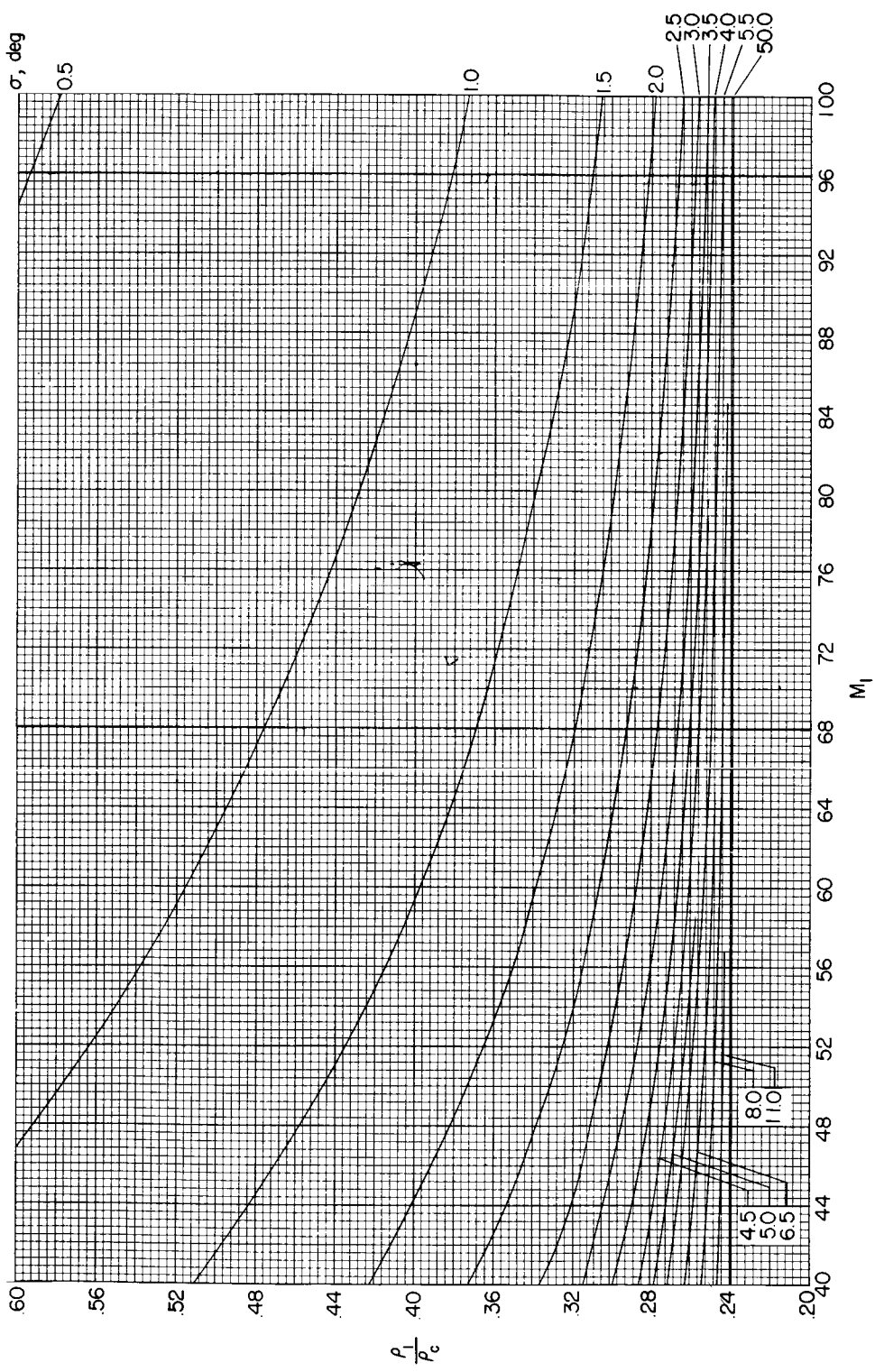
(h)  $M_1 = 25$  to 40;  $\rho_1/\rho_c = 0.2$  to 0.6.

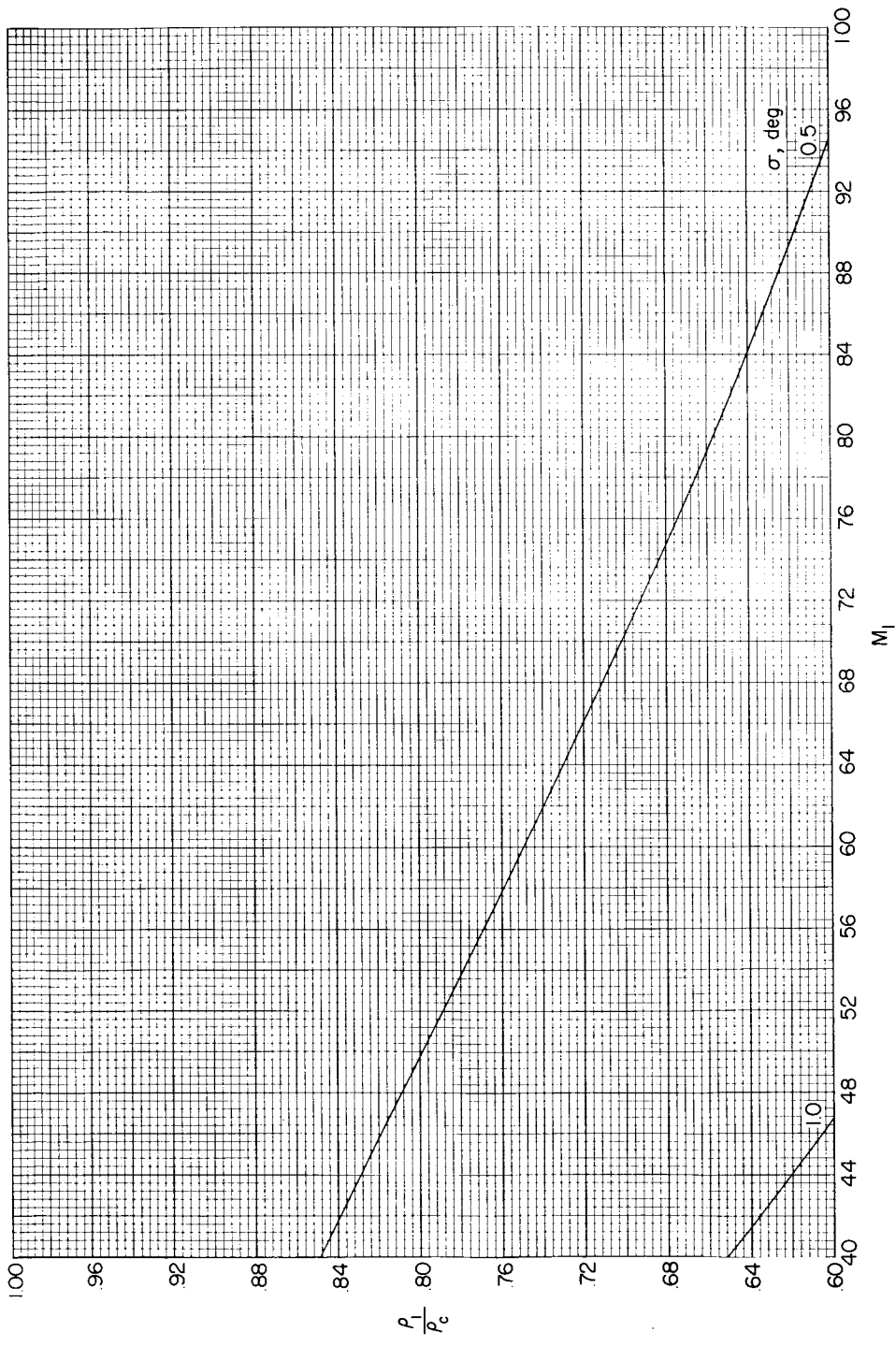
Figure 5.- Continued.



(i)  $M_1 = 25$  to 40;  $\rho_1/\rho_c = 0.6$  to 1.

Figure 5.- Continued.





(k)  $M_{1\perp} = 40$  to 100;  $\rho_1/\rho_c = 0.6$  to 1.

Figure 5. - Concluded.

(a)  $M_1 = 1$  to 100;  $\epsilon = 0^\circ$  to  $90^\circ$ .

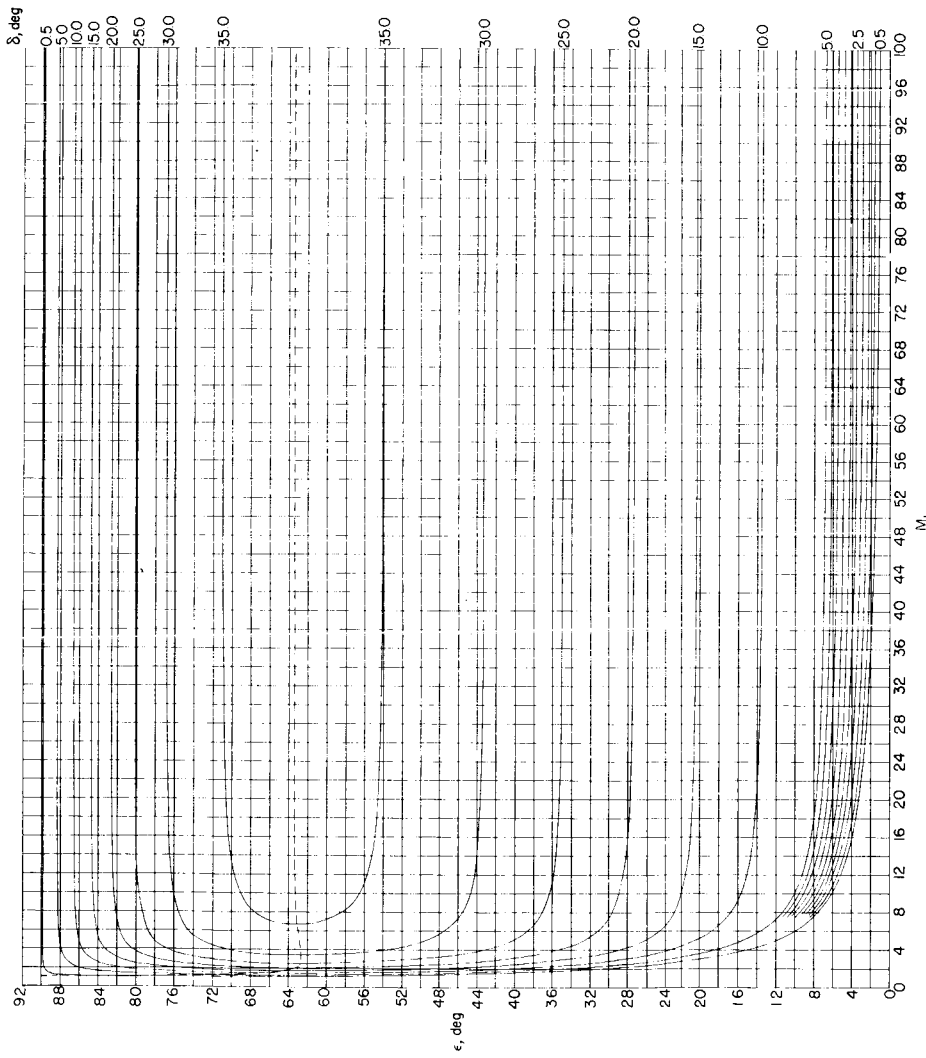
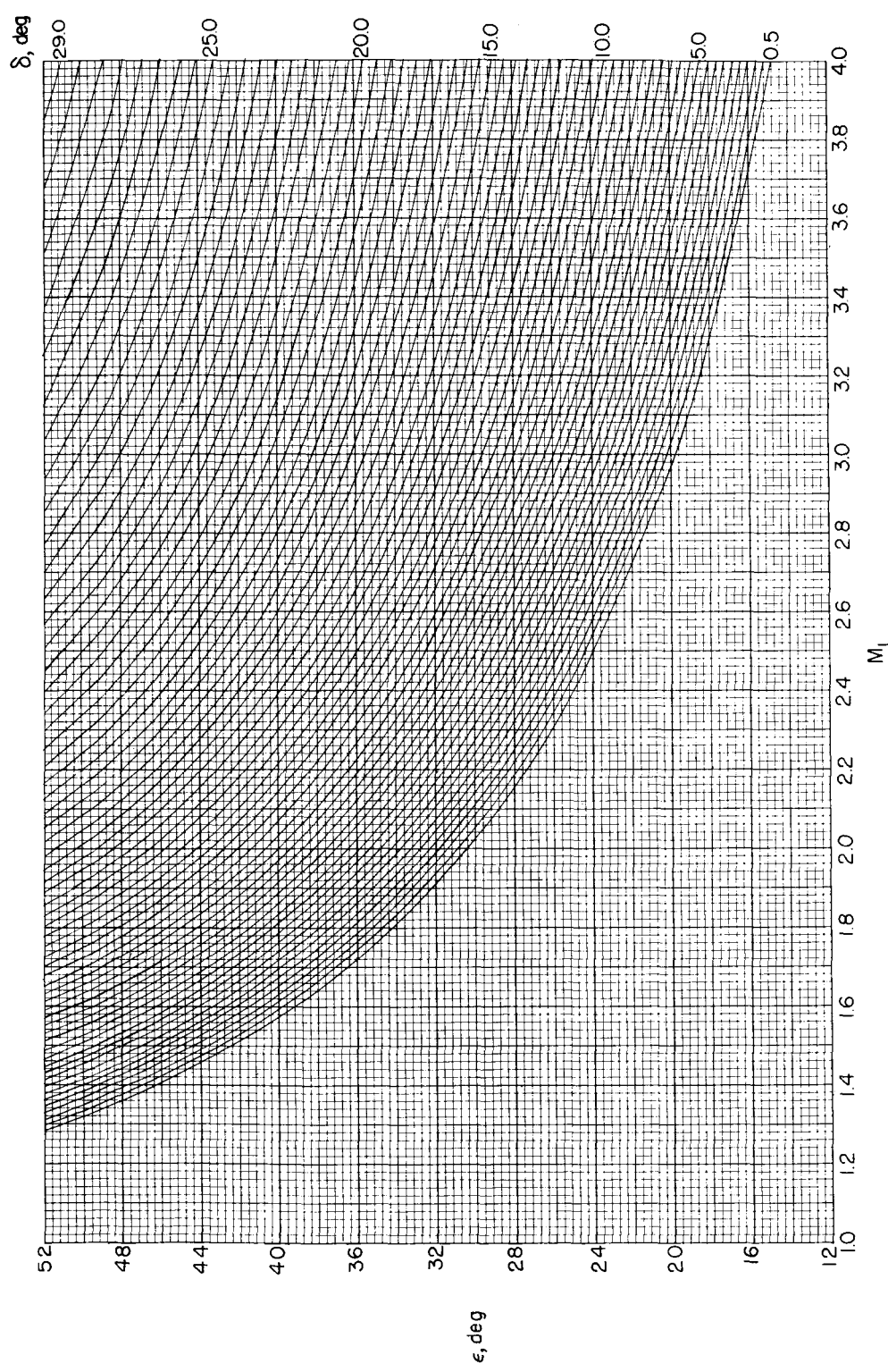


Figure 6.- Variation of two-dimensional shock angle with free-stream Mach number for various flow-deflection angles. (Dashed line denotes boundary between weak and strong shock solutions. Weak shock solutions are below dashed line.)



(b)  $M_1 = 1$  to 4;  $\epsilon = 12^\circ$  to  $52^\circ$ .

Figure 6. - Continued.

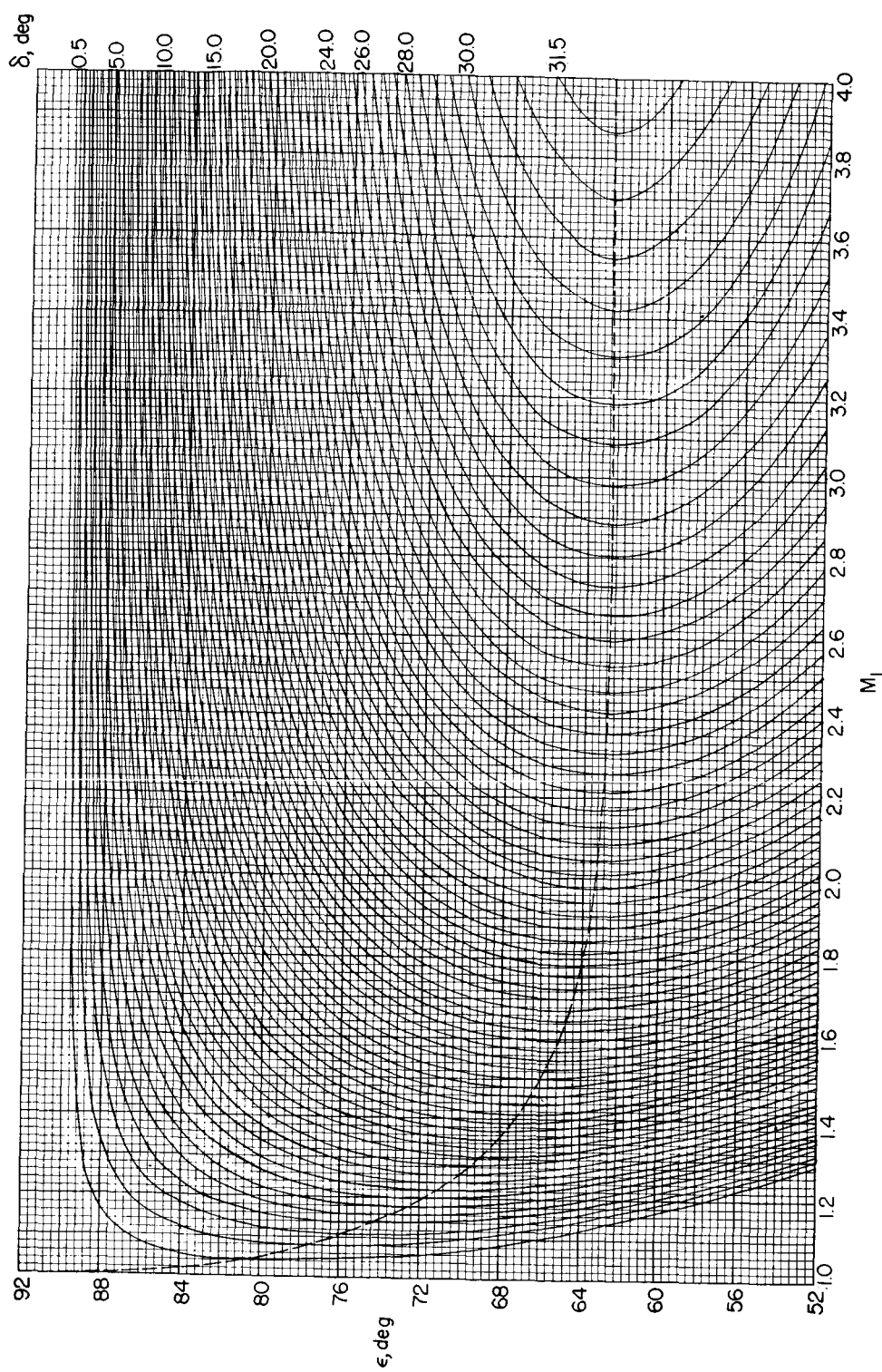
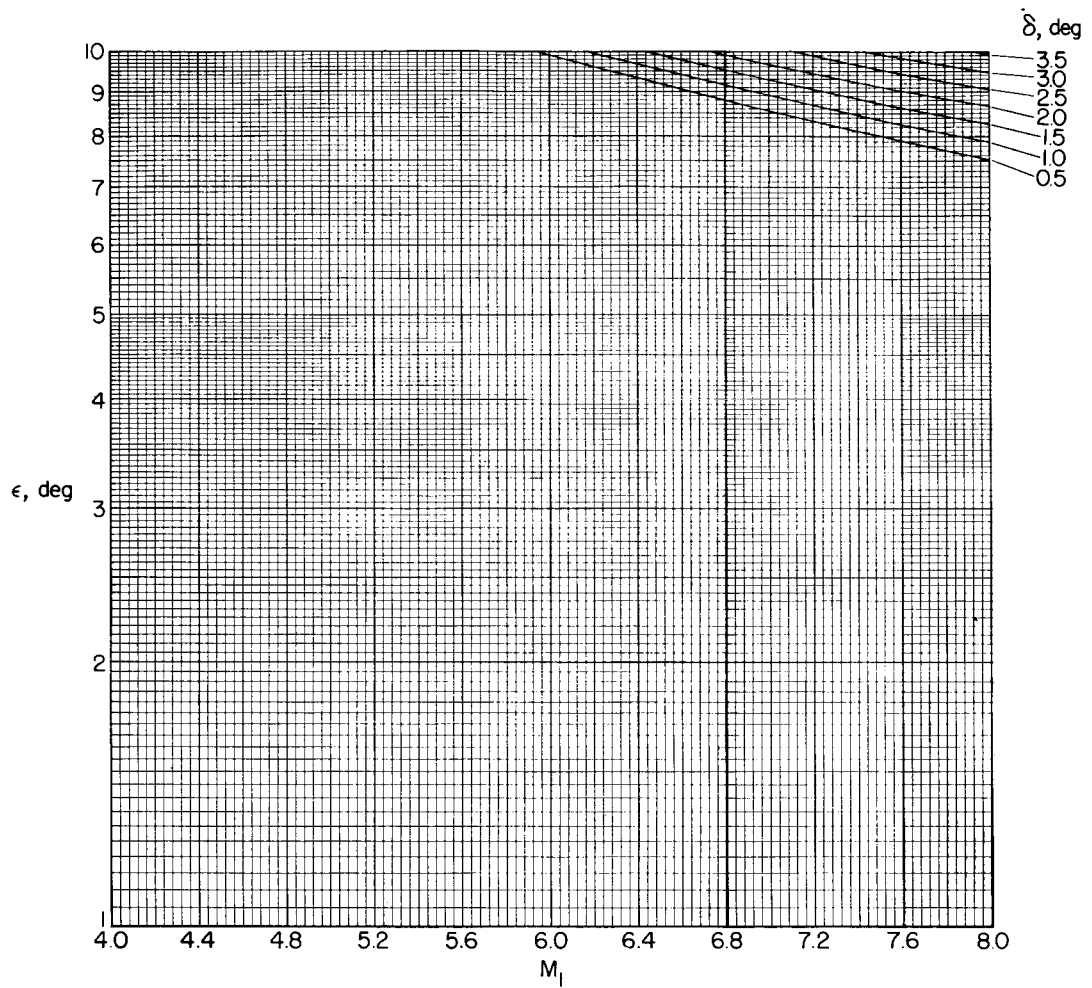
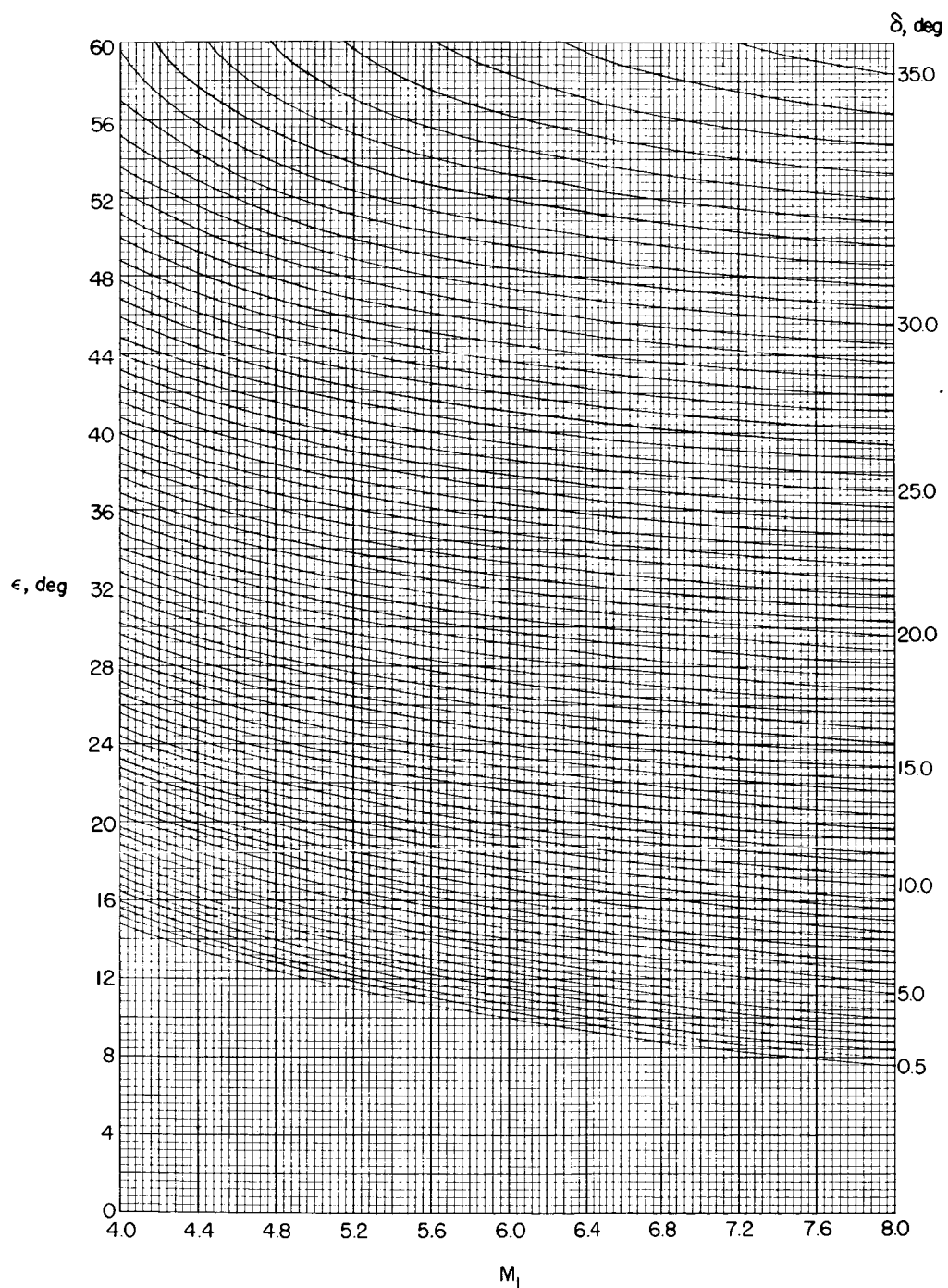
(c)  $M_1 = 1$  to 4;  $\epsilon = 52^\circ$  to  $90^\circ$ .

Figure 6.- Continued.



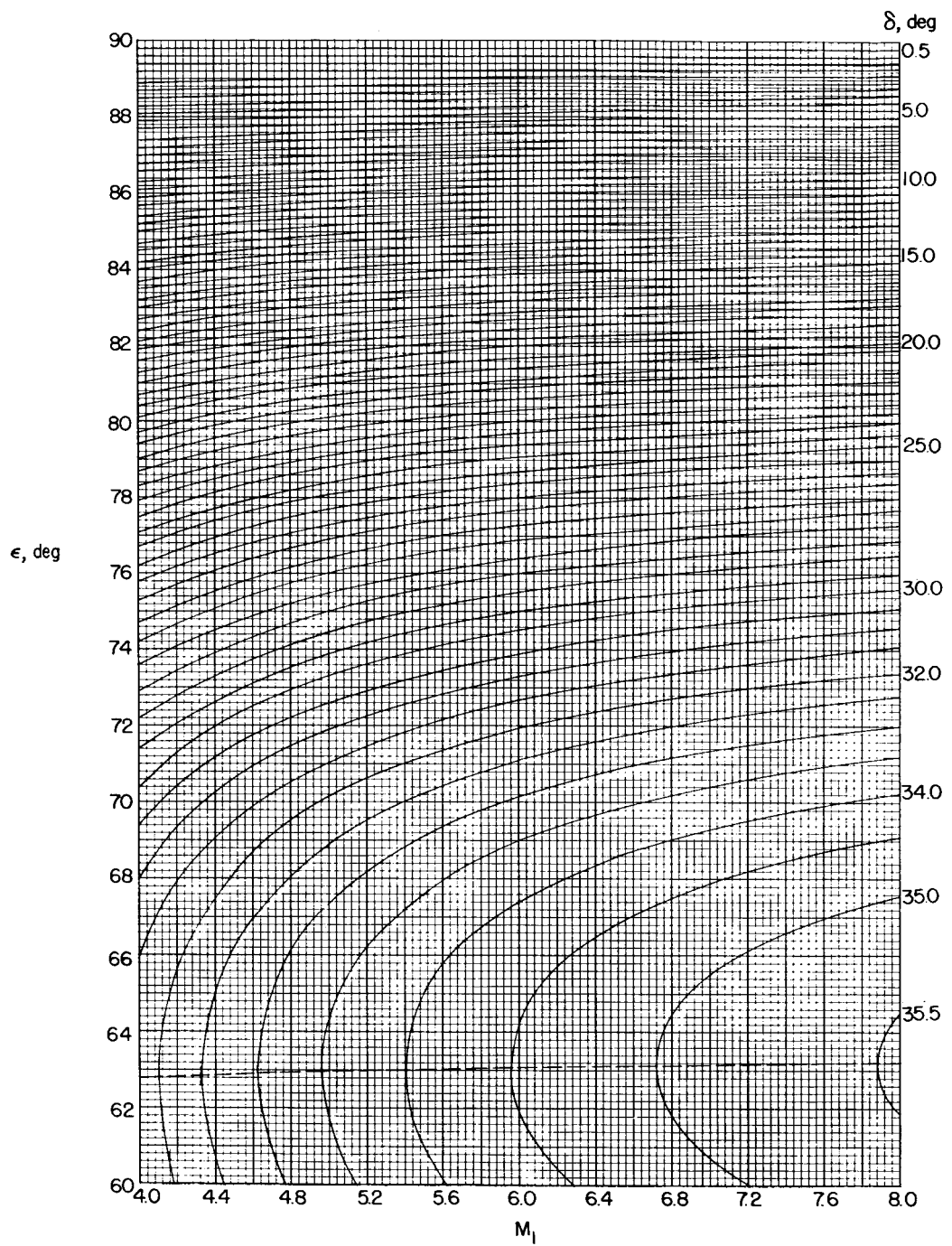
(d)  $M_1 = 4$  to 8;  $\epsilon = 1^\circ$  to  $10^\circ$ .

Figure 6.- Continued.



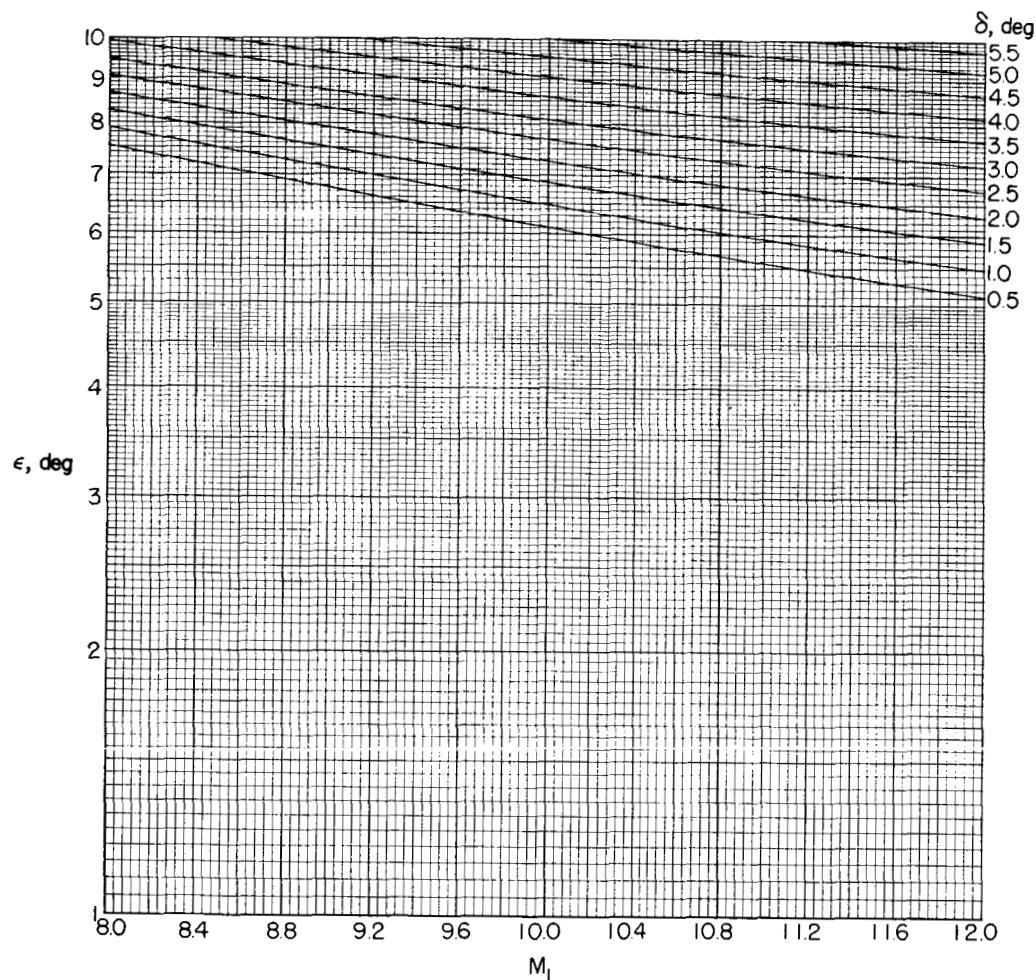
(e)  $M_1 = 4$  to  $8$ ;  $\epsilon = 0^\circ$  to  $60^\circ$ .

Figure 6.- Continued.



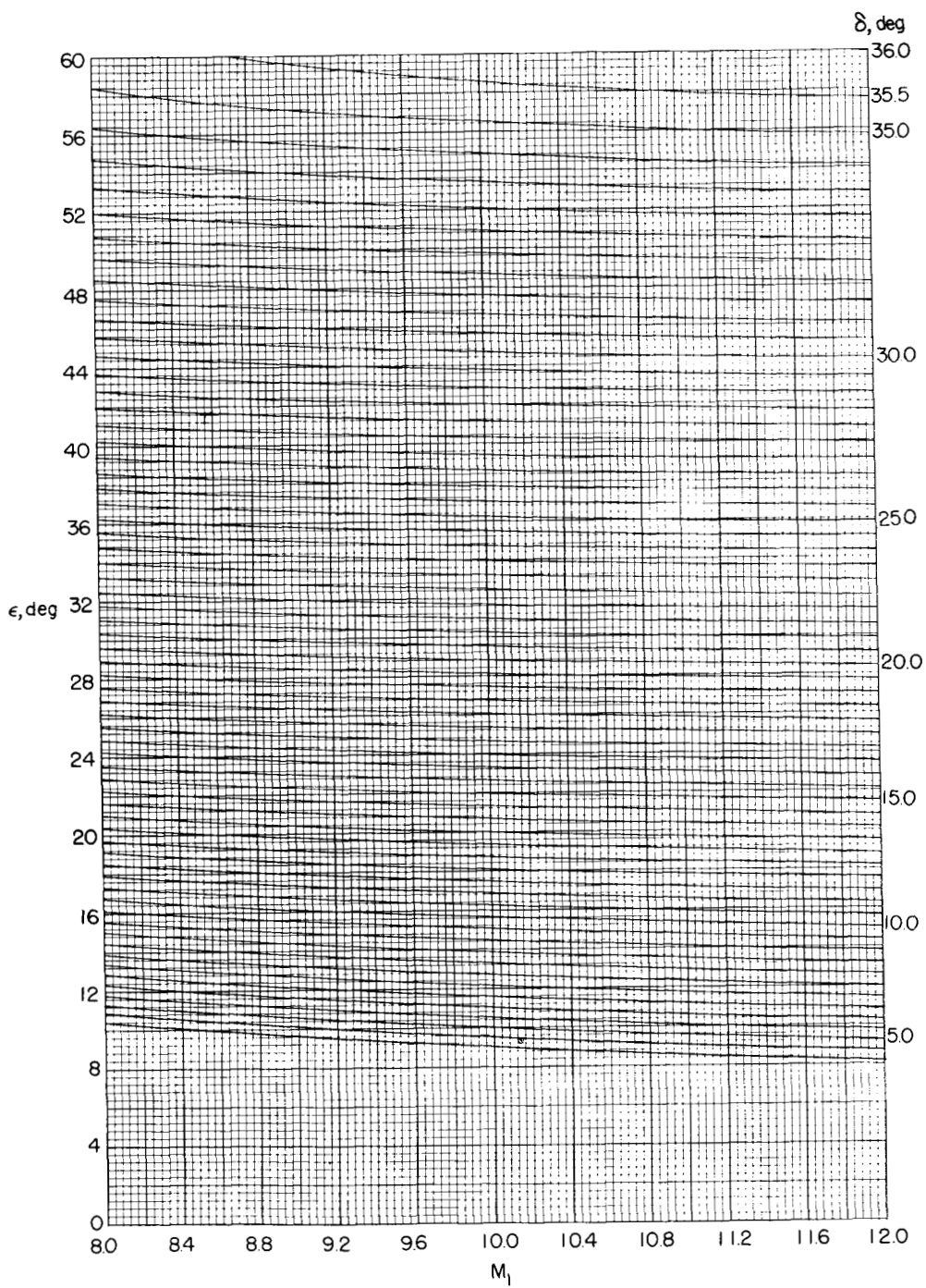
(f)  $M_l = 4$  to 8;  $\epsilon = 60^\circ$  to  $90^\circ$ .

Figure 6.- Continued.



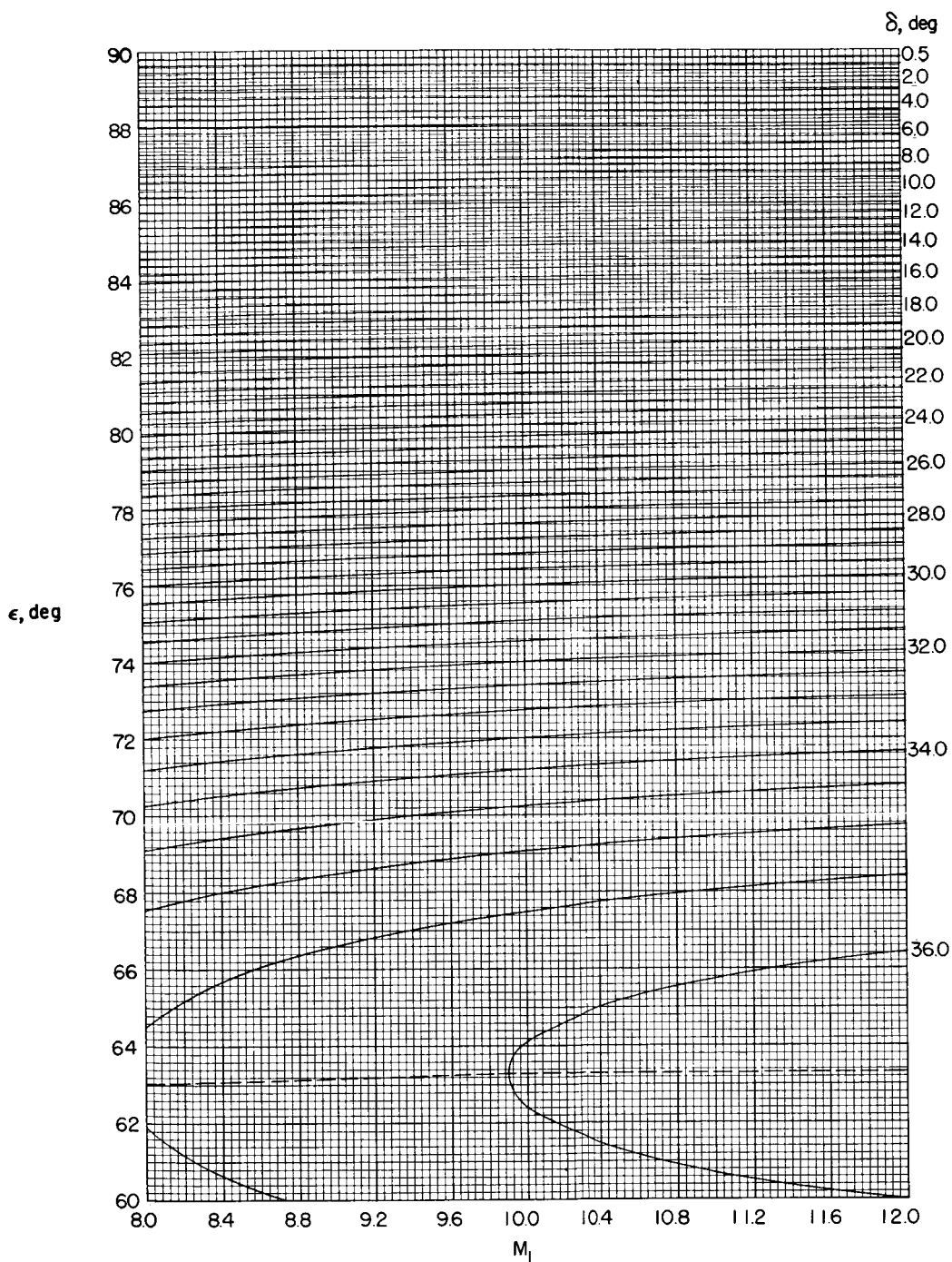
(g)  $M_1 = 8$  to  $12$ ;  $\epsilon = 1^\circ$  to  $10^\circ$ .

Figure 6.- Continued.



(h)  $M_1 = 8$  to  $12$ ;  $\epsilon = 0^\circ$  to  $60^\circ$ .

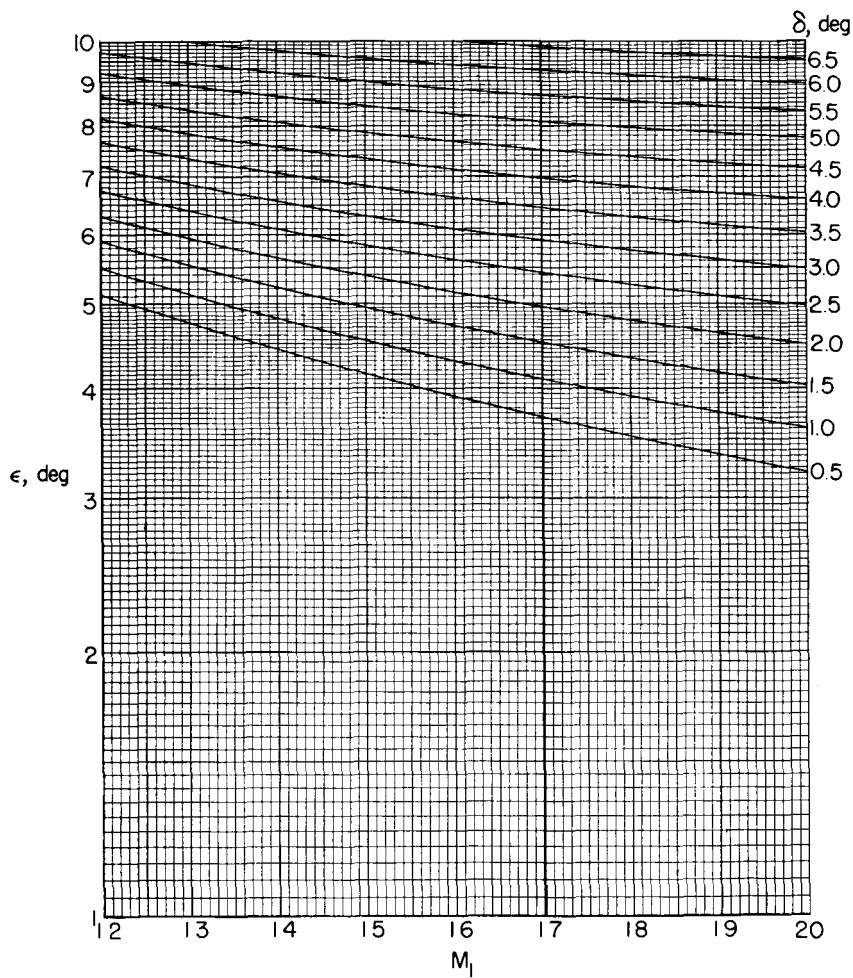
Figure 6.- Continued.



(i)  $M_1 = 8$  to  $12$ ;  $\epsilon = 60^\circ$  to  $90^\circ$ .

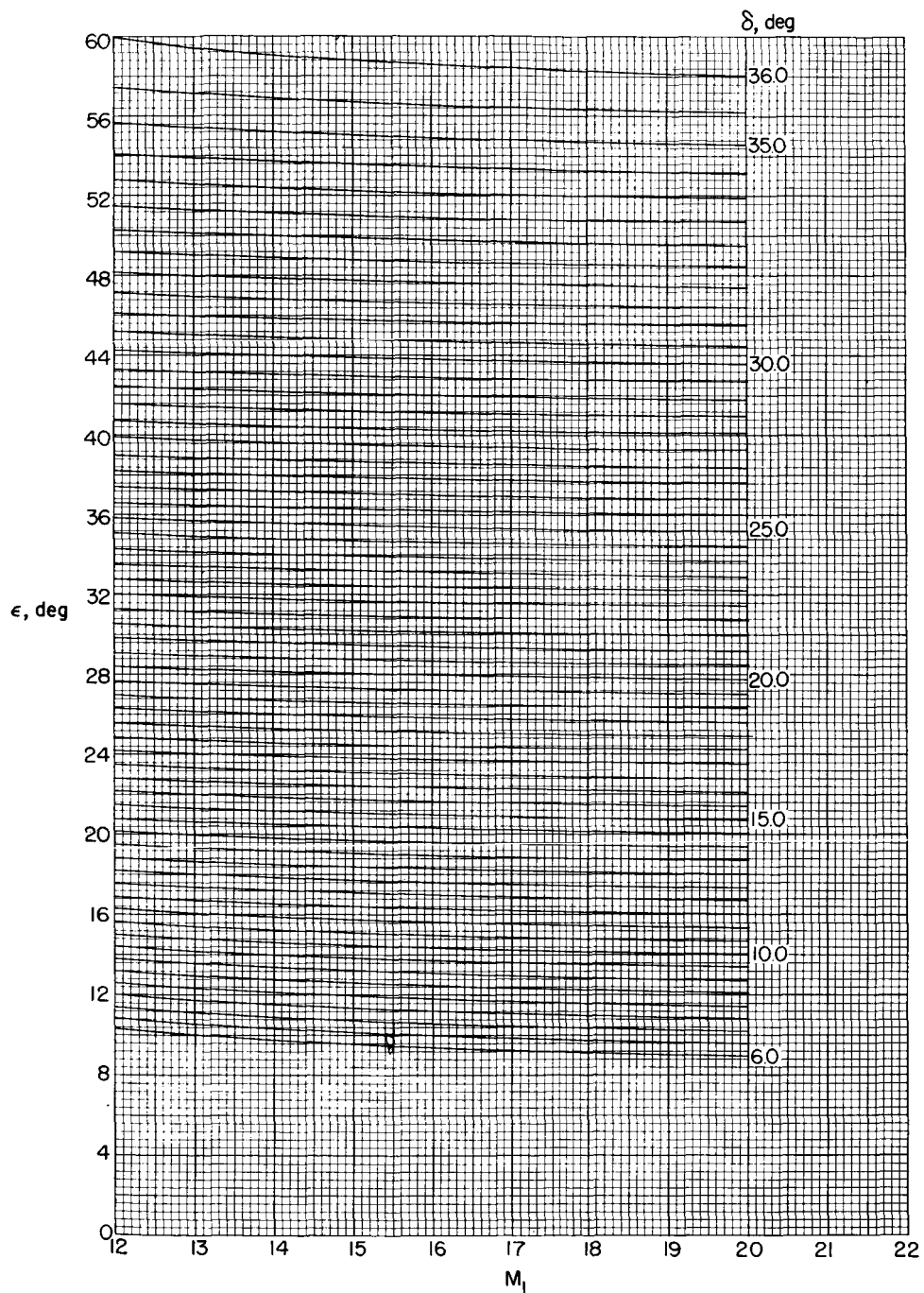
Figure 6.- Continued.

$10^4$



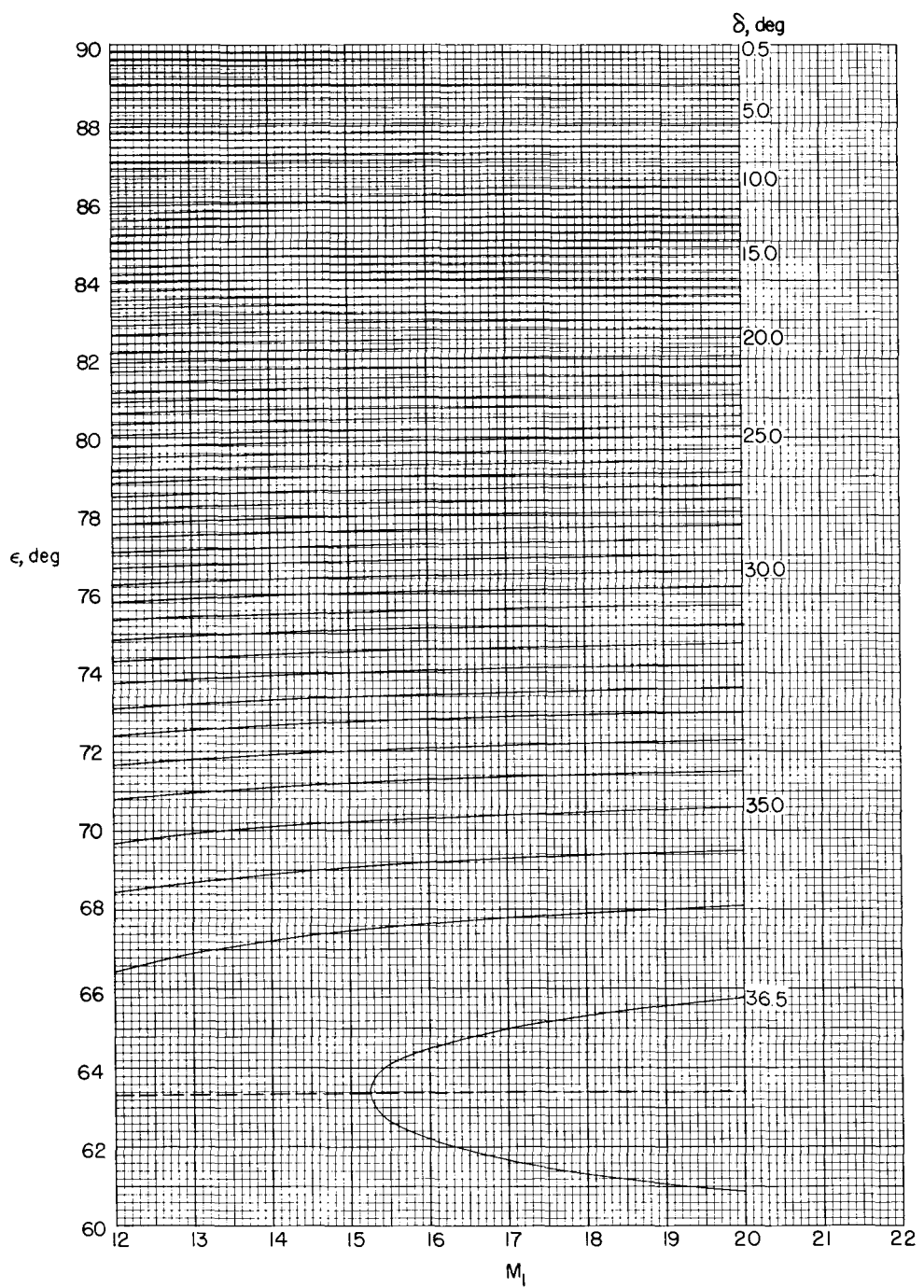
(j)  $M_l = 12$  to  $20$ ;  $\epsilon = 1^\circ$  to  $10^\circ$ .

Figure 6.- Continued.



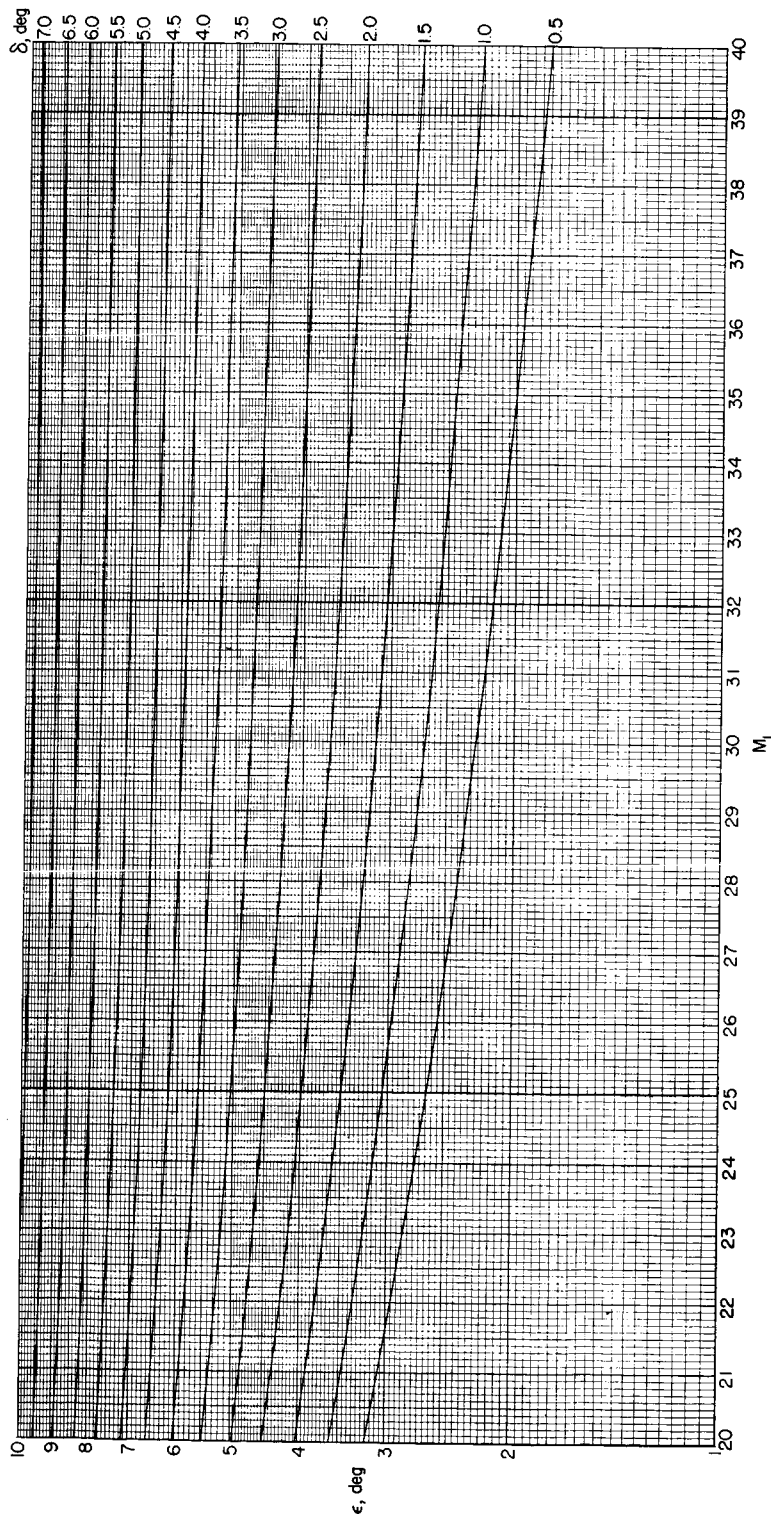
(k)  $M_1 = 12$  to  $20$ ;  $\epsilon = 0^\circ$  to  $60^\circ$ .

Figure 6.- Continued.



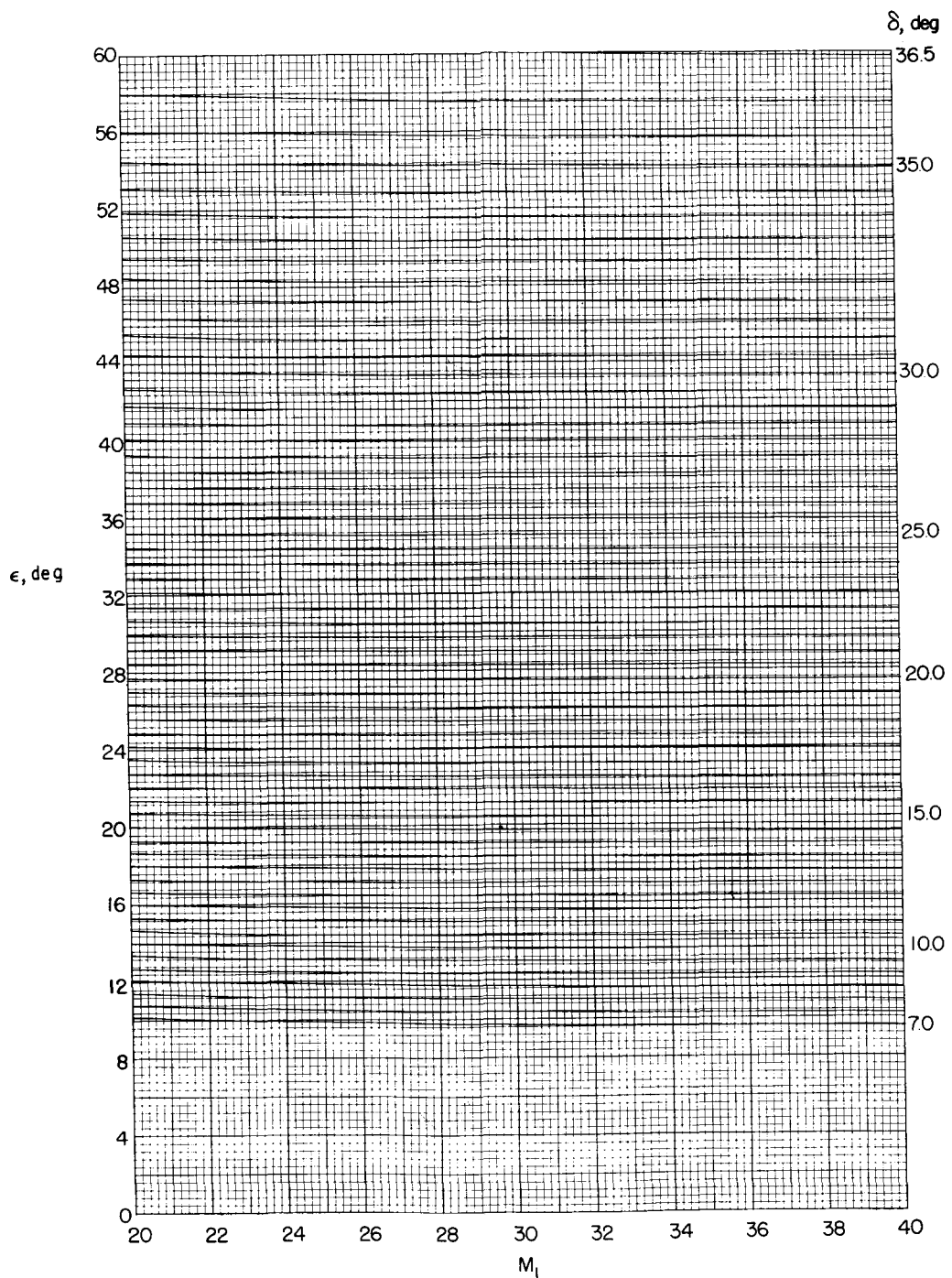
(i)  $M_1 = 12$  to  $20$ ;  $\epsilon = 60^\circ$  to  $90^\circ$ .

Figure 6.- Continued.



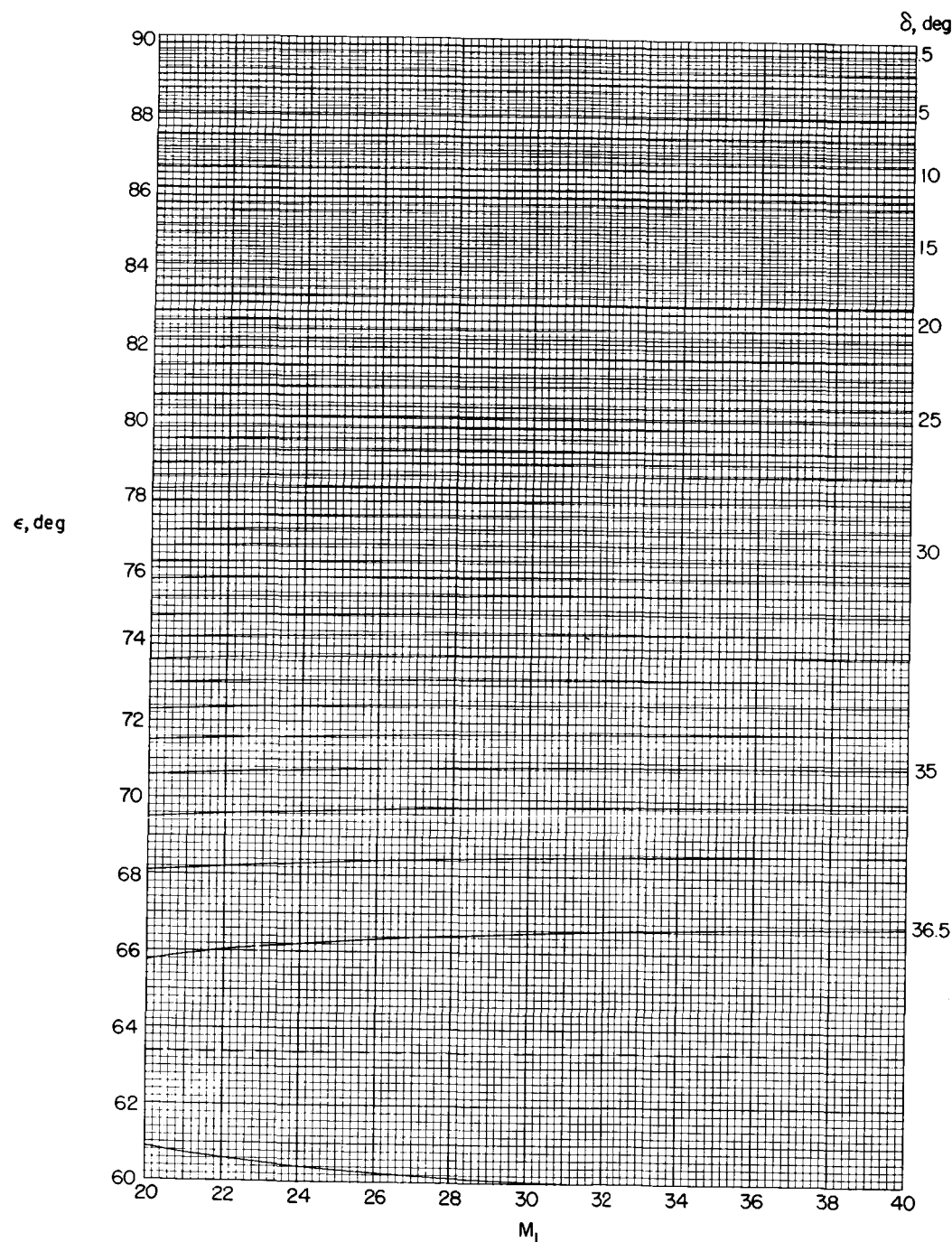
(m)  $M_1 = 20$  to  $40$ ;  $\epsilon = 1^\circ$  to  $10^\circ$ .

Figure 6.- Continued.



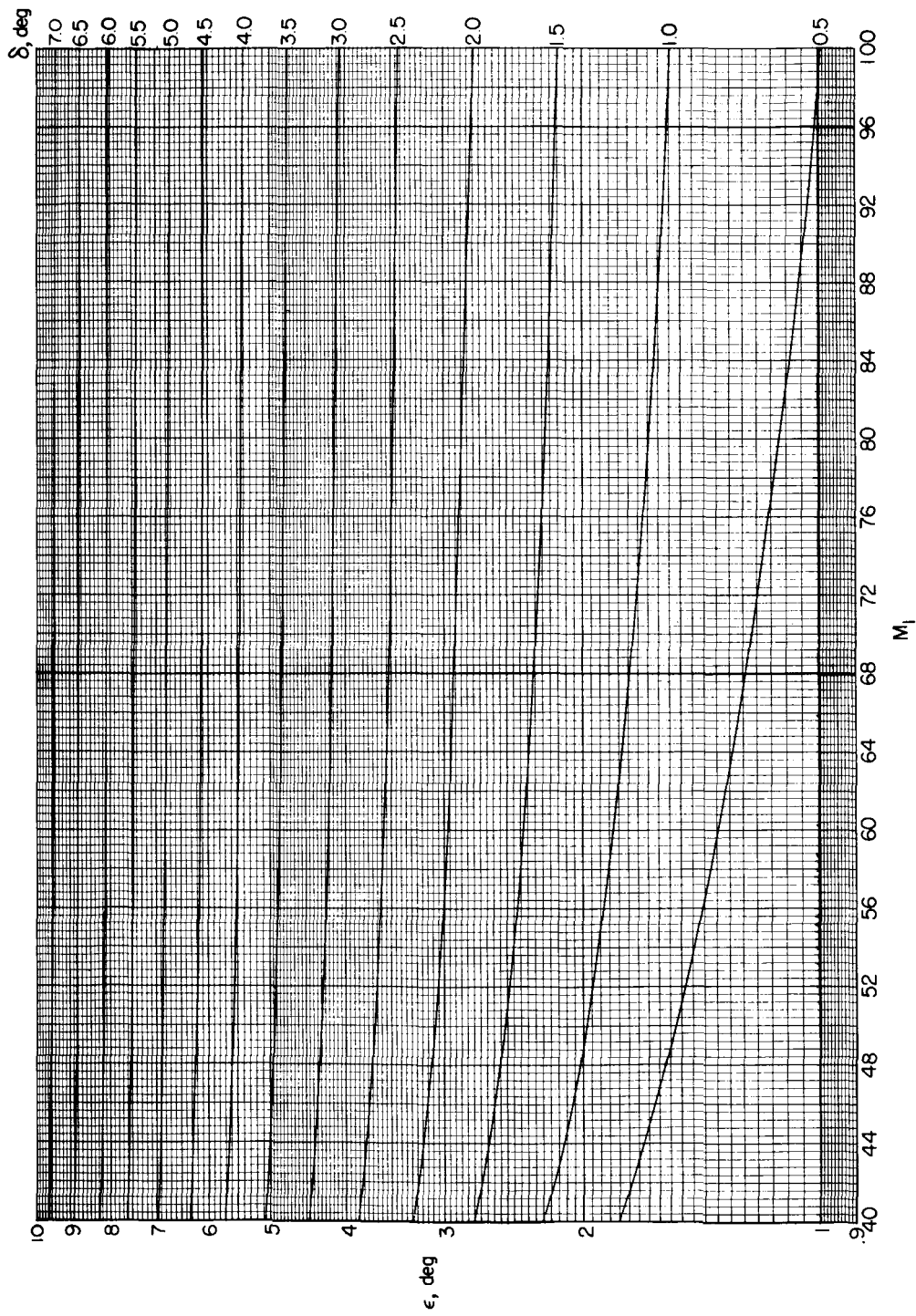
(n)  $M_1 = 20$  to  $40$ ;  $\epsilon = 0^\circ$  to  $60^\circ$ .

Figure 6.- Continued.



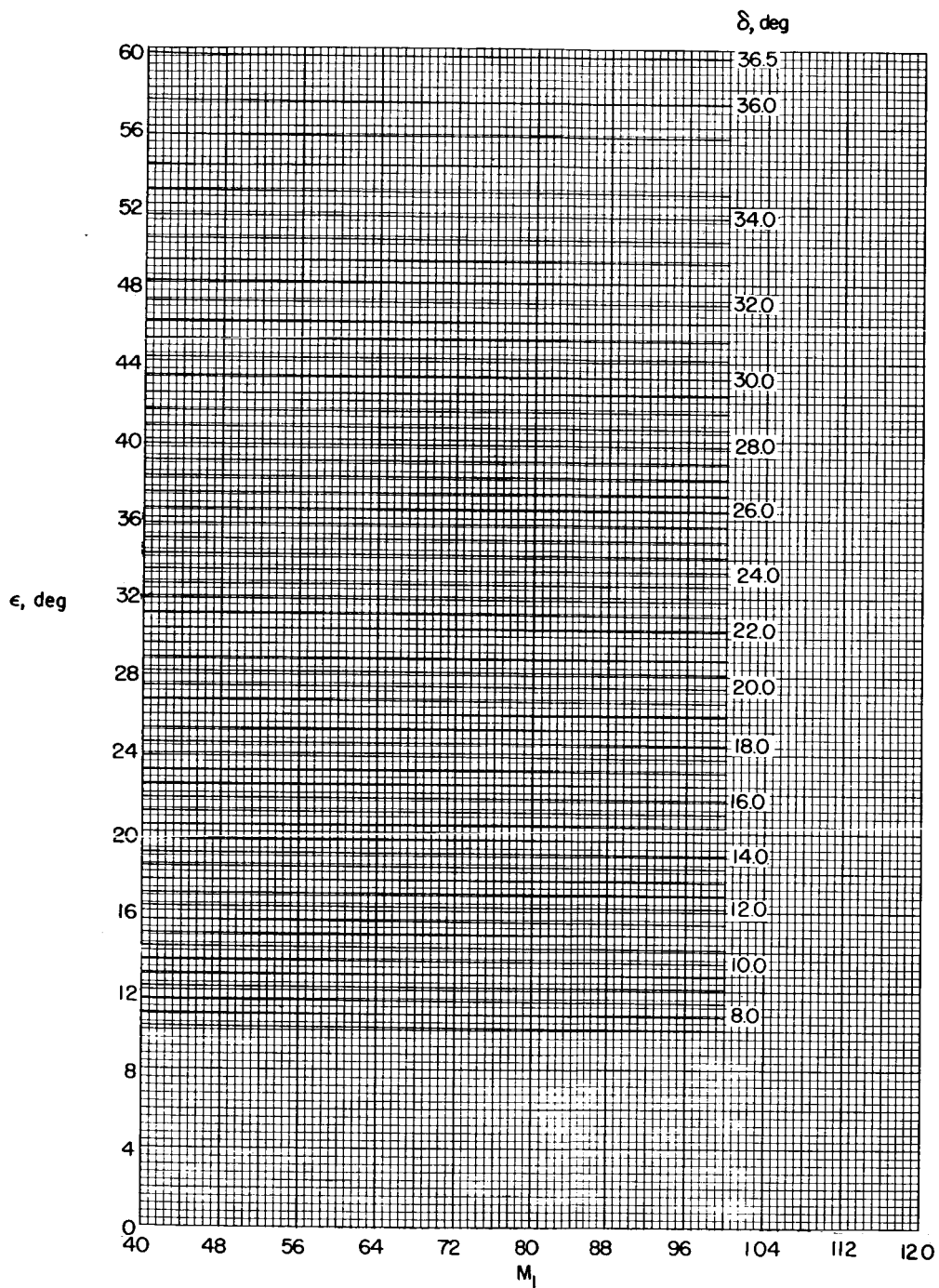
(o)  $M_1 = 20$  to  $40$ ;  $\epsilon = 60^\circ$  to  $90^\circ$ .

Figure 6.- Continued.



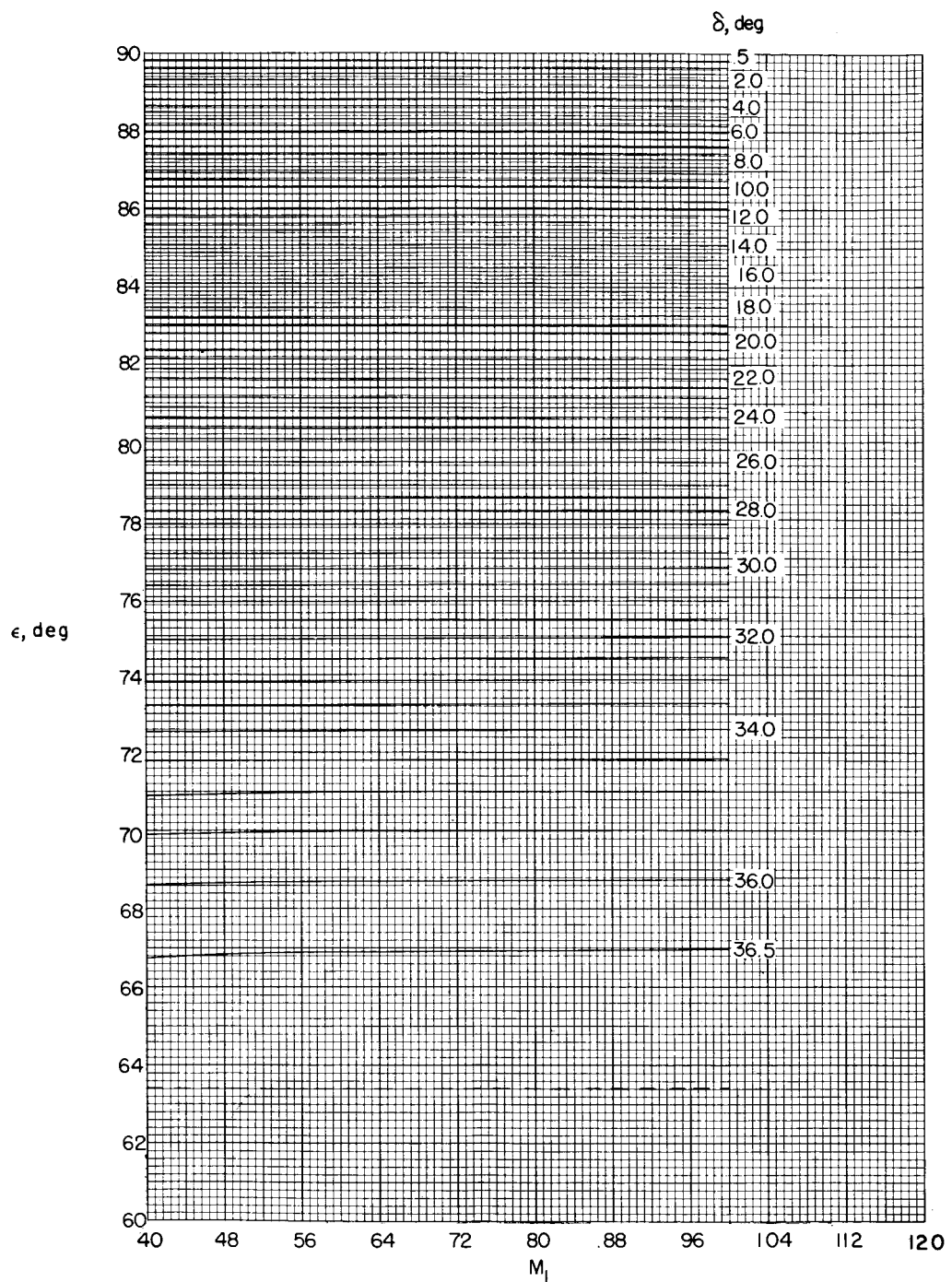
(p)  $M_1 = 40$  to  $100$ ;  $\epsilon = 0.90$  to  $10^\circ$ .

Figure 6.- Continued.



(q)  $M_1 = 40$  to  $100$ ;  $\epsilon = 0^\circ$  to  $60^\circ$ .

Figure 6.-- Continued.



(r)  $M_1 = 40$  to  $100$ ;  $\epsilon = 60^\circ$  to  $90^\circ$ .

Figure 6.- Concluded.

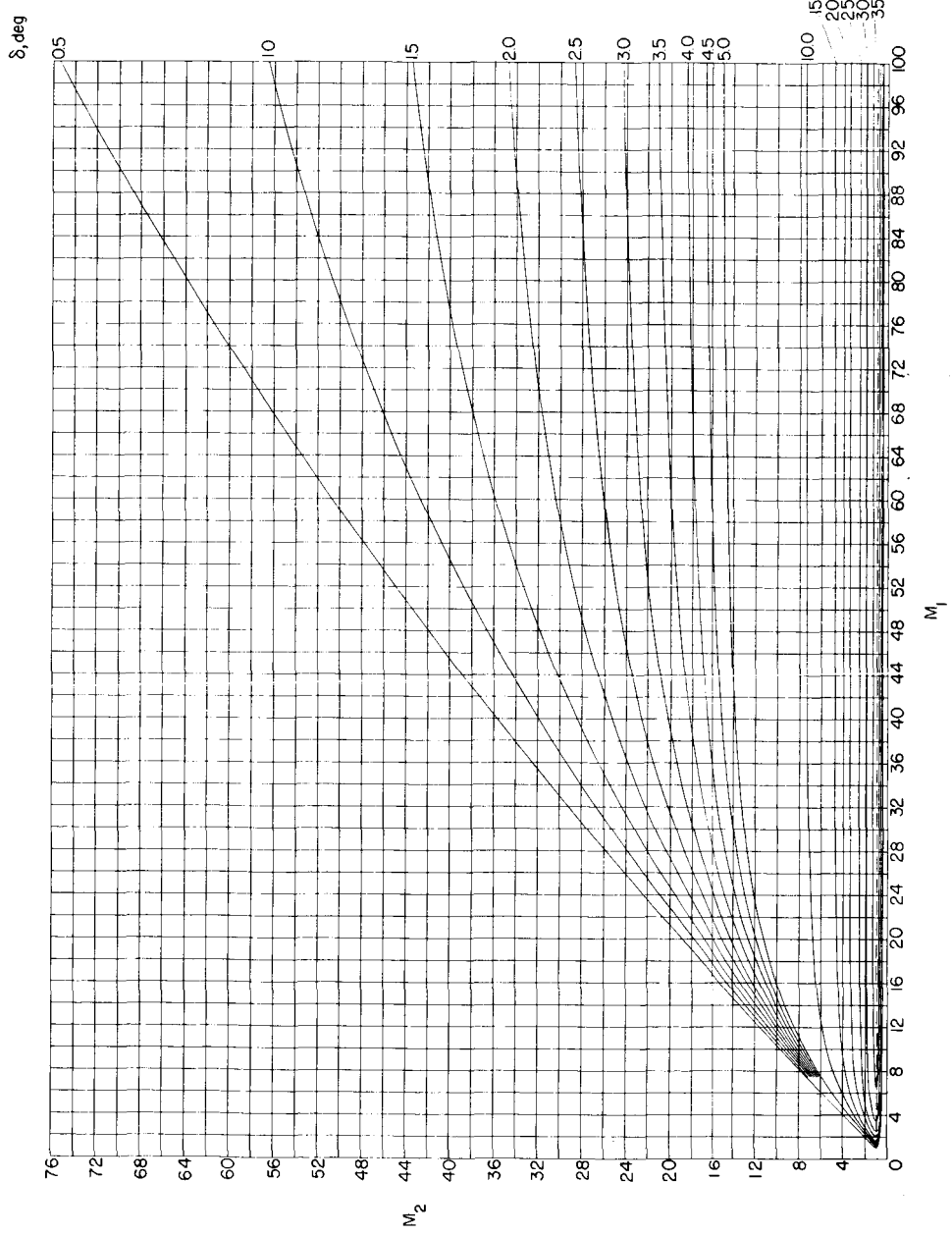
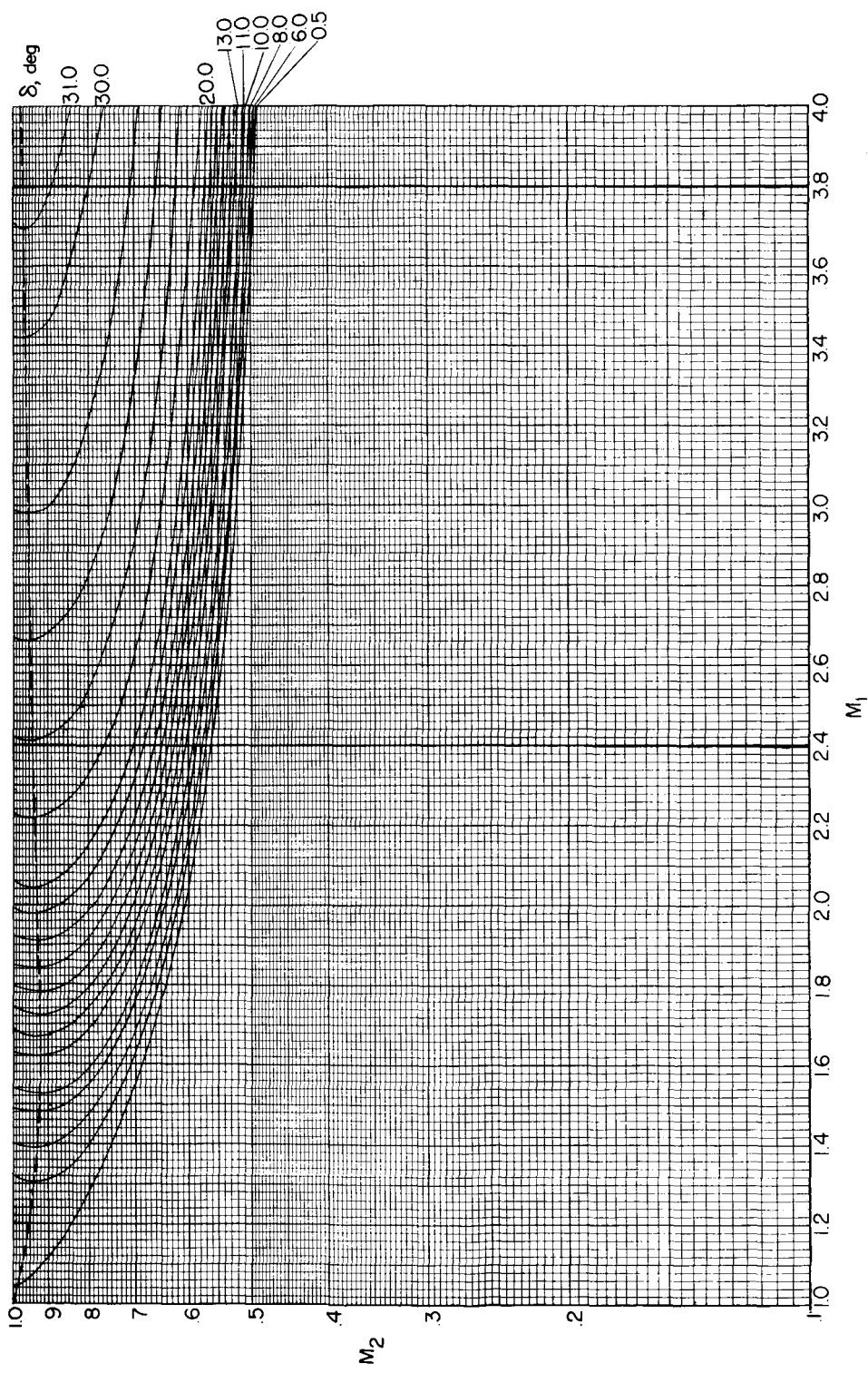
(a)  $M_1 = 1$  to 100;  $M_2 = 0$  to 76.

Figure 7.- Variation of Mach number behind two-dimensional shock with free-stream Mach number for various flow-deflection angles. (Dashed line denotes boundary between weak and strong shock solutions. Weak shock solution is above dashed line.)



(b)  $M_1 = 1$  to 4;  $M_2 = 0.1$  to 1.

Figure 7.- Continued.

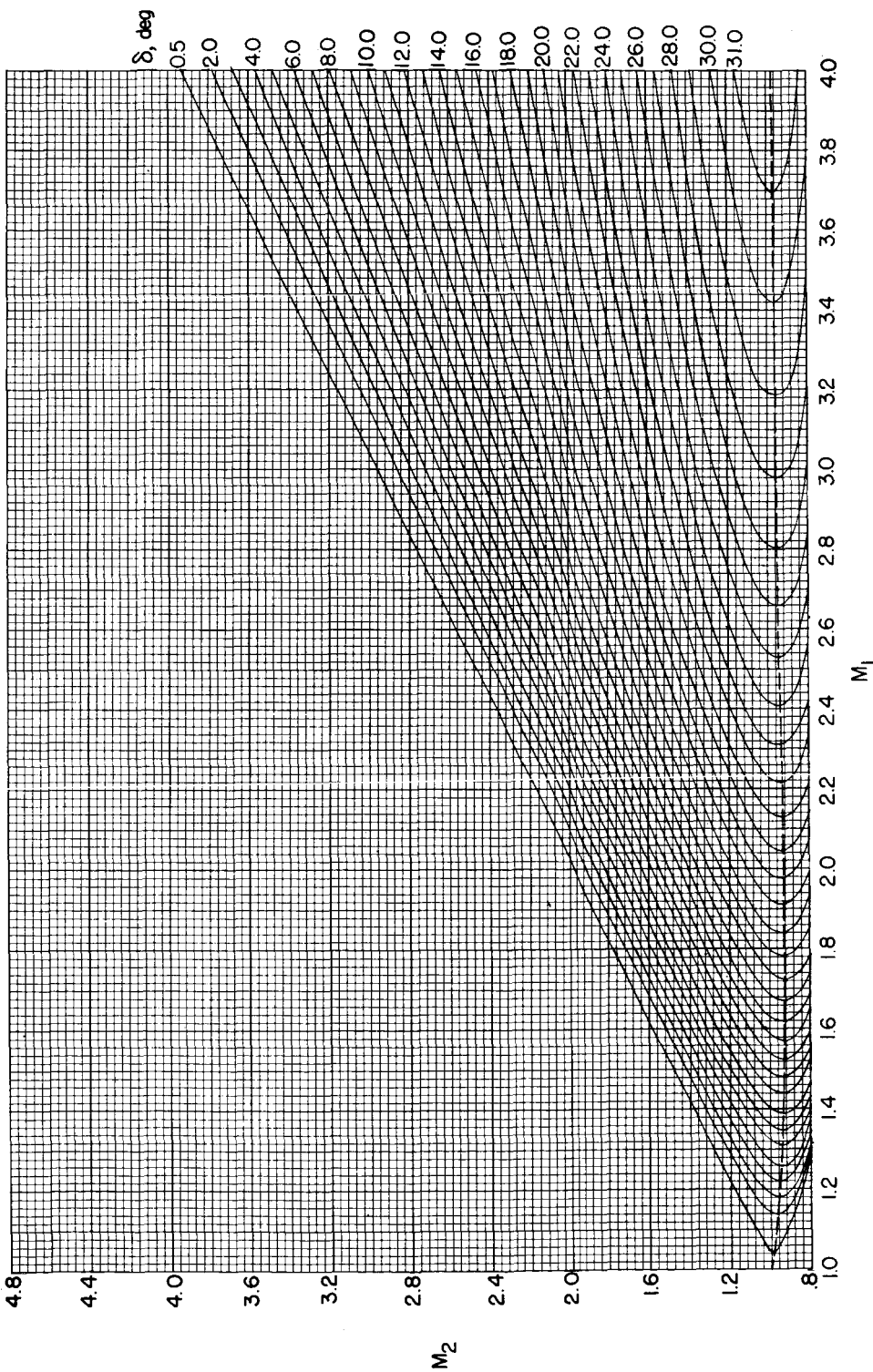
(c)  $M_1 = 1$  to 4;  $M_2 = 0.8$  to 4.8.

Figure 7.- Continued.

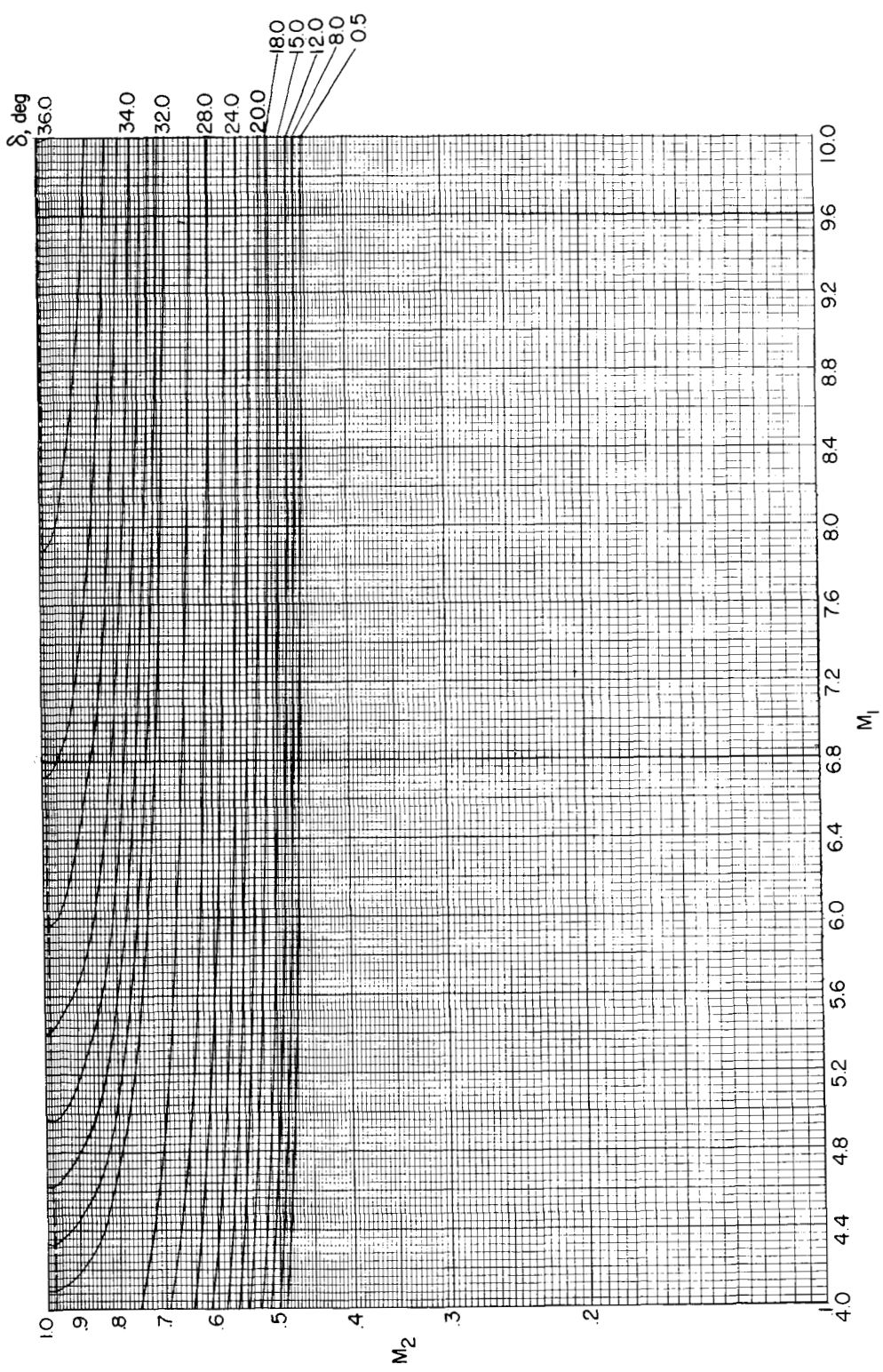
(d)  $M_1 = 4$  to 10;  $M_2 = 0.1$  to 1.

Figure 7.- Continued.

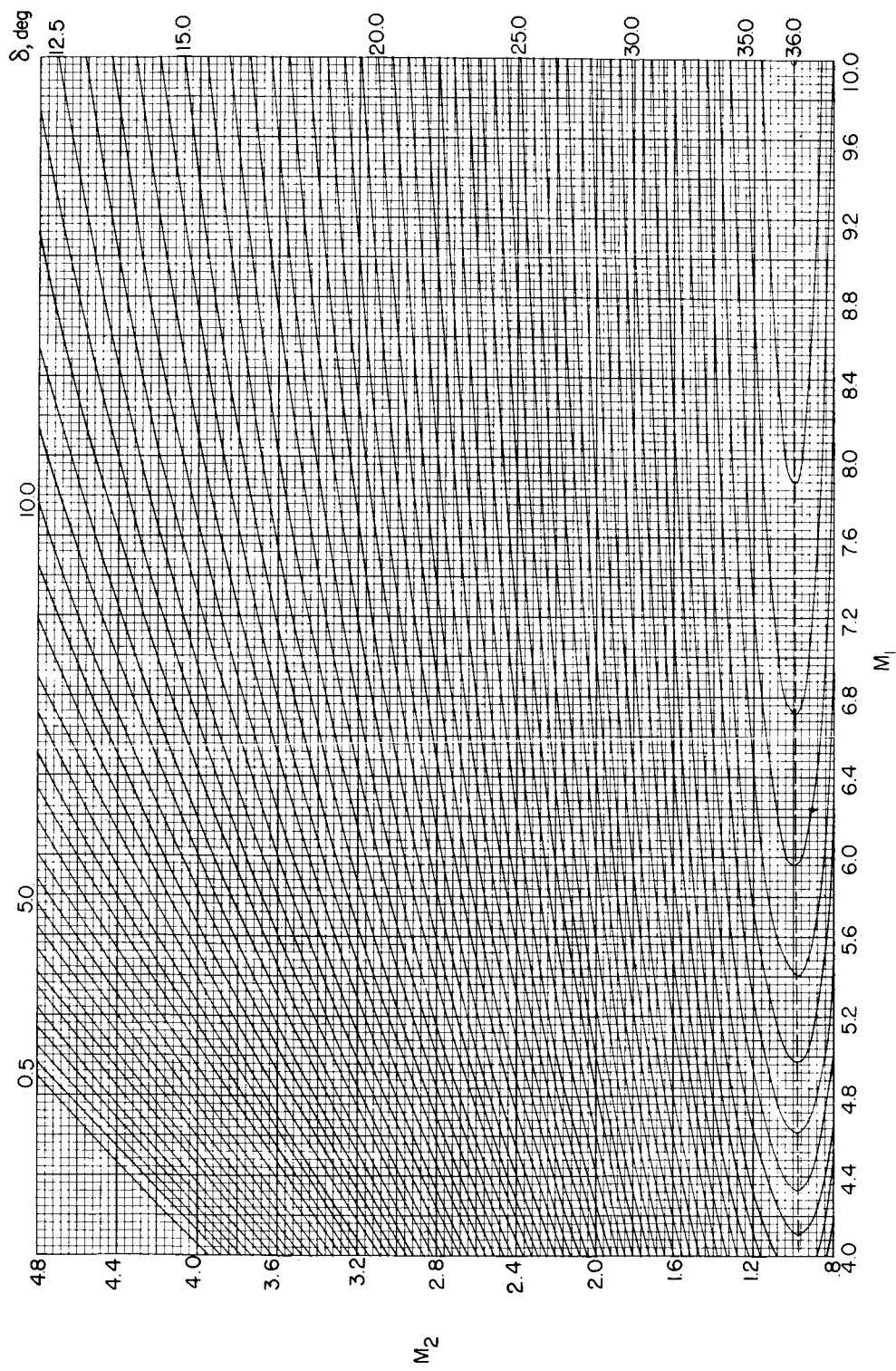
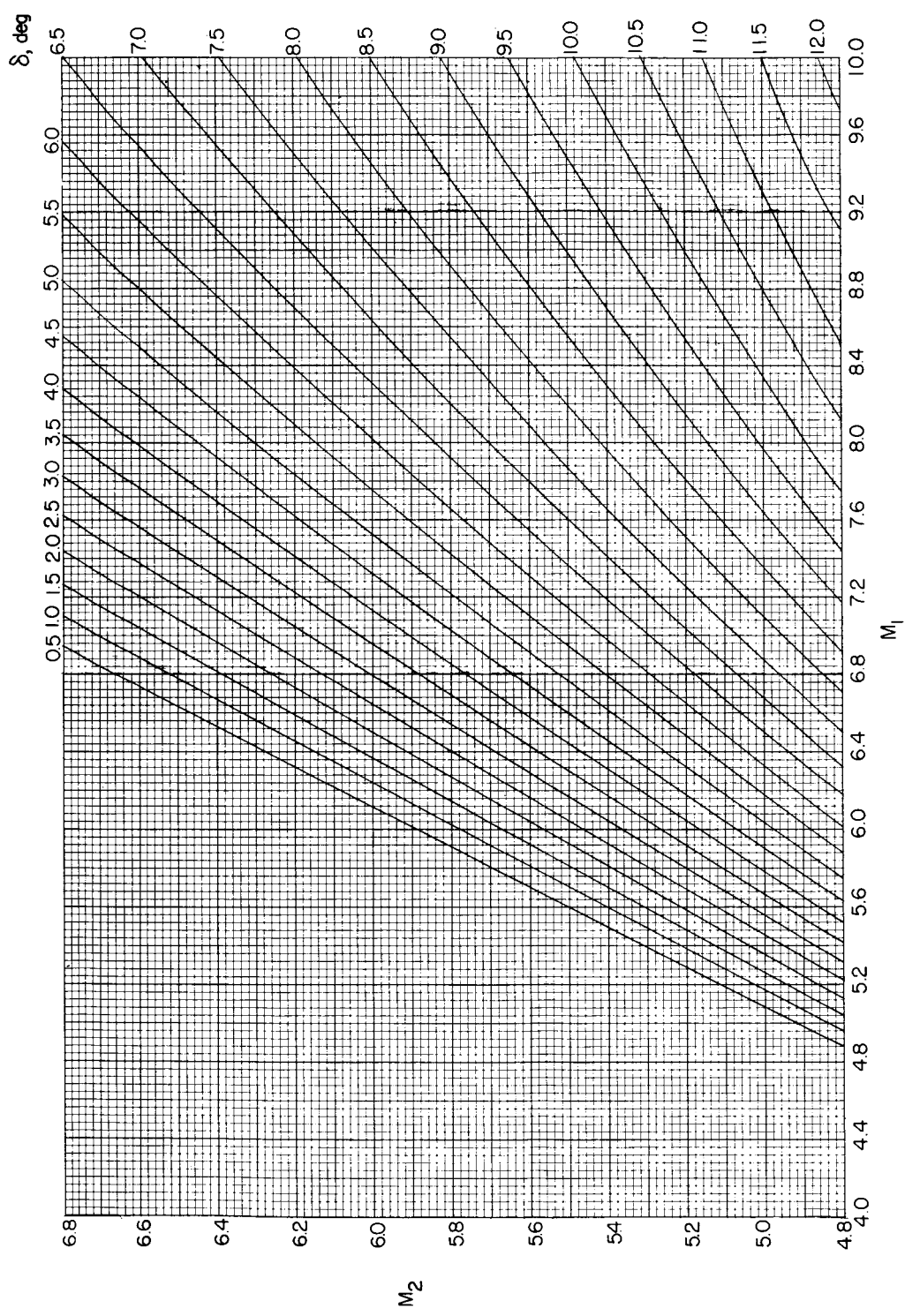
(e)  $M_1 = 4$  to 10;  $M_2 = 0.8$  to 4.8.

Figure 7.- Continued.



(f)  $M_1 = 4$  to 10;  $M_2 = 4.8$  to 6.8.

Figure 7.- Continued.

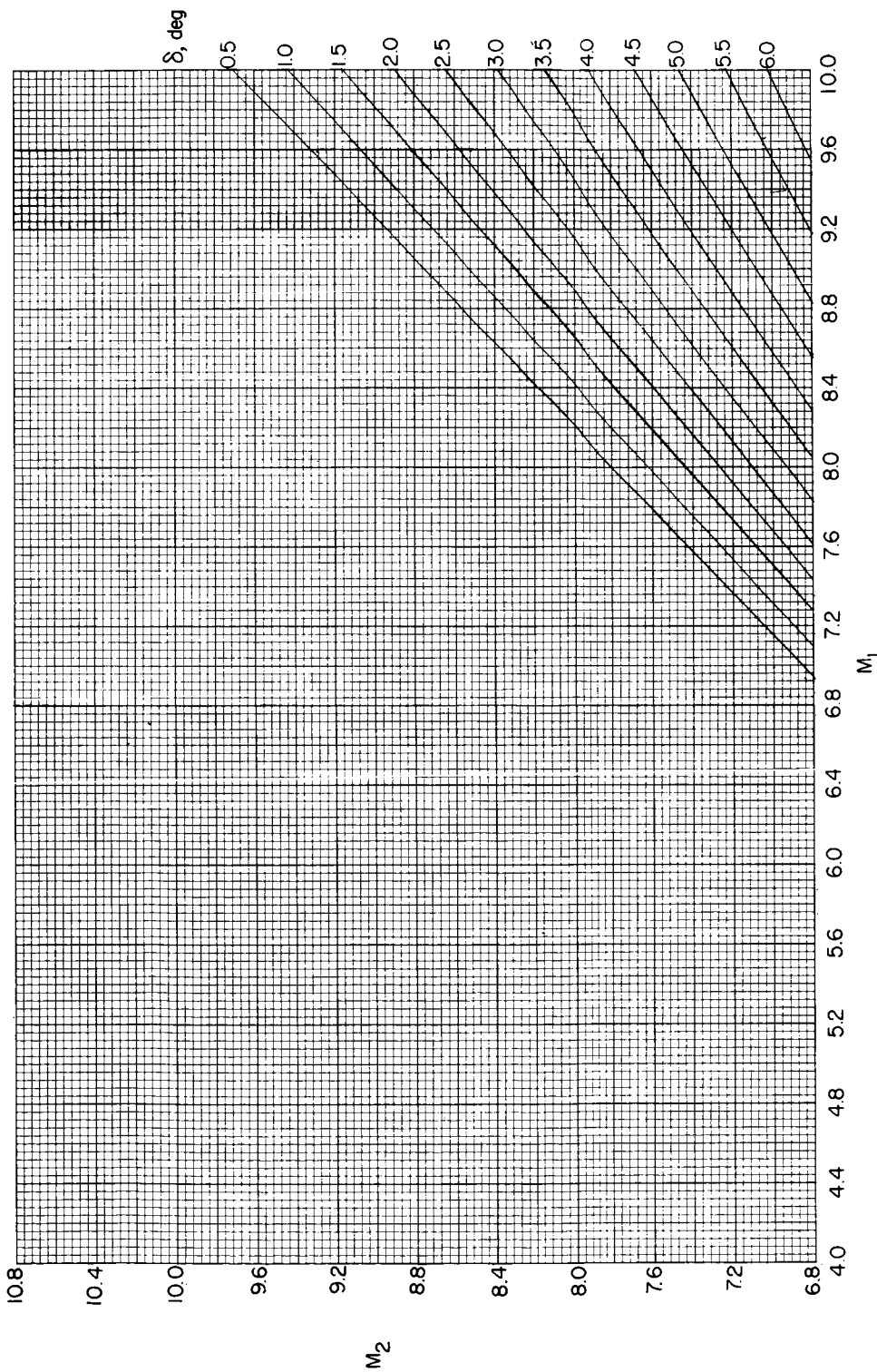
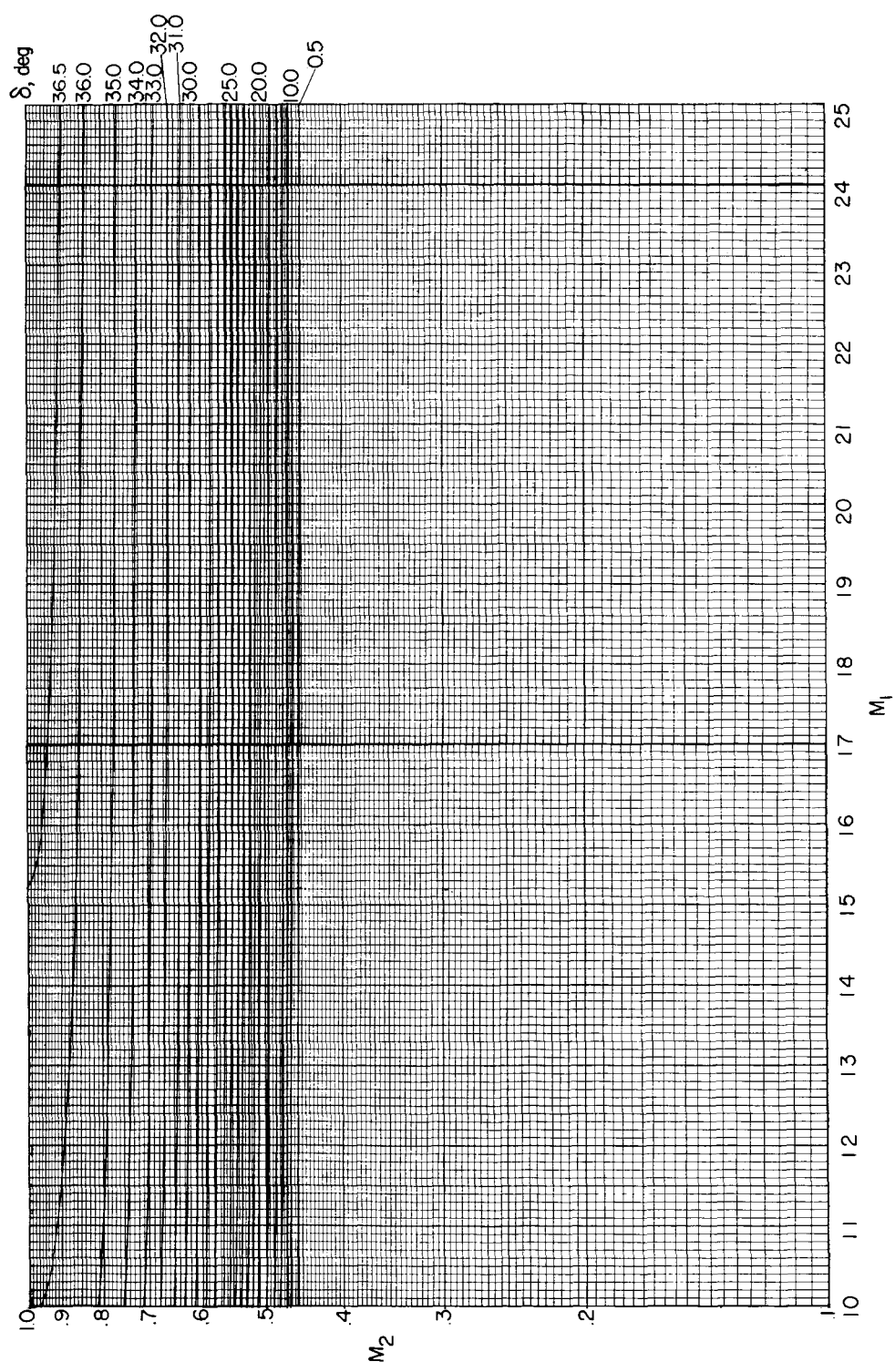
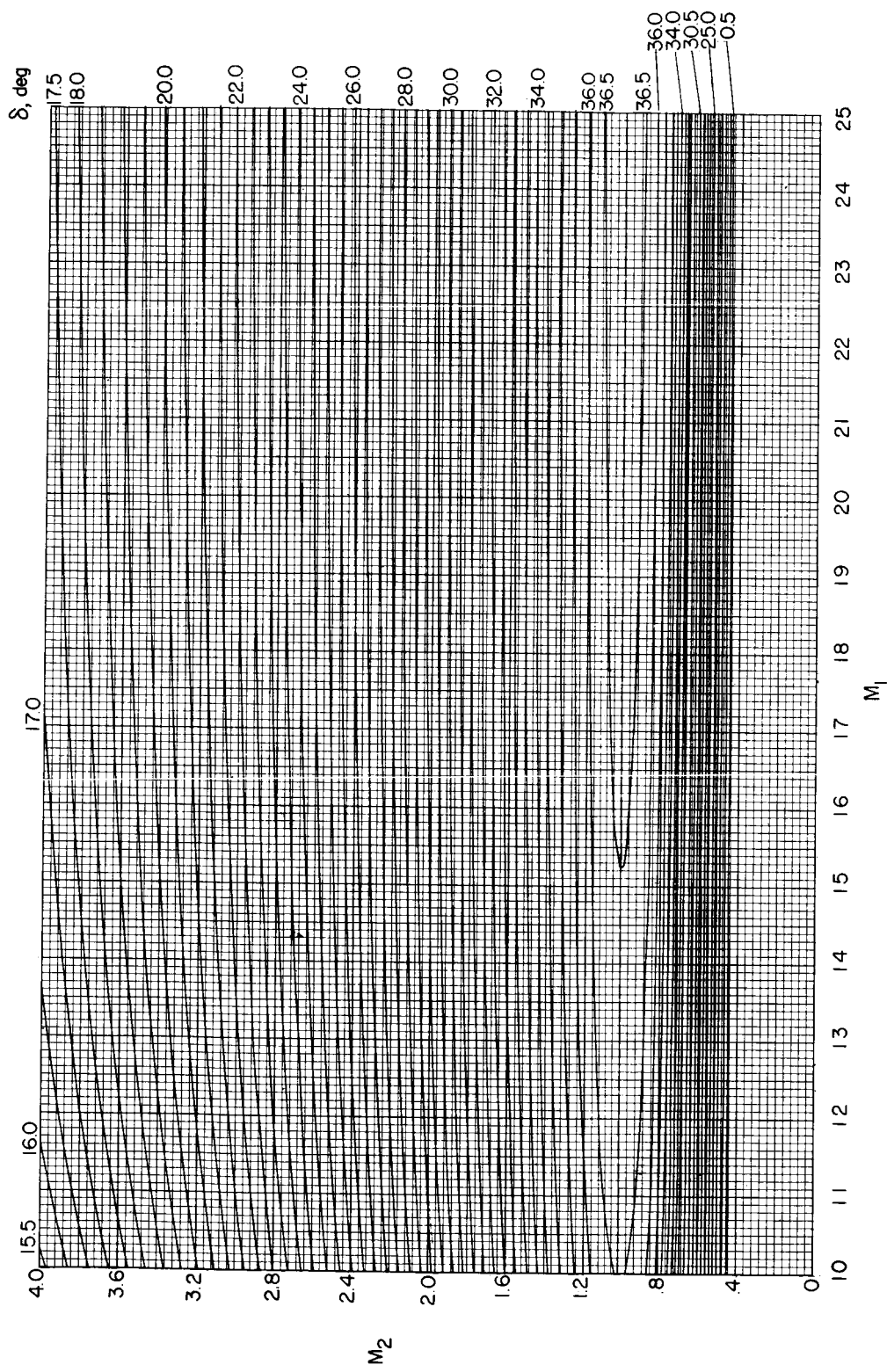


Figure 7.- Continued.



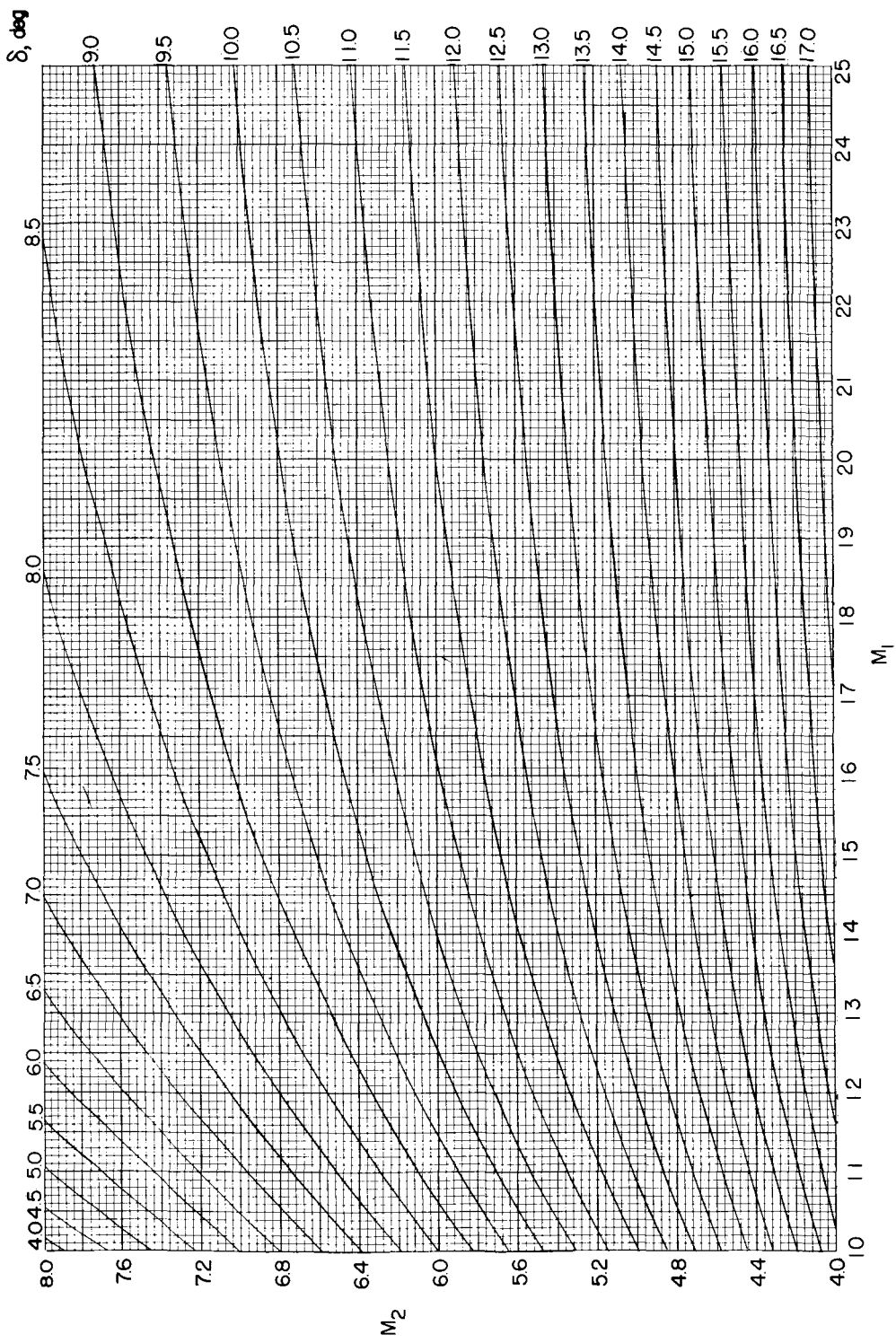
(h)  $M_1 = 10$  to 25;  $M_2 = 0.1$  to 1.

Figure 7.- Continued.



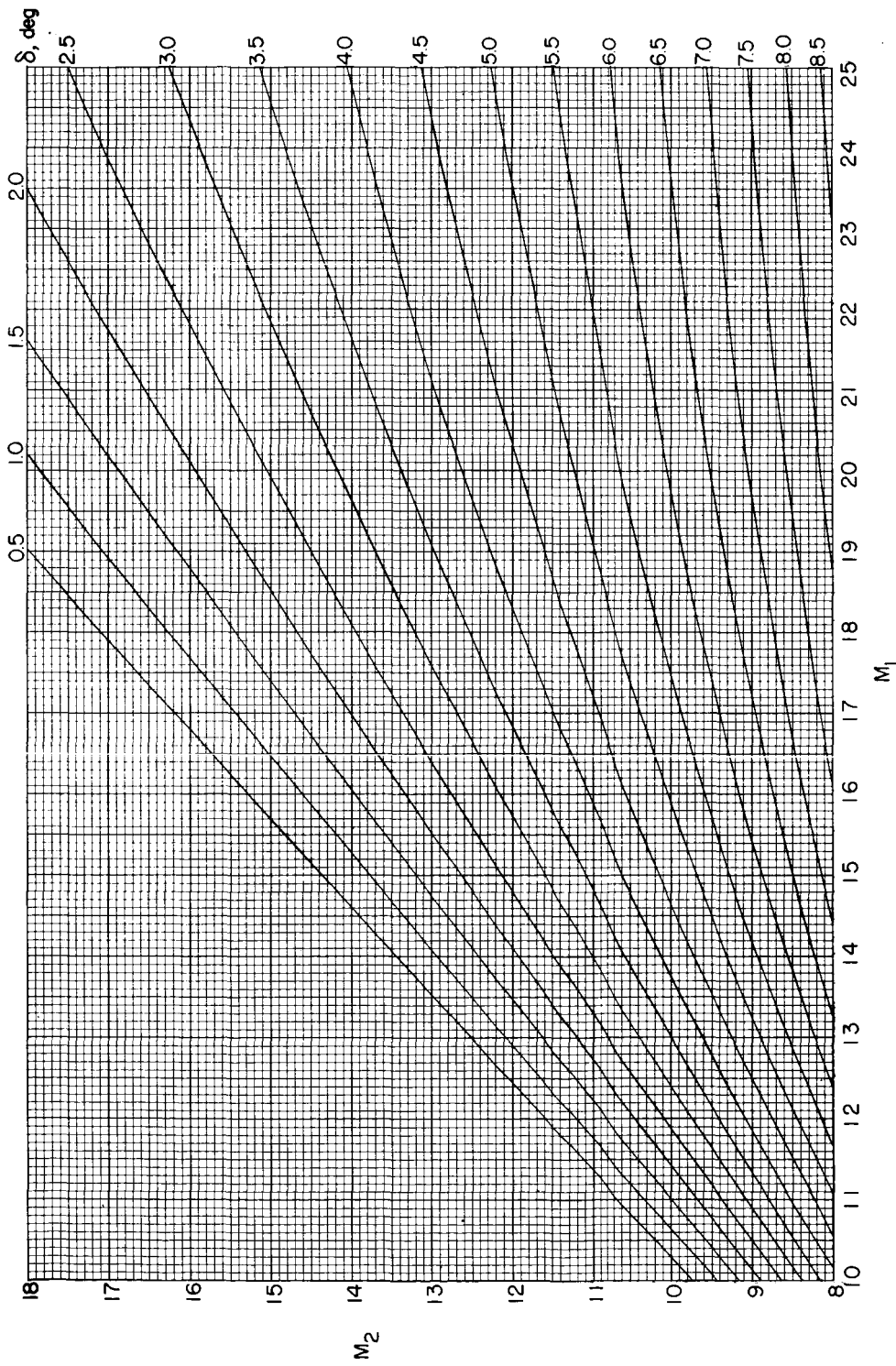
(1)  $M_1 = 10 \text{ to } 25; M_2 = 0 \text{ to } 4.$

Figure 7.- Continued.



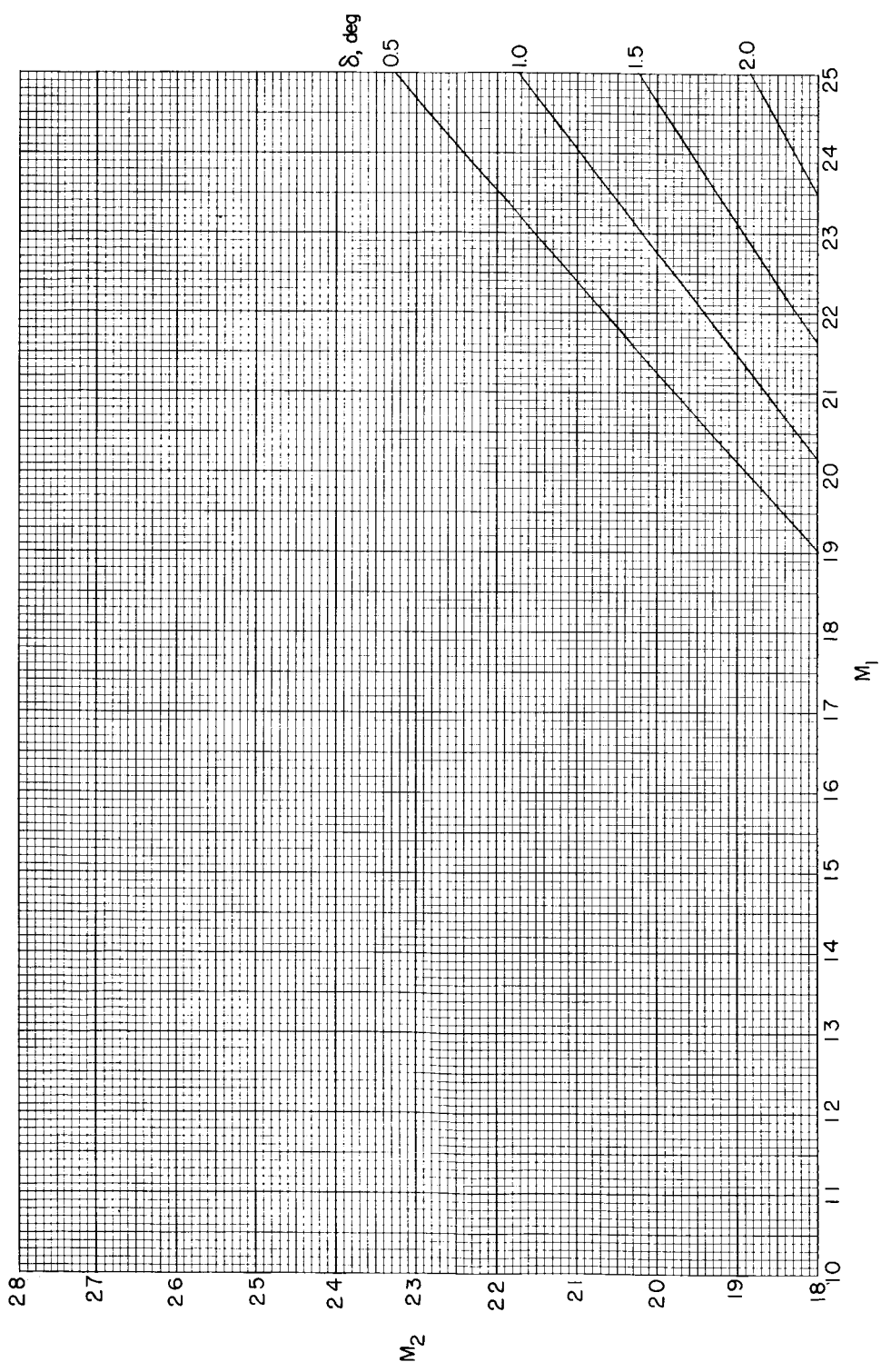
(j)  $M_1 = 10$  to  $25$ ;  $M_2 = 4$  to  $8$ .

Figure 7.- Continued.



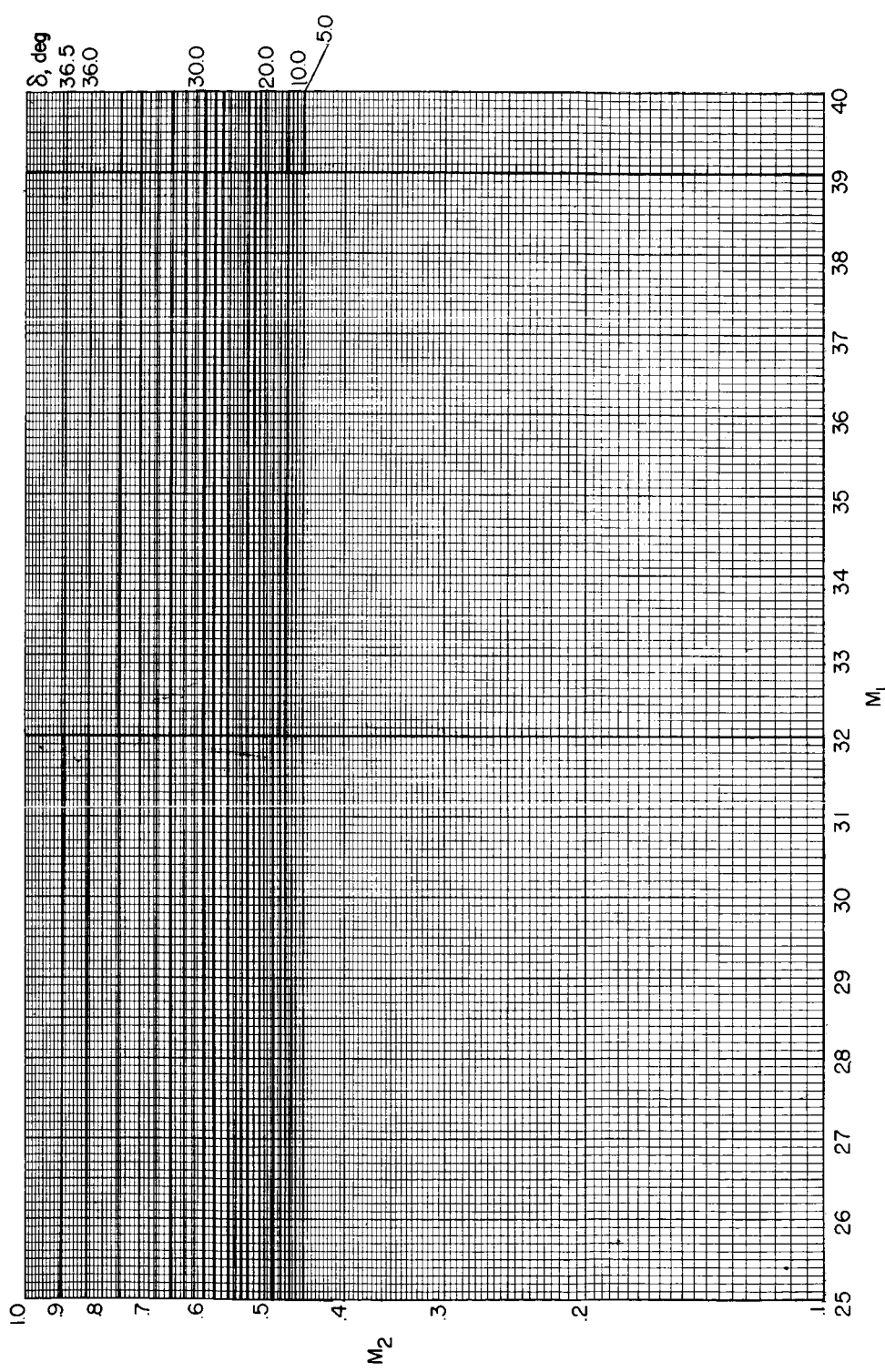
(k)  $M_1 = 10$  to 25;  $M_2 = 8$  to 18.

Figure 7.- Continued.



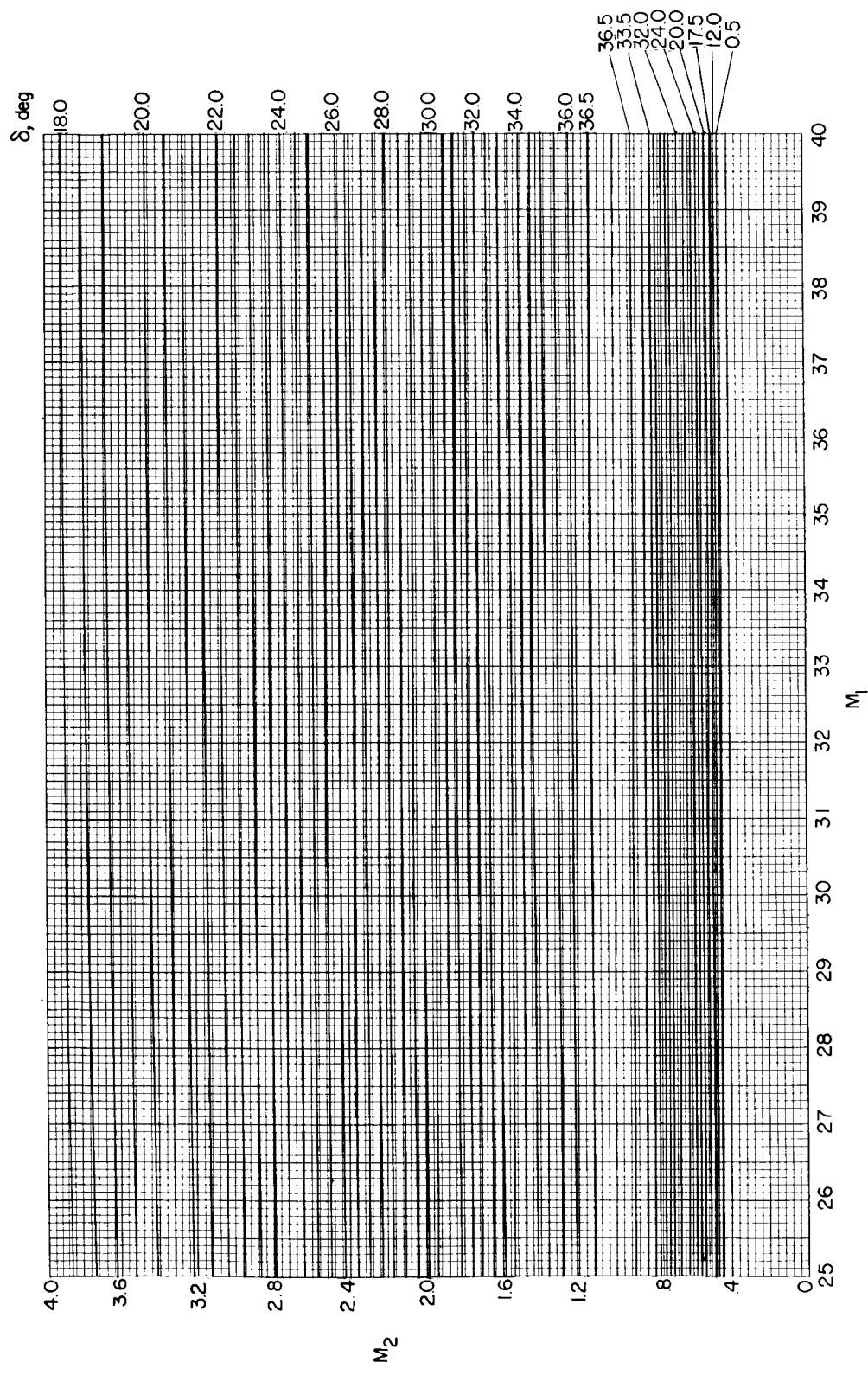
(l)  $M_1 = 10$  to  $25$ ;  $M_2 = 18$  to  $28$ .

Figure 7.- Continued.



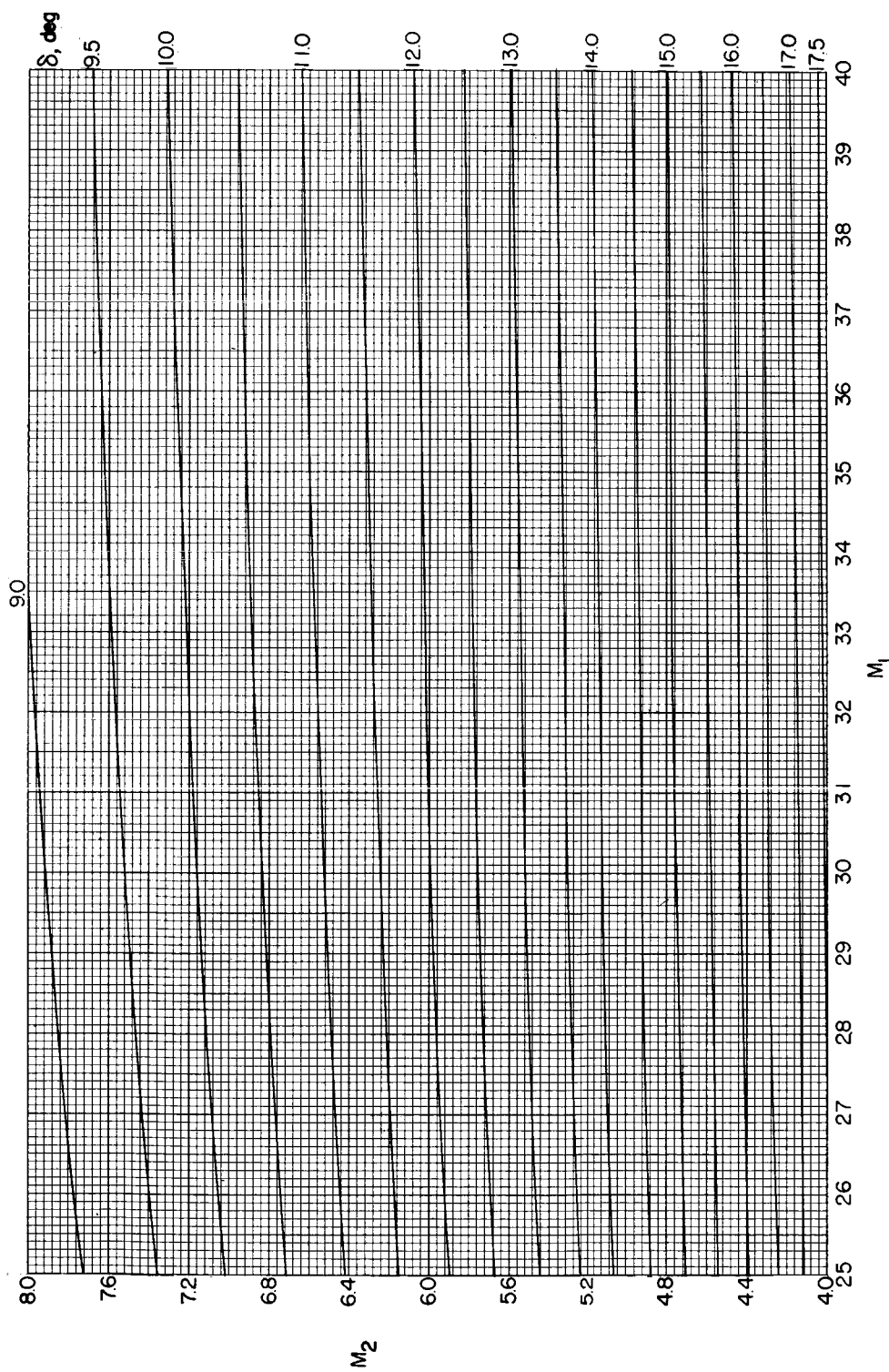
(m)  $M_1 = 25$  to 40;  $M_2 = 0.1$  to 1.

Figure 7.- Continued.



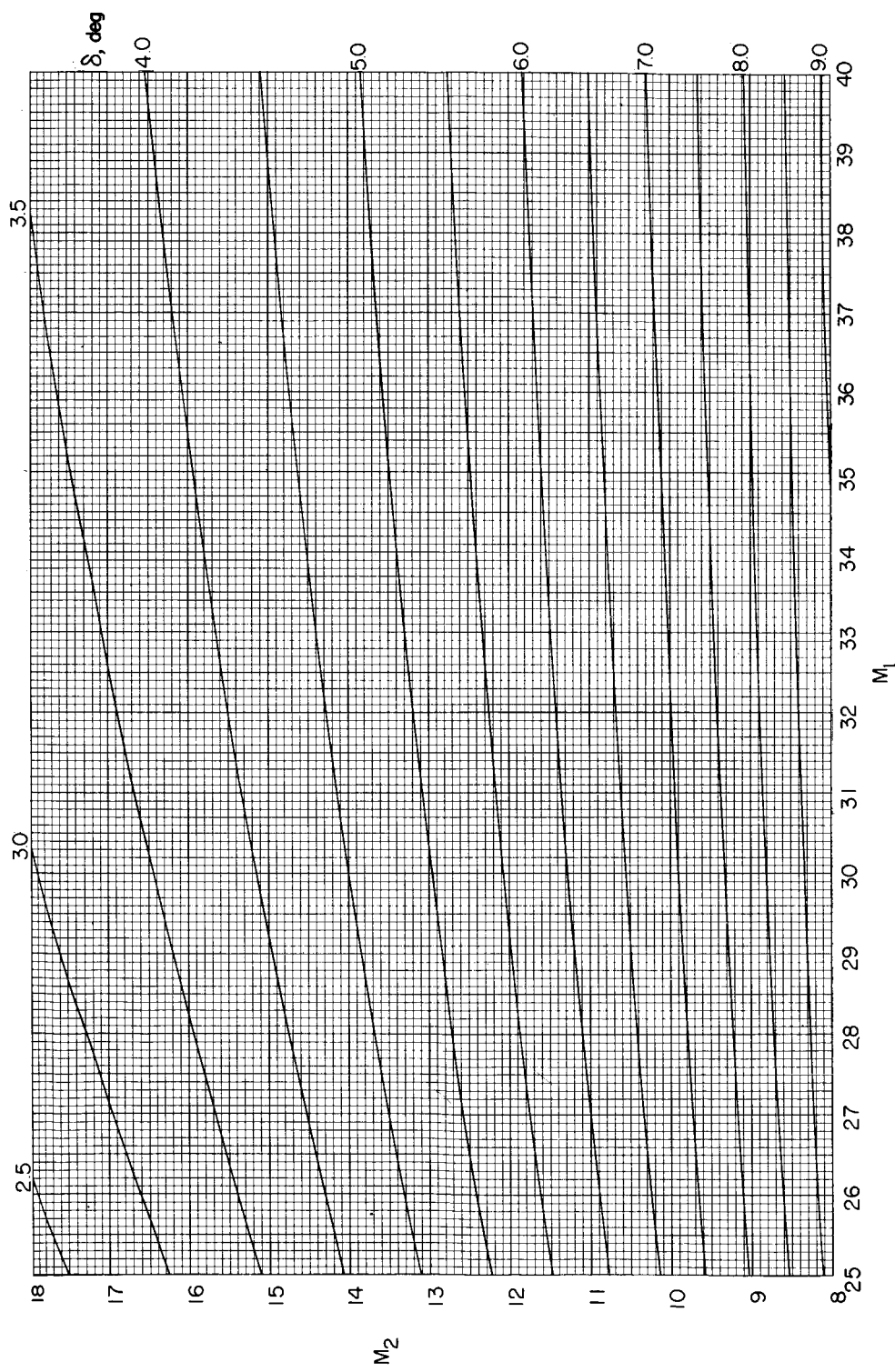
(n)  $M_1 = 25$  to 40;  $M_2 = 0$  to 4.

Figure 7.- Continued.



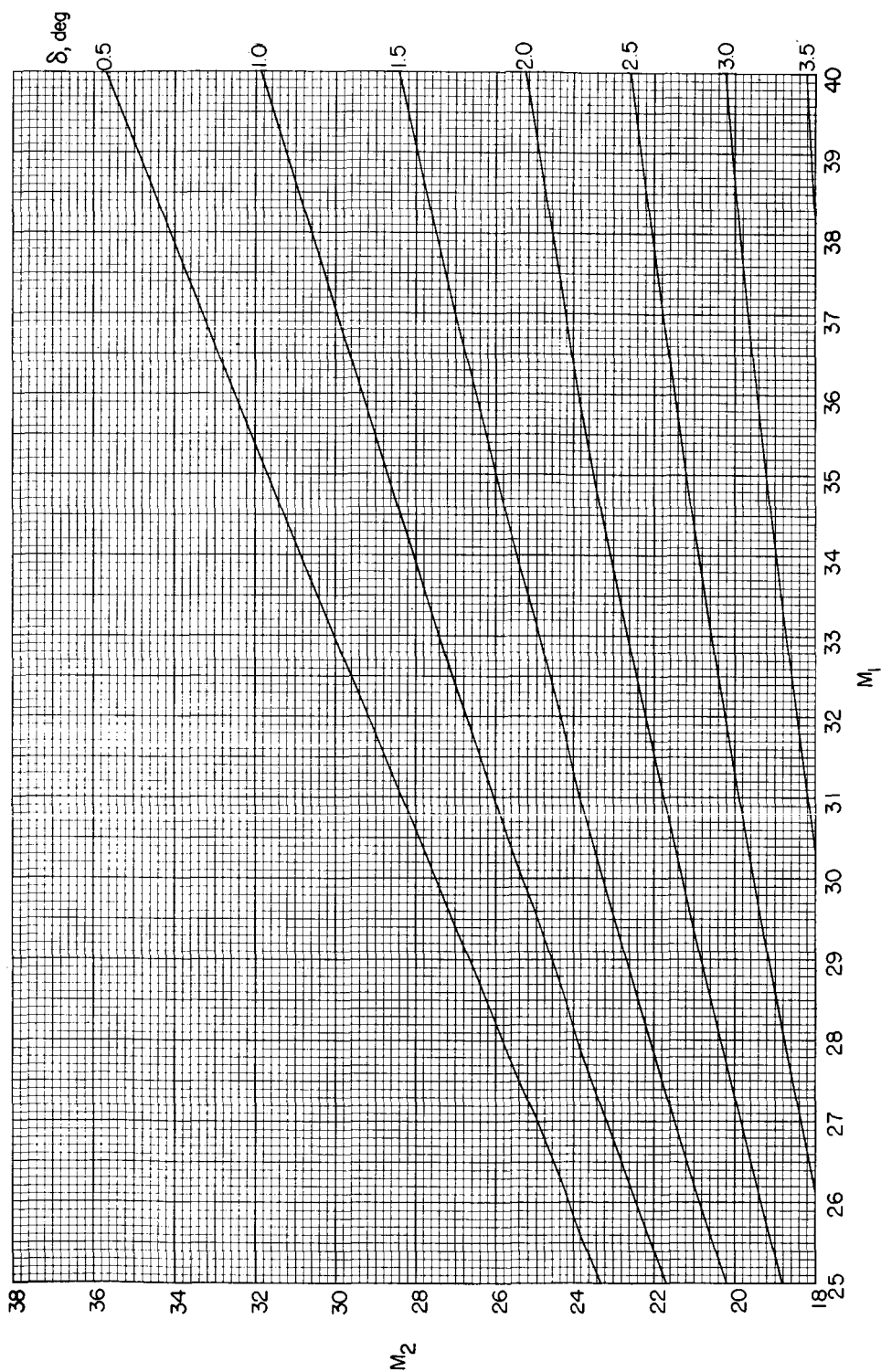
(o)  $M_1 = 25$  to 40;  $M_2 = 4$  to 8.

Figure 7.- Continued.



(p)  $M_1 = 25$  to 40;  $M_2 = 8$  to 18.

Figure 7.- Continued.



(q)  $M_1 = 25$  to 40;  $M_2 = 18$  to 38.

Figure 7.- Continued.

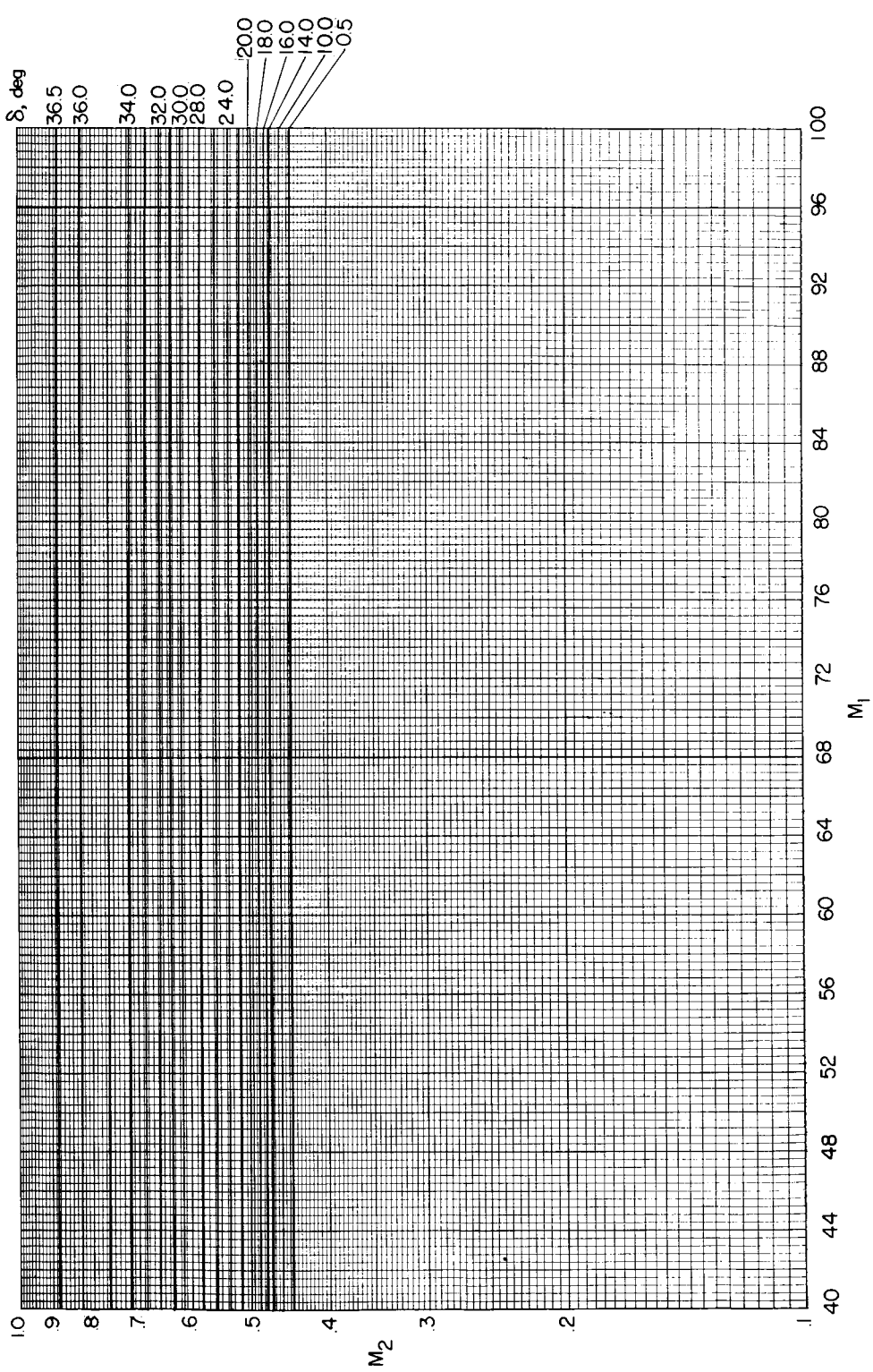
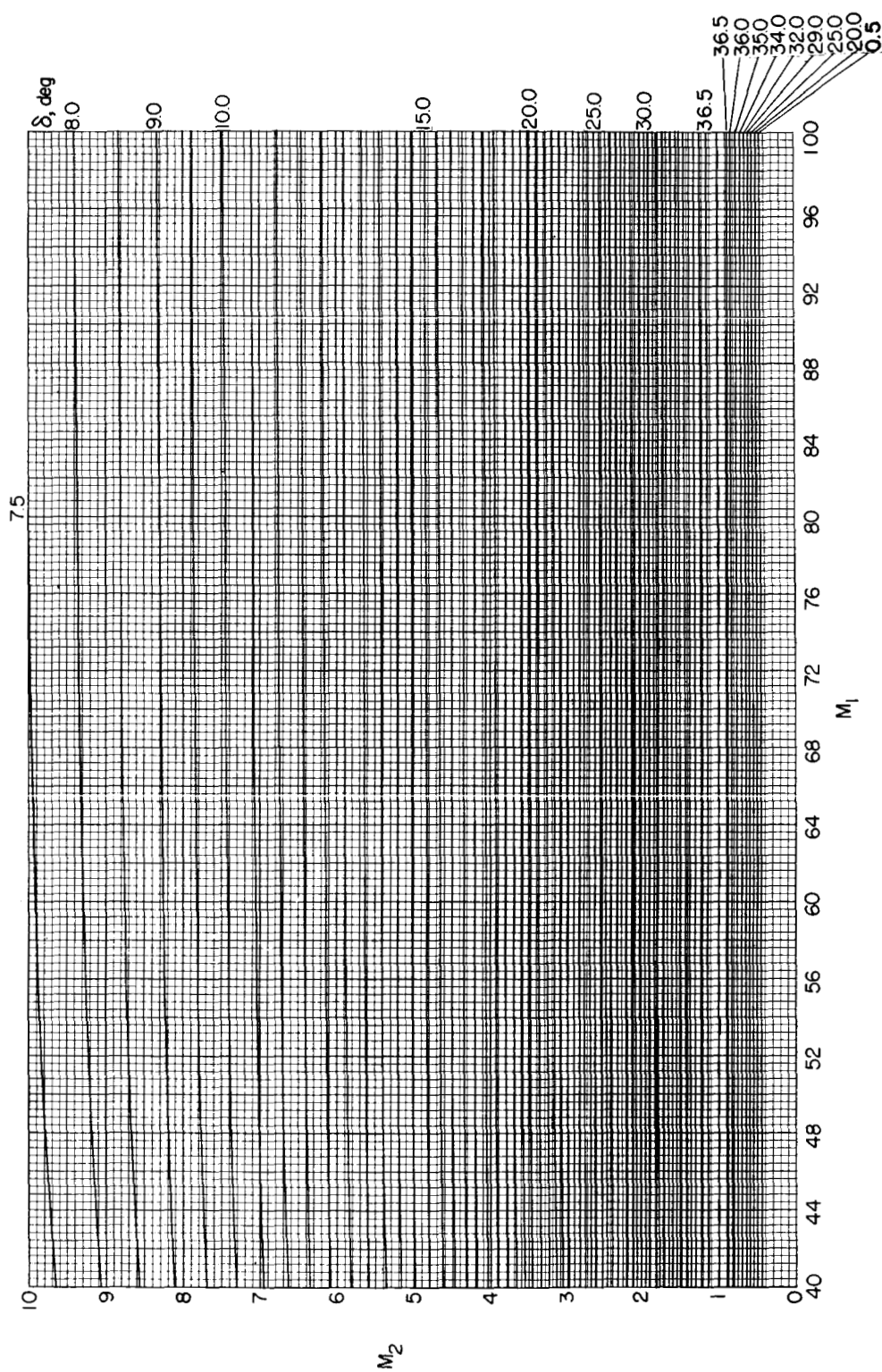
(r)  $M_1 = 40$  to  $100$ ;  $M_2 = 0.1$  to  $1$ .

Figure 7.- Continued.



(s)  $M_1 = 40$  to 100;  $M_2 = 0$  to 10.

Figure 7.- Continued.

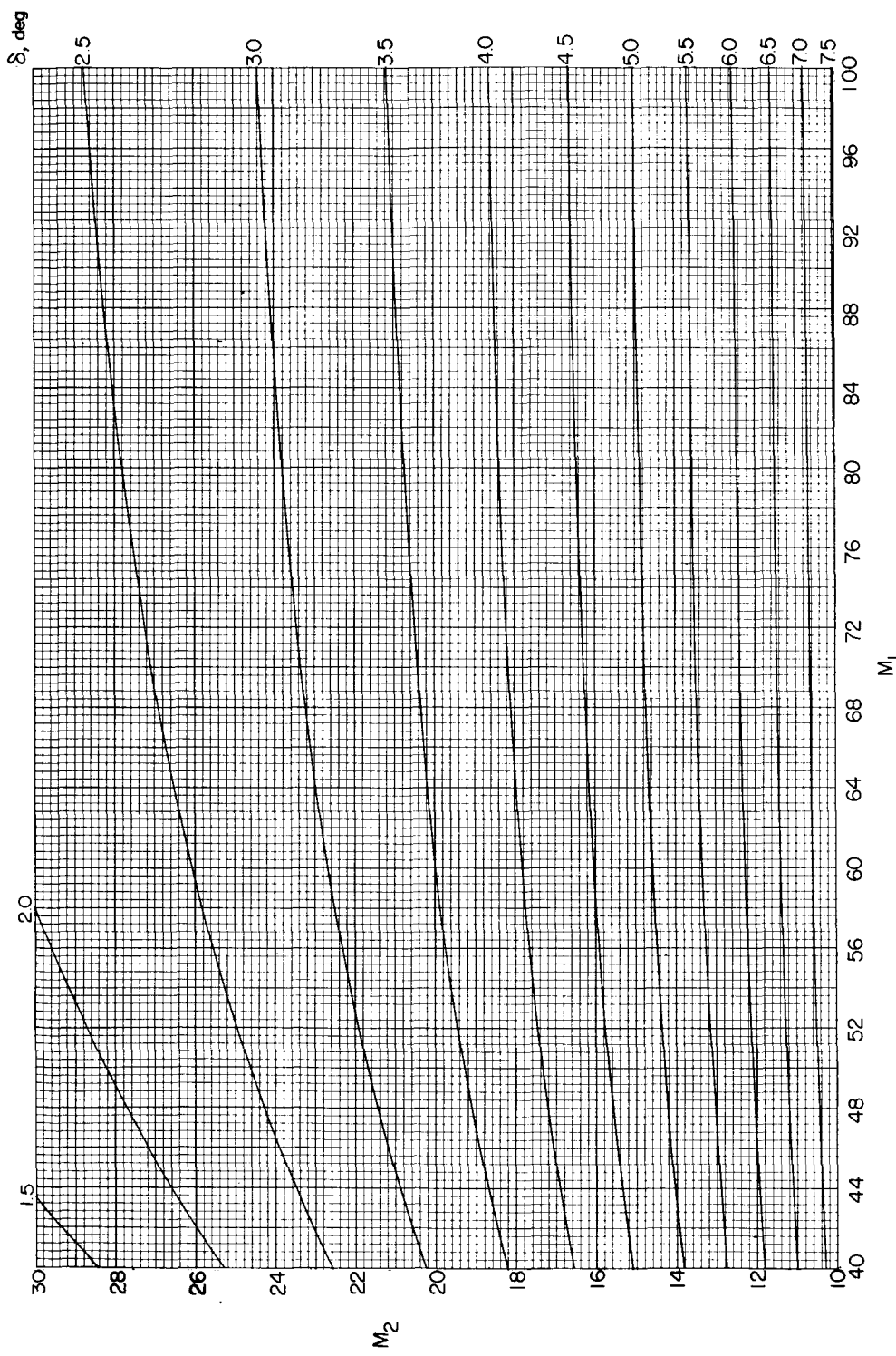
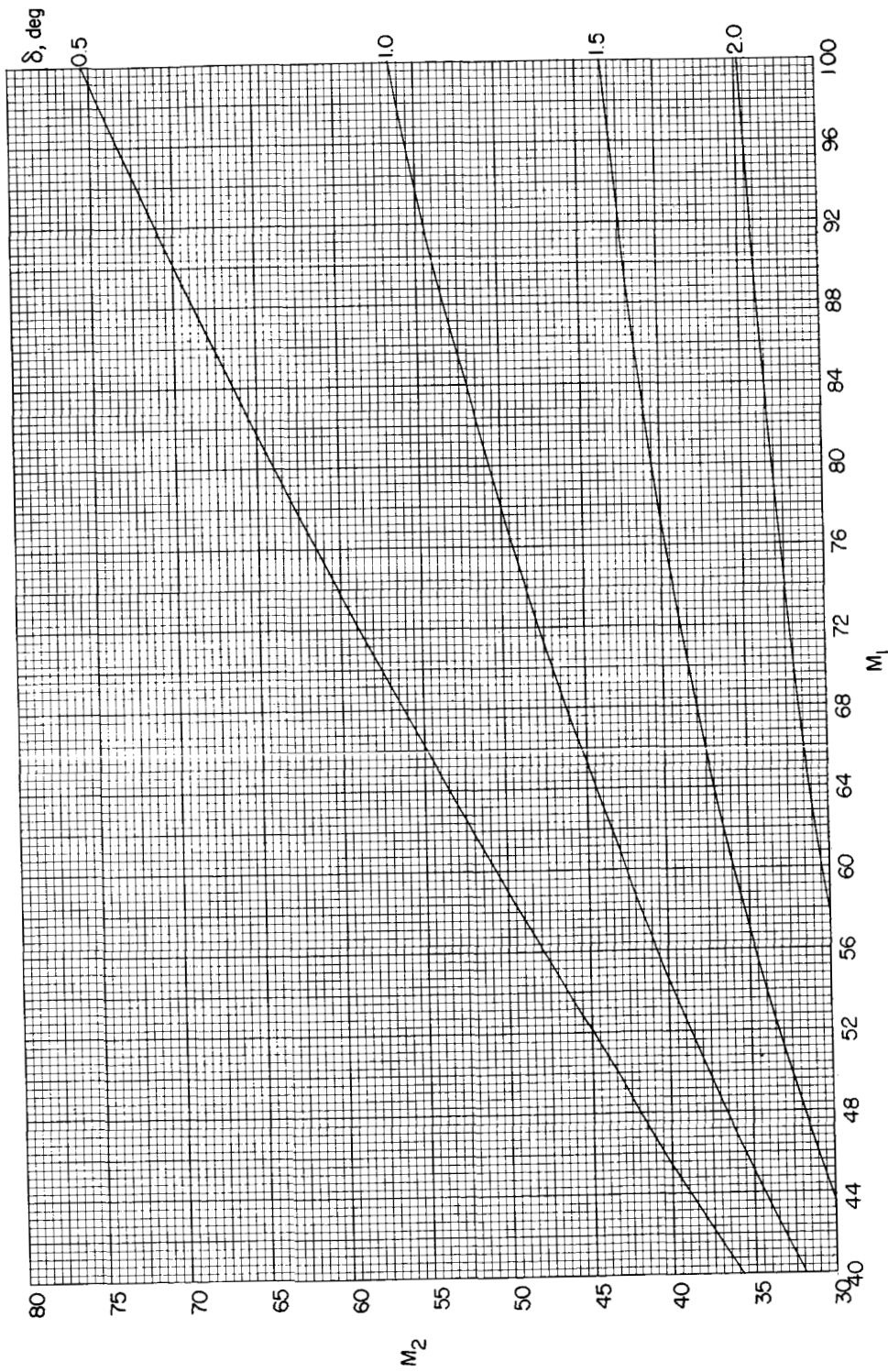
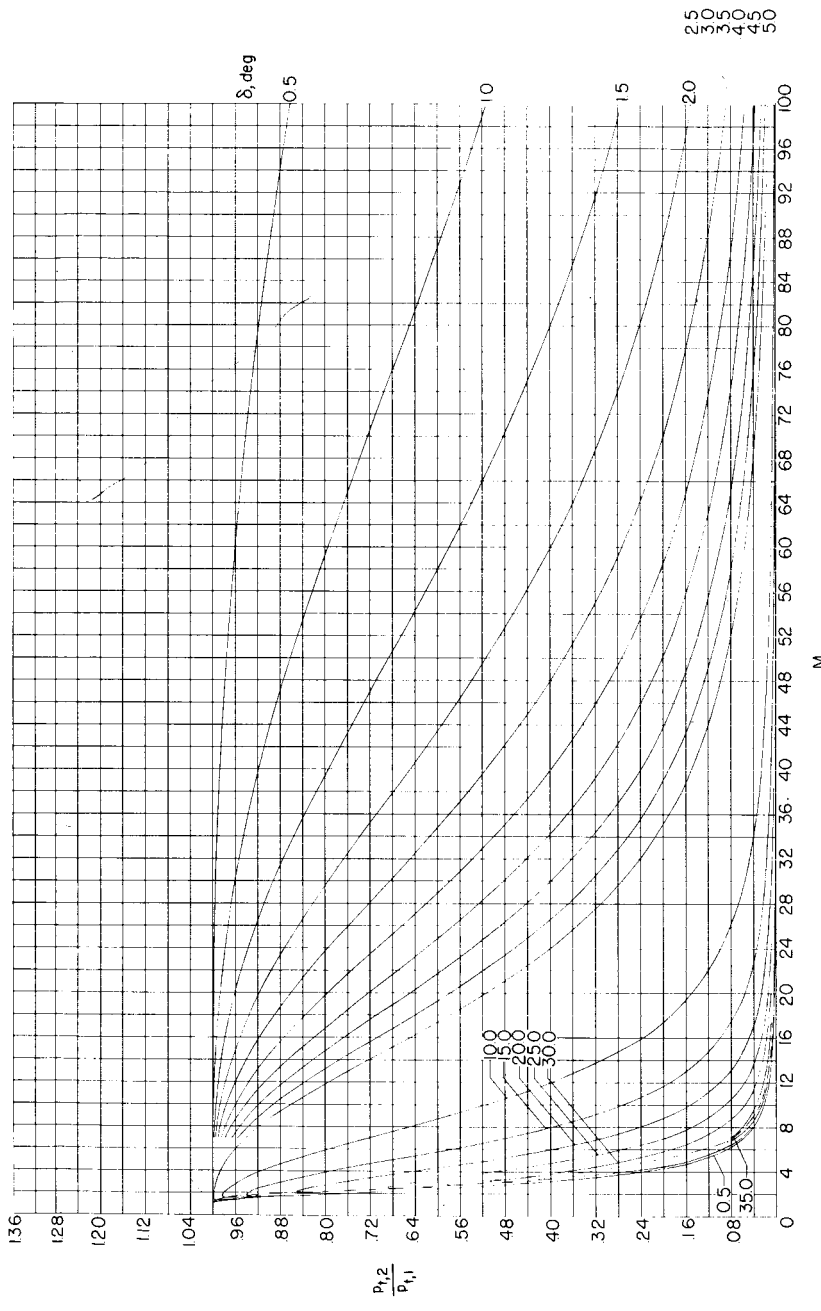
(t)  $M_1 = 40$  to  $100$ ;  $M_2 = 10$  to  $30$ .

Figure 7.- Continued.



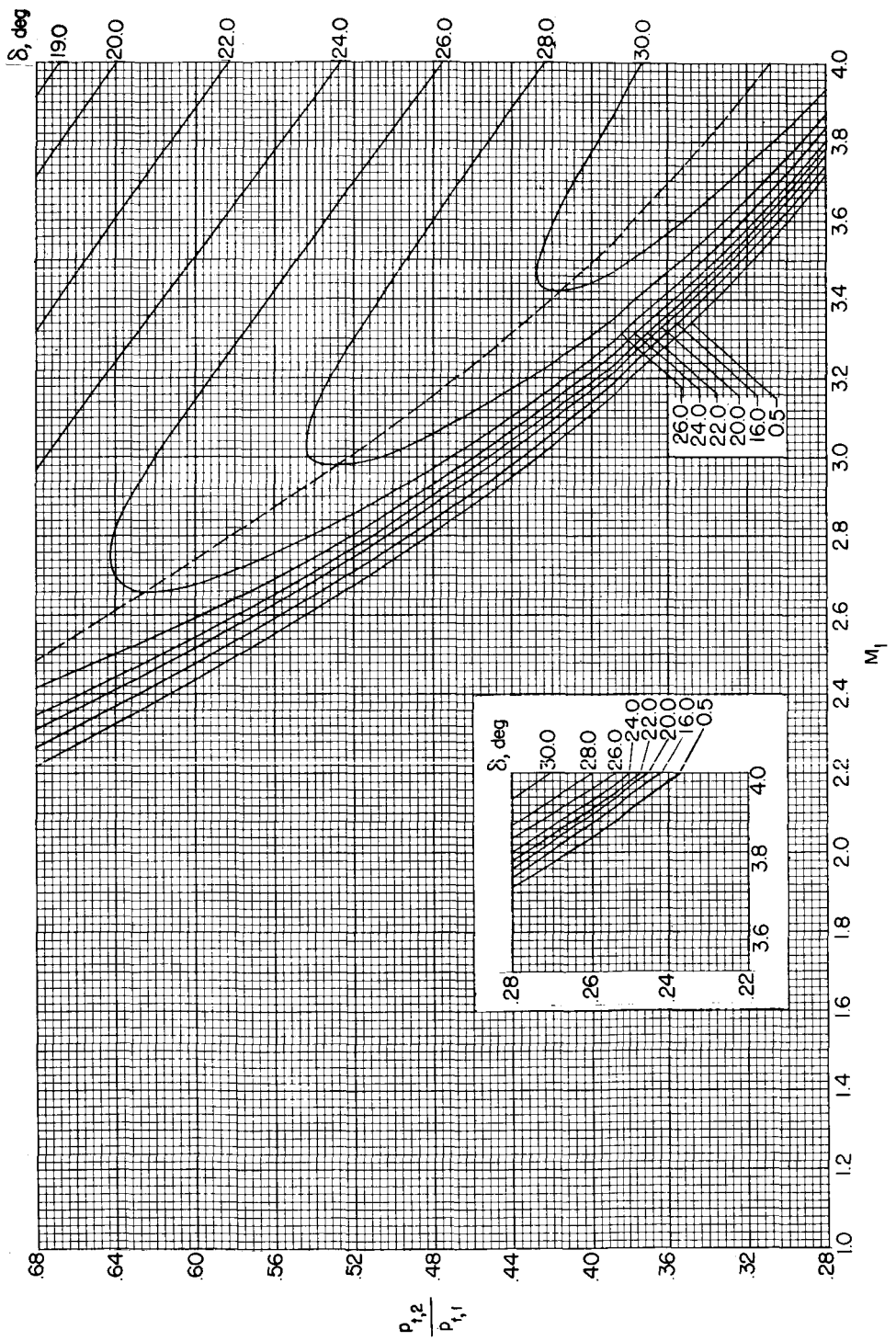
(u)  $M_1 = 40$  to 100;  $M_2 = 30$  to 80.

Figure 7.— Concluded.



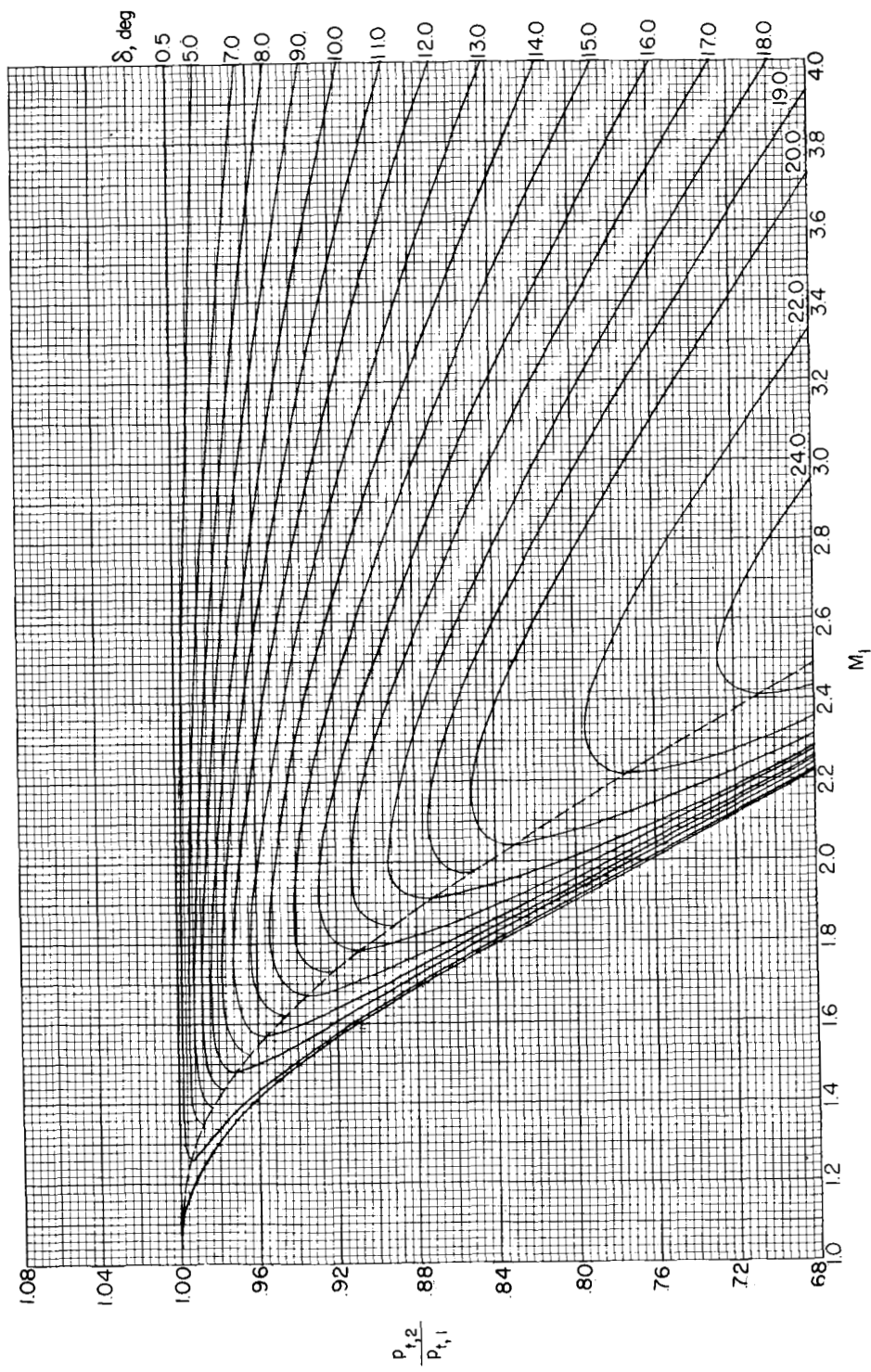
(a)  $M_1 = 1$  to  $100$ ;  $\frac{p_{t,2}}{p_{t,1}} = 0$  to  $1$ .

Figure 8.- Variation of ratio of total pressure behind a two-dimensional shock to free-stream total pressure with free-stream Mach number for various flow-deflection angles. (Dashed line denotes boundary between weak and strong shock solutions. Weak shock solution is above dashed line.)



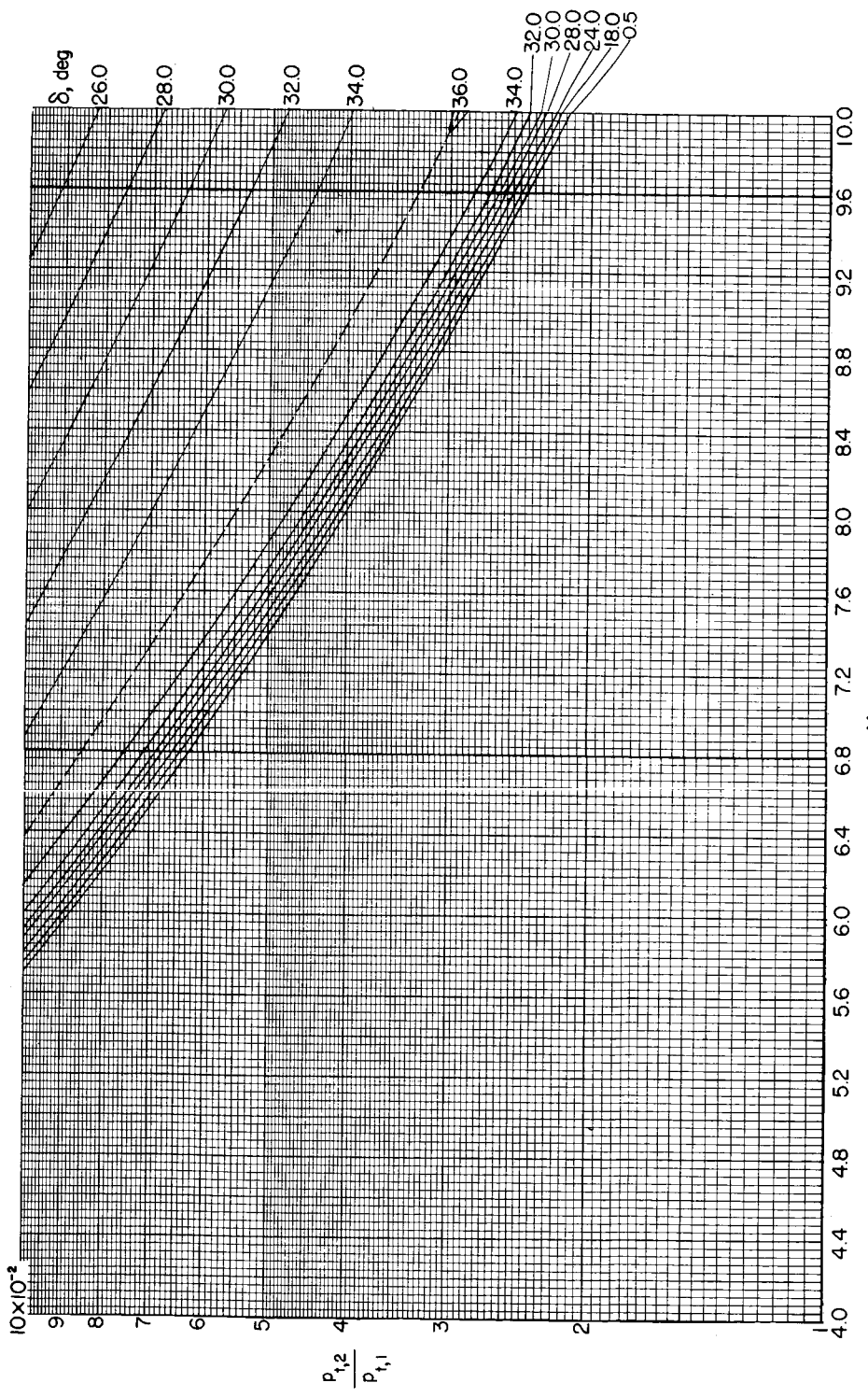
(b)  $M_1 = 1$  to 4;  $\frac{p_{t,2}}{p_{t,1}} = 0.22$  to 0.68.

Figure 8. - Continued.



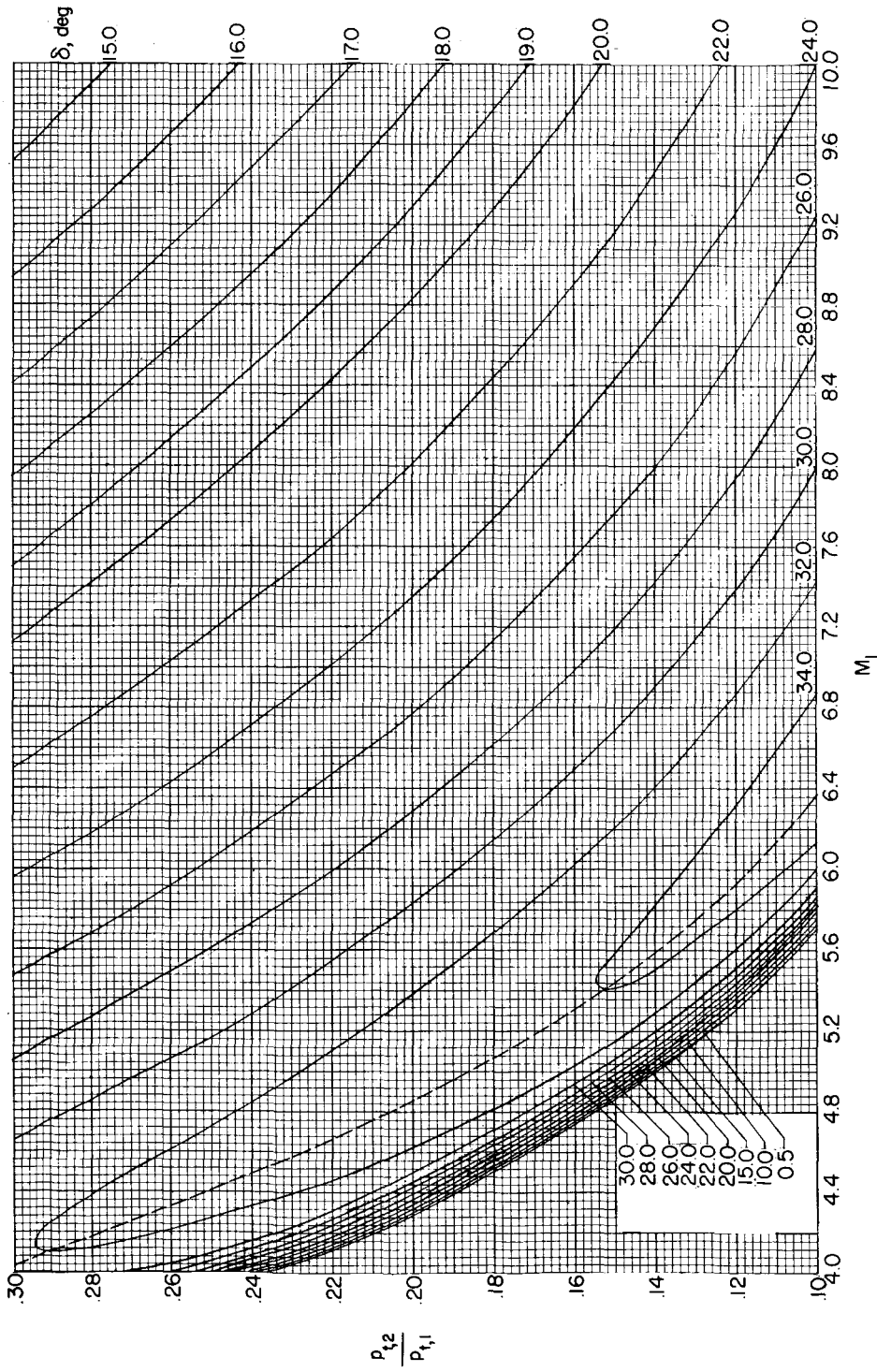
(c)  $M_1 = 1$  to 4;  $\frac{P_{t,2}}{P_{t,1}} = 0.68$  to 1.

Figure 8.- Continued.



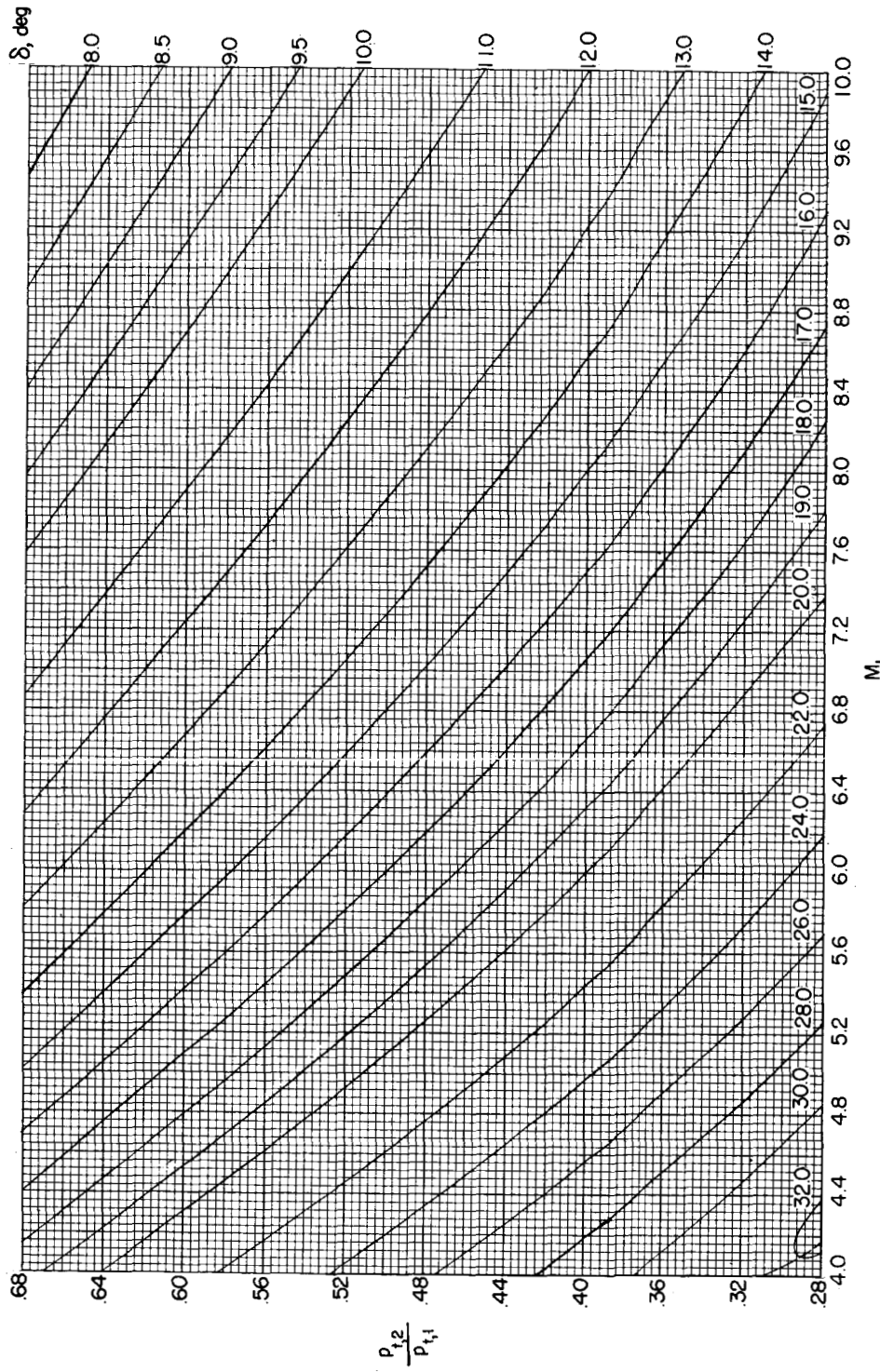
(d)  $M_1 = 4$  to 10;  $\frac{P_{t,2}}{P_{t,1}} = 1 \times 10^{-2}$  to  $10 \times 10^{-2}$ .

Figure 8.- Continued.



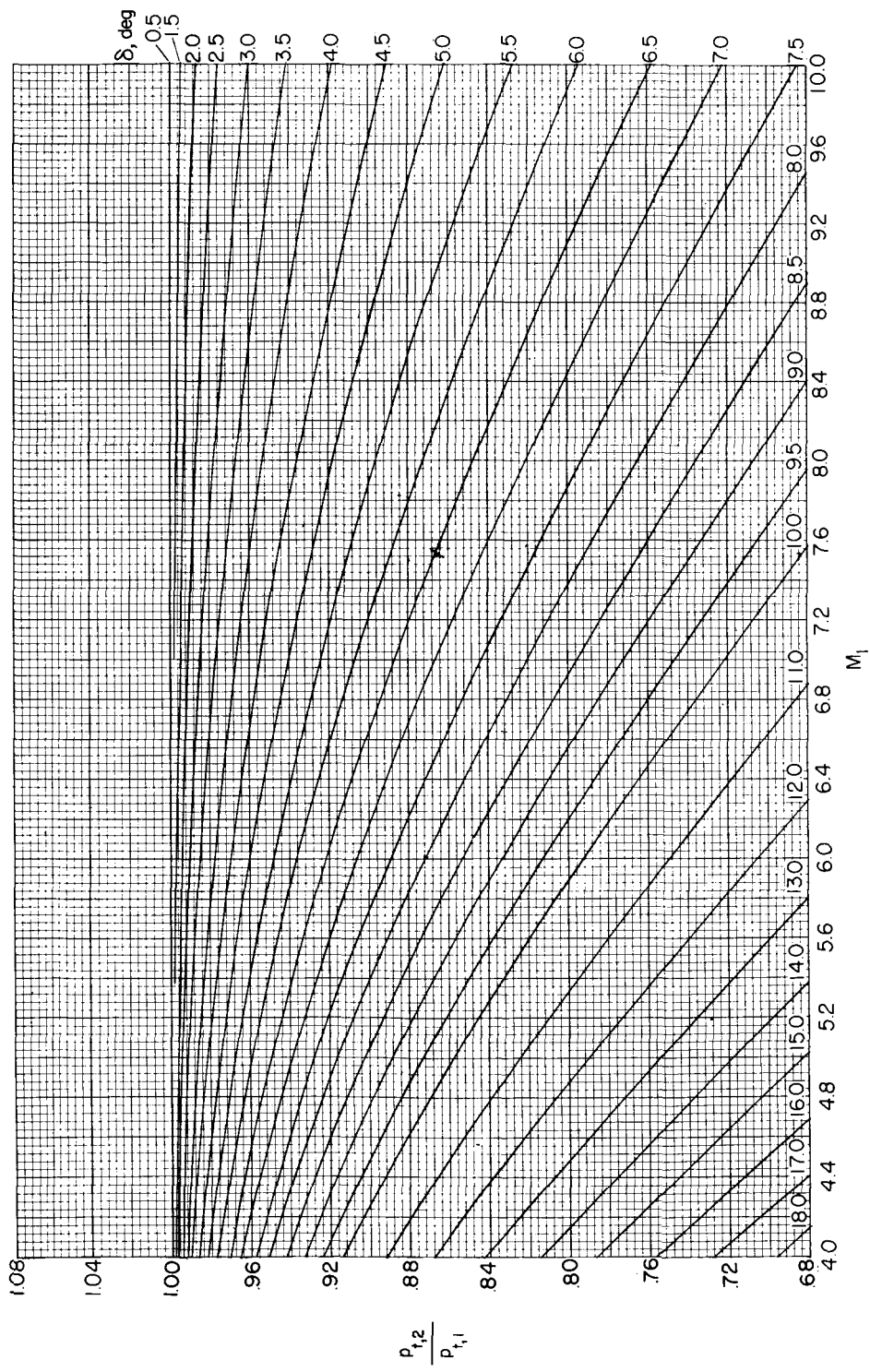
(e)  $M_1 = 4$  to 10;  $\frac{P_{t,2}^2}{P_{t,1}^2} = 0.1$  to 0.3.

Figure 8.- Continued.



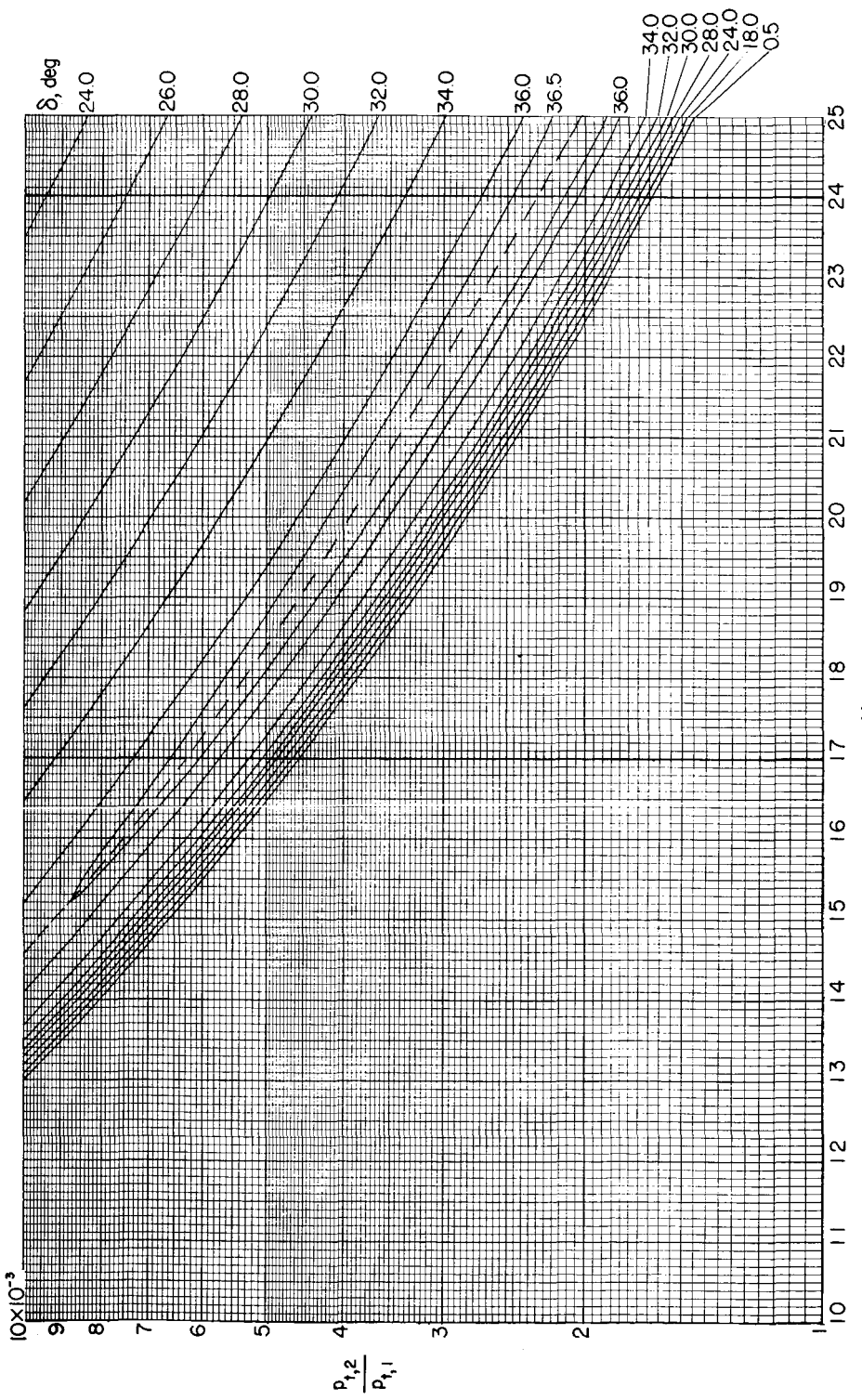
$$(f) \quad M_1 = 4 \text{ to } 10; \quad \frac{P_{t,2}}{P_{t,1}} = 0.28 \text{ to } 0.68.$$

Figure 8.- Continued.



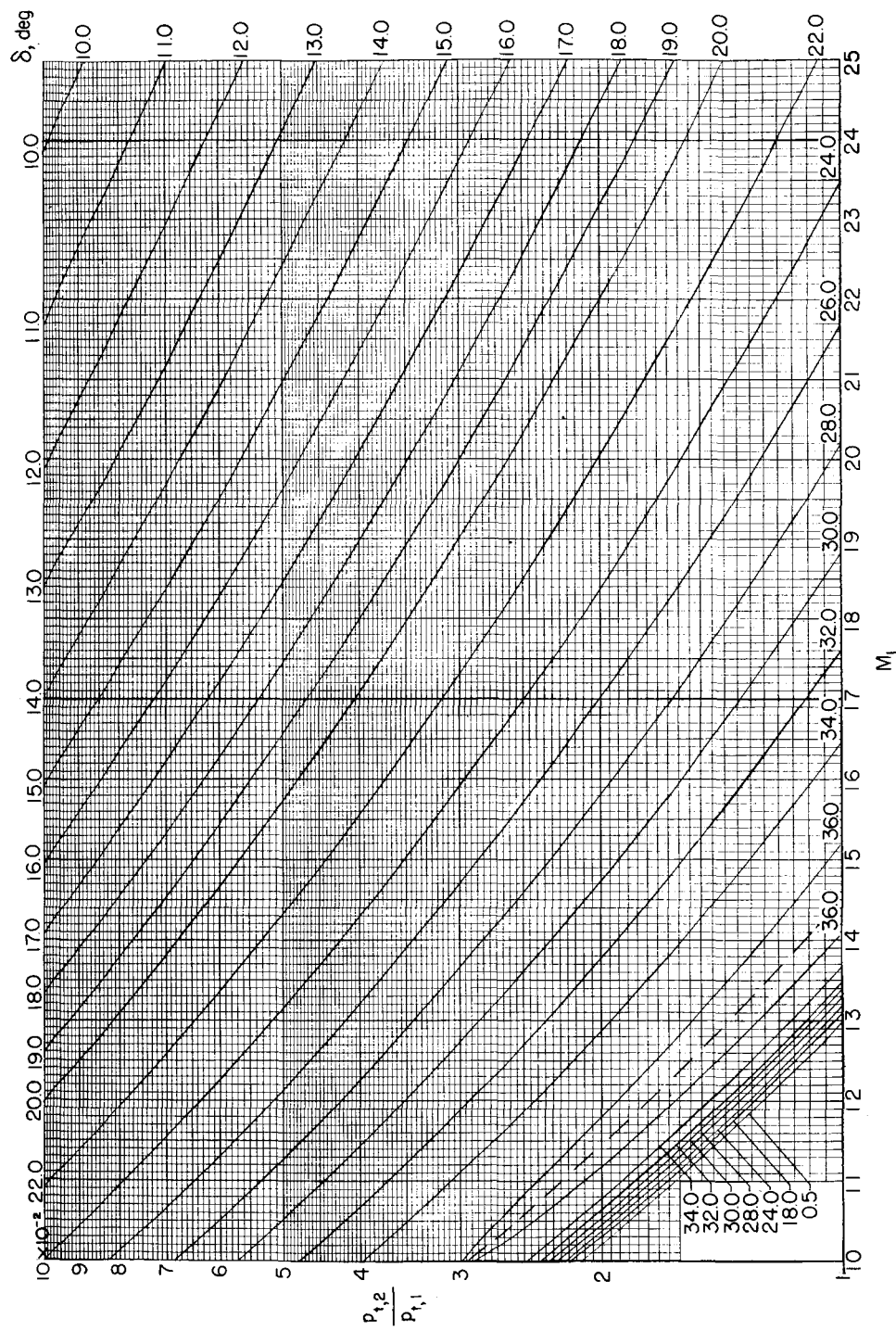
(g)  $M_1 = 4$  to 10;  $\frac{p_{t,2}}{p_{t,1}} = 0.68$  to 1.

Figure 8.- Continued.



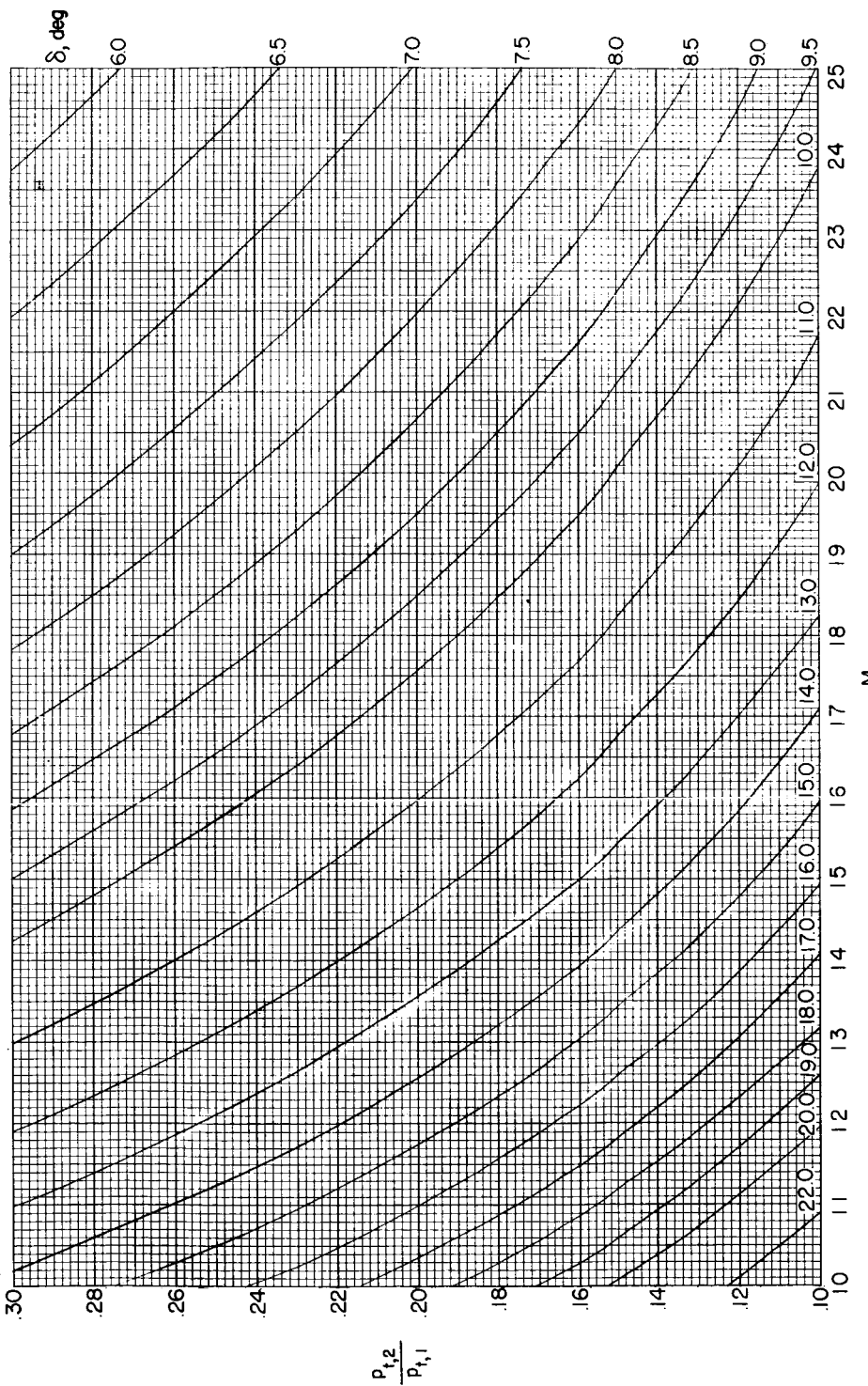
(h)  $M_{\perp} = 10$  to  $25$ ;  $\frac{p_{t,2}}{p_{t,1}} = 1 \times 10^{-3}$  to  $10 \times 10^{-3}$ .

Figure 8.- Continued.



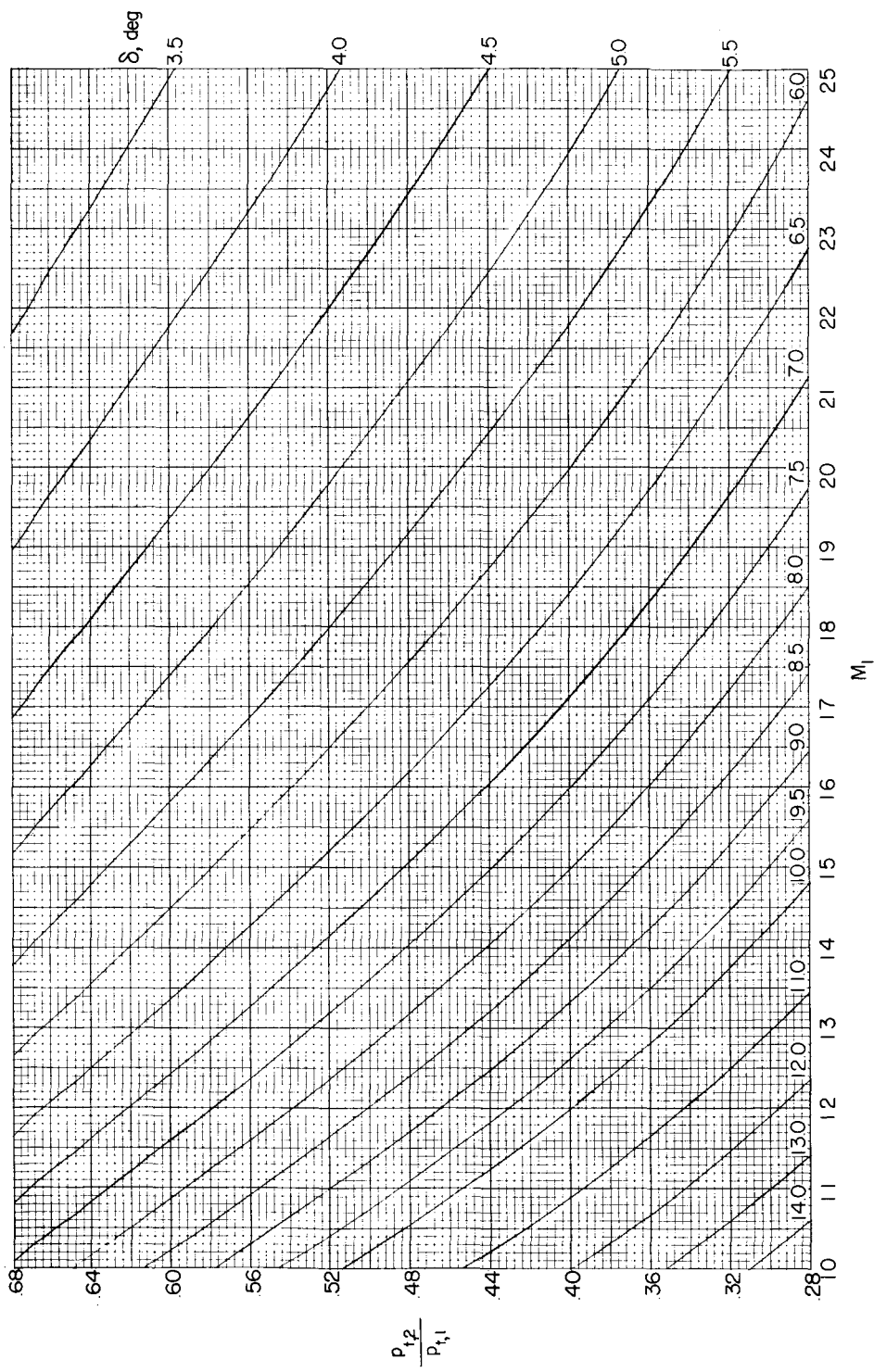
(1)  $M_1 = 10$  to  $25$ ;  $\frac{p_{t,2}}{p_{t,1}} = 1 \times 10^{-2}$  to  $10 \times 10^{-2}$ .

Figure 8.- Continued.



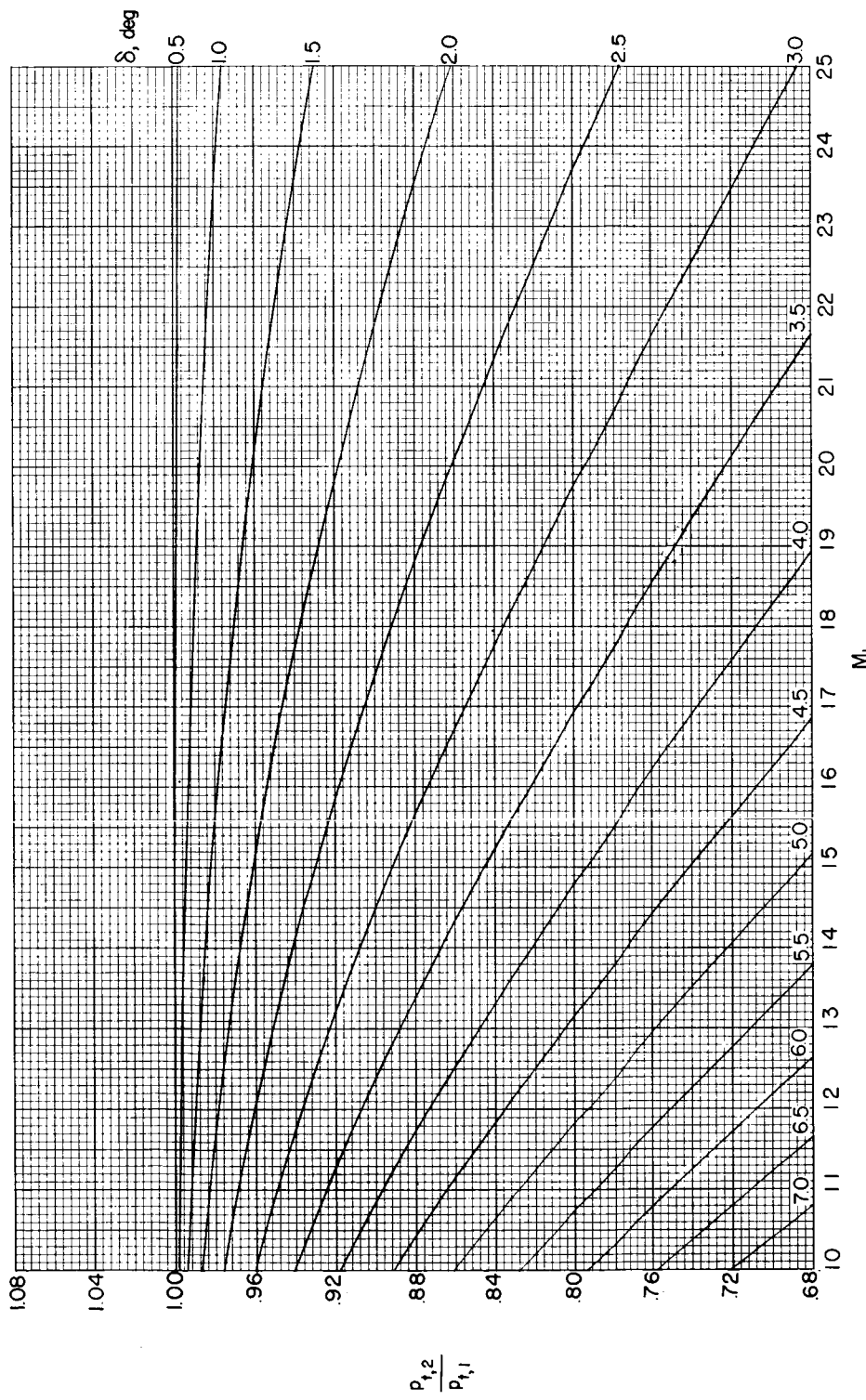
(j)  $M_1 = 10 \text{ to } 25; \frac{P_{t,2}}{P_{t,1}} = 0.1 \text{ to } 0.3.$

Figure 8.- Continued.



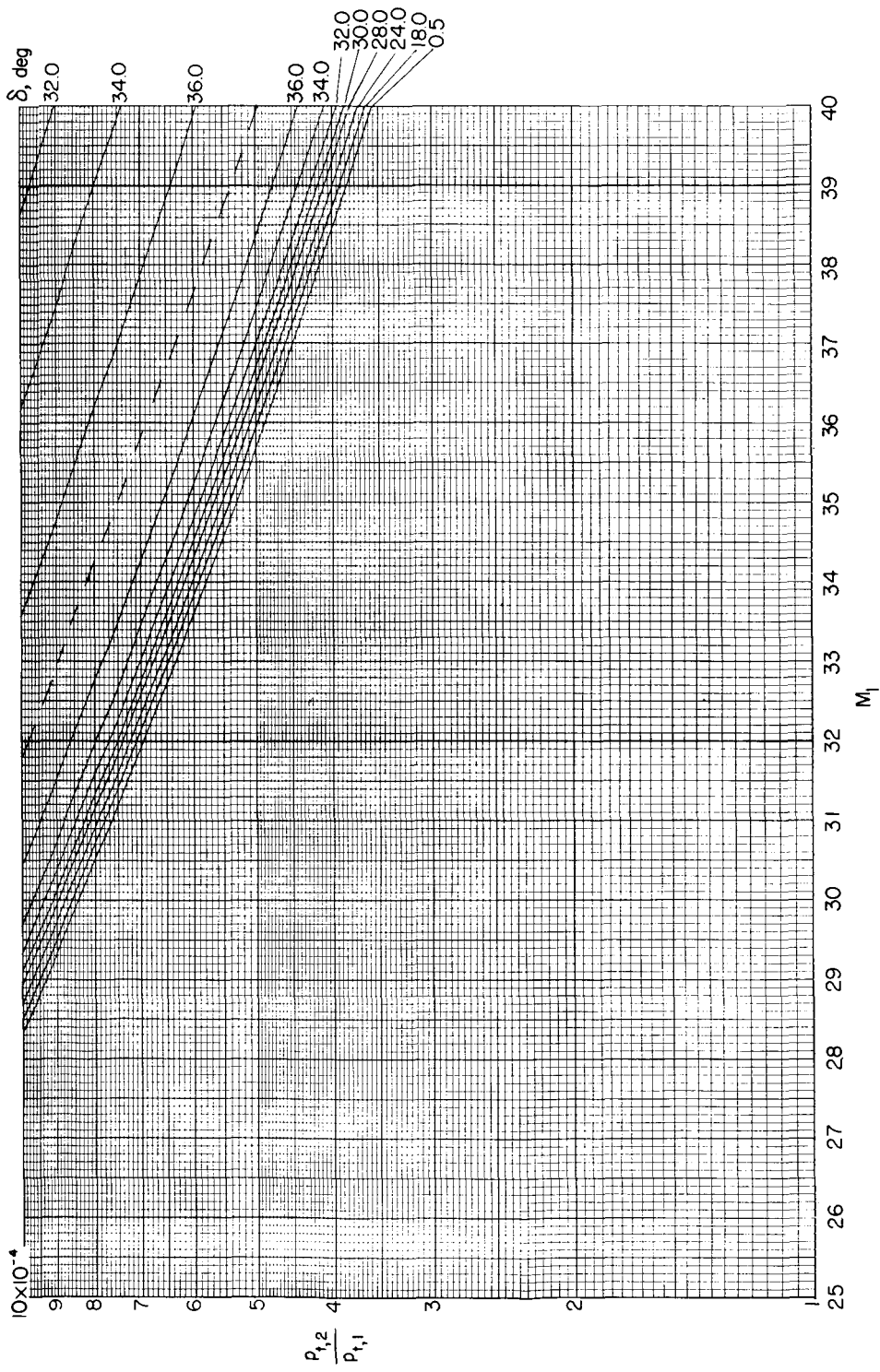
(k)  $M_1 = 10$  to  $25$ ;  $\frac{P_{t2}}{P_{t1}} = 0.28$  to  $0.68$ .

Figure 8.- Continued.



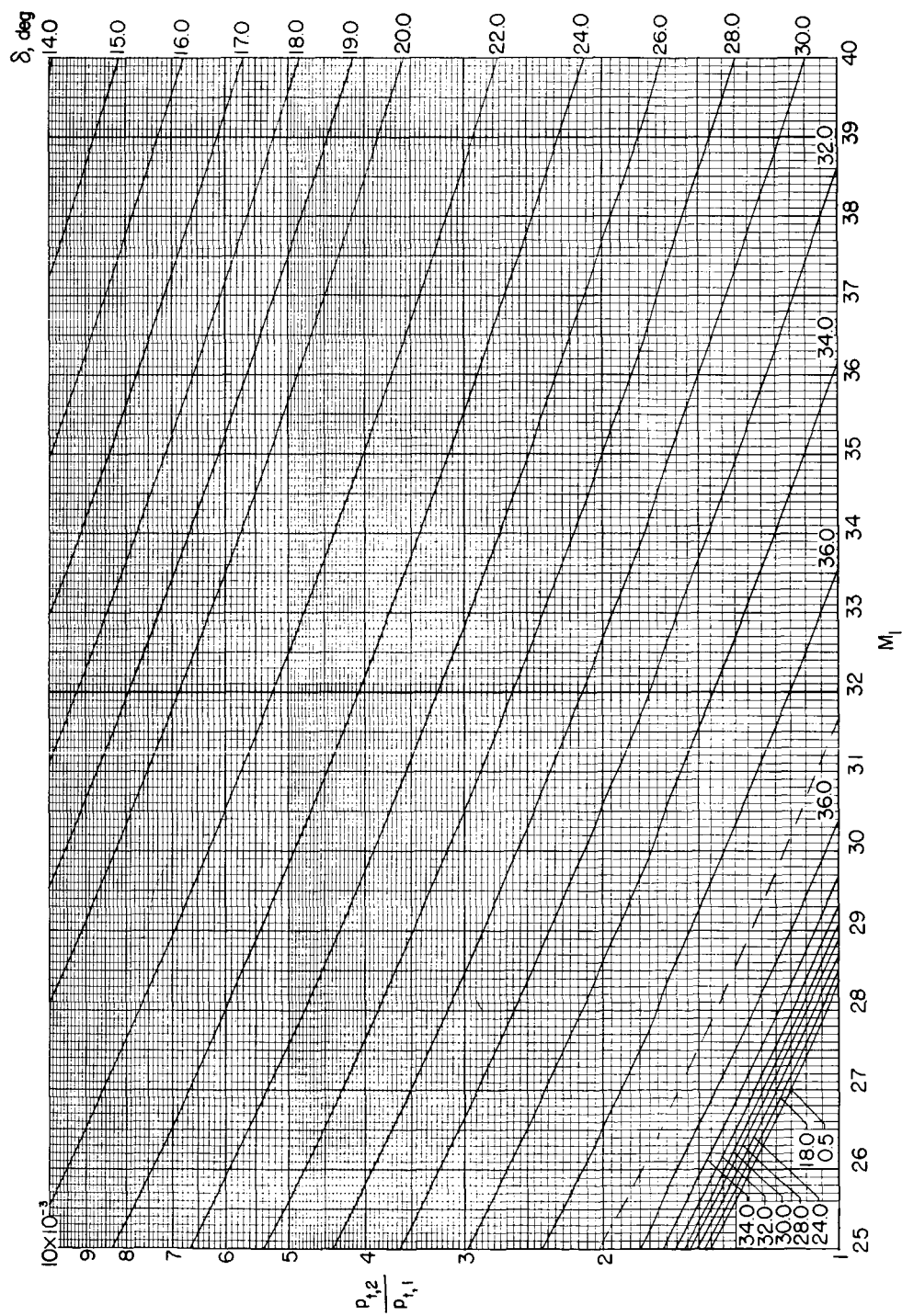
(1)  $M_1 = 10$  to 25;  $\frac{p_{t,2}^2}{p_{t,1}} = 0.68$  to 1.

Figure 8.- Continued.



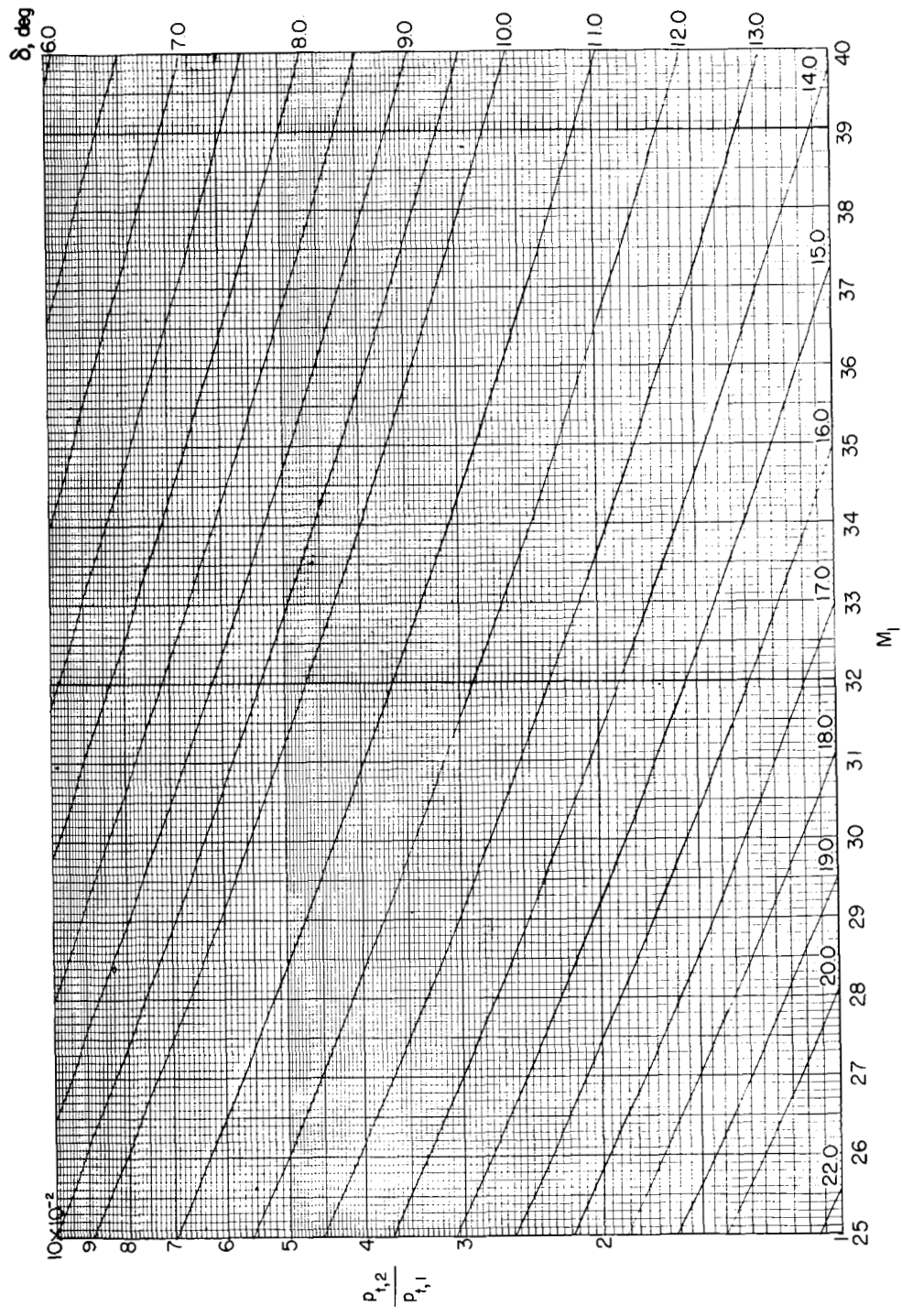
(m)  $M_t = 25$  to 40;  $\frac{P_{t,2}}{P_{t,1}} = 1 \times 10^{-4}$  to  $10 \times 10^{-4}$ .

Figure 8.- Continued.



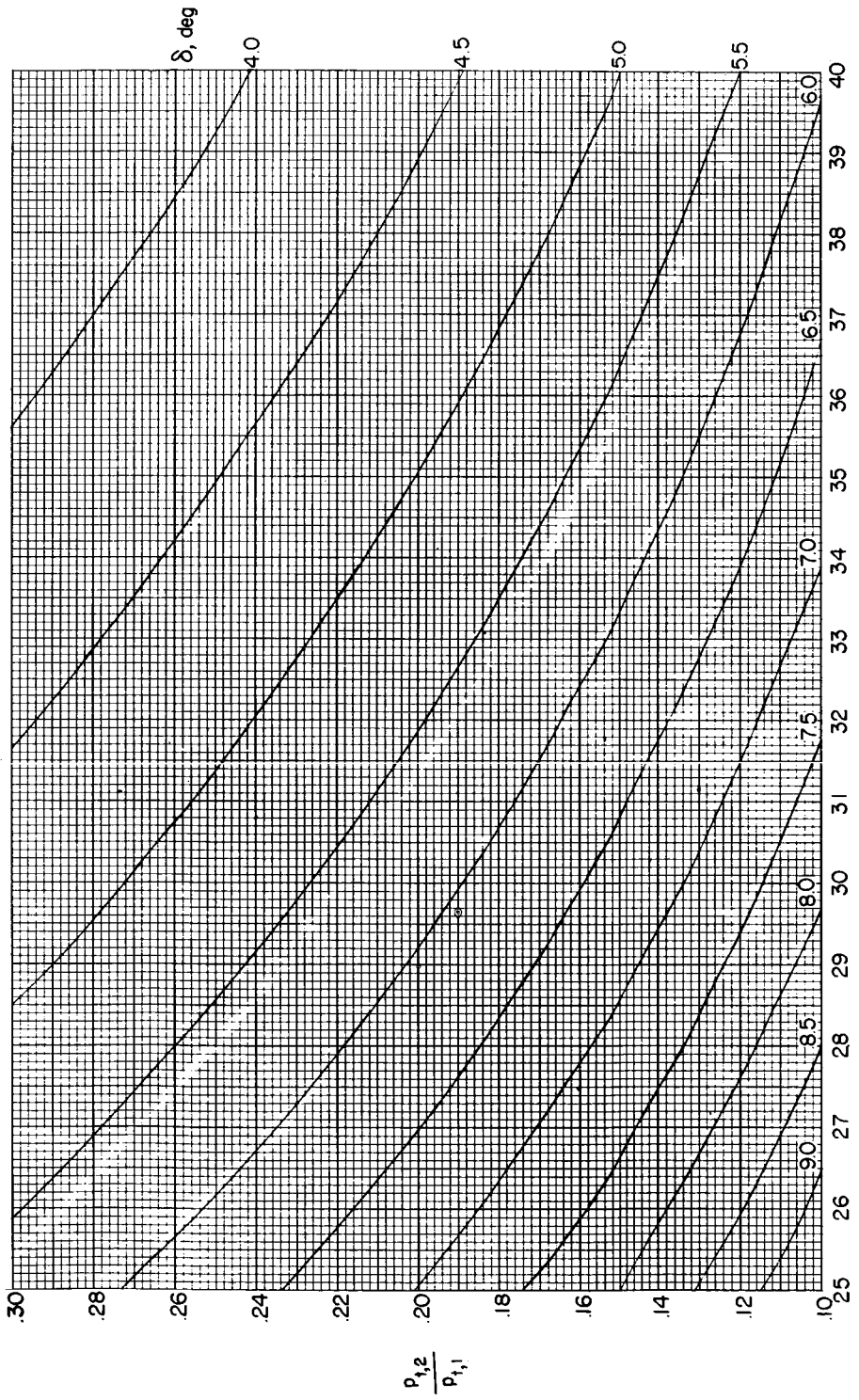
(n)  $M_1 = 25$  to 40;  $\frac{P_{t,2}}{P_{t,1}} = 1 \times 10^{-3}$  to  $10 \times 10^{-3}$ .

Figure 8.- Continued.



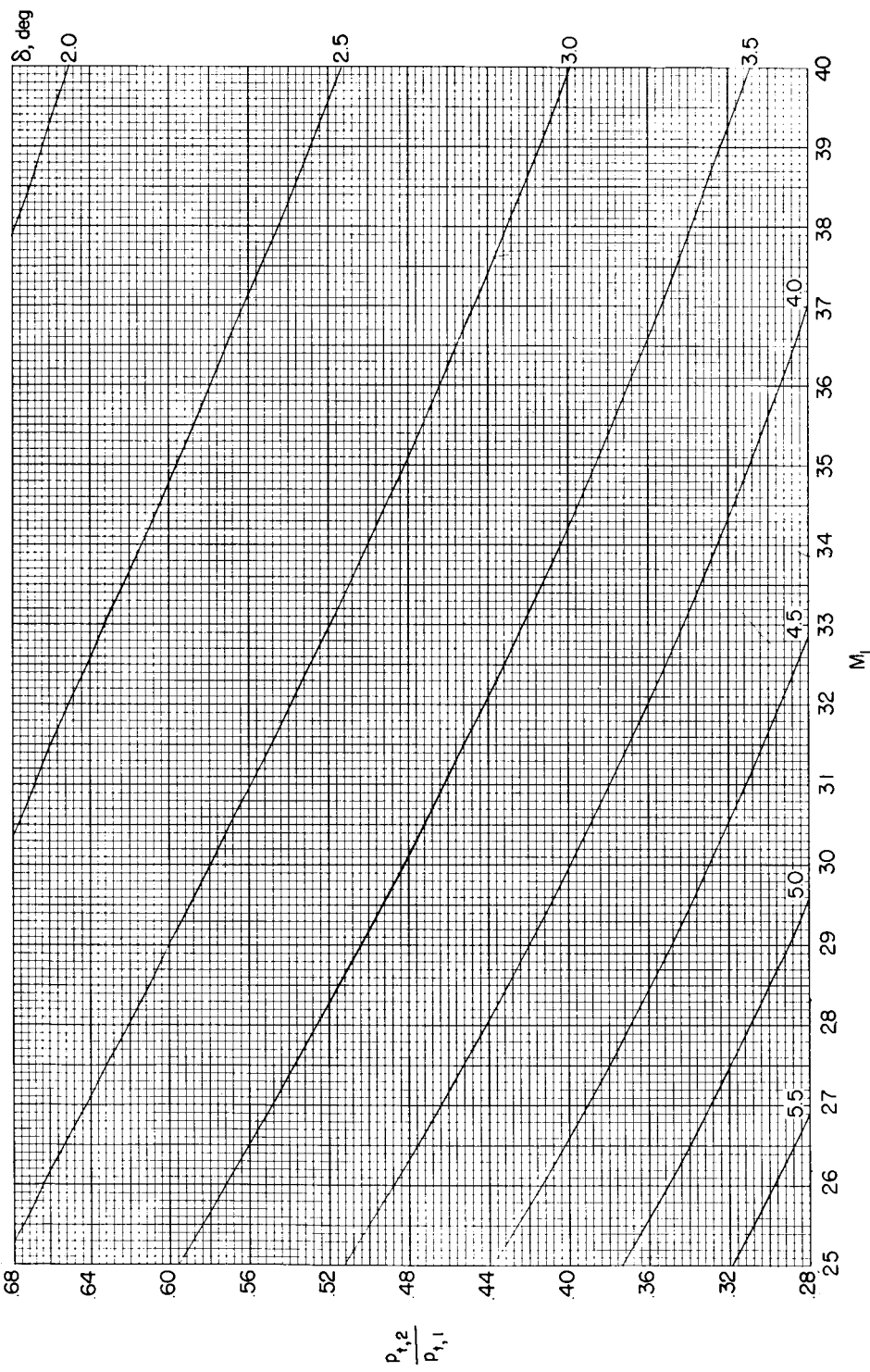
(o)  $M_1 = 25$  to 40;  $\frac{p_{t,2}}{p_{t,1}} = 1 \times 10^{-2}$  to  $10 \times 10^{-2}$ .

Figure 8.- Continued.



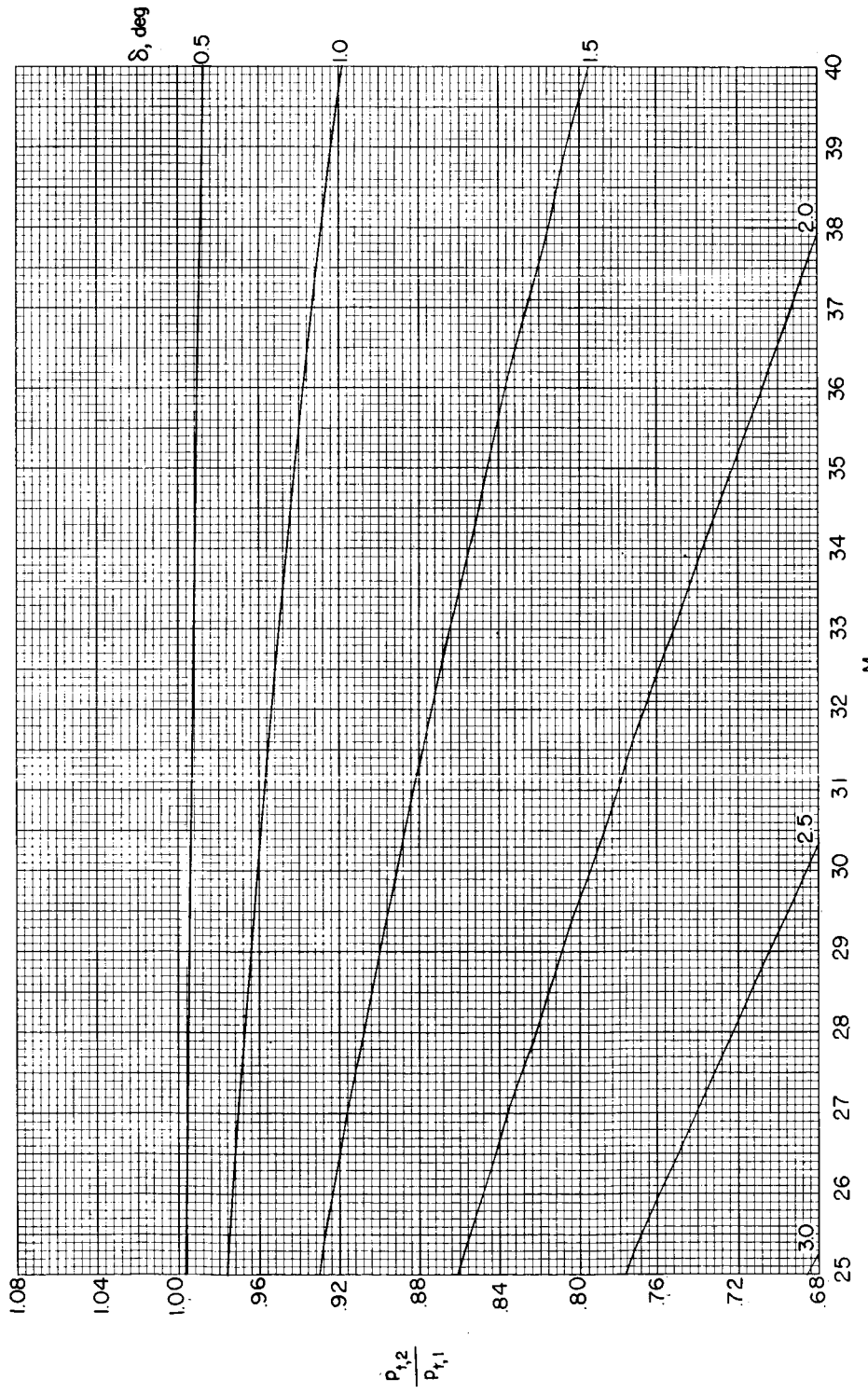
(p)  $M_1 = 25$  to 40;  $\frac{p_{t,2}}{p_{t,1}} = 0.1$  to 0.3.

Figure 8.- Continued.



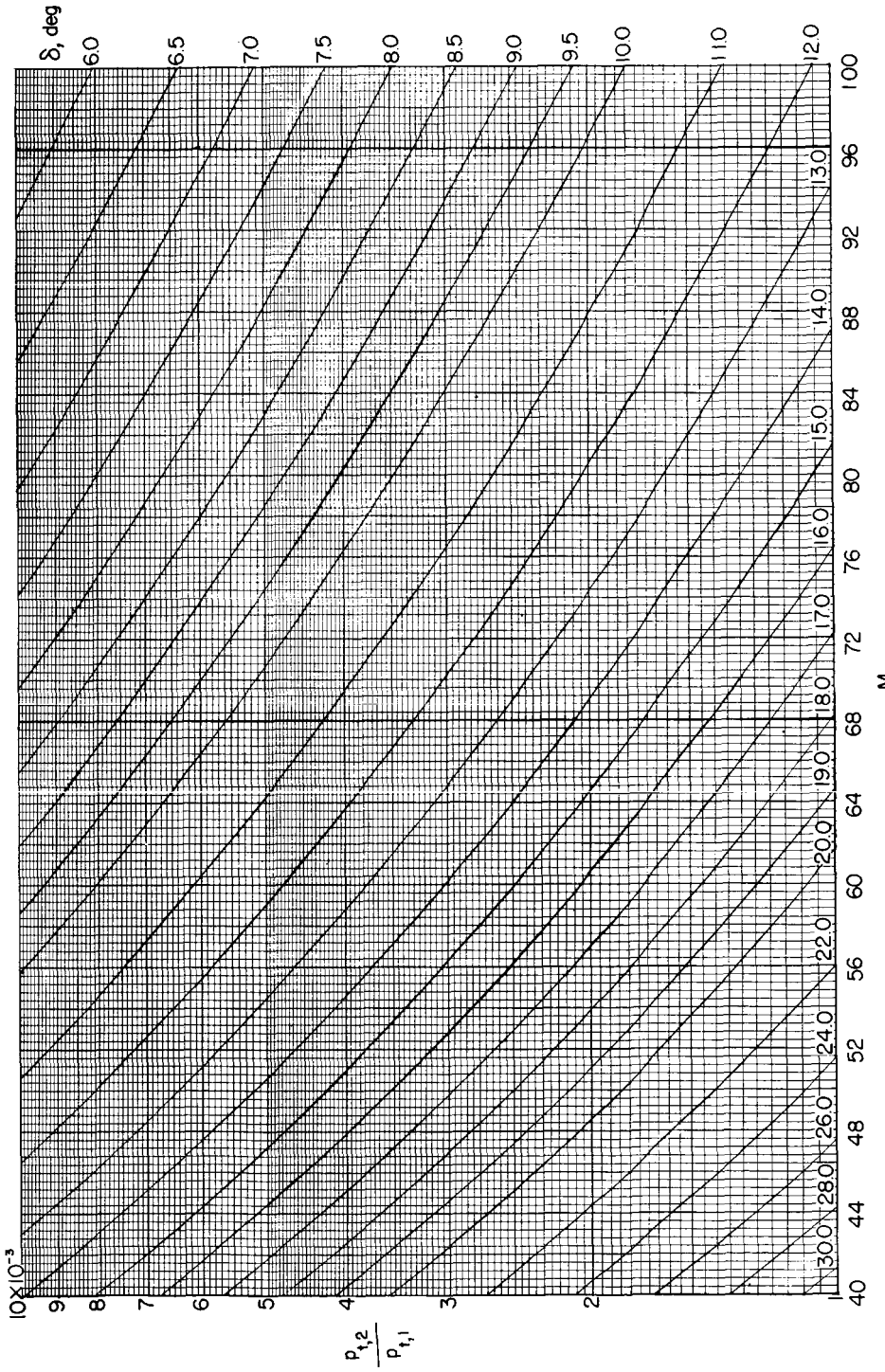
(a)  $M_1 = 25$  to 40;  $\frac{p_{t,2}}{p_{t,1}} = 0.28$  to 0.68.

Figure 8.- Continued.



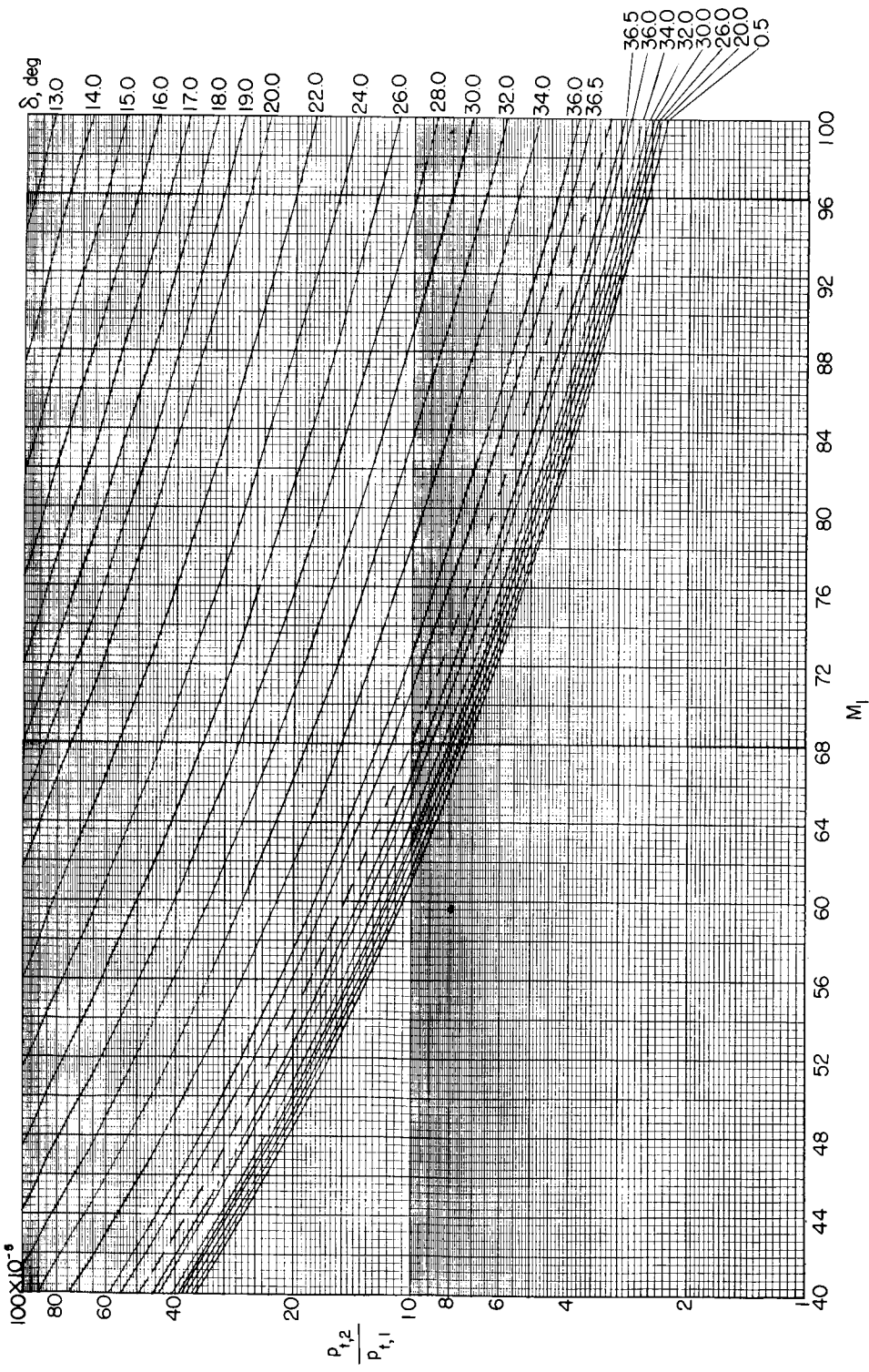
(r)  $M_1 = 25$  to  $40$ ;  $\frac{p_{t,2}}{p_{t,1}} = 0.68$  to  $1$ .

Figure 8.- Continued.



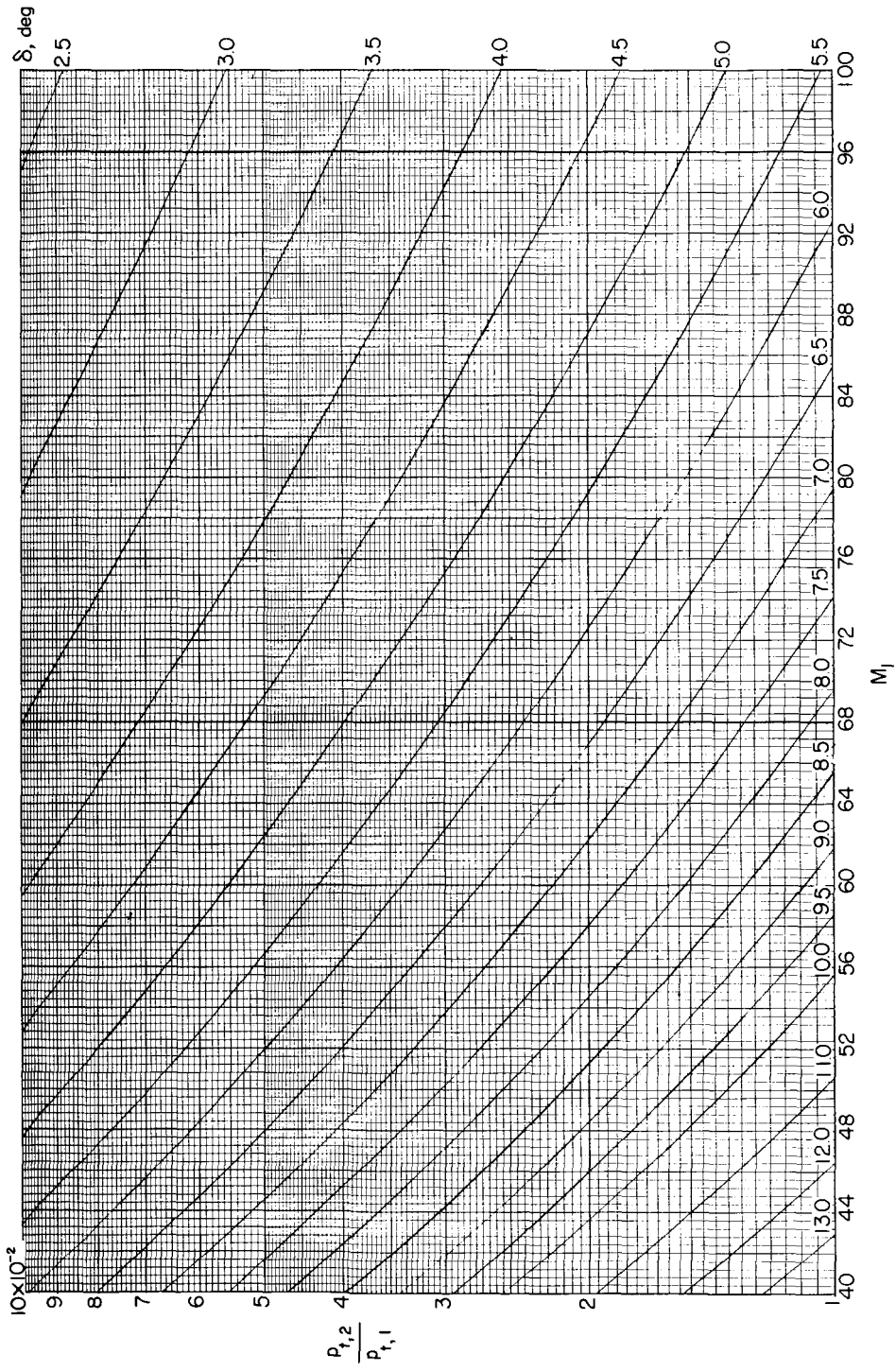
(t)  $M_1 = 40$  to 100;  $\frac{p_{t,2}}{p_{t,1}} = 1 \times 10^{-3}$  to  $10 \times 10^{-3}$ .

Figure 8.- Continued.



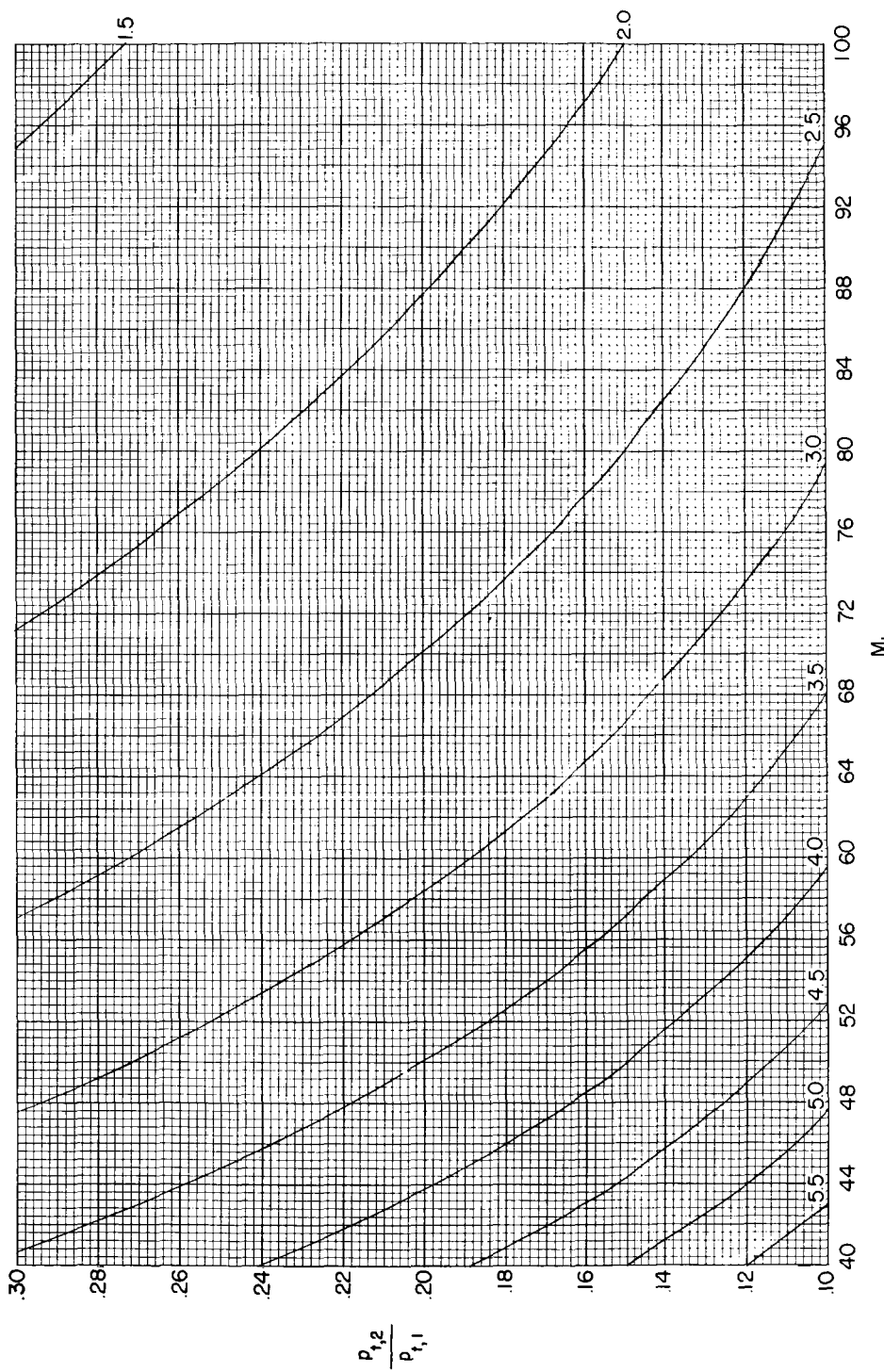
(s)  $M_1 = 40$  to 100;  $\frac{P_{t,2}}{P_{t,1}} = 1 \times 10^{-5}$  to  $100 \times 10^{-5}$ .

Figure 8.- Continued.



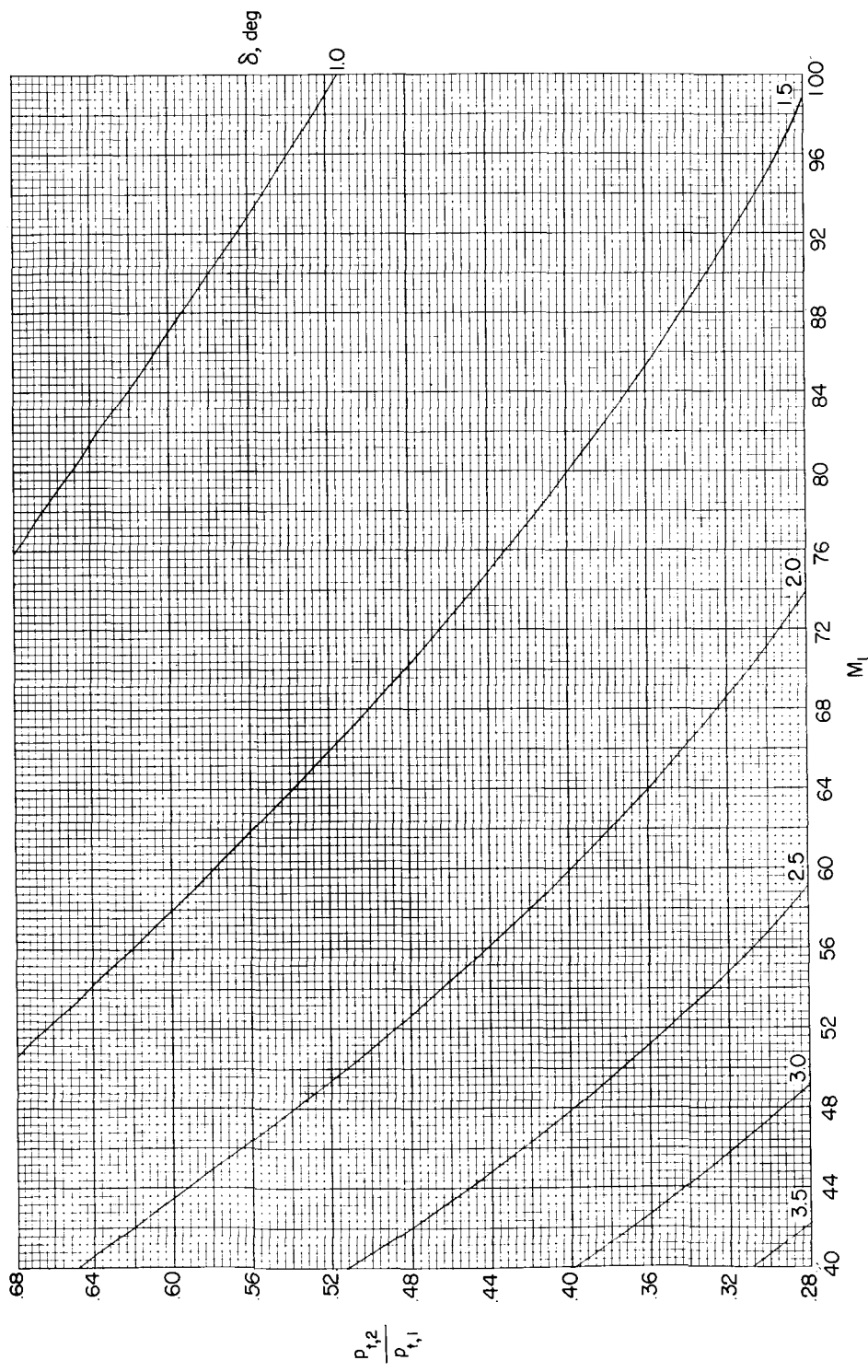
(u)  $M_{1\perp} = 40$  to 100;  $\frac{p_{t,2}}{p_{t,1}} = 1 \times 10^{-2}$  to  $10 \times 10^{-2}$ .

Figure 8.- Continued.



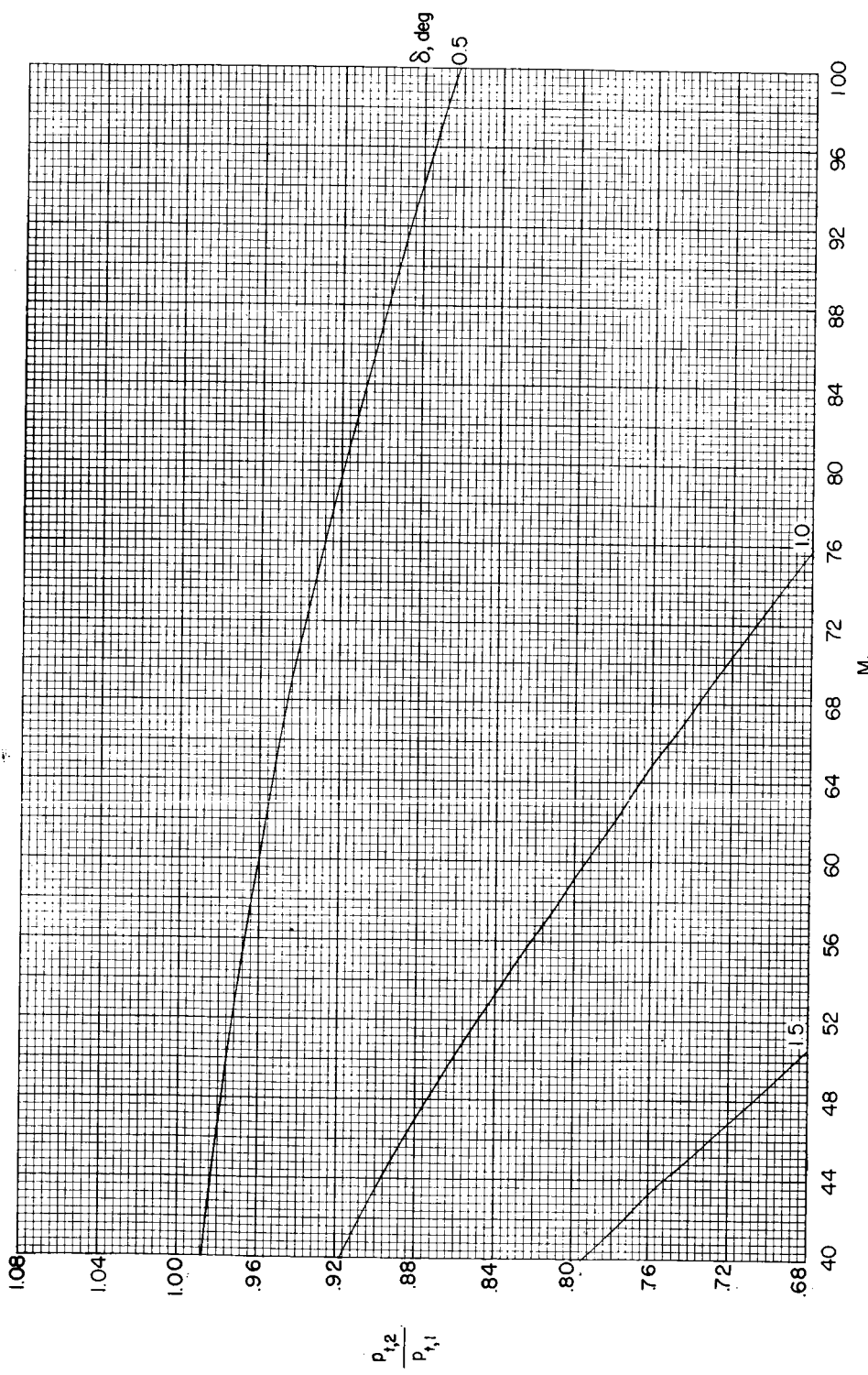
(v)  $M_1 = 40$  to  $100$ ;  $\frac{P_{t,2}^2}{P_{t,1}} = 0.1$  to  $0.3$ .

Figure 8.- Continued.



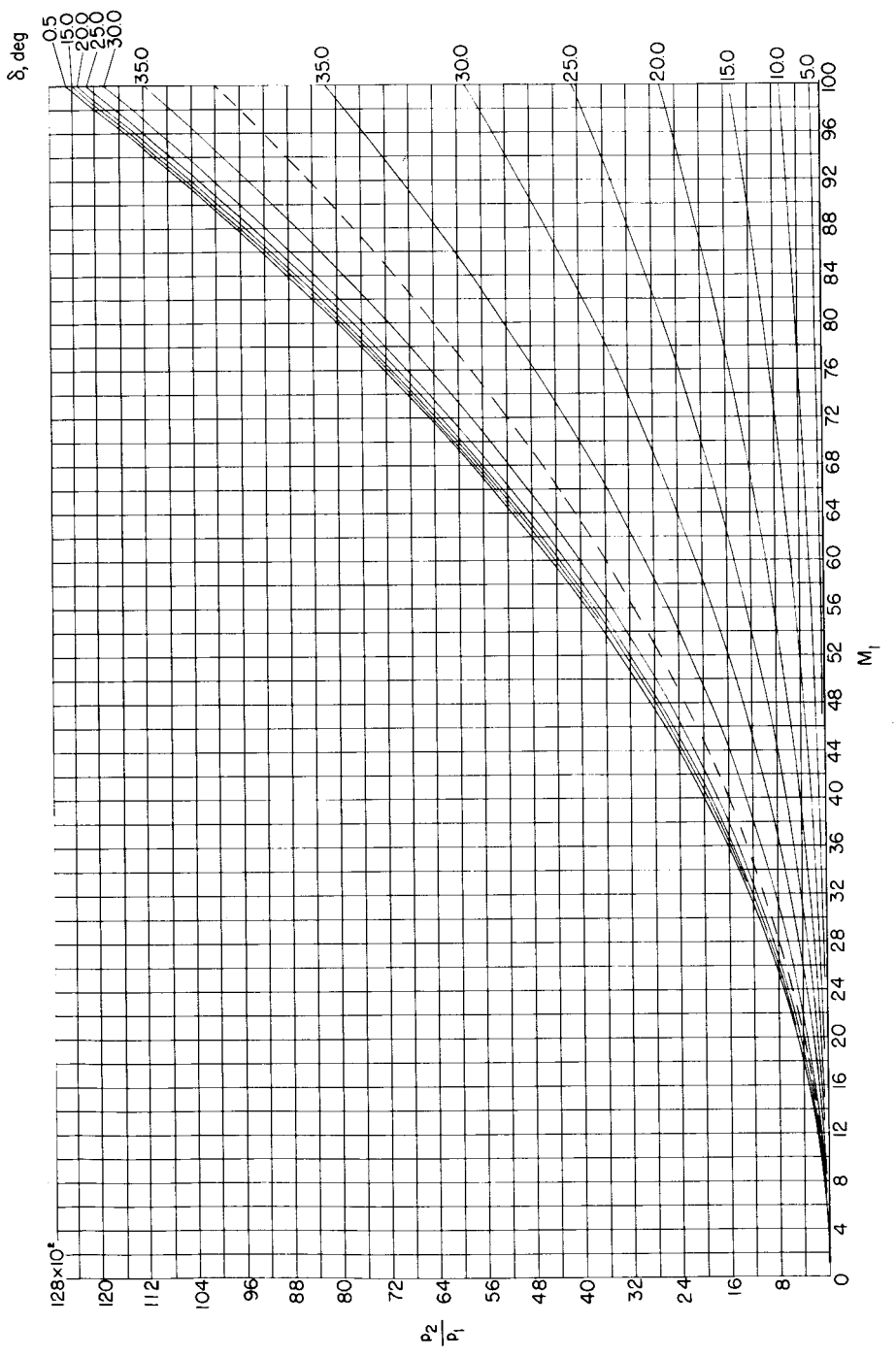
(v)  $M_1 = 40$  to 100;  $\frac{P_{t,2}}{P_{t,1}} = 0.28$  to 0.68.

Figure 8.- Continued.



(x)  $M_1 = 40$  to  $100$ ;  $\frac{p_{t,2}}{p_{t,1}} = 0.68$  to  $1$ .

Figure 8. - Concluded.



(a)  $M_1 = 1$  to  $100$ ;  $p_2/p_1 = 0$  to  $128 \times 10^2$ .

Figure 9.- Variation of ratio of static pressure behind a two-dimensional shock to free-stream static pressure with free-stream Mach number for various flow-deflection angles. (Dashed line denotes boundary between weak and strong shock solutions. Weak shock solution is below dashed line.)

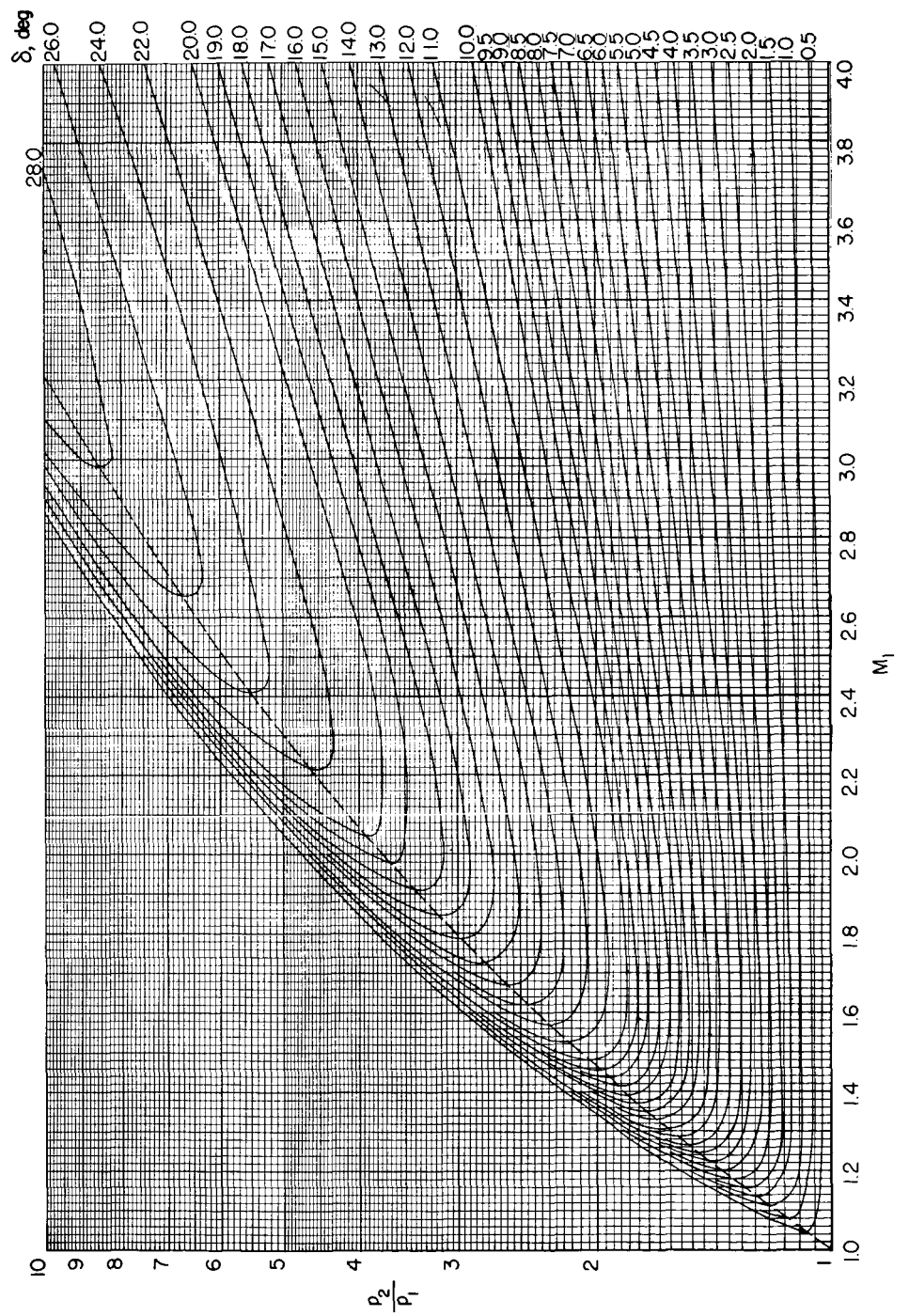
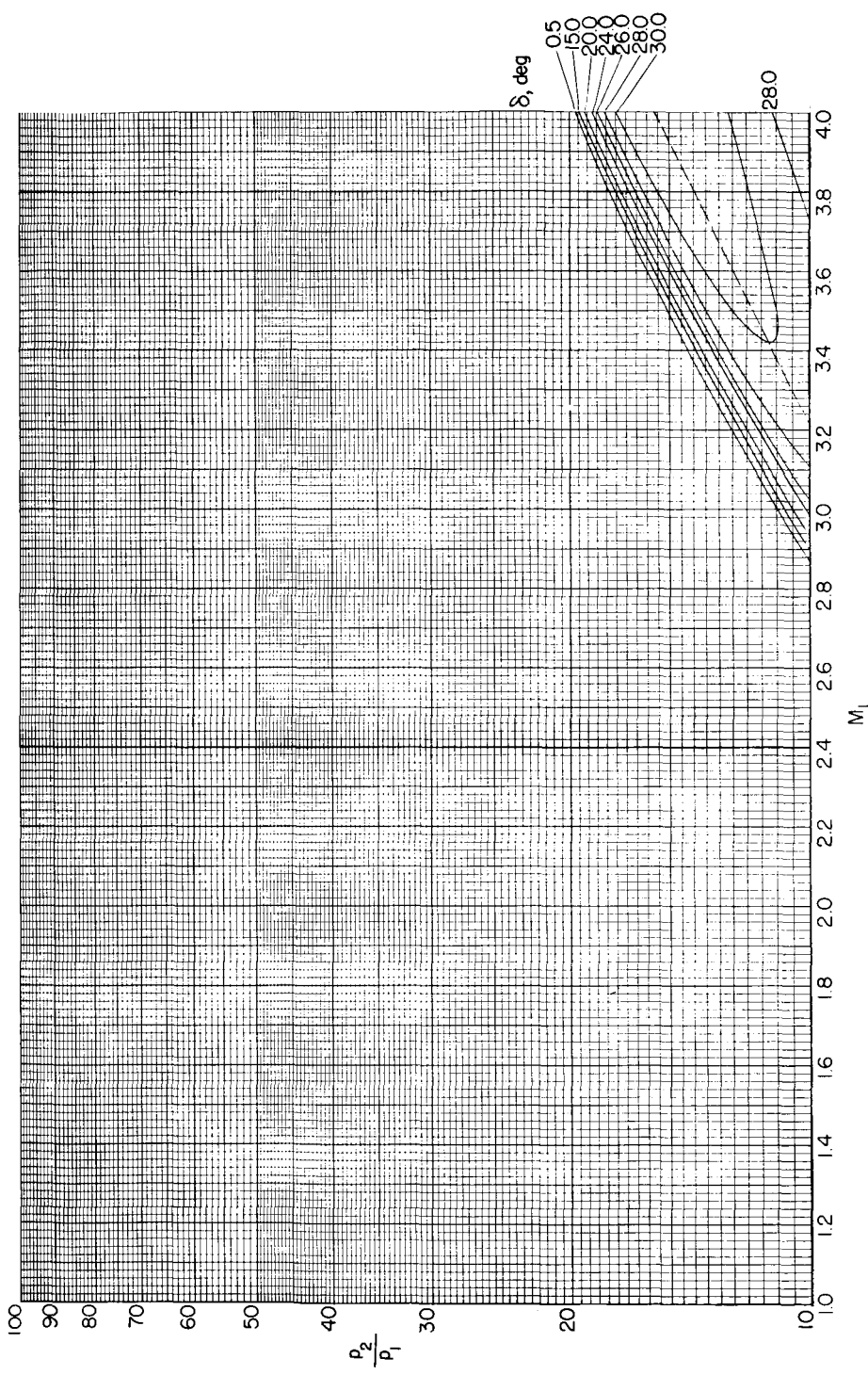
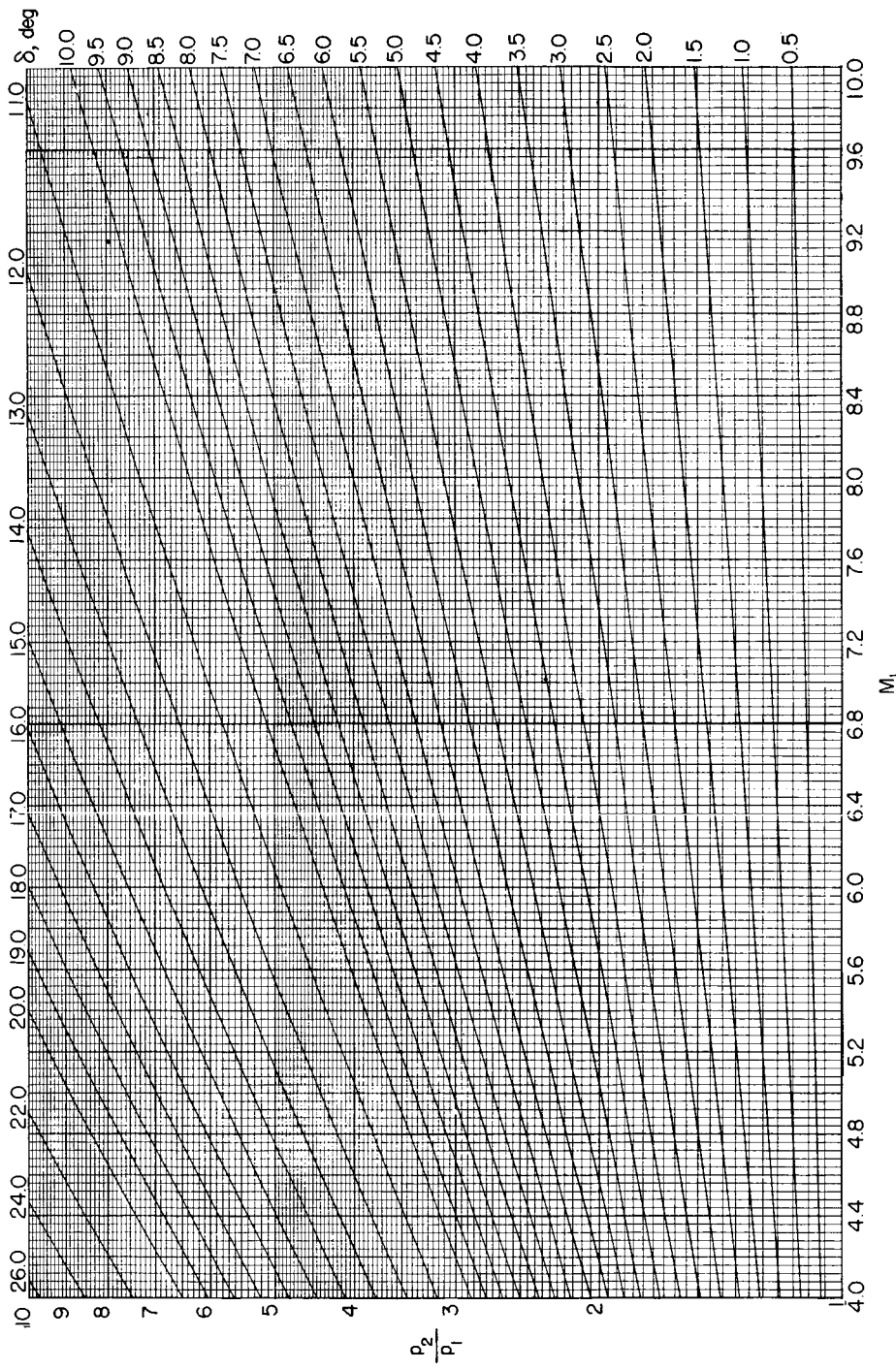
(b)  $M_1 = 1 \text{ to } 4; p_2/p_1 = 1 \text{ to } 10.$ 

Figure 9.- Continued.



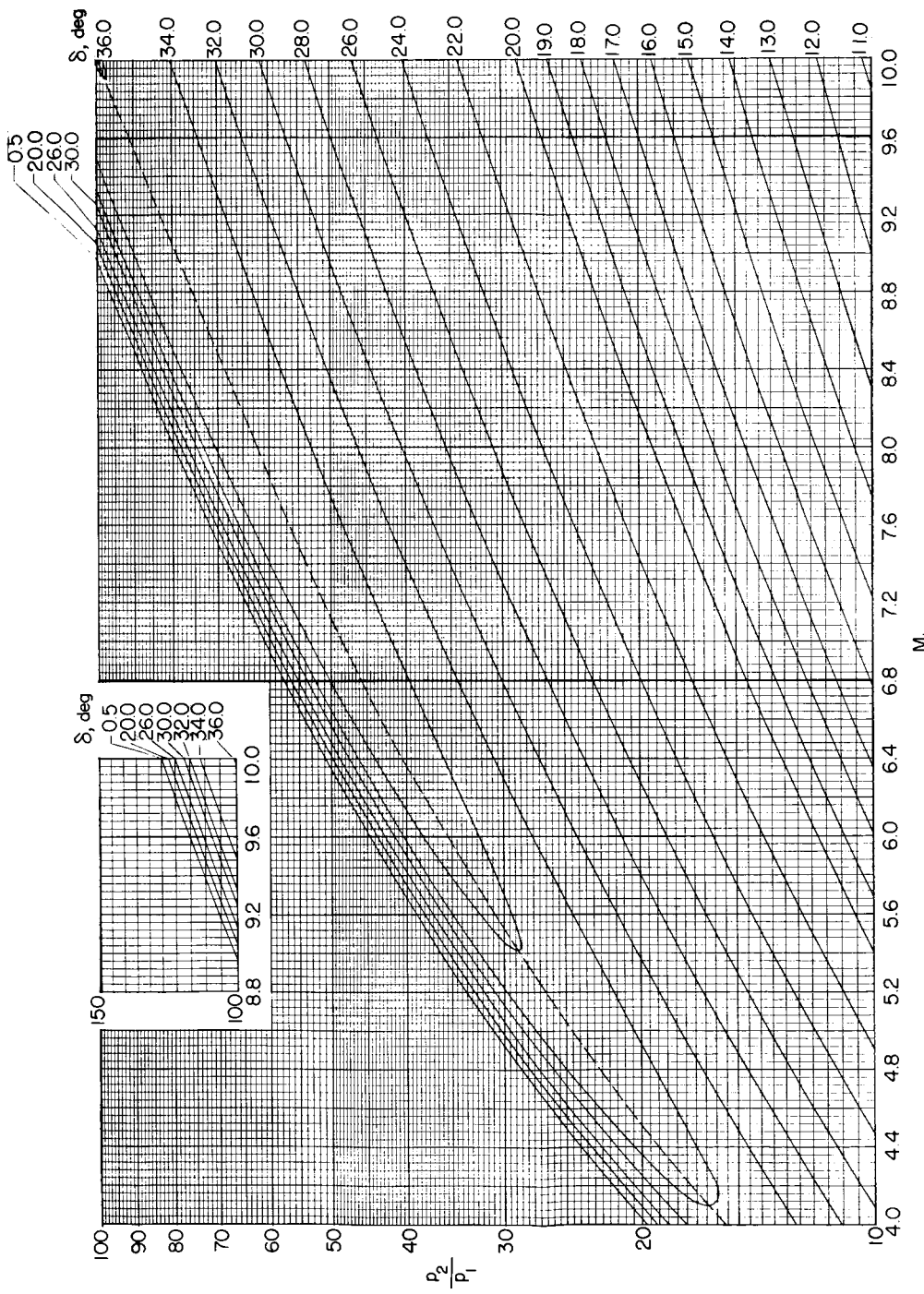
(c)  $M_1 = 1$  to  $4$ ;  $p_2/p_1 = 10$  to  $100$ .

Figure 9 - Continued.



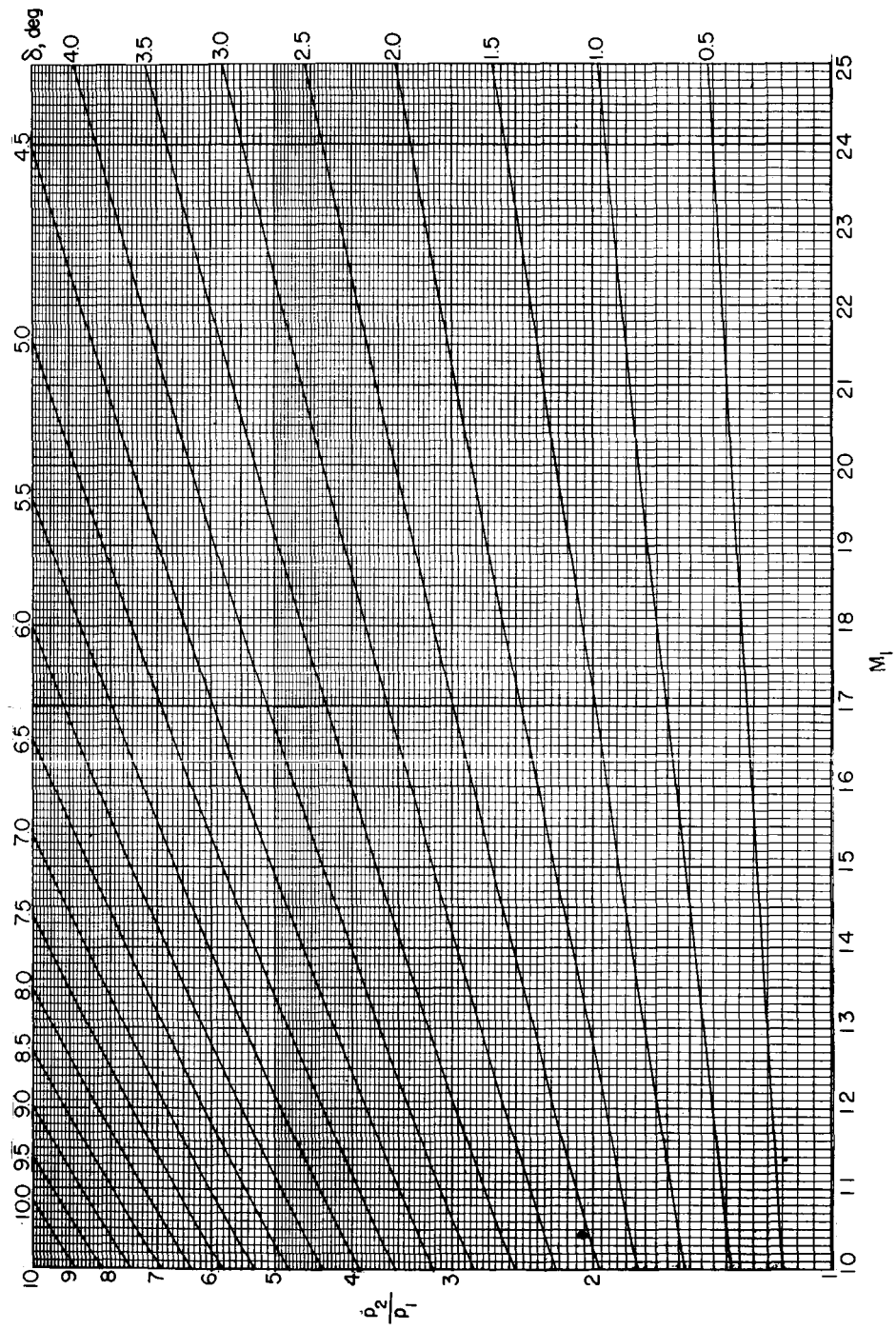
(d)  $M_1 = 4$  to 10;  $p_2/p_1 = 1$  to 10.

Figure 9.- Continued.



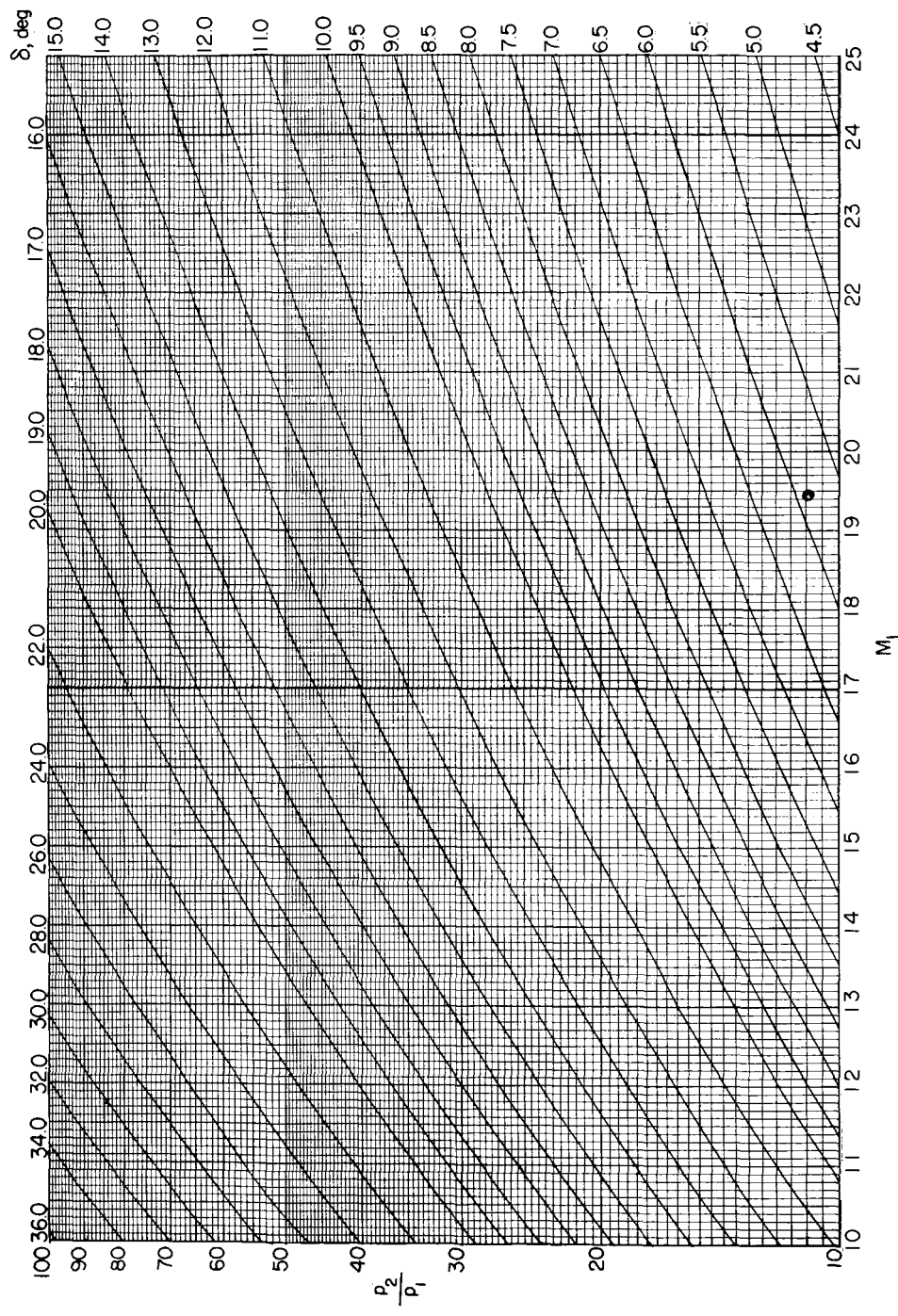
(e)  $M_1 = 4$  to 10;  $p_2/p_1 = 10$  to 150.

Figure 9.- Continued.



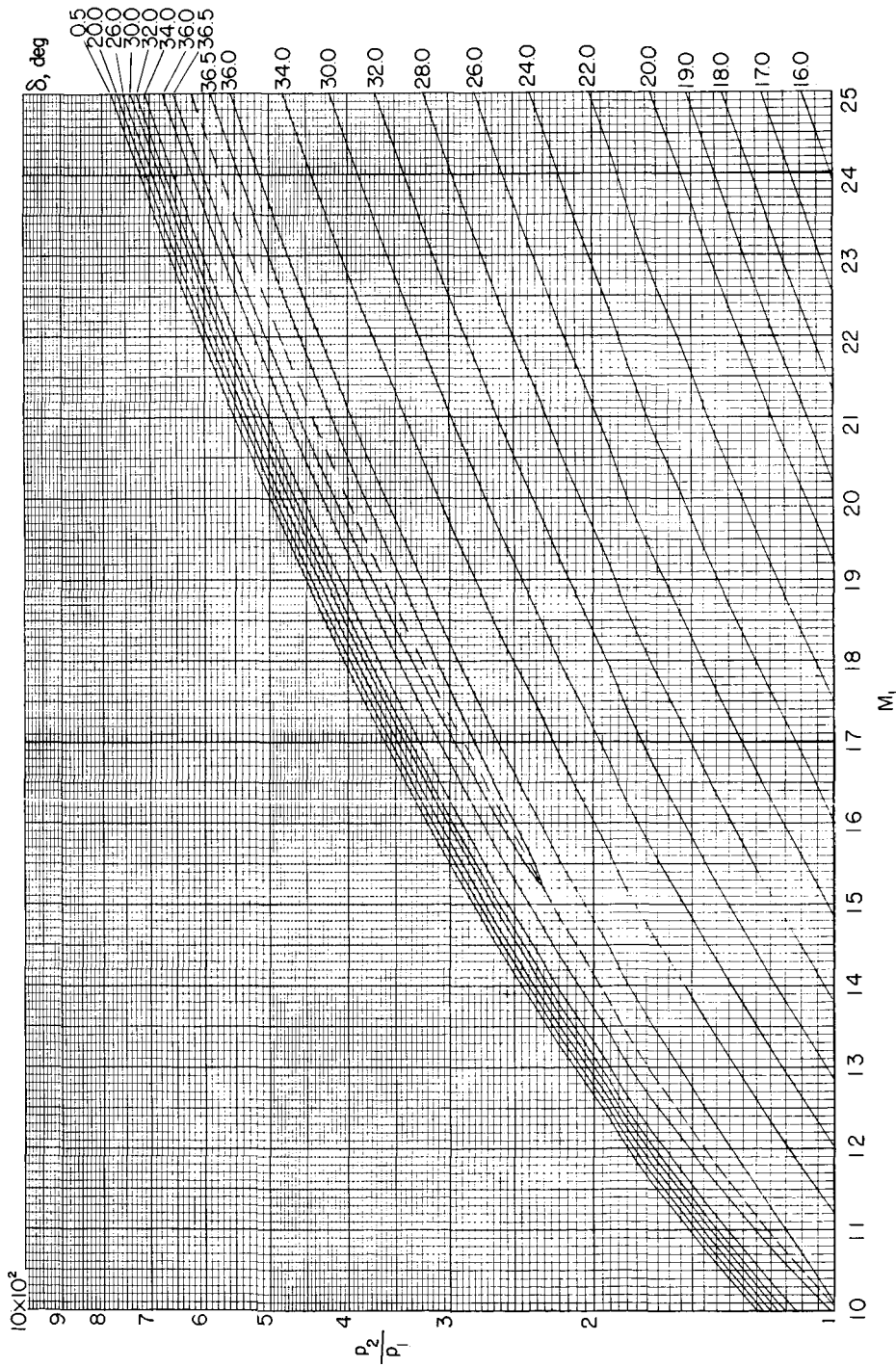
(f)  $M_1 = 10$  to 25;  $p_2/p_1 = 1$  to 10.

Figure 9.- Continued.



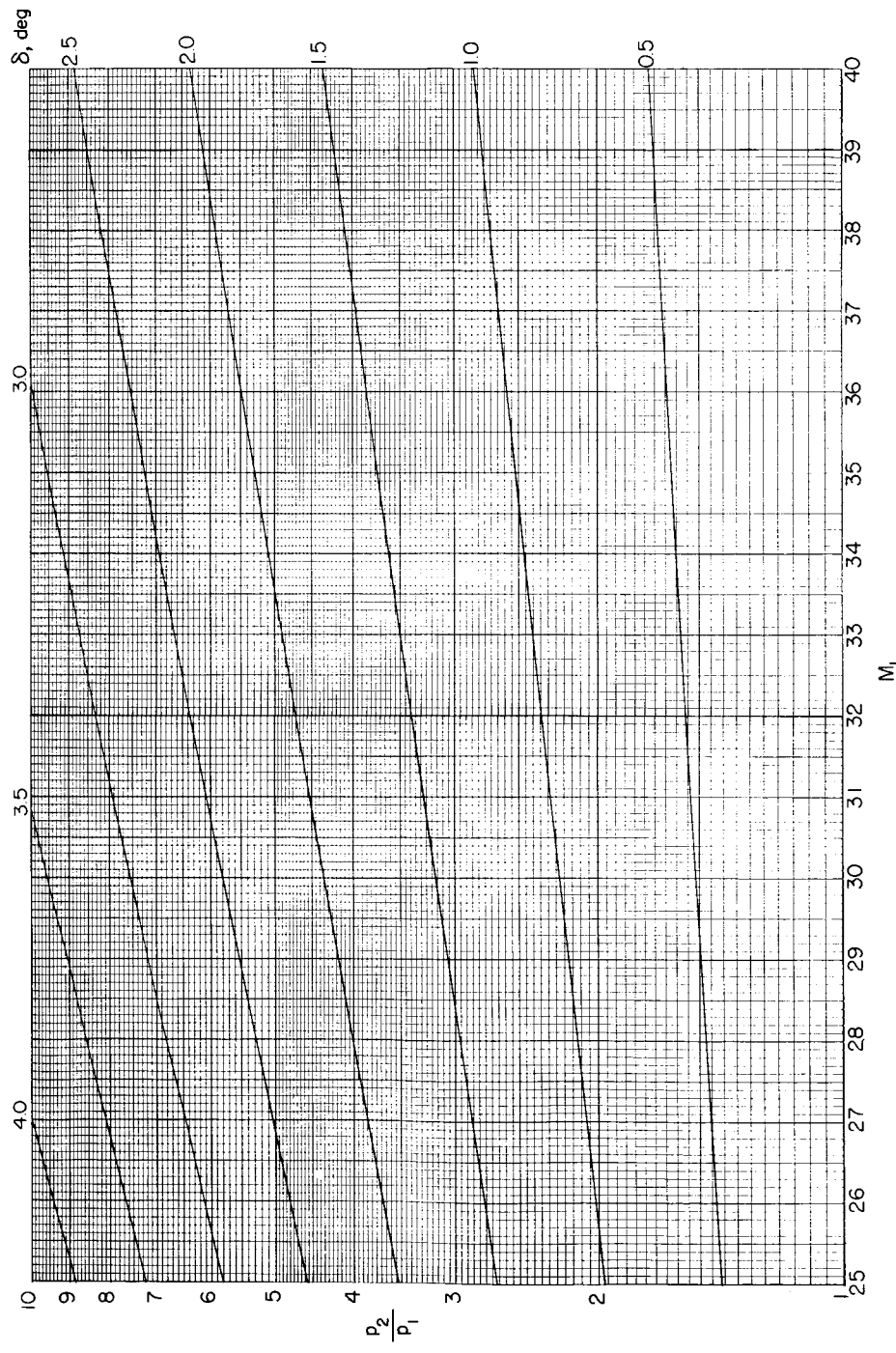
(g)  $M_1 = 10$  to 25;  $p_2/p_1 = 10$  to 100.

Figure 9. - Continued.



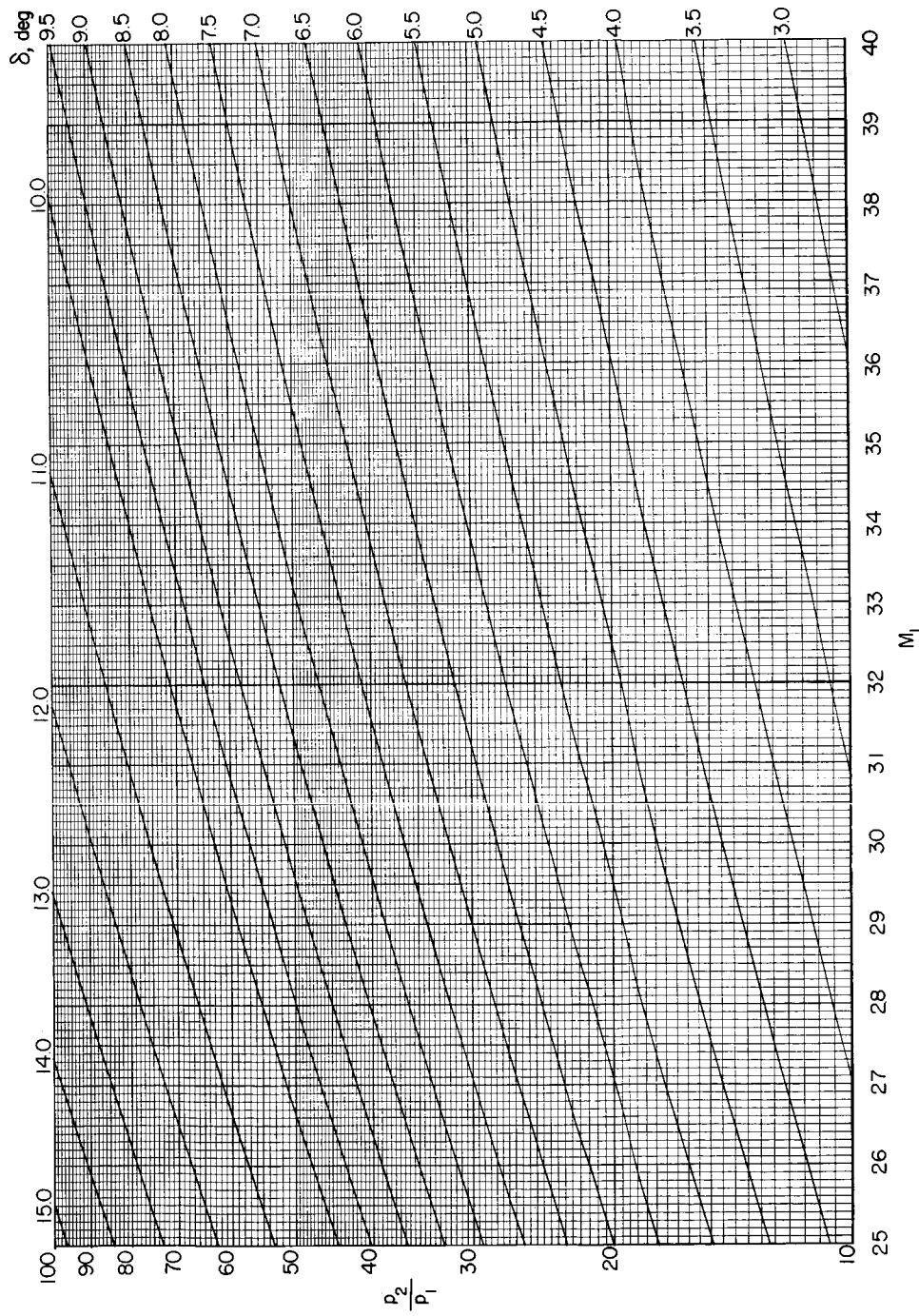
(h)  $M_1 = 10$  to  $25$ ;  $p_2/p_1 = 1 \times 10^2$  to  $10 \times 10^2$ .

Figure 9.- Continued.



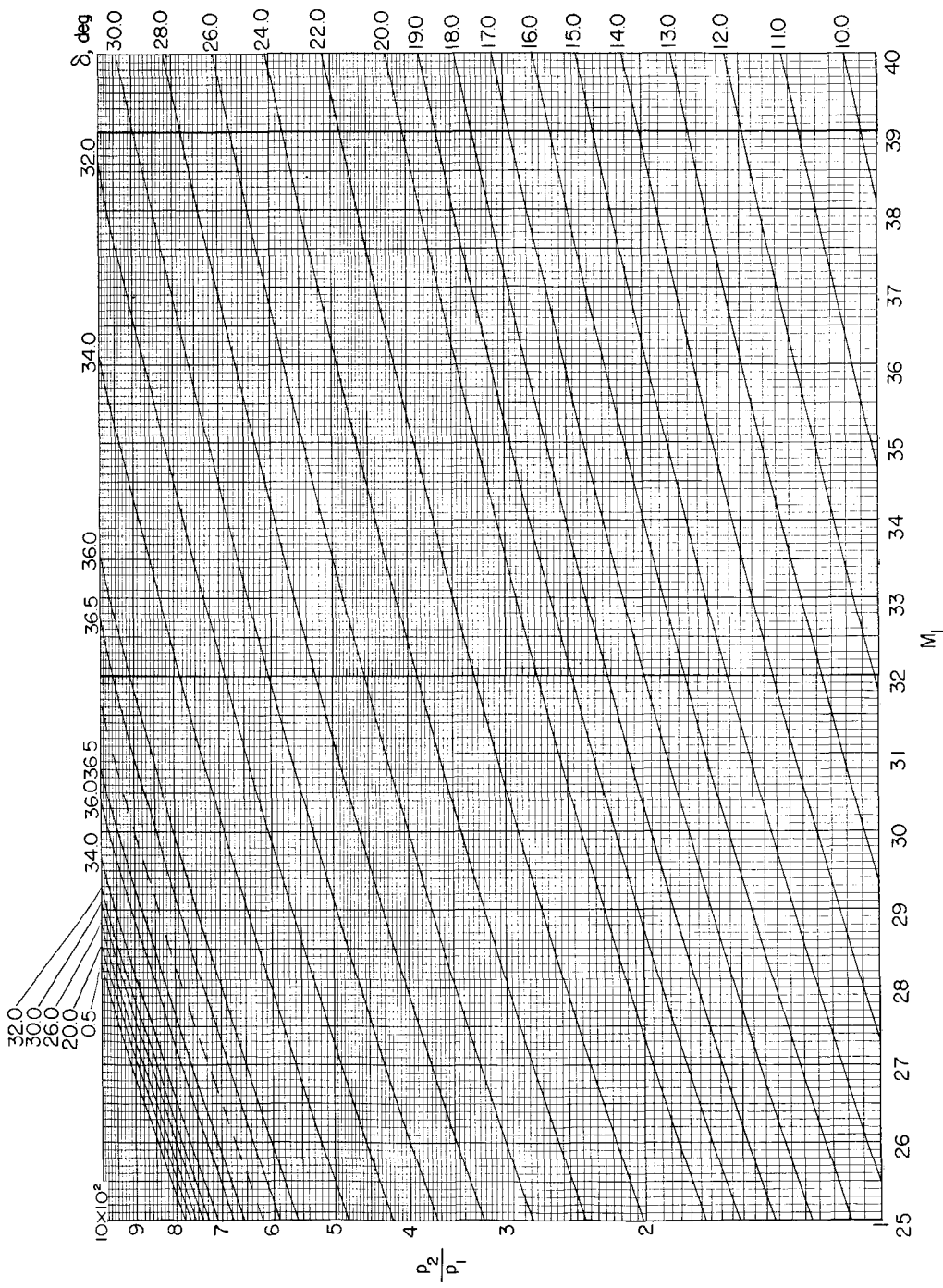
(i)  $M_1 = 25$  to 40;  $p_2/p_1 = 1$  to 10.

Figure 9.- Continued.



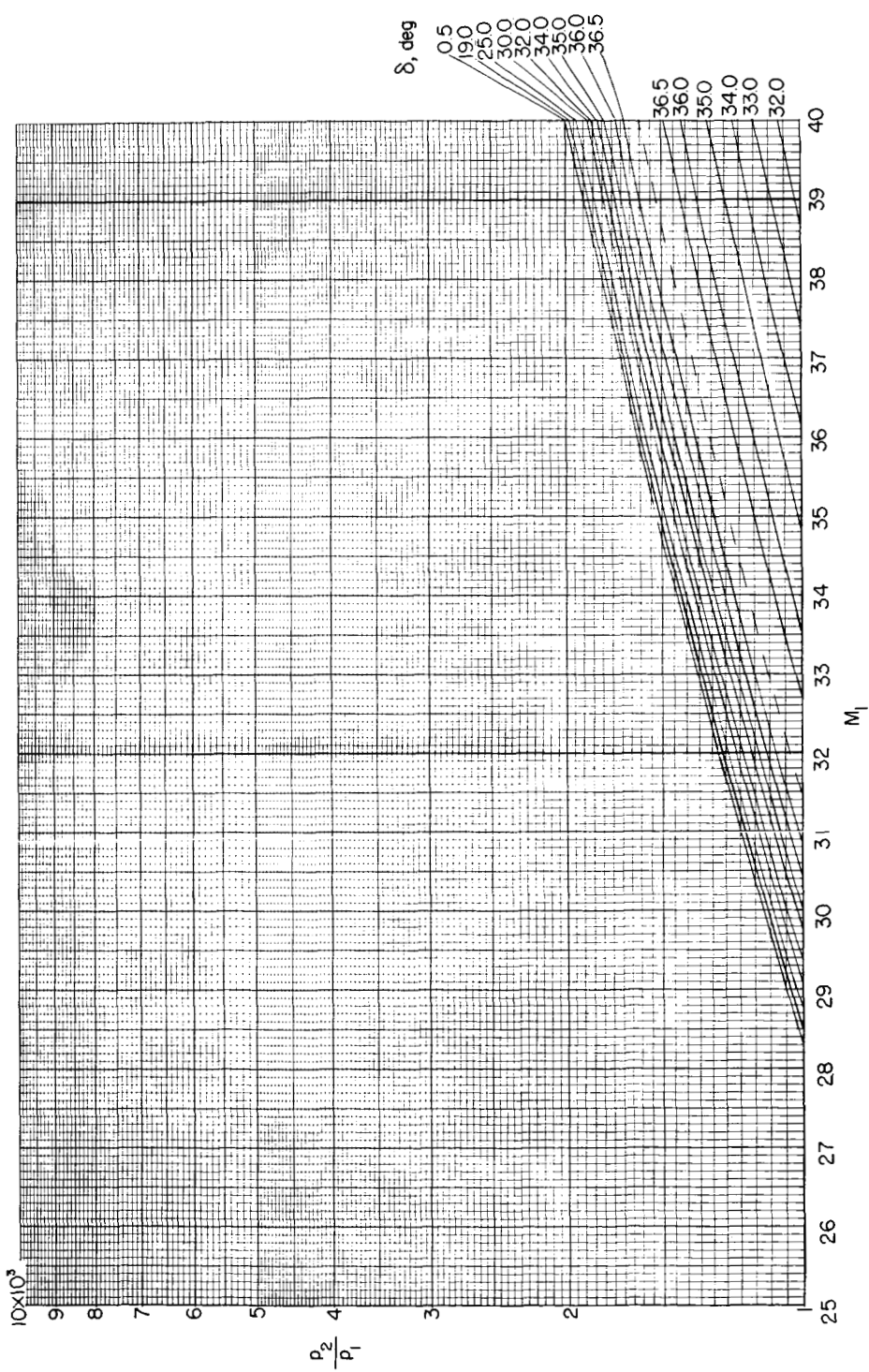
(j)  $M_{\perp} = 25$  to 40;  $p_2/p_1 = 10$  to 100.

Figure 9.- Continued.



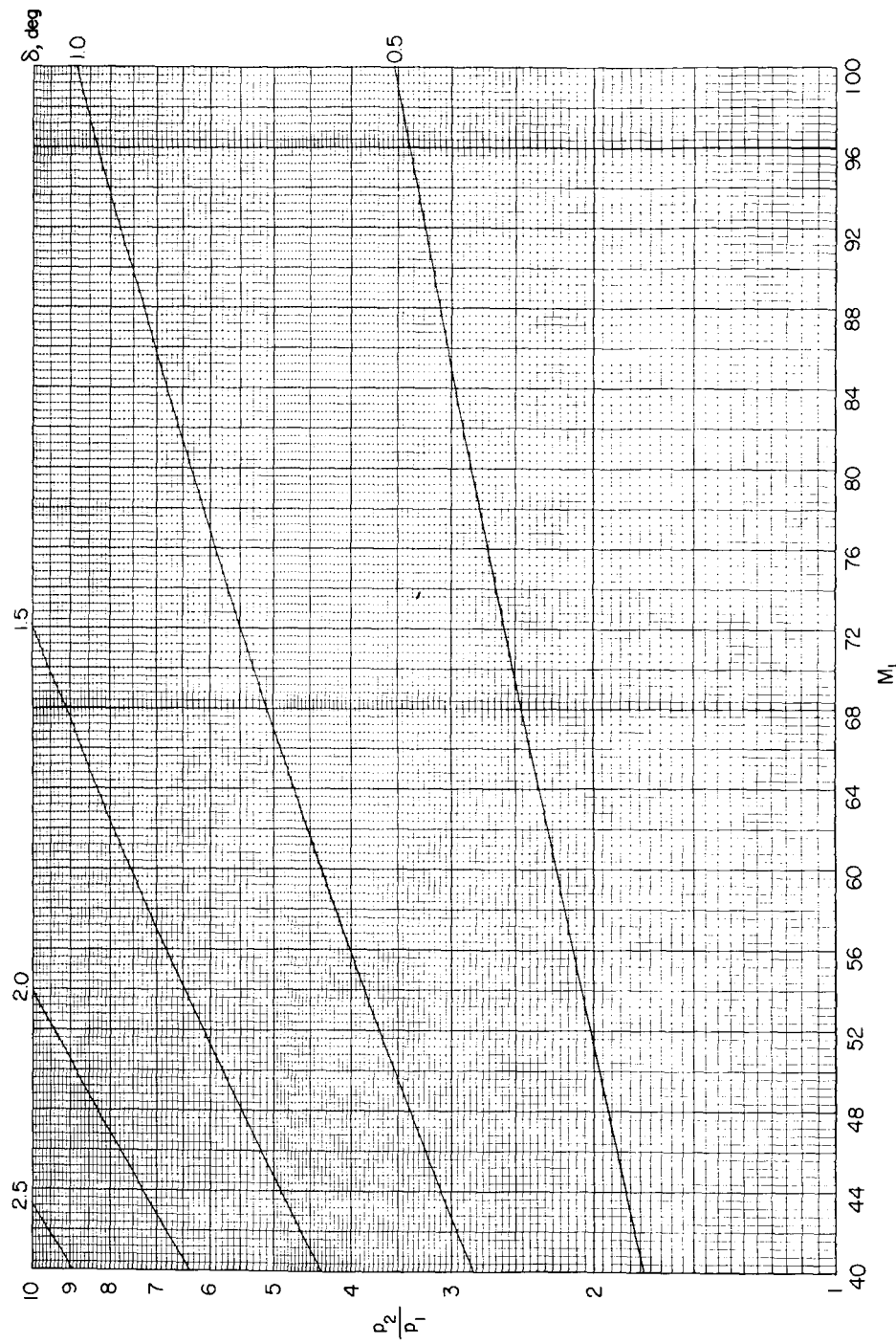
(k)  $M_1 = 25$  to  $40$ ;  $p_2/p_1 = 1 \times 10^2$  to  $10 \times 10^2$ .

Figure 9. - Continued.



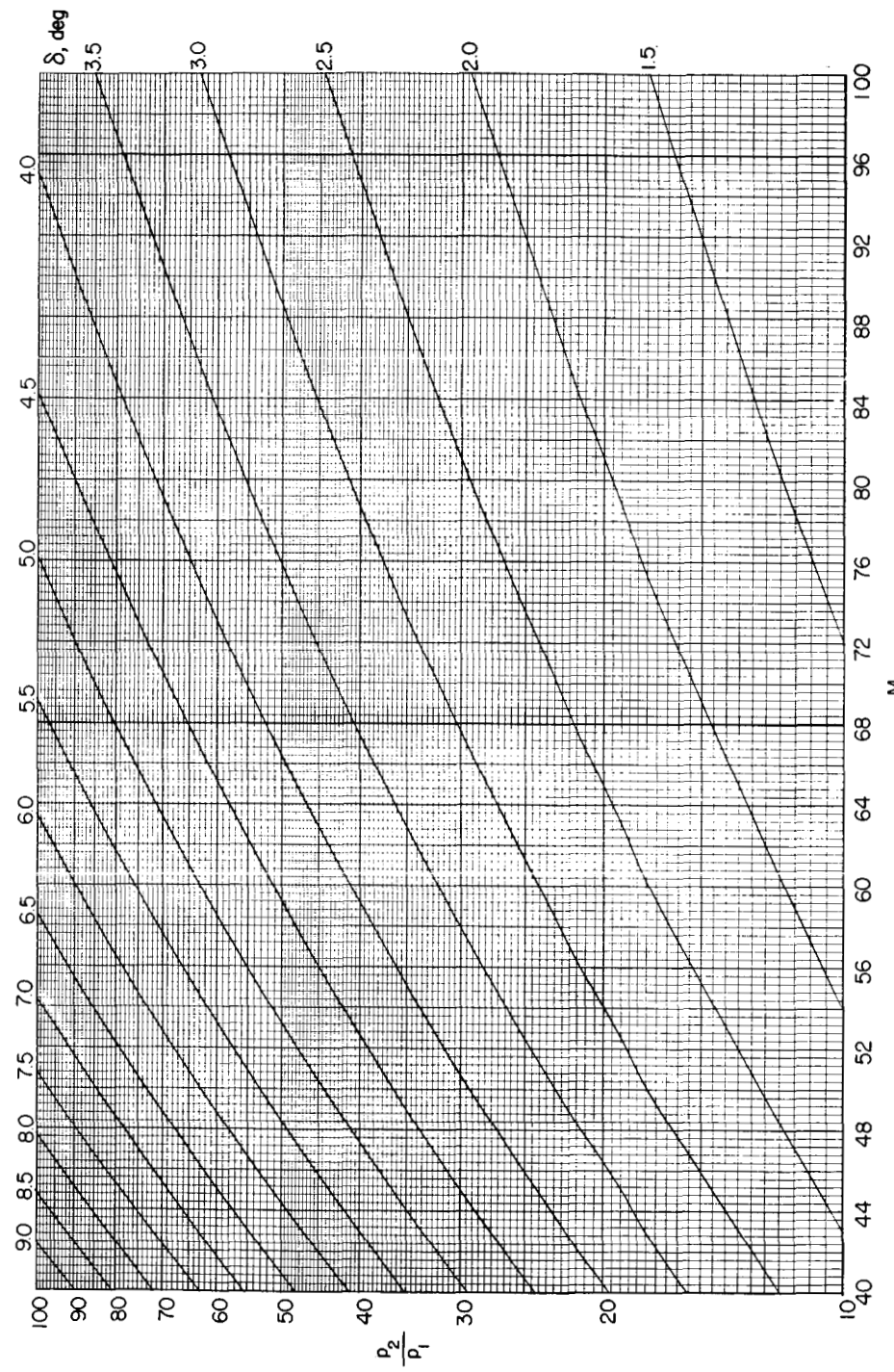
(1)  $M_1 = 25$  to 40;  $P_2/P_1 = 1 \times 10^3$  to  $10 \times 10^3$ .

Figure 9.- Continued.



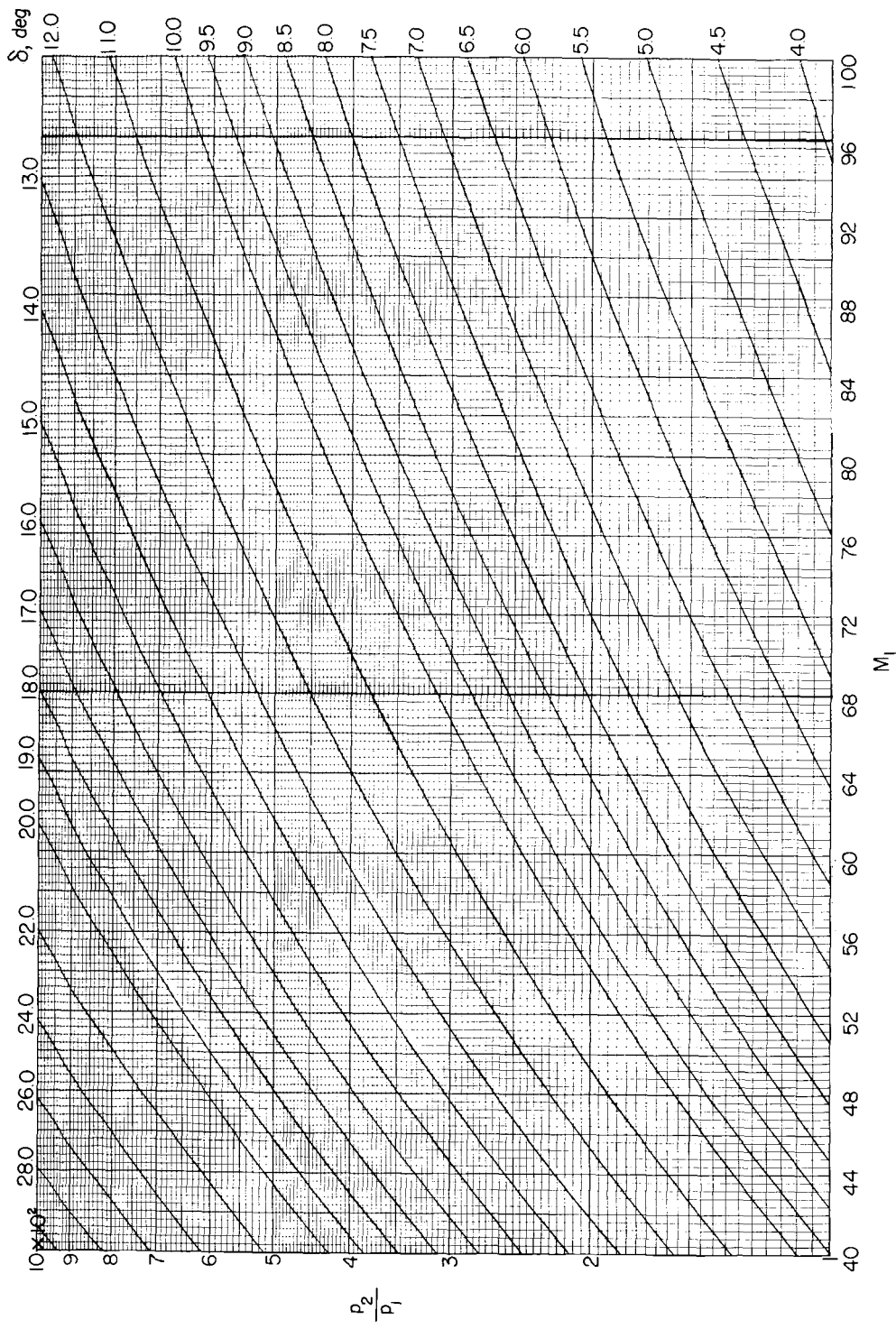
(m)  $M_1 = 40$  to  $100$ ;  $p_2/p_1 = 1$  to  $10$ .

Figure 9.- Continued.



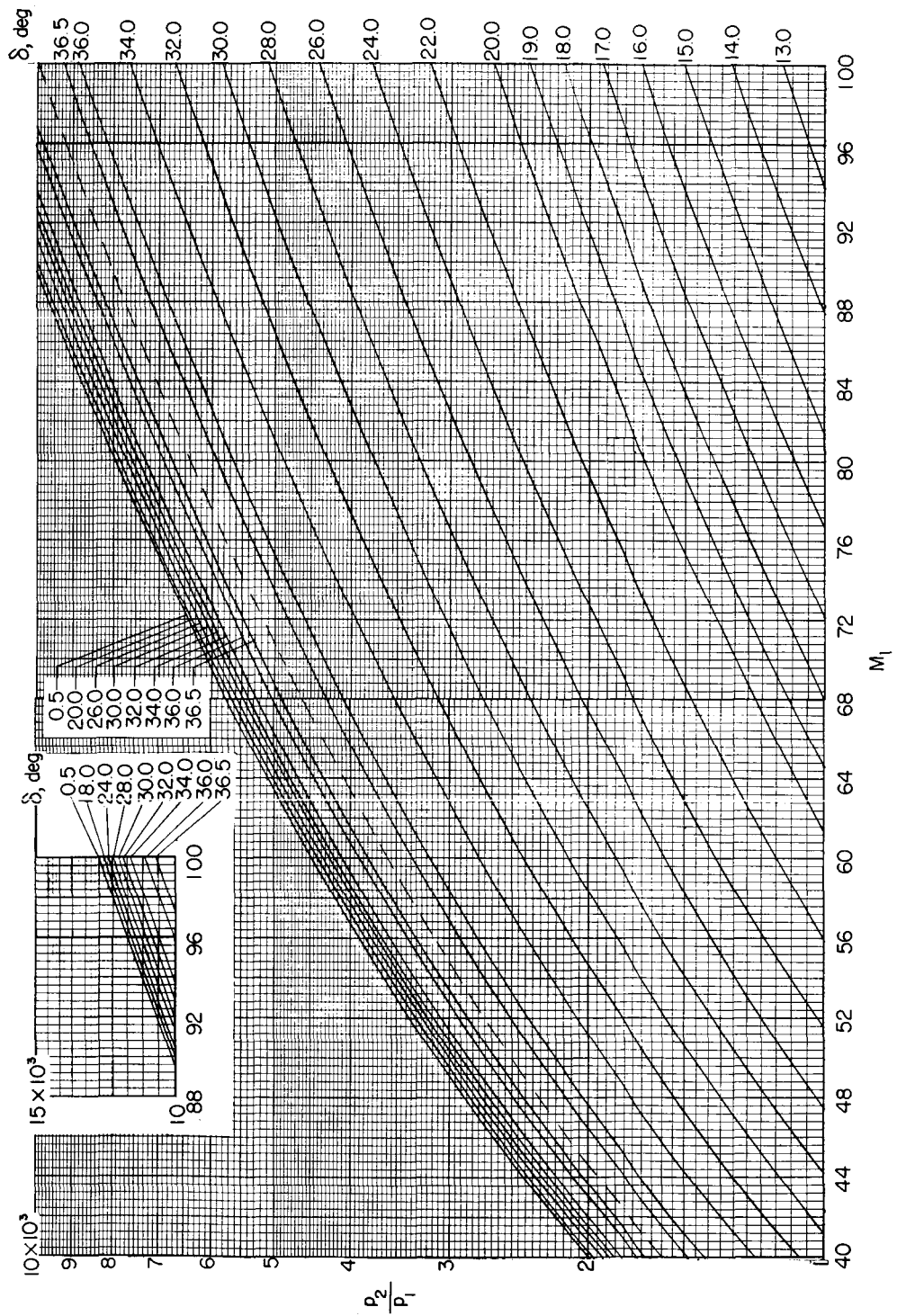
(n)  $M_1 = 40$  to  $100$ ;  $p_2/p_1 = 10$  to  $100$ .

Figure 9.- Continued.



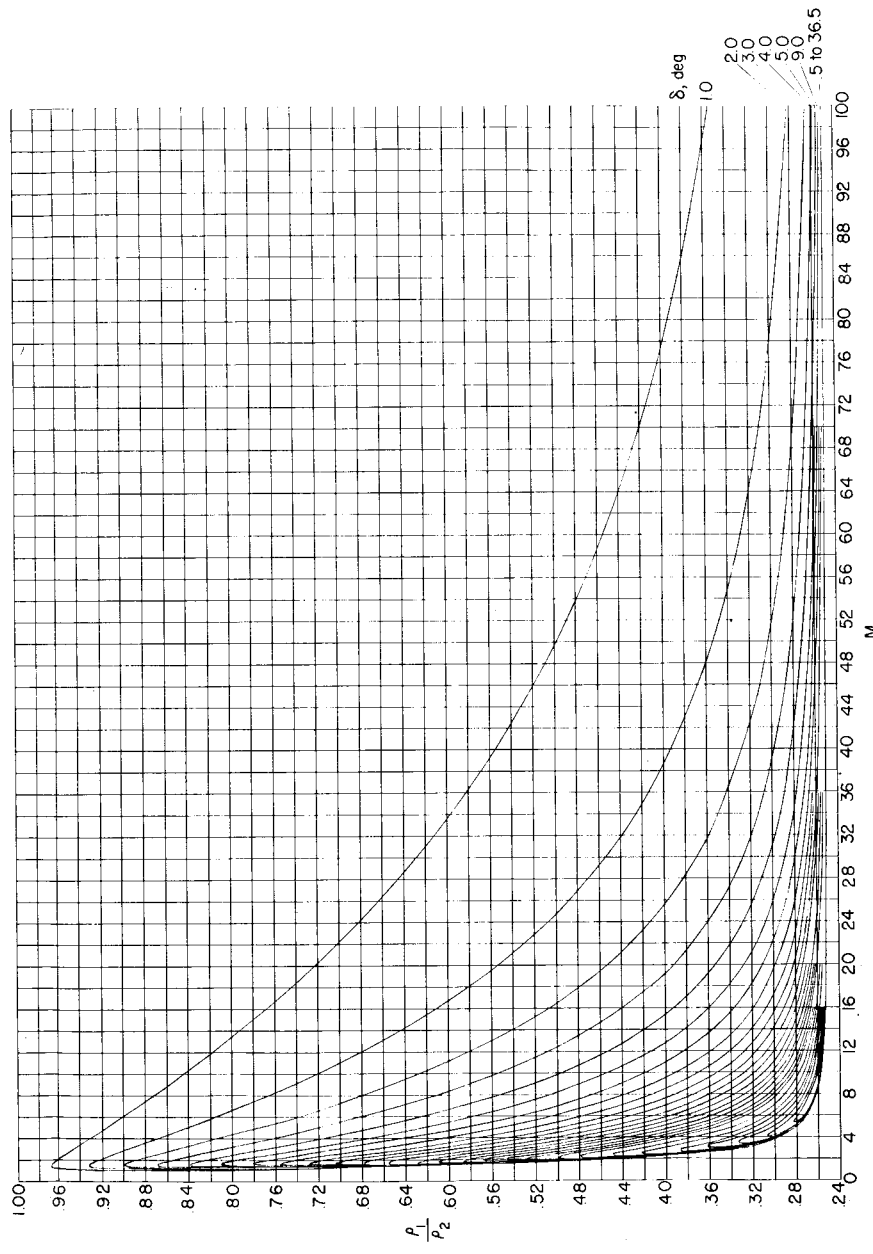
(o)  $M_1 = 40$  to 100;  $p_2/p_1 = 1 \times 10^2$  to  $10 \times 10^2$ .

Figure 9.- Continued.



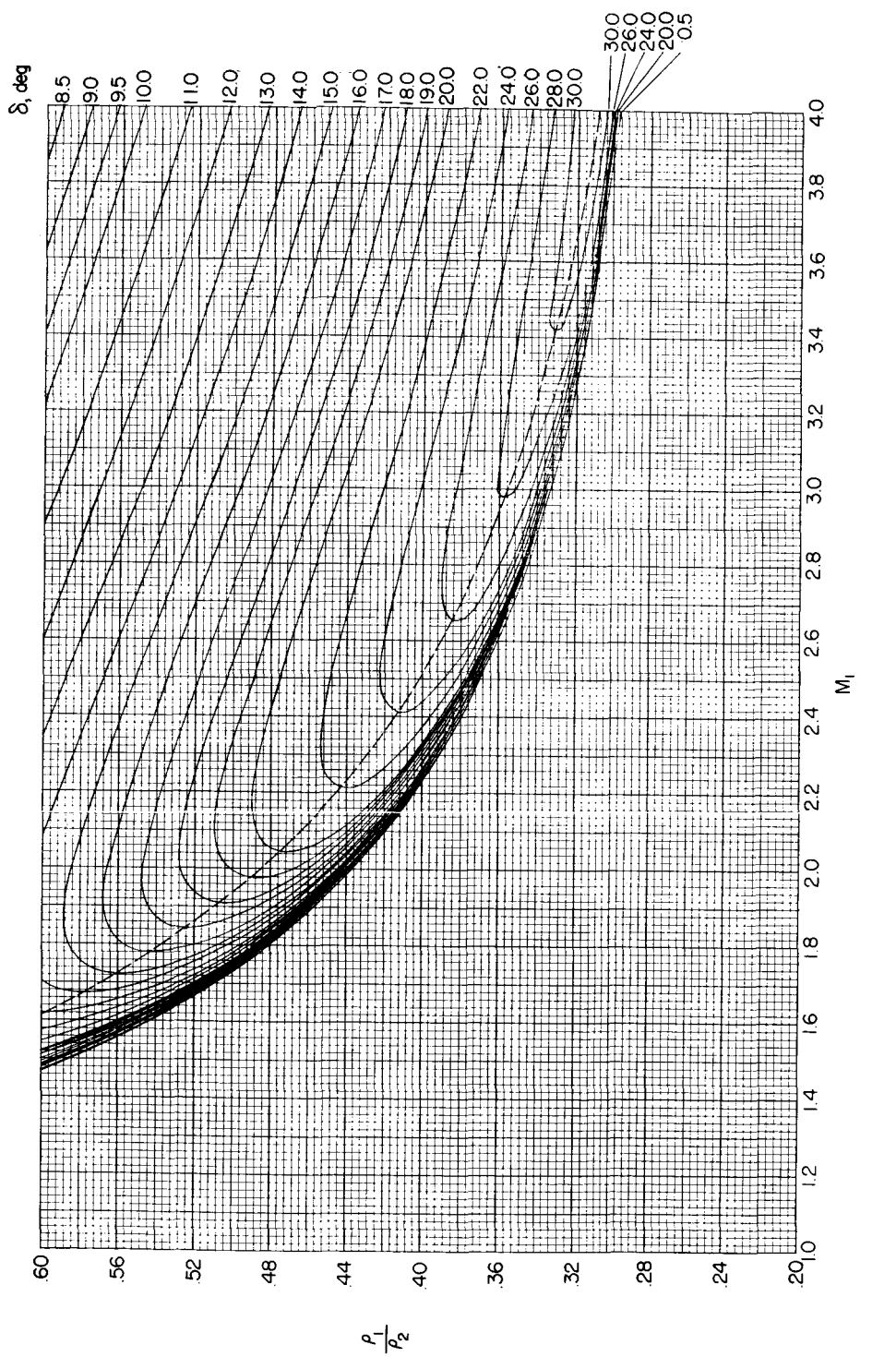
(p)  $M_1 = 40$  to 100;  $p_2/p_1 = 1 \times 10^3$  to  $10 \times 10^3$ .

Figure 9.- Concluded.



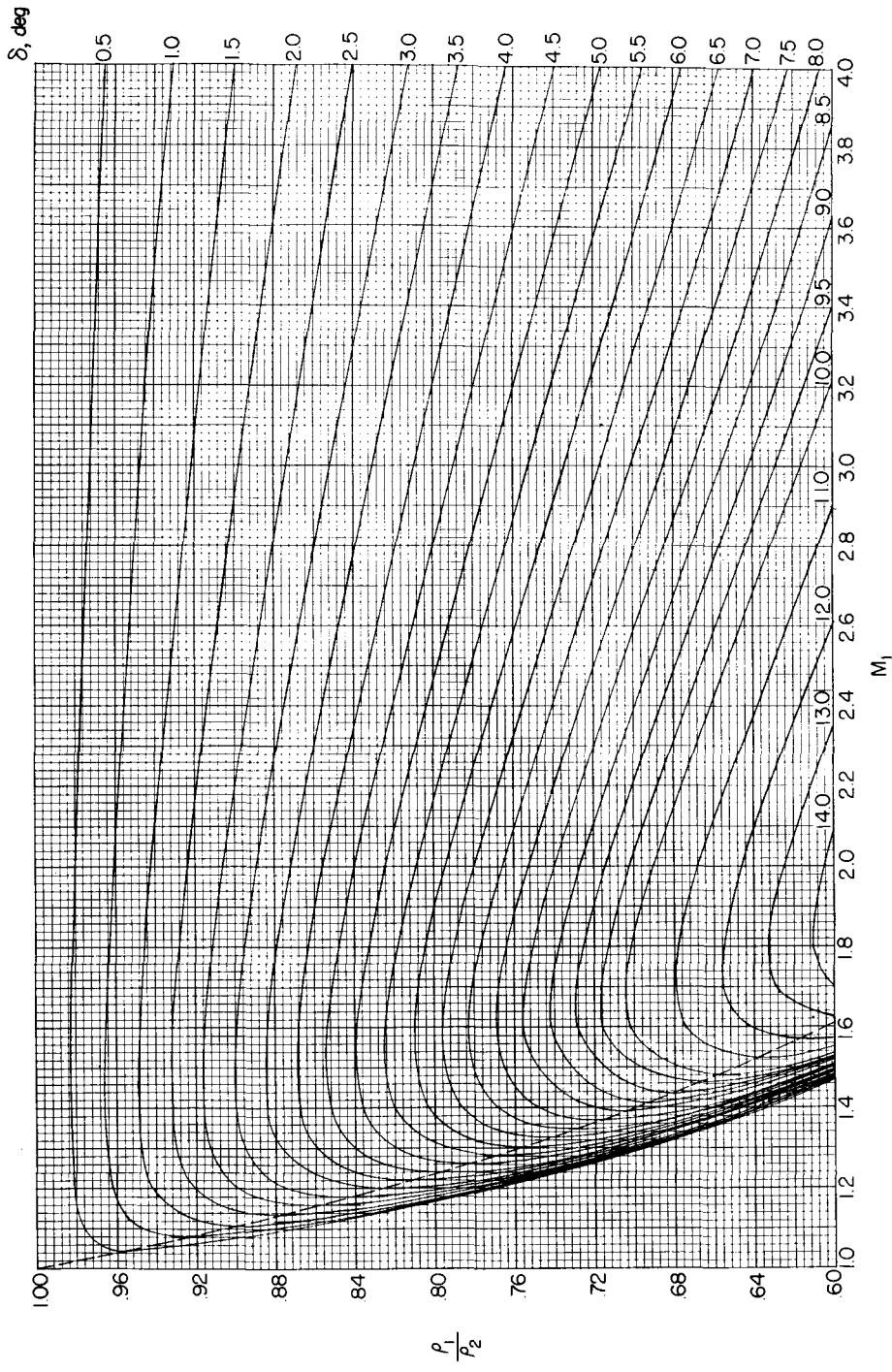
(a)  $M_1 = 1$  to 100;  $\rho_1 / \rho_2 = 0.24$  to 1.

Figure 10.- Variation of ratio of free-stream static density to static density behind a two-dimensional shock with free-stream Mach number for various flow-deflection angles. (Dashed line denotes boundary between weak and strong shock solutions. Weak shock solution is above dashed line.)



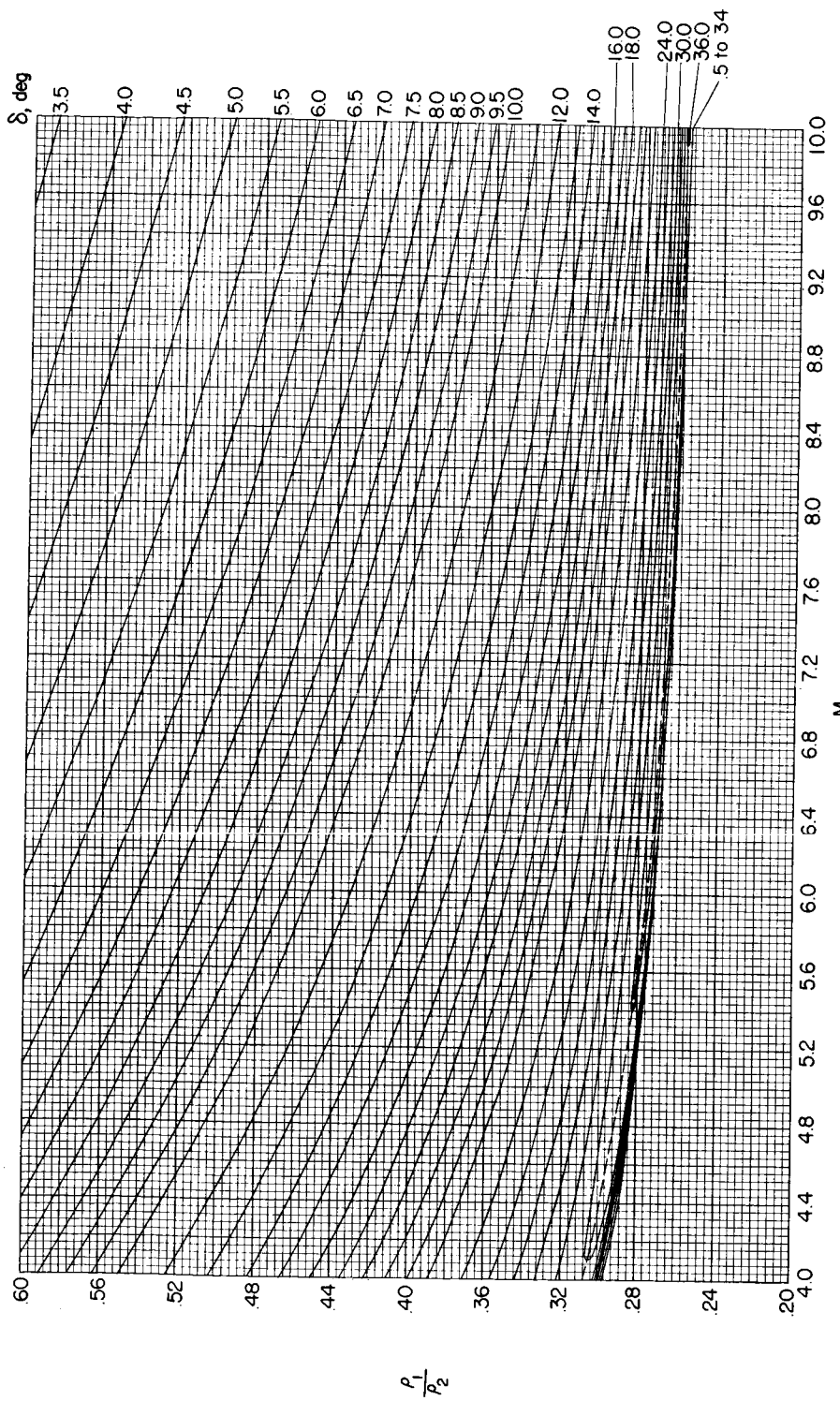
(b)  $M_1 = 1$  to 4;  $\rho_1/\rho_2 = 0.2$  to 0.6.

Figure 10.- Continued.



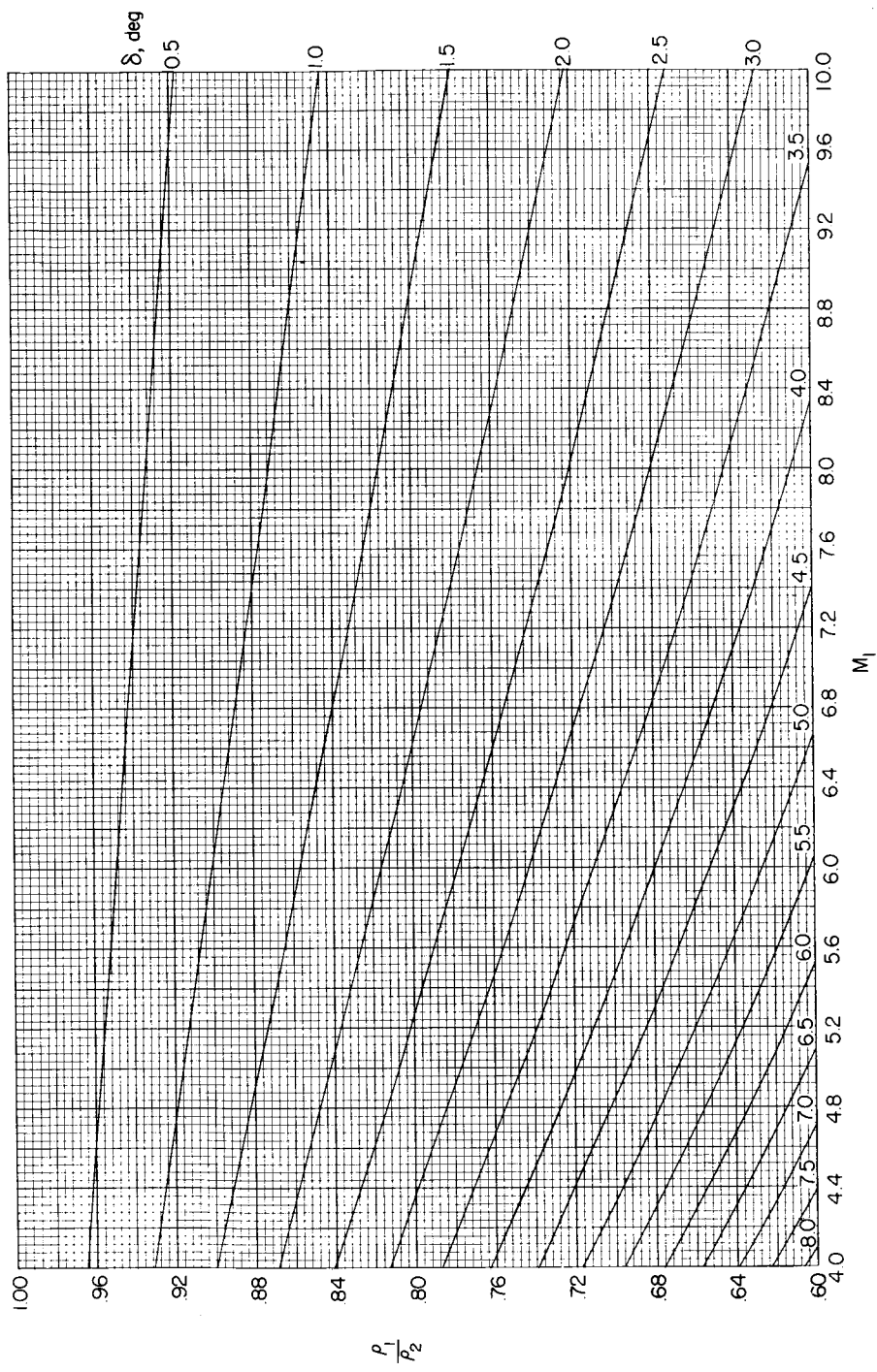
(c)  $M_1 = 1$  to 4;  $\rho_1/\rho_2 = 0.6$  to 1.

Figure 10.- Continued.



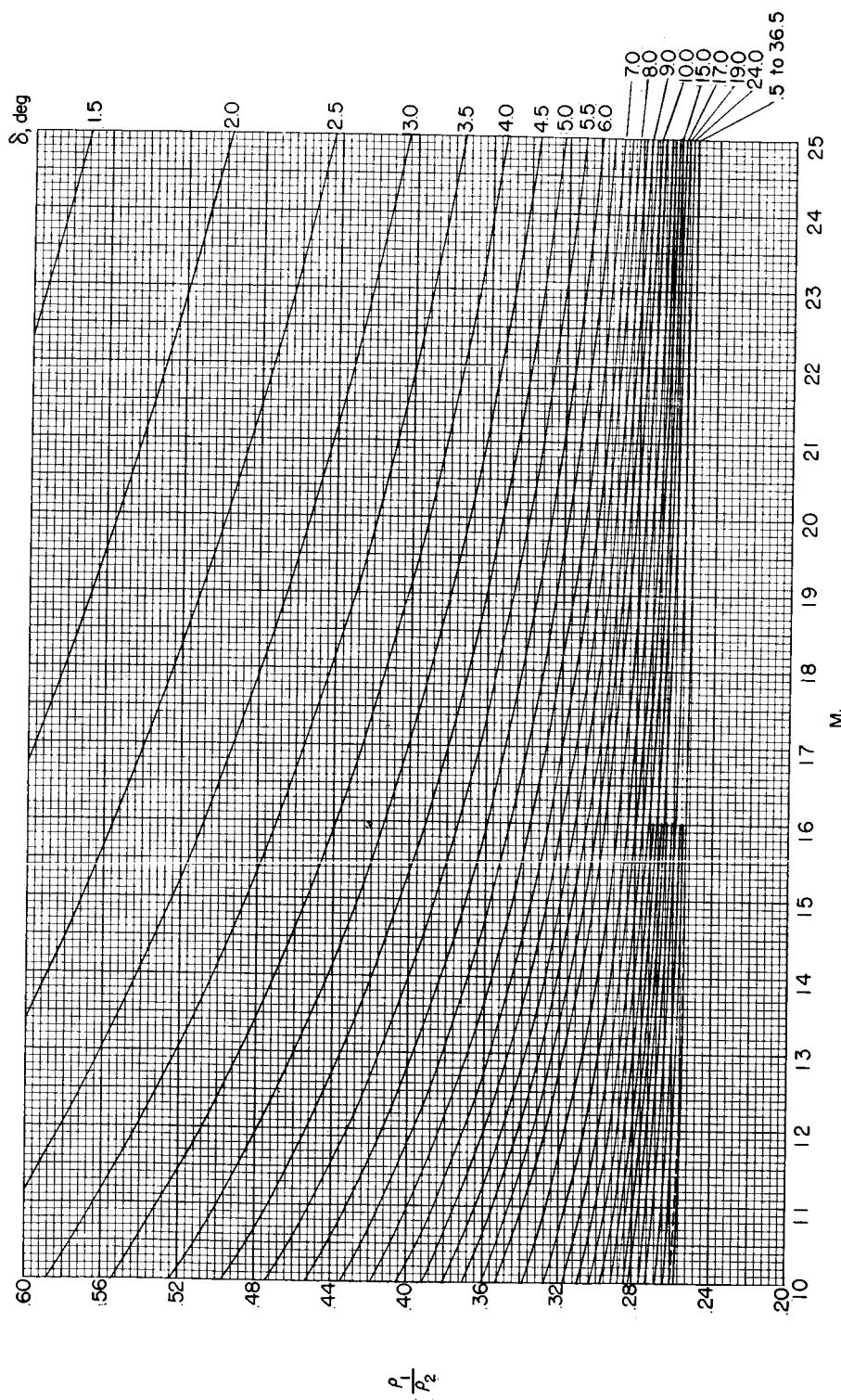
(d)  $M_1 = 4$  to 10;  $\rho_1/\rho_2 = 0.2$  to 0.6.

Figure 10.- Continued.



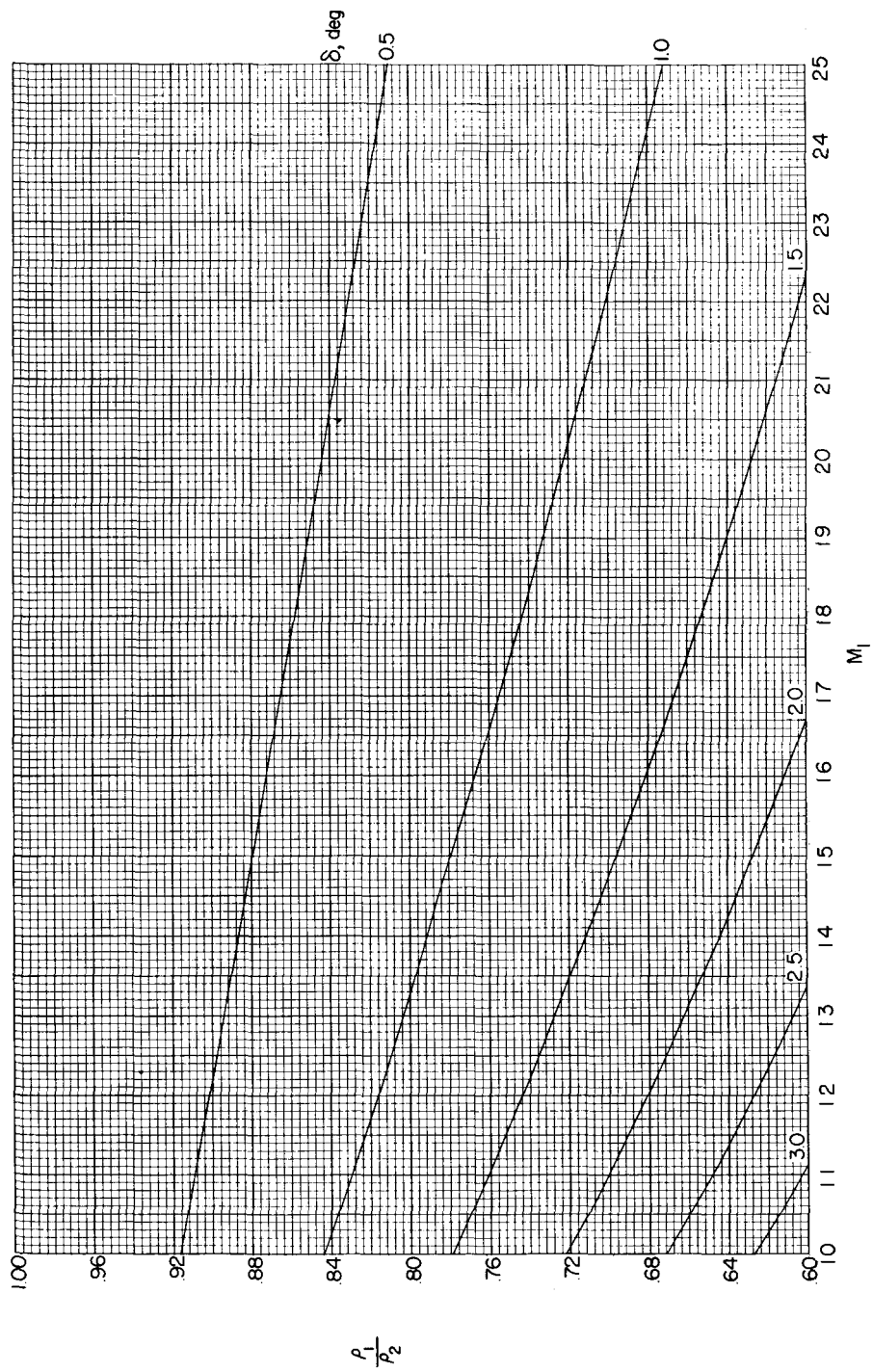
(e)  $M_1 = 4$  to 10;  $\rho_1/\rho_2 = 0.6$  to 1.

Figure 10.- Continued.



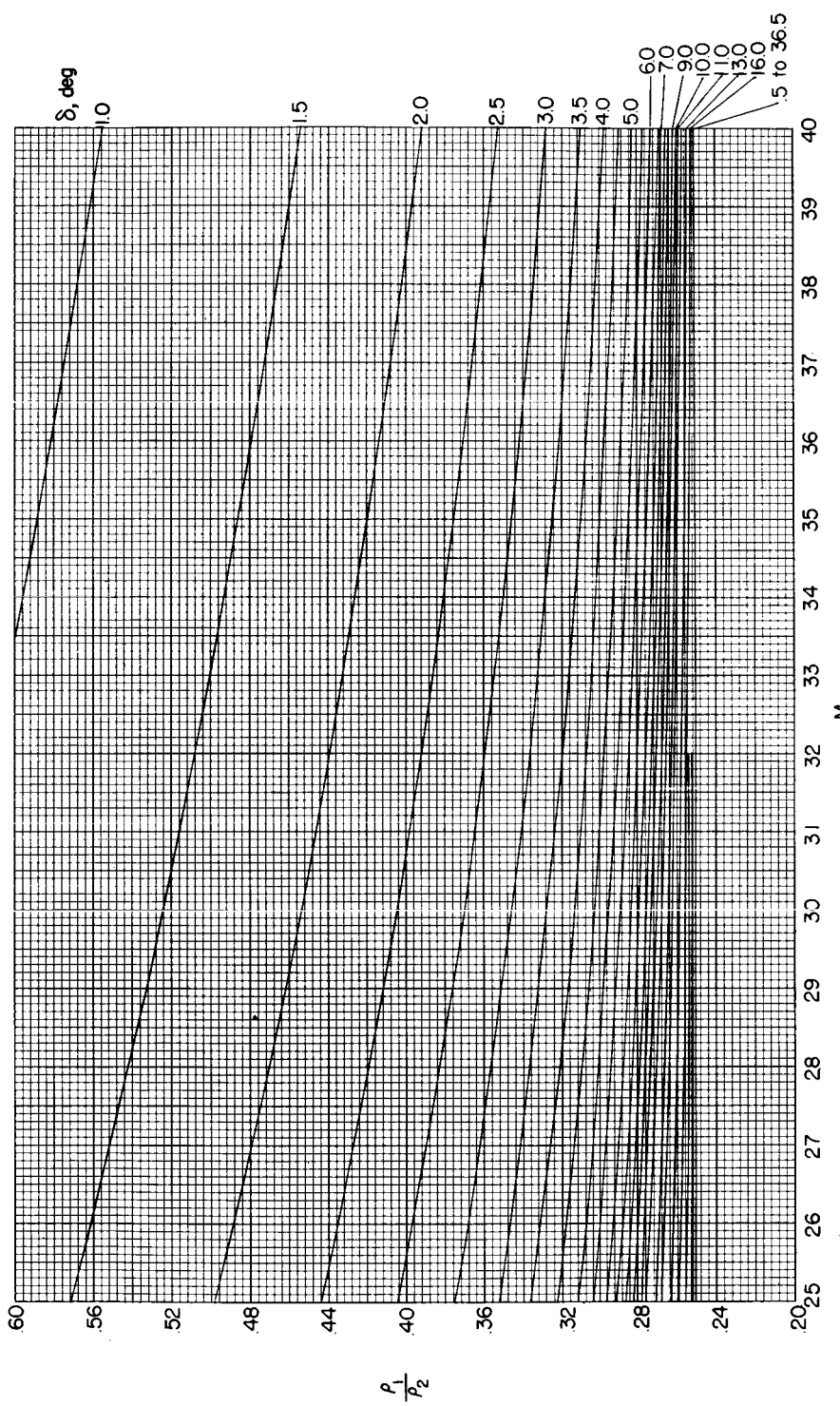
(f)  $M_1 = 10$  to  $25$ ;  $\rho_1/\rho_2 = 0.2$  to  $0.6$ .

Figure 10.- Continued.



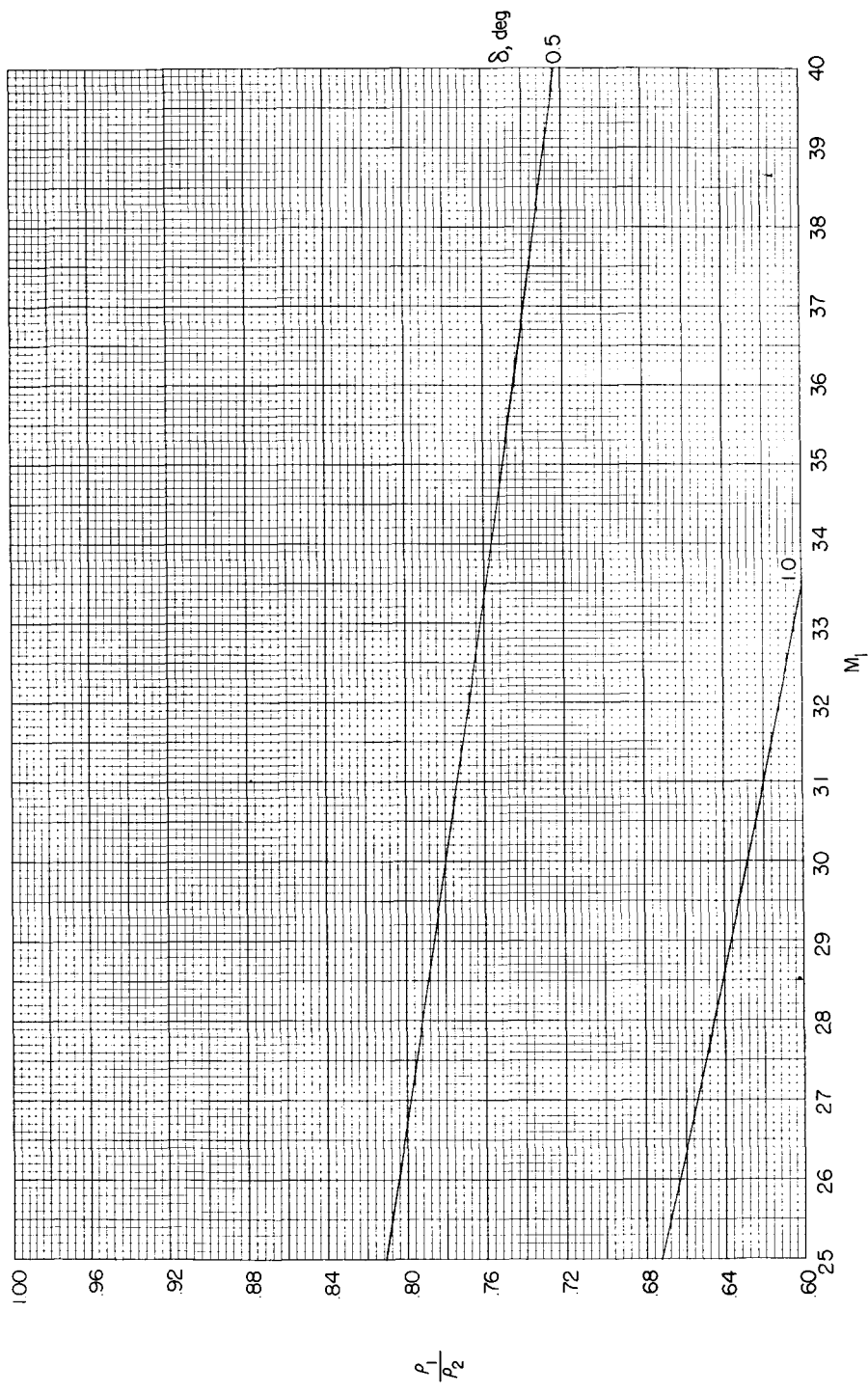
(g)  $M_1 = 10$  to 25;  $\rho_1/\rho_2 = 0.6$  to 1.

Figure 10.- Continued.



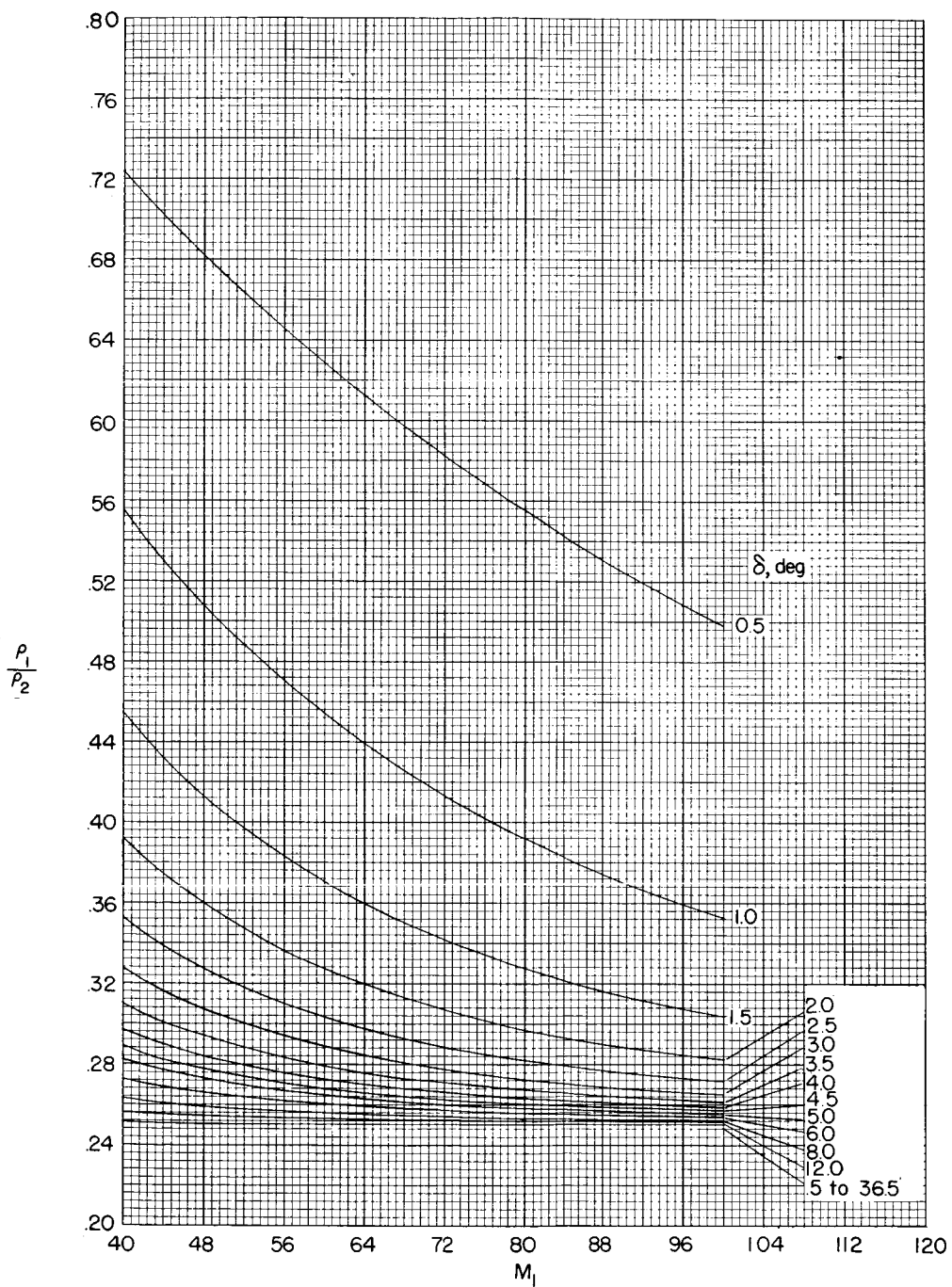
(h)  $M_1 = 25$  to 40;  $\rho_1/\rho_2 = 0.2$  to 0.6.

Figure 10.- Continued.



(1)  $M_1 = 25$  to 40;  $\rho_1/\rho_2 = 0.6$  to 1.

Figure 10.- Continued.



(j)  $M_1 = 40$  to  $100$ ;  $\rho_1/\rho_2 = 0.2$  to  $0.8$ .

Figure 10.- Concluded.